
Electronic Thesis and Dissertation Repository

12-15-2014 12:00 AM

Mouse Models of Intervertebral Disc Development, Degeneration and Mechanical Loading

Matthew R. McCann, *The University of Western Ontario*

Supervisor: Dr. Cheryle Séguin, *The University of Western Ontario*

Joint Supervisor: Dr. Frank Beier, *The University of Western Ontario*

A thesis submitted in partial fulfillment of the requirements for the Doctor of Philosophy degree in Physiology

© Matthew R. McCann 2014

Follow this and additional works at: <https://ir.lib.uwo.ca/etd>



Part of the [Medical Physiology Commons](#)

Recommended Citation

McCann, Matthew R., "Mouse Models of Intervertebral Disc Development, Degeneration and Mechanical Loading" (2014). *Electronic Thesis and Dissertation Repository*. 2623.
<https://ir.lib.uwo.ca/etd/2623>

This Dissertation/Thesis is brought to you for free and open access by Scholarship@Western. It has been accepted for inclusion in Electronic Thesis and Dissertation Repository by an authorized administrator of Scholarship@Western. For more information, please contact wlsadmin@uwo.ca.

MOUSE MODELS OF INTERVERTEBRAL DISC DEVELOPMENT,
DEGENERATION AND MECHANICAL LOADING

(Thesis Format: Integrated-Article)

by

Matthew Robert M^cCann

Graduate Program in
Physiology

Submitted in partial fulfillment
of the requirements for the degree of
Doctor of Philosophy

School of Graduate and Postdoctoral Studies
The University of Western Ontario
London, Ontario, Canada

© Matthew Robert M^cCann 2014

ABSTRACT

Intervertebral disc degeneration is a complex and multi-factorial process that is influenced by aging, genetic predispositions and environmental influences, such as altered mechanical loading. While recent studies have begun to characterize changes in the IVD associated with degeneration, the underlying etiology remains elusive. It is thought that the loss notochord cells from the nucleus pulposus is one initiating factor contributing to the cascade of disc degeneration. However, questions remain about the function of the notochord cell within the disc, including their capacity as tissue specific progenitor cells for the nucleus pulposus. We have demonstrated, with the use of the novel notochord-specific Cre mouse (*Noto-Cre*), that all cells in the adult NP are derived from the embryonic notochord (Chapter 2). Using this mouse strain, we performed transcriptional profiling paired with bioinformatic analysis of NP tissues from various time points and determined that TGF- β , PPAR and PI3K-AKT pathways are associated with NP aging, while mineralization, calcium and WNT signalling pathways are associated with NP degeneration (Chapter 3). We further characterized the proteomic signature of the healthy murine IVD to gain insight into the composition of this complex structure and provide a comprehensive catalogue of proteins enriched within the disc (Chapter 4). Lastly, we studied the effects of mechanical loading, in the form of whole-body vibration on the intervertebral disc. Whole-body vibration platforms are becoming increasingly popular in the fitness industry as well as clinic practice for and the treatment of musculoskeletal disorders. Our results demonstrate a transient beneficial effect of acute exposure to whole body vibration on the IVD. Furthermore, we demonstrate that this response is both frequency-dependent and tissue autonomous (Chapter 5). In follow

up studies, we demonstrated that repeated exposure to vibration resulted in dramatic catabolic effects leading to degeneration of the IVD. These detrimental effects were also detected in tissues of the knee joint, mediated in both joints by the activation of matrix metalloproteinases (Chapter 6). In summary, this work uses novel mouse models to provide insight to intervertebral disc development, degeneration and the response of the IVD to mechanical loading.

KEYWORDS

Intervertebral Disc; Nucleus Pulposus; Notochord; Transcriptional Profiling; Proteomics;
Whole Body Vibration; Bioinformatics; Disc Degeneration; Mouse Models

EPIGRAPH

"Life itself is a school, and Nature always a fresh study"

Hugh Miller

ACKNOWLEDGEMENTS

As I look back on the completion of this thesis, I have reminded that I am not here alone. My progress in graduate school would not be possible without amazing mentorships, exciting collaborations and great friendships that I have been fortunate enough to experience while at Western. It has been a privilege and honour to work with such talented people, who strive to make their community a positive one for all involved. The Department of Physiology and Pharmacology, the Collaborative Program in Developmental Biology and the Joint Motion Program have all been amazing groups who have contributed to my success both directly and indirectly.

First and foremost, I would like to thank my primary supervisor, Dr. Cheryle Séguin, for the support and guidance you have given me throughout my PhD. Even before I entered into the Master's program, you have been in my corner fighting for something that you saw in me. If it wasn't for your persistence and belief in me, I would not have had the opportunity to fully understand my passion for science and the satisfaction that scientific exploration can bestow. With your guidance, I have learned critical thinking skills, interpretation of data, how to present my work eloquently and effectively, and the ability to set up a well-designed experiment to answer new and exciting scientific questions. Your ability to make time for your students, the support you offer them and your ability to challenge them is a model that I hope to, at least partially, achieve in my own future mentoring. I will always appreciate the time you spent training me and the time I spent in your lab.

In addition, I would like to thank my co-supervisor, Dr. Frank Beier for your scientific guidance, honesty, encouragement, insight and wit. Your advice has been instrumental in my graduate career thus far and will have lasting affects on my future scientific advances.

During my time in the research labs at Western, I have had the opportunity to work a great number of supervisors, particularly those who are members of the musculoskeletal labs. I would like to thank Dr. Andrew Leask for giving me the opportunity to experience what "actual science" is like during my undergraduate years. If it weren't for you opening the doors to your lab, I would not have started this journey in science. Furthermore, you scientific insights mixed with popular culture references always makes me laugh and reminds me of the fun of science. I would also like to thank Dr. Jeff Dixon for your kind hearted and optimistic approach to this job. Through exciting collaborations, you have been become a fundamental in my group of mentors who I can count for great insights and opportunities. I would like to thank my committee members, Drs. Dean Betts, Tom Drysdale and Mark Hurtig for your input, not just within my experiments, but also in my career and future development. I could not have graduated without you help, both figuratively and literally.

Special thanks must go out to my past and present lab members who have made coming to work a fun and enjoyable venture. Without your encouraging, open atmosphere, I would not be where I am today. Particularly, I would like to thank the following people (in no particular order): Priya Patel, Jake Bedore, Dr. Christine Bell, Neil Tenn, Mike Sattin, Sumeeta Warraich, Meg Kamphuis, Courtney Brooks, Ahmed

Shah, Ryan Huff, Diana Quinonez, Teresa Dean and Dr. Hisataka Ii. You guys made the lab what it was, day in and day out.

There is a group of graduate students that I always looked up to and admired for their hard work, scientific advances as graduate students and their ability to stick together through the good and the bad. This group consists of Matt Grol, Kim Beaucage, Shirine Usmani, Lauren Solomon, Veronica Ulici and Erik Holm. You will always be the senior graduate students in my eyes. This is in contrast to the four master's students that joined the Beier and Séguin labs back in June 2009. To Nicole Watts, Emily LeBlanc and Ryan Perlus. You guys made the start to this long process an enjoyable one and I am grateful that we went through it together. I look back on this year fondly and will always remember our ability to do everything together, from coffee runs and late nights to JuMP events and softball games.

I would also like to thank members of Beier lab. While I always joked that I was never a member of your lab unless I need supplies; that was never the feeling that I received. Members of your lab, past and present, have been nothing short of amazing and I can't think of better lab to share an office with. Again in no particular order, I would like to thank the following: Mike Pest, Anusha Ratneswaran, Sadia Ladhani Paxton Moon, Margaret Sun, Dr. Jason Bush, Dawn Bryce, Holly Dupuis, Ryan Gillespie, Laura Aubrey, Sara Ohora, and Chantel Tacchino. I would also like to thank Katie Rabicki for the friendship, support and guidance she has offered me.

There is a core group of friends, while having no ties to my graduate career, have

made my years at Western truly unforgettable. Whether we were watching hockey or playing our own table version, going to Tuesday Trivia, hanging out at my house or going downtown, it was always a story. Members of the Brain Trust (Brad St Croix, Darren Schryvers, Ryan Ghuman, Andreas Clesle) as well as Stephan MacDonald, Matt Waghorn, Julian Restivo, Paul Tucker, Dan Pepe, Jess Brunnock-Hann, Sonya Corson, Carrie Charters, Elizabeth Skinner, Kendra Flagg, and Caleb & Jenna Butler. Also, to my frosh and best friend Brandon Mastromartino, thank you for the years of friendship during university and the years ahead.

I have also been fortunate enough throughout my doctoral studies to receive stipend support from the Joint Motion Program, The University of Western Ontario and the Canadian Institutes for Health Research in the form of a Fredrick Banting and Charles Best Canada Graduate Scholarship. These awards allowed me to focus on my studies and not be pressured to find alternative funding. Furthermore, CIHR, NSERC and the Canadian Arthritis Network have funded experiments that I have undertaken in the lab of Dr. Séguin. The Canadian public funded the support from these institutions and I hope that one day my research will lead to the development of an effective treatment or a cure disc degeneration and lower back pain.

I would like to finish by thanking my loving and understanding family. My grandparents for instilling in me that you should always be accountable for your actions and your performance at work but encouraged me to enjoy the time you have off with friends and family. I would like to thank my brother Andrew and Uncle Ian for your humour and friendship and my parents for your support of my ambitions even when they

seamed to be the tough road head. Your guidance and instilling in me the fortitude to never to give up has taught more than you will ever know.

TABLE OF CONTENTS

	PAGE
<i>Abstract and Keywords</i>	ii
<i>Epigraph</i>	iv
<i>Acknowledgements</i>	v
<i>Table of Contents</i>	x
<i>List of Tables</i>	xv
<i>List of Figures</i>	xvi
<i>List of Appendices</i>	xix
<i>List of Abbreviations</i>	xx
CHAPTER 1	1
INTRODUCTION AND REVIEW OF THE LITERATURE	1
1.1 <i>Co-Authorship Statement</i>	2
1.2 <i>Overview</i>	3
1.3 <i>Function and Structure of the Intervertebral Disc</i>	4
1.3.1 <i>Composition of the Intervertebral Disc</i>	4
1.4 <i>Intervertebral Disc Development</i>	7
1.4.1 <i>Early Embryo and Node Development</i>	7
1.4.2 <i>Notochord Development</i>	8
1.4.3 <i>Role of the Mesenchyme in Intervertebral Disc Development</i>	9
1.5 <i>Cellular Composition of the Nucleus Pulposus</i>	10
1.6 <i>Intervertebral Disc Degeneration</i>	12
1.7 <i>Animal Models to Study Intervertebral Disc Development and Degeneration</i>	13
1.7.1 <i>Notochord Cells in Animal Models</i>	13
1.7.2 <i>Notochord Specific Cre Mouse Strains</i>	14
1.8 <i>Nucleus Pulposus Tissue Regeneration</i>	19
1.8.1 <i>Nucleus Pulposus Progenitor Cells</i>	19
1.8.2 <i>Stem Cell-based Nucleus Pulposus Regeneration</i>	20
1.8.3 <i>Need for Notochord Cell Phenotype in Cell Differentiation Studies</i>	21
1.8.4 <i>Understanding the Phenotype of Nucleus Pulposus Cells</i>	24
1.9 <i>Mechanical Loading and the Musculoskeletal System</i>	25
1.9.1 <i>Biomechanical Loading Regulates Bone Physiology</i>	25
1.9.2 <i>Mechanical Loading in Knee Joint Health</i>	26
1.9.3 <i>Mechanical Loading and Intervertebral Disc Homeostasis</i>	27
1.10 <i>Whole Body Vibration as Mechanical Stimulus</i>	28
1.10.1 <i>Whole Body Vibration on Bone</i>	28
1.10.2 <i>Whole Body Vibration and Joint Health</i>	30
1.10.3 <i>Whole Body Vibration and the Intervertebral Disc</i>	31
1.11 <i>Rationale, Hypotheses and Objectives</i>	32
1.12 <i>References</i>	36
CHAPTER 2	57

TRACING NOTOCHORD-DERIVED CELLS USING A NOVEL NOTO-CRE MOUSE: IMPLICATIONS FOR INTERVERTEBRAL DISC DEVELOPMENT.....	57
2.1 <i>Co-Authorship Statement</i>	58
2.2 <i>Chapter Summary</i>	59
2.3 <i>Introduction</i>	60
2.4 <i>Materials and Methods</i>	63
2.4.1 Generation of Notochord-Specific Note-Cre Mouse Strain.....	63
2.4.2 Genotyping of Mice.....	65
2.4.3 Whole Mount In Situ Hybridization.....	68
2.4.4 Lineage Tracing and β -galactosidase Stain.....	70
2.4.5 Histology.....	72
2.4.6 Immunohistochemistry.....	72
2.5 <i>Results</i>	73
2.5.1 Generation of the Noto-Cre Mouse Line.....	73
2.5.2 Tracing Notochord-derived Cells in the Embryonic Mouse.....	74
2.5.3 Lineage Tracing the Cells of the Adult Nucleus Pulposus.....	77
2.6 <i>Discussion</i>	79
2.7 <i>References</i>	84
 CHAPTER 3	89
ELUCIDATING THE PHENOTYPE OF NOTOCHORD AND NUCLEUS PULPOSUS CELLS: CHANGES ASSOCIATED WITH AGING AND DEGENERATION.....	89
3.1 <i>Co-Authorship Statement</i>	90
3.2 <i>Chapter Summary</i>	91
3.3 <i>Introduction</i>	92
3.4 <i>Materials and Methods</i>	94
3.4.1 Mice.....	94
3.4.2 Histology.....	95
3.4.3 RNA Isolation and Purification.....	95
3.4.4 Global Gene Expression Analysis.....	96
3.4.5 Gene Ontology (GO) and Kyoto Encyclopedia of Genes and Genomes (KEGG) Pathway Analysis.....	97
3.5 <i>Results</i>	97
3.5.1 Nucleus Pulposus Degeneration with Age.....	97
3.5.2 Genetic Labeling and Isolation of Notochord-derived Cells.....	100
3.5.3 Assessment of Gene Expression Profiles in Age-induced Degeneration of the Nucleus Pulposus.....	102
3.5.4 KEGG Pathway Analysis.....	107
3.5.5 Extracellular Matrix Cluster Analysis and Specific Gene Queries.....	110
3.6 <i>Discussion</i>	113
3.7 <i>References</i>	116
 CHAPTER 4	121

PROTEOMIC SIGNATURE OF THE MURINE INTERVERTEBRAL DISC.....	121
4.1 <i>Co-Authorship Statement</i>	122
4.2 <i>Chapter Summary</i>	123
4.3 <i>Introduction</i>	124
4.4 <i>Materials and Methods</i>	126
4.4.1 <i>Animals</i>	126
4.4.2 <i>Intervertebral Disc Harvest, Protein Extraction and Tryptic Digestion</i>	126
4.4.3 <i>Liquid Chromatography Electrospray Ionization Tandem Mass Spectrometry (LC-ESI-MS/MS)</i>	127
4.4.4 <i>Bioinformatic Analysis</i>	128
4.4.5 <i>Validation using Previously Published IVD Markers</i>	128
4.4.6 <i>Histology and Immunohistochemistry</i>	128
4.5 <i>Results</i>	129
4.5.1 <i>Identification of Proteins in the Mature Murine Intervertebral Disc</i>	129
4.5.2 <i>Classification of the Proteomic Signature of the Murine Intervertebral Disc</i>	130
4.5.3 <i>Validation of Identified Proteins in the Murine Intervertebral Disc</i>	132
4.6 <i>Discussion</i>	135
4.7 <i>References</i>	138
 CHAPTER 5	 143
ACUTE VIBRATION INDUCES TRANSIENT EXPRESSION OF ANABOLIC GENES IN THE MURINE INTERVERTERBRAL DISC.....	143
5.1 <i>Co-Authorship Statement</i>	144
5.2 <i>Chapter Summary</i>	145
5.3 <i>Introduction</i>	146
5.4 <i>Materials and Methods</i>	149
5.4.1 <i>Ex Vivo Spine Organ Culture</i>	149
5.4.2 <i>Ex Vivo Vibration Apparatus</i>	149
5.4.3 <i>In Vivo Vibration</i>	153
5.4.4 <i>Harvesting of Murine IVDs and RNA Extraction</i>	155
5.4.5 <i>Real-time Polymerase Chain Reaction (PCR)</i>	155
5.4.6 <i>Protein Extraction and Trypsin Digestion</i>	157
5.4.7 <i>Liquid Chromatography Electrospray Ionization Tandem Mass Spectrometry (LC-ESI-MS/MS)</i>	157
5.4.8 <i>Histological Analysis</i>	158
5.4.9 <i>Immunofluorescence Analysis</i>	159
5.4.10 <i>Statistical Analysis</i>	159
5.5 <i>Results</i>	161
5.5.1 <i>Acute Ex Vivo High-Frequency, Low-Amplitude Vibration Affects on the Intervertebral Disc</i>	161
5.5.2 <i>Affect of Frequency of Vibration on the IVD</i>	163
5.5.3 <i>High-Frequency, Low-Amplitude Whole-body Vibration</i>	

In Vivo Model.....	163
5.5.4 High-Frequency, Low-Amplitude Whole body Vibration Affect on Protein Abundance in the IVD.....	165
5.6 <i>Discussion</i>	172
5.7 <i>References</i>	177
 CHAPTER 6	143
REPEATED EXPOSURE TO HIGH-FREQUENCY LOW-AMPLITUDE VIBRATION INDUCES DEGENERATION OF THE INTERVERTEBRAL DISC AND KNEE JOINT IN A MURE MODEL.....	182
6.1 <i>Co-Authorship Statement</i>	183
6.2 <i>Chapter Summary</i>	184
6.3 <i>Introduction</i>	185
6.4 <i>Materials and Methods</i>	187
6.4.1 In Vivo Vibration.....	187
6.4.2 Tissue Harvest and RNA Extraction.....	188
6.4.3 Quantitative Polymerase Chain Reaction (qPCR).....	188
6.4.4 Histology.....	190
6.4.5 Immunohistochemistry.....	190
6.4.6 Cell Death Assay.....	191
6.4.7 Micro-computed tomography (micro-CT).....	191
6.4.8 Statistical Analysis.....	192
6.5 <i>Results</i>	193
6.5.1 Effects of Repeated Exposure to WBV on the Intervertebral Disc.....	193
6.5.2 Effects of Repeated Exposure to WBV on the Knee Joint.....	199
6.5.3 Repeated Exposure to WBV did not Alter Bone Morphometry.....	210
6.6 <i>Discussion</i>	210
6.7 <i>References</i>	217
 CHAPTER 7	223
CONCLUSIONS AND GENERAL DISCUSSION.....	223
7.1 <i>Summary and Conclusions</i>	184
7.2 <i>Contributions to the Current State of Knowledge</i>	231
7.2.1 Intervertebral Disc Development.....	231
7.2.2 Transcriptional and Proteomic Profiling of the Nucleus Pulposus.....	233
7.2.3 Effects of Whole-body Vibration on the Intervertebral Disc.....	235
7.3 <i>Limitations of the Research and Future Directions</i>	236
7.3.1 Origin of Chondrocyte-like Cells in the Nucleus Pulposus.....	236
7.3.2. Gene Expression Analysis and Proteomics of the Intervertebral Disc.....	238
7.3.3 Whole-body Vibration and the Intervertebral Disc.....	241
7.4 <i>References</i>	249

Appendix A	
<i>Gene Expression Analysis from Chapter 3</i>	250
Appendix B	
<i>Characterized Proteins from Chapter 4</i>	263
Appendix C	
<i>Permissions to Reuse Copyrighted Material from Springer for Chapter 1</i>	300
Appendix D	
<i>Permissions to Reuse Copyrighted Material from The Company of Biologist for Chapter 2</i>	304
Appendix E	
<i>Permissions to Reuse Copyrighted Material from Wiley for Chapter 4</i>	308
Appendix F	
<i>UWO Council on Animal Care – Animal Care Protocol Approval</i>	316
Curriculum Vitae.....	318

LIST OF TABLES

Table	Page
1.1 <i>Identified knockout and transgenic mouse models with IVD phenotypes.....</i>	15
3.1 <i>Primers for Noto^{Cre/+} and lacZ reporter mice.....</i>	69
4.1 <i>Validation using previously identified genes and proteins in the intervertebral disc.....</i>	133
5.1 <i>Primers for real-time PCR.....</i>	156
6.1 <i>Primers for real-time PCR.....</i>	189

LIST OF FIGURES

Figure	Page
1.1. <i>Morphology and composition of the intervertebral disc.....</i>	5
1.2. <i>Lack of specific phenotypic markers limits strategies for notochord cell generation.....</i>	24
1.3. <i>Schematic illustrations of whole-body vibration platforms.....</i>	29
2.1. <i>Schematic representation of the main stages in axial skeletogenesis.....</i>	64
2.2. <i>Generation of notochord-specific Cre mouse line.....</i>	67
2.3. <i>Whole mount examination of β-galactosidase staining in $Noto^{Cre/+};R26^{R/+}$ embryos.....</i>	75
2.4. <i>β-galactosidase staining at postnatal time points in $Noto^{Cre/+};R26^{R/+}$ mice.....</i>	76
2.5. <i>Co-localization of β-galactosidase and cytokeratin-8 in the nucleus pulposus.....</i>	78
3.1. <i>Characterization of the nucleus pulposus composition with aging in 2.5, 6, and 21 month old mice.....</i>	99
3.2. <i>Genetic mouse models to distinguish notochord-derived cell within the intervertebral disc and nucleus pulposus microdissection.....</i>	101
3.3. <i>Phenotypic comparison of genes altered in the aging nucleus pulposus.....</i>	104
3.4. <i>Gene ontology enrichment analyses of differentially expressed genes.....</i>	106
3.5. <i>KEGG pathway analyses for differentially expressed mRNA.....</i>	109
3.6. <i>Heat map and hierarchical clustering of gene annotated through Gene Ontology for extracellular matrix.....</i>	112
4.1. <i>Proteomic signature of the murine intervertebral disc.....</i>	131
4.2. <i>Immunohistochemical staining validating the localization of proteins in the murine intervertebral disc.....</i>	134
5.1. <i>Histological appearance of murine spinal segments used in ex vivo organ culture model.....</i>	150

5.2	<i>Experimental design and platforms developed for ex vivo and in vivo studies of the effects of vibration on murine intervertebral disc.....</i>	<i>151</i>
5.3	<i>Representative graphs illustrate the waveform generated during in vivo vibration.....</i>	<i>154</i>
5.4	<i>Transient effects of acute vibration on anabolic and catabolic gene expression in murine intervertebral disc ex vivo.....</i>	<i>162</i>
5.5	<i>Frequency-dependent effects of acute vibration on anabolic and catabolic gene expression in the murine intervertebral disc ex vivo.....</i>	<i>164</i>
5.6	<i>Effects of acute whole-body vibration in vivo on anabolic and catabolic gene expression in the murine IVD.....</i>	<i>167</i>
5.7	<i>Effect of acute whole-body vibration in vivo on the abundance of extracellular matrix proteins in the murine intervertebral disc.....</i>	<i>169</i>
5.8	<i>Effect of acute whole-body vibration in vivo on histologic features of the murine intervertebral disc.....</i>	<i>171</i>
6.1	<i>Repeated exposure to whole-body vibration negatively affects the lumbar intervertebral disc.....</i>	<i>194</i>
6.2	<i>Repeated exposure to whole-body vibration negatively affects the caudal intervertebral disc.....</i>	<i>196</i>
6.3	<i>Matrix degradation in mouse intervertebral discs following whole-body vibration.....</i>	<i>198</i>
6.4	<i>TUNEL staining of intervertebral discs after repeated exposure to whole-body vibration.....</i>	<i>200</i>
6.5	<i>Histological sections of mouse medial knee joints after exposure to whole-body vibration.....</i>	<i>201</i>
6.6	<i>Histological sections of the lateral compartment of the mouse knee joints after exposure to whole-body vibration.....</i>	<i>203</i>
6.7	<i>Histological sections of the mouse medial knee joint after 4 weeks of exposure to whole-body vibration.....</i>	<i>204</i>
6.8	<i>Matrix degradation in mouse the medial knee joint compartment following whole-body vibration.....</i>	<i>206</i>

6.9	<i>Catabolic activities in the lateral mouse knee joint following whole-body vibration.....</i>	<i>209</i>
6.10	<i>Analysis of bone microarchitecture and gene expression following whole-body vibration.....</i>	<i>212</i>

LIST OF APPENDICES

Appendix	Page
Appendix A <i>Gene Expression Analysis from Chapter 3.....</i>	250
Appendix B <i>Characterized Proteins from Chapter 4.....</i>	263
Appendix C <i>Permissions to Reuse Copyrighted Material from Springer for Chapter 1.....</i>	300
Appendix D <i>Permissions to Reuse Copyrighted Material from The Company of Biologist for Chapter 2.....</i>	304
Appendix E <i>Permissions to Reuse Copyrighted Material from Wiley and Sons for Chapter 5.....</i>	308
Appendix F <i>UWO Council on Animal Care – Animal Care Protocol Approval.....</i>	316

LIST OF ABBREVIATIONS

AC	articular cartilage
ACAN	aggrecan
ADAMTS	a disintegrin-like and metallopeptidase with thrombospondin type motif
AF	annulus fibrosus
ANOVA	analysis of variance
ATP	adenosine triphosphate
BCA	bicinchoinic acid
BGN	biglycan
BMC	bone mineral content
BMD	bone mineral density
BSP	bone sialprotein
BVF	bone volume fraction
C1,2C	epitopes generated at the C-terminus of types I and II collagen
CA3	carbonic anhydrase III
CCN1	cysteine rich protein 61
cDNA	complementary deoxyribonucleic acid
CEP	cartilage end-plates
CID	collision-induced dissociation
CNOT1	CCR4-NOT transcription complex, subunit 1
CO ₂	carbon dioxide
Col1A1	collagen, type I, alpha 1

Cre	cre recombinase
C _T	cycle threshold
CTGF	connective tissue growth factor
DAB+	1-5% biphenyl-3,3',4,4'-tetrayltetraammonium tetrachloride
DAPI	4,6'-diamidino-2-phenylindole
DCN	decorin
DMEM	Dulbecco's modified Eagle's medium
DMP1	dentin matrix protein 1
DNA	deoxyribonucleic acid
DNase I	deoxyribonuclease I
DUSP1	dual specificity phosphatase 1
E	embryonic day
ECM	extracellular matrix
EDTA	ethylenediaminetetraacetic acid
FITC	fluorescein isothiocyanate
FLH	floating Head
FLPe	flippase
FOXA2	forkhead box A2
FRT	flippase recognition target
g	gravitational
GAPDH	glyceraldehyde-3-phosphate dehydrogenase
GFP	green fluorescence protein
HIF1A	hypoxia inducible factor 1, alpha subunit

HNF-3	hepatocyte nuclear factor 3
HU	Hounsfield units
Hz	hertz
IBSP	integrin binding sialoprotein
ICR	Institute for Cancer Research
IgG	immunoglobulin G
IRES	internal ribosome entry site
IVD	intervertebral disc
K ₃ [Fe(CN) ₆]	potassium ferricyanide
K ₄ [Fe(CN) ₆]	potassium ferrocyanide
KRT8	cytokeratin-8
KRT18	cytokeratin-18
KET19	cytokeratin-19
KVp	peak kilovoltage
L	lumber
LC-ESI-MS/MS	liquid chromatography electrospray ionization tandem mass spectrometry
MAB	malic acid buffer
MeOH	methanol
MgCl ₂	magnesium chloride
Micro-CT	micro-computed tomography
mm	millimetre
mRNA	messenger ribonucleic acid

MS/MS	mass spectrometry/mass spectrometry
MYOM1	myomesin 1
NaCl	sodium chloride
NCCM	notochord-cell conditioned media
NEO	neomycin
NFAT	nuclear factor of activated T-cells
NGN	neogenin
NH ₄ HCO ₃	ammonium bicarbonate
NLS	nuclear localization signal
NOTO	notochord homeobox
NP	nucleus pulposus
NPR3	natriuretic peptide receptor 3
NTMT	(tris-HCl)-MgCl ₂ -NaCl-Tween-20
PANTHER	protein analysis through evolutionary relationships
PBS	phosphate buffered saline
PBST	phosphate buffered saline with tween
PCR	polymerase chain reaction
PGK	phosphoglycerine kinase
RANK	receptor activator of nuclear factor κ B
RNA	ribonucleic acid
ROI	region of interest
SEM	standard error of the mean
SHH	sonic hedgehog

SOX5	SRY (sex determining region Y)-box
SPARC	secreted acidic cysteine rich glycoprotein
T	brachyury
Tb.N.	trabecular number
Tb.Sp.	trabecular spacing
Tb.Th.	trabecular thickness
TGF- β 3	transforming growth factor, beta 3
TIMP	tissue inhibitor of metalloproteinase
TNT	tris-hydrochloride-NaCl-Tween20 buffer
TUNEL	terminal deoxynucleotidyl transferase dUTP nick-end labeling
w	watt
WBV	whole-body vibration
WISP1	WNT1 inducible signaling pathway protein 1
WNT10b	wingless-type MMTV integration site family, member 10B
MMP	matrix metalloproteinase
X-Gal	5-bromo-4-chloro-3-indolyl- β -D-galactopyranoside

CHAPTER ONE

INTRODUCTION AND REVIEW OF THE LITERATURE

Sections of this chapter have been reproduced with permission from:

McCann, M. R., Bacher C.A., Séguin C.A. Exploiting notochord cells from stem cell-based regeneration of the intervertebral disc. *Journal of Cell Communication and Signalling* (2011) Mar;5(1):39-43

1.1 Co-Authorship Statement

Portions of the text in Chapter 1 are adapted from McCann, M.R., Bacher, C.A., and Séguin, C.A. (2011). Exploiting notochordal cells for stem cell-based regeneration of the intervertebral disc. *Journal of Cell Communication and Signalling Mar;5(1):39-43*. Figures and text are reproduced with permissions from the Journal of Cell Communication and Signalling (Appendix C). C.A Bacher provided insight into the topic and approved the final manuscript. M.R. McCann developed topic, prepared figures and wrote the manuscript with suggestions from Dr. C.A. Séguin

1.2 Overview

Non-specific low back pain (LBP) has become one of the most common global health care problems, with recent reports indicating a lifetime prevalence as high as 84% (Balague et al. 2012). Back pain has been reported to cause chronic pain in 23% of the global population (Balague et al. 2012); numbers that are mirrored in the Canadian population (Lim et al. 2006). In fact, according to the most recent Global Burden of Disease study, LBP is the leading musculoskeletal disorder and the leading cause of years lived with disability in all developed countries (Vos et al. 2012). Alarming, while the prevalence of LBP has increased over the past three decades (Hoy et al. 2012), current treatment options do not adequately provide improved outcomes (Friedman et al. 2012). Even though the etiology of LBP remains unknown, the first manifestations are thought to be a result of degeneration of the intervertebral disc (IVD). While symptomatic treatments are available for LBP, the current lack of disease-modifying therapies for disc degeneration is linked to our limited understanding of the mechanisms that regulate IVD development, homeostasis, aging and degeneration.

This chapter will provide an overview of IVD biology, with a specific emphasis on the development of the IVD and how transient embryonic structures play an essential role in the adult IVD. Also described is the potential function of notochord cells in regulating IVD homeostasis, the benefits of animal models to study the IVD and the use of mouse models to better understand the phenotype and function of distinct cell populations within the IVD. Lastly, the importance of mechanical loading on the IVD and other tissues in the musculoskeletal system will be discussed in the context of the whole-body vibration-based mechanical loading.

1.3 Function and Structure of the Intervertebral Disc

IVDs are complex connective tissue structures that serve to anchor adjacent vertebral bodies along the spinal column. IVDs are essential for mechanical stabilization of the spine and load bearing during axial compression. Furthermore, the IVD forms a cartilaginous joint that serves to provide flexibility and movement of the spinal column.

1.3.1 Composition of the Intervertebral Disc

The IVD consists of three distinct, yet interdependent specialized tissues: the outer fibrillar annulus fibrosus (AF), the central viscous nucleus pulposus (NP), and the cartilage end-plates (CEP) that anchor the composite tissue to the adjacent vertebral bones (**Figure 1.1**). The diversity in the structure of these tissues is due to the specific organization of their extracellular matrix (ECM), which is produced and maintained by distinct cell populations.

The AF is a highly organized fibrocartilagenous structure that consists of distinct lamellae (25 lamellae in a human disc), which are composed of bundles of type-I collagen fibers oriented at oblique angles that alternate within each consecutive lamella to form an angle-ply structure (Cassidy et al. 1989). The outer AF contains elastic fibers that directly associate with the adjacent vertebra and extend into the bone as Sharpey's fibers to anchor the IVD into bone (Smith and Fazzalari 2009). The inner AF contains an increasing amount of glycosaminoglycans (GAG) and type-II collagen in the interlamellar matrix, which makes the inner AF a transition zone between the fibrous outer AF and the gelatinous structured NP (Li et al. 2014). The NP is composed

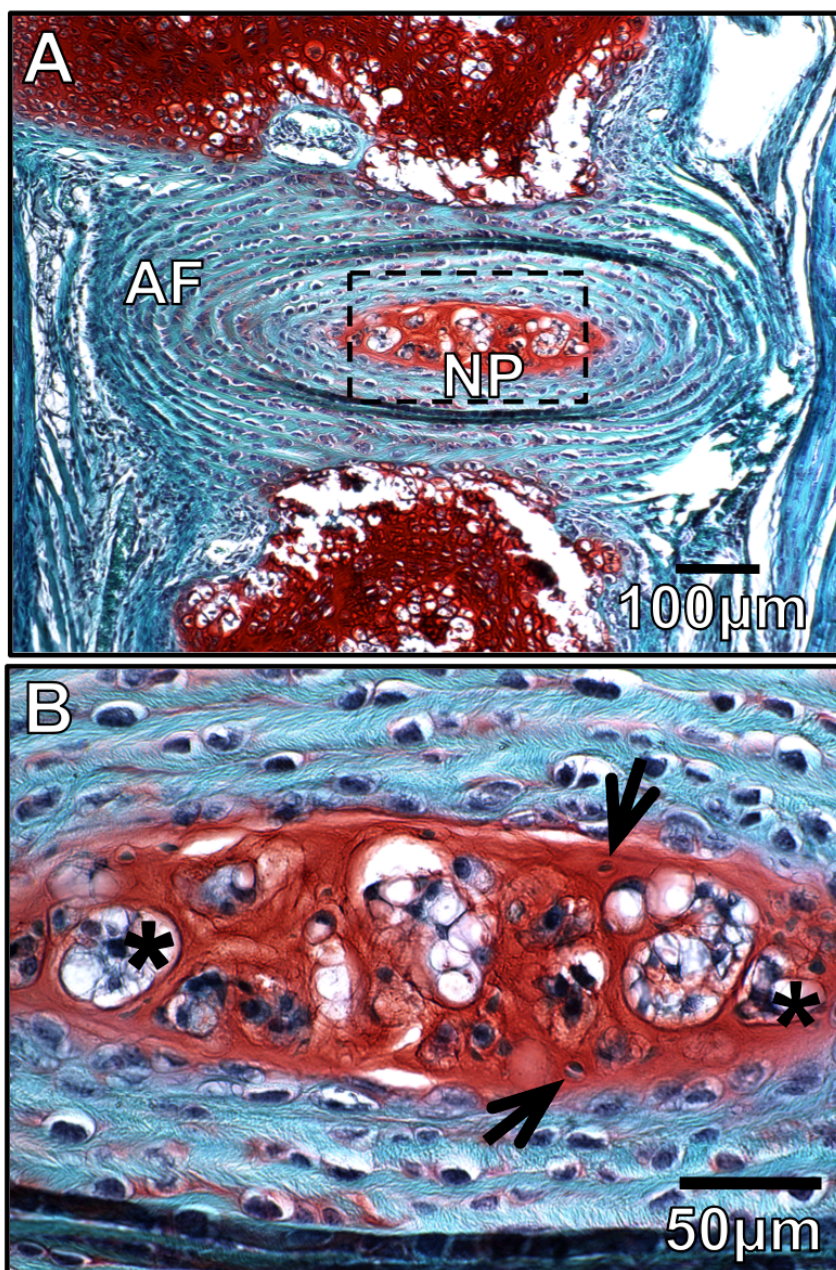


Figure 1. 1 Morphology and composition of the intervertebral disc.

A. Histological section of an IVD from a 4-week-old mouse, stained with Safranin-O/fast green demonstrates IVD morphology and regionalization of the nucleus pulposus (NP), annulus fibrosus (AF). Proteoglycan content is indicated by red stain. **B.** Enlarged view of the nucleus pulposus region in A. Asterisks indicate aggregations of vacuolated notochord cells and arrows indicate the smaller more disperse cartilage-like NP cells.

primarily of proteoglycans that are held together loosely by an irregular network of type-II collagen and elastin fibers. Specifically, the large aggregating proteoglycans are highly sulfated aggrecan monomers, which are cross-linked to hyaluronic acid via cartilage link protein (Moreland 2003). The monomers consist of a core protein with several covalently attached GAGs, notably chondroitin sulfate and keratin sulfate. These bound GAGs allow aggrecan molecules to acquire their negative charge and attract larger numbers of counter ions and therefore water molecules (Nap and Szleifer 2008; Chandran and Horkay 2012). The influx of water into the NP is created by osmotic pressure (Kraemer et al. 1985), and the water molecules are retained in the matrix in part by the irregular meshwork of type II collagen (Mwale 2014). Thus, osmotic pressure provides the intrinsic compressive stiffness required of the NP to maintain its height and turgor against compressive loads. With sustained loads, such as daily activity, the disc is no longer able to maintain turgor pressure and roughly 20-25% of the water slowly diffuses out of the disc into the paravertebral muscles (Urban et al. 2000; Matsumura et al. 2009). Upon removal of the compressive load, water molecules are reabsorbed back into the matrix, resulting in a re-expansion of the tissue and an increase in disc height. (Watanabe et al. 1998; Adams and Roughley 2006; Setton and Chen 2006)

The disc is anchored superiorly and inferiorly to the adjacent vertebral bodies through the CEPs, which are thin layers of hyaline cartilage that cover the vertebral bone creating an interface with the inner AF and NP. The CEP functions both as a mechanical barrier and as a gateway for nutrient transport into the disc. The adult NP is the largest avascular tissue in the body, which is dependent on nutrient, metabolic by-products and O₂ gas exchange through the CEPs via passive diffusion from the highly vascularized vertebral bone (Urban et al. 2004). Since the CEP is hyaline cartilage, it is formed by

chondrocytes similar to those found in articular cartilage (AC), which secrete a type II collagen and proteoglycan rich extracellular matrix.

1.4 Intervertebral Disc Development

1.4.1 Early Embryo and Node Development

To understand IVD development, it is important to start from the early embryo. During early embryogenesis, cells within the inner cell mass contribute to the formation of the embryo proper through differentiation into either the hypoblast or epiblast. While the hypoblast gives rise to the extraembryonic endoderm, the epiblast gives rise to all three germ layers (endoderm, ectoderm and mesoderm) through a process known as gastrulation. While there is diversity in the shape of the epiblast amongst mammalian species (i.e. the mouse epiblast is cup-shaped and the human epiblast is disc-shaped), the cellular and molecular processes that govern gastrulation are largely conserved.

During gastrulation the primitive streak (a band of cells that forms along the longitudinal axis) is formed and establishes the longitudinal (anterior/posterior) and the bilateral (left/right) symmetry of the embryo. In the mouse, a cluster of cells located near the anterior end of the primitive streak ingress to form the node. The node is a transient pit-shaped structure located at the distal tip the early embryo, responsible for establishing the left asymmetry of the of the body plan. Monocilia localized specifically to the apical surface of cells within the cup-shaped node beat in a clockwise rotation (when viewed from the ventral side) to drive a leftward flow of extraembryonic fluid containing morphogens, such as Nodal, secreted by the columnar epithelial cells of ventral node (Davidson and Tam 2000; Brennan et al. 2002; Hirokawa et al. 2006). This leftward flow

of morphogens causes left side specification via two possible mechanisms: either directly inducing a differentiation cascade on the left side of the embryo, or the fluid flow produced by the cilia is sensed by the perinodal crown cells that lie directly left of the nodal pit, which respond via elevated calcium signalling which then induces cell specification. While the underlying mechanisms remain to be established, the node and resultant nodal flow are necessary for asymmetric differentiation of the left axis of the embryo (Nonaka et al. 1998; Tanaka et al. 2005; Babu and Roy 2013).

1.4.2 Notochord Development

In the mouse, the first stages in notochord development originate at the notochordal plate at E8.0-E8.5. This plate like structure lays in the ventral midline of the embryo and is continuous with the dorsal gut endoderm. At E9.0, the notochord plate folds off the gut endoderm to form the anterior notochord, where it rests in a central position in the embryo, flanked by the ventral ridge of the neural tube (the floor plate) and dorsally by the gut endoderm (the endoderm plate). Laterally, the notochord is flanked by the paraaxial mesoderm, which will go on to form the somites.

The notochord is morphologically and molecularly distinct and plays two important roles in the developing embryo. First, the notochord forms the primitive anterior/posterior axis of the embryo; a continuous rod-like structure that runs along the axis of the embryo, surrounded by an acellular notochordal sheath, and this sheath structure is similar in composition to cartilage with an extracellular matrix rich in collagens, laminins, and proteoglycans (Gotz et al. 1995). The notochord remains in place until the development of permanent skeletal components such as the vertebrae, which will

take over the functional role of axial support. Secondly, the notochord is generally considered to be a signalling centre, secreting factors such as Shh and noggin, and is responsible for patterning of surrounding tissues, including the neural tube (Yamada et al. 1991), the sclerotome of the somites (Fan and Tessier-Lavigne 1994), the pancreas (Kim et al. 1997) and the aorta (Meadows et al. 2012).

While the importance of the notochord in early embryonic development is well established, the fate of notochord cells after embryogenesis has been a source of controversy for decades. Studies have shown that the notochord disappears in areas where the vertebral bodies form but expands within the perichordal disc, to form the central NP pulposus (Choi et al. 2008). Within the newly formed NP, notochord cells begin to proliferate and subsequently produce the glycosaminoglycan-rich extracellular matrix, which separates the original cell mass into a network of cell clusters.

1.4.3 Role of the Mesenchyme in Intervertebral Disc Development

Axial skeleton development is a multi-step process beginning with notochord formation and requiring fine-tuned coordination and pre-patterning of individual skeletal segments. From embryonic days E7.5-E11.5 in the mouse, the paraxial mesoderm undergoes segmentation to form the somites, which are metameric structures that exist transiently during vertebrate development (Forsberg et al. 1998). The somites lie adjacent to the neural tube and the notochord. In response to bone morphogenetic protein (BMP) and Wnt signals from the ectoderm and Shh signaling from the notochord and neural tube floorplate, the dorsal aspect of the somites differentiates to form the dermomyotome, which gives rise to the dermis. At E12.5, the ventral portion of the somites differentiates

to form the sclerotome that will give rise to the ribs, vertebral bodies and CEP and AF of the IVD (Brent and Tabin 2002). The sclerotome cells migrate and aggregate around the notochord to form a continuous perichordal tube (Christ and Wilting 1992). At E15.5, these mesenchymal cells acquire a metameric pattern of condensed and non-condensed segments along the anterior/posterior axis. This process is regulated by Notch and Wnt signaling to maintain somite polarity (Zhang and Gridley 1998; Barrantes et al. 1999). Lineage tracing using both the *Gdf5*-Cre (Mundy et al. 2011) and *Tbx18*-Cre (Bruggeman et al. 2012) demonstrated the mesenchymal origin of the AF. The condensed segments will later contribute to the mesenchyme-derived AF, whereas the less-condensed segments form the templates of the future vertebral bones.

The notochord secretes Shh thereby regulating differentiation of the sclerotome in the formation of the axial skeleton. Notably, the vertebral column is not formed in mice lacking *Shh* (Chiang et al. 1996); however, targeted deletion of *Shh* in the floorplate does not alter IVD development, and deletion of *Shh* in both the floorplate and notochord results in the loss of IVD and vertebral body structures (Choi et al. 2012). Shh signaling is also necessary to maintain the notochord sheath, as deletion of *Smo* (Smoothed, an essential component in hedgehog signal transduction) in the notochord and floor plate results in small NP structures with reduced cellularity and notochordal cells dispersed throughout the vertebral body during embryogenesis (Choi and Harfe 2011).

1.5 Cellular Composition of the Nucleus Pulposus

Unlike the cells in the AF and CEP that remain relatively stable throughout life, the cells of the NP undergo drastic changes within the first decade of life in humans. In

most vertebrates, including humans and mice, there is a progressive loss of large vacuolated notochord cells immediately after birth and the NP becomes populated by small chondrocyte-like cells (Roberts 2002; Hunter et al. 2003). Interestingly, the loss of notochordal cells is associated with the onset of disc degeneration, suggesting that these cells are required for the maintenance of the NP (Aguiar et al. 1999; Boos et al. 2002; Hunter et al. 2003). Despite this correlation, only recently has there been insight into the specific origin of the cells within the adult NP or the reason for their loss.

There have historically been two conflicting hypotheses regarding the origin of the cartilage-like cells of the NP. It was originally suggested that these cells were of mesenchymal origin, resulting from migration of cells to the NP from the surrounding CEP (Vujovic et al. 2006) or migration of a population of transient amplifying cells located in the perichondrium on the periphery of the IVD (Henriksson et al. 2009). During IVD formation, notochordal cells were believed to direct mesenchymal cell migration, stimulate matrix synthesis, and upon completion of their role undergo apoptosis or necrosis (Trout et al. 1982; Kim et al. 2003). Alternatively, it has been suggested that notochordal cells are progenitors for all NP cells, and undergo terminal differentiation to give rise to small chondrocyte-like cells (Pazzaglia et al. 1989; Boos et al. 2002; Liebscher et al. 2010). In these two scenarios notochordal cells play distinct roles, that of organizer and tissue-specific progenitor, respectively. Studies by Choi *et al.* and our lab have used lineage-tracing approaches to understand the composition of the adult NP and have established that, in mice, all cells of the healthy NP are notochord derived (E15.5 until 21 months of age) (Choi et al. 2008; McCann et al. 2011b).

1.6 Intervertebral Disc Degeneration

The most common cause of back pain is disc degeneration, the etiology of which is poorly defined. However, due to a general lack of understanding of the biological processes associated with disc degeneration, there are no specific criteria to distinguish degeneration from the physiological processes of growth, aging or adaptive remodeling (Adams and Roughley 2006). Disc degeneration has perhaps been best defined as a cell-mediated response to progressive structural failure (Adams and Roughley 2006). This process is thought to initiate with changes to the cellular microenvironment within the disc and progress over decades, resulting in structural breakdown and functional deficiency (Mwale et al. 2004; Smith et al. 2011). Degeneration of the IVD is associated with increased extracellular matrix breakdown, abnormal (fibrotic) matrix synthesis, inflammation, and in-growth of nociceptive nerves and blood vessels into a typically aneural and avascular tissue.

Initiation of the degenerative process is thought to originate specifically at the NP (Pearce et al. 1987; Sobajima et al. 2004). The deterioration of the major structural proteoglycan aggrecan (Roughley 2004; Boxberger et al. 2006), along with decreased production of other ECM contents in the NP, leads to reduced hydration (Buckwalter 1995), loss of disc height, and an overall inability to absorb compressive load (O'Connell et al. 2009; Barbir et al. 2011). Compressive forces are therefore distributed to the surrounding AF, which results in altered mechanical properties and structural deterioration including radial and circumferential tears in the AF (Haefeli et al. 2006; Natarajan et al. 2006). These tears often precede radial bulges or herniations of the NP substance into the adjacent spinal cord, resulting in pain (Nilsson et al. 2011; Smith et al.

2011). Currently, there are symptomatic treatments for late stages of degenerative disc disease but no disease-modifying therapeutics (Risbud et al. 2011) as disc degeneration has been hard to classify from normal physiological aging.

1.7 Animal Models to Study Intervertebral Disc Development and Degeneration

1.7.1 Notochord Cells in Animal Models

Animal models have become invaluable to study the IVD due to the difficulty of obtaining human IVD tissue, specifically “healthy” intact discs and cells (Alini et al. 2008). These animal models have been incorporated into studies aimed at characterizing disc development, disease progression and to develop therapeutic interventions. In all mammals, development of the IVD involves common pathways associated with node formation, notochord elongation and aggregation of the mesenchyme around the central notochord (as described above). Although the overall process is similar, there are important differences between the persistence of notochord cells in the NP between species, an important factor to consider when studying NP aging or degeneration. Unlike humans, species such as the rat, pig, cat, and rabbit, retain notochord cells throughout their life (Urban et al. 2000). Large animals such as bovine and sheep resemble humans in that the notochord cells present at birth rapidly decline in numbers early in life.

The murine NP is predominantly composed of notochordal cells in the first months of life, but like humans there is a decline in notochord cells and a concomitant

increase in smaller chondrocyte-like cells with age (Hunter et al. 2004). While mice have inherent limitations due to their size and limited amount of disc material, they have become instrumental in studying disease progression due to the high degree of conservation between the mouse and human genomes and the ease of murine genomic manipulation (Nagy et al. 2003) (**Table 1**, transgenic mouse models with an identified IVD phenotype). An important tool in mouse genetics to understand cellular and/or gene function is the Cre/loxP method for conditional mutagenesis. In this system, expression of Cre recombinase is regulated by a tissue-specific and/or temporally-regulated promoter, that can excise target loxP-flanked (“floxed”) genes via intra-chromosomal recombination to generate conditional knockouts. This strategy confers the ability to track specific cell types during development/aging, or assess the function of a specific gene within a given tissue, depending on the specificity of Cre recombinase expression (Nagy 2000).

1.7.2 Notochord Specific Cre Mouse Strains

Several gene loci have been targeted for the generation of Cre expressing mouse strains and demonstrated Cre expression in the notochord, including the T-box transcription factor brachyury, *T*-Cre (Perantoni et al. 2005), flat-top (*Cfap126*), a cilia and flagella associated protein, *Fltp*^{T2AiCre} (Lange et al. 2012), and type-II collagen *Col2a1*-Cre (Ovchinnikov et al. 2000; Sakai et al. 2001; Schipani et al. 2001; Terpstra et al. 2003). However, in these strains Cre expression was not notochord-specific, detected in structures such as lateral mesoderm, the neural tube floorplate, head mesenchyme and cartilaginous tissues throughout the body, respectively. Consequently, novel notochord-

Table 1: Identified knockout and transgenic mouse models with IVD phenotypes

Gene	Allele type	Nucleus Pulposus Phenotype	Annulus Fibrosus Phenotype	Reference
<i>Acan</i>	Universal KO	Increased Degeneration	Increased Degeneration	(Watanabe et al. 1997)
<i>ApoE</i>	Universal KO	Abnormal	Abnormal	(Zhang et al. 2013)
<i>Bgn</i>	Universal KO	Abnormal Development	Abnormal Development	(Furukawa et al. 2009)
<i>c-Jun</i>	Conditional – KO in cartilage	Reduced in size	Normal	(Behrens et al. 2003)
<i>Cav1</i>	Universal KO	Abnormal	Normal	(Smolders et al. 2013)
<i>Ccn2</i>	Conditional – KO in notochord	Abnormal Development and Increased Degeneration	Increased Degeneration	(Bedore et al. 2013)
<i>Clec3b</i>	Universal KO	Increased Degeneration	Increased Degeneration	(Iba et al. 2001)
<i>Coll1a1</i>	Universal KD	Normal	Abnormal Development	(Sarver and Elliott 2004)
<i>Col2a1</i>	i. Universal KO ii. Universal KO	i. Abnormal ii. Normal	i. Absent ii. Abnormal Development	i. (Aszodi et al. 1998) ii. (Sahlman et al. 2001)
<i>Col9a1</i>	Universal KO	Normal	Abnormal Development	(Boyd et al. 2008; Allen et al. 2009)
<i>Cox2</i>	Conditional – KO in ectoderm	Abnormal	Abnormal	(Shim et al. 2010)
<i>Creb</i>	Notochord specific – Dominant Negative	Absent	Absent	(Lopez and Fan 2013)
<i>Ext1</i>	Conditional – KO in annulus	Abnormal Development	Abnormal Development	(Mundy et al. 2011)
<i>Flnb</i>	Universal KO	Absent	Absent	(Zhou et al. 2007)

<i>Foxa1</i> & <i>Foxa2</i>	Conditional – KO in notochord	Double cKO - abnormal, Single KO - Normal	Normal	(Maier et al. 2013)
<i>Gdf5</i>	i. Universal KO ii. Conditional – KO in notochord	i. Reduced in size ii. Normal	i. Abnormal Development ii. Normal	i. (Li et al. 2004) ii. (Maier and Harfe 2011)
<i>Gli2</i>	Universal KO	Abnormal Development	Abnormal	(Mo et al. 1997)
<i>Has2</i>	Conditional – KO in cartilage	Enlarged in size	Abnormal Development	(Roughley et al. 2011)
<i>Hes7</i>	Universal KO	Abnormal Development	Abnormal Development	(Bessho et al. 2001)
<i>Hif1α</i>	Conditional – KO in notochord	Reduced in size	Normal	(Merceron et al. 2014)
<i>Hsp47</i>	Conditional – KO in cartilage	Enlarged in size	Normal	(Masago et al. 2012)
<i>Hspg</i>	Universal KO	Abnormal Development	Absent	(Gustafsson et al. 2003)
<i>ky</i>	Autosomal Recessive Mutation	Abnormal Development	Abnormal Development	(Semba et al. 2006)
<i>Meox1</i> & <i>Meox2</i>	Double Universal KO	Absent in double KO	Absent in double KO	(Mankoo et al. 2003)
<i>Mesp2</i>	Universal KO	Absent	Absent	(Saga et al. 1997)
<i>Mfh1</i>	Universal KO	Absent	Absent	(Winnier et al. 1997)
<i>Mfh1</i> & <i>Pax1</i>	Double Universal KO	Absent in double KO	Absent in double KO	(Furumoto et al. 1999)
<i>Nfix</i>	Universal KO	Reduced in size	Abnormal	(Driller et al. 2007)
<i>Nkx3.2</i>	Universal KO	Absent	Absent	(Lettice et al. 1999)
<i>Nkx3.2</i>	Universal KO	Reduced in size	Reduced in size	(Tribioli and Lufkin 1999)
<i>Npr3</i>	Universal KO	Abnormal Development	Normal	(Jaubert et al. 1999)
<i>p63</i> & <i>p73</i>	Universal Heterozygous	Increased Degeneration	Increased Degeneration	(Flores et al. 2005)

<i>Pax1</i>	Universal KO	Absent	Absent	(Wilm et al. 1998)
<i>Pax1</i> & <i>Pax9</i>	Double Universal KO	- Absent in double KO - Abnormal Development in single KOs	Absent in double KO - Abnormal Development in single KOs	(Wallin et al. 1994; Furumoto et al. 1999; Peters et al. 1999)
<i>Skt</i>	Gene trap	Absent	Normal	(Semba et al. 2006)
<i>Smo</i> (Shh Signaling)	Conditional – KO in notochord	Reduced in size	Abnormal Development	(Choi and Harfe 2011)
<i>Sox5</i> , <i>Sox6</i>	Double Universal KO	Absent in double KO - Reduced in size in single KO	Abnormal in both double and single KO	(Smits and Lefebvre 2003)
<i>Sox9</i>	Conditional – Universal KO	Absent	Absent	(Barrionuevo et al. 2006)
<i>Sparc</i>	Universal KO	Increased Degeneration	Increased Degeneration	(Millecamps et al. 2012)
<i>Tbx18</i>	Universal KO	Abnormal Development	Normal	(Bussen et al. 2004)
<i>Tgfbβ2</i>	Conditional – KO in cartilage	Reduced in size	Reduced in size	(Baffi et al. 2004)
<i>Traf4</i>	Universal KO	Abnormal Development	Abnormal	(Regnier et al. 2002)
<i>Tsg</i>	Universal KO	Abnormal Development	Normal	(Zakin and De Robertis 2004)
<i>β-catenin</i>	i. Conditional – Act in cartilage	Abnormal Development	Abnormal Development	(Wang et al. 2012)
<i>δEF1</i>	Universal KO	Reduced in size	Normal	(Takagi et al. 1998)

OK = knockout, O/E = overexpression, Act = activation, DomNeg = dominant negative

specific Cre strains were required to fate map the notochord and trace the lineage of NP cells. The first reported and most commonly used notochord-Cre mouse is the *Shh*-Cre strain (Harfe et al. 2004), which when crossed with conditional lacZ reporter mice *Gt(ROSA)26^{tm1Sor}* (Soriano 1999) marked cells throughout the notochord at E10.5, notochord cells during segmentation at E12.5, and the presumptive NP at E16.5 (Choi et al. 2008). Importantly, no β -galactosidase-positive cells were detected in the surrounding AF or CEPs. Interestingly, the authors report a small population of β -galactosidase-positive cells that failed to be incorporated into the NP but remained in the developing vertebral bone. The authors suggested that these notochord remnant cells are equivalent to benign notochord tumors in humans, which can give rise to chordoma. Since it was unknown if mature NP cells would gain *Shh* expression leading to Cre expression in the mature tissue, a tamoxifen-inducible *Shh-CreER^{T2}* (Harfe et al. 2004) was used to transiently induce Cre expression in the notochord between E8.5-E12.5. This experiment demonstrated that all the cells the mature NP (≥ 19 months) expressed β -galactosidase and therefore were derived from the *Shh* expressing cells of the node and notochord (Choi et al. 2008).

The sickle tail (*Skt*) gene, has been reported to play a role in the development of the notochord and IVD. The Skt protein is localized to the cytoplasm and is thought to act as a structural element or a scaffolding protein. *Skt* was an interesting target for the development of a notochord-specific Cre strain since in gene-trapping experiments, intense β -galactosidase expression was detected in the notochord and at birth the mice had kinky tails, compressed IVDs, and disorganized NP tissues (Semba et al. 2006). *Skt*-Cre mice were subsequently generated and when crossed to a conditional Rosa26-LacZ

reporter mouse, β -galactosidase expression was detected in the notochord at E9.5 and E12.5. At E15.5 β -galactosidase expression was predominantly detected in the NP however, small populations of the cells were also detected in the primitive AF. In adult mice, β -galactosidase expression was detected in the NP but large populations of AF were LacZ positive (Abe et al. 2012), making the *Skt*-Cre mouse not suitable for NP-specific genetic experiments.

Forkhead box protein A2 (FoxA2), also known as hepatocyte nuclear factor 3- β , is a transcription factor first discovered to be necessary for the formation and maintenance of the definitive endoderm (Ang et al. 1993) and subsequently found to be required for node and notochord formation (Ang and Rossant 1994). Since then, the *FoxA2*-Cre strain (Park et al. 2008; Uetzmänn et al. 2008) and the inducible *FoxA2^{mcm}* Cre strain (Park et al. 2008) have been generated and when crossed to a conditional Rosa26-LacZ reporter mouse, LacZ staining was detected in the endoderm but also in the node, floorplate, and notochord (Park et al. 2008). Recently the *FoxA2*-Cre was used to knockout hypoxia inducing factor-1 α , which demonstrate a NP specific phenotype (Merceron et al. 2014).

1.8 Nucleus Pulposus Tissue Regeneration

1.8.1 Nucleus Pulposus Progenitor Cells

In a recent study by Sakai *et. al.* the authors identified a population of *Tie2* and *Gd2* positive progenitor cells in the NP of both mice and humans. The injection of these multipotent cells into the IVD of immunodeficient mice led to reorganization of the NP

tissue, marked by increased detection of sulphated proteoglycans and type II collagen (Sakai et al. 2012). While their numbers in the IVD were reported to diminish with age, it is yet to be determined if these progenitor cells are notochord cells or if they are of notochordal origin. . This study demonstrates the potential for cell-based therapies to regenerate the NP. In such strategies, notochordal cells are a prime target as a potential source of growth factors and mitogens, similar to their role during early development. The potential of notochord cells to regulate NP cell function was exemplified in a classical experiment that demonstrated that co-culture of purified notochord cells with mature NP cells increased proteoglycan secretion from the latter (Aguiar et al. 1999). This study also established this to be cell contact-independent, since culture of NP cells in notochord cell-conditioned media (NCCM) was capable of recapitulating the anabolic effects. Given the effect of NCCM on NP cell metabolism, notochord cells are considered an excellent source of signals for potential cell-based IVD therapies. However, the development of strategies to exploit this potential is limited by the fact that these cells are no longer detected in human IVDs within the first decade of life (Liebscher et al. 2010). This limitation prevents the direct therapeutic application of notochord cells and highlights the need for an alternate source of cells for IVD therapy.

1.8.2 Stem Cell-based Nucleus Pulposus Regeneration

Mesenchymal stem cells (MSC) provide an obvious source for stem cell-based therapy due to their ease of availability (Van et al. 1976; Castro-Malaspina et al. 1980; Majumdar et al. 1998), overall plasticity (Jiang et al. 2002) and ability to undergo

chondrogenic differentiation (Pittenger et al. 1999). In fact, many studies have focused on the use of co-culture systems using NP cells to drive MSC differentiation towards a NP-like phenotype (Vadala et al. 2008; Chen et al. 2009; Niu et al. 2009; Allon et al. 2010).

There are multiple factors that may prove important for the regeneration of NP tissue; however, of particular importance is the origin of the stem cells source used for differentiation and the ability to assess cell fate following differentiation. Firstly, using mature cell types to direct cellular differentiation might have unknown molecular and physiological effects as mature MSC showed decreased ability to undergo chondrocyte differentiation (O'Driscoll et al. 2001; Sethe et al. 2006). Secondly, we have only recently begun to understand the phenotype of NP cells (Lee et al. 2007; Minogue et al. 2010a), and the cell-type specific molecular signature of these cells has yet to be characterized either during early IVD development or as cells persist in the mature IVD. Without knowing the phenotype NP cells, our ability to properly assess the success of cell differentiation experiments is limited.

1.8.3 Need for Notochord Cell Phenotype in Cell Differentiation Studies

In a paper by Korecki *et. al.* (Korecki et al. 2010), the authors demonstrated the ability of NCCM to stimulate the differentiation of human bone MSCs towards to a NP-like phenotype, using as direct comparison MSC treated with TGF- β (used extensively for chondrogenic differentiation) (Barry et al. 2001; Worster et al. 2001). The authors observed that culture of MSCs in the presence of NCCM produced differentiated cells secreting higher levels of glycosaminoglycans (GAG) and type III collagen when

compared to cells treated with TGF- β . Further suggesting that NCCM induced the differentiation of potential notochord cells rather than chondrocyte-like NP cells, differentiated MSCs demonstrated increased expression of laminin β -1 and tissue inhibitor of metalloproteinases-1 (TIMP-1), genes previously shown to be upregulated in the subset of notochord cells within the NP when compared to adjacent IVD cell types (Hayes et al. 2001). The authors state that NCCM has the potential to differentiate MSCs towards a “young” NP cell phenotype (although not classifying it as a notochord cell) based on the expression of type III collagen which is the first collagen to be expressed during early IVD development in rats (Hayes et al. 2001) and humans (McAlinden et al. 2002). However, type III collagen is also expressed during disc repair and disc degeneration (Adam and Deyl 1984; Roberts et al. 1991; Kaapa et al. 1994). The upregulation of type III collagen reported during MSC differentiation may be associated with the advanced age of the sample population from which the MSCs were obtained (mean age 64.3). With age, MSC chondrocyte differentiation potential decreases and apoptosis increases (Stolzing et al. 2008), indicating that these “mature” MSCs may be stimulating a fibrotic repair rather than tissue regeneration.

While the potential of notochord cells and NCCM to contribute to IVD repair has been demonstrated, the generation of so-called notochord cells *in vitro* is limited by the lack of cell type-specific markers to assess the notochord phenotype (**Figure 1.2**). Currently, the phenotype of notochord cells during the stages of embryonic patterning, IVD formation, and in mature IVD tissues remains to be established. *In vitro* differentiation of MSCs may lead to any of the aforementioned stages of notochord cell

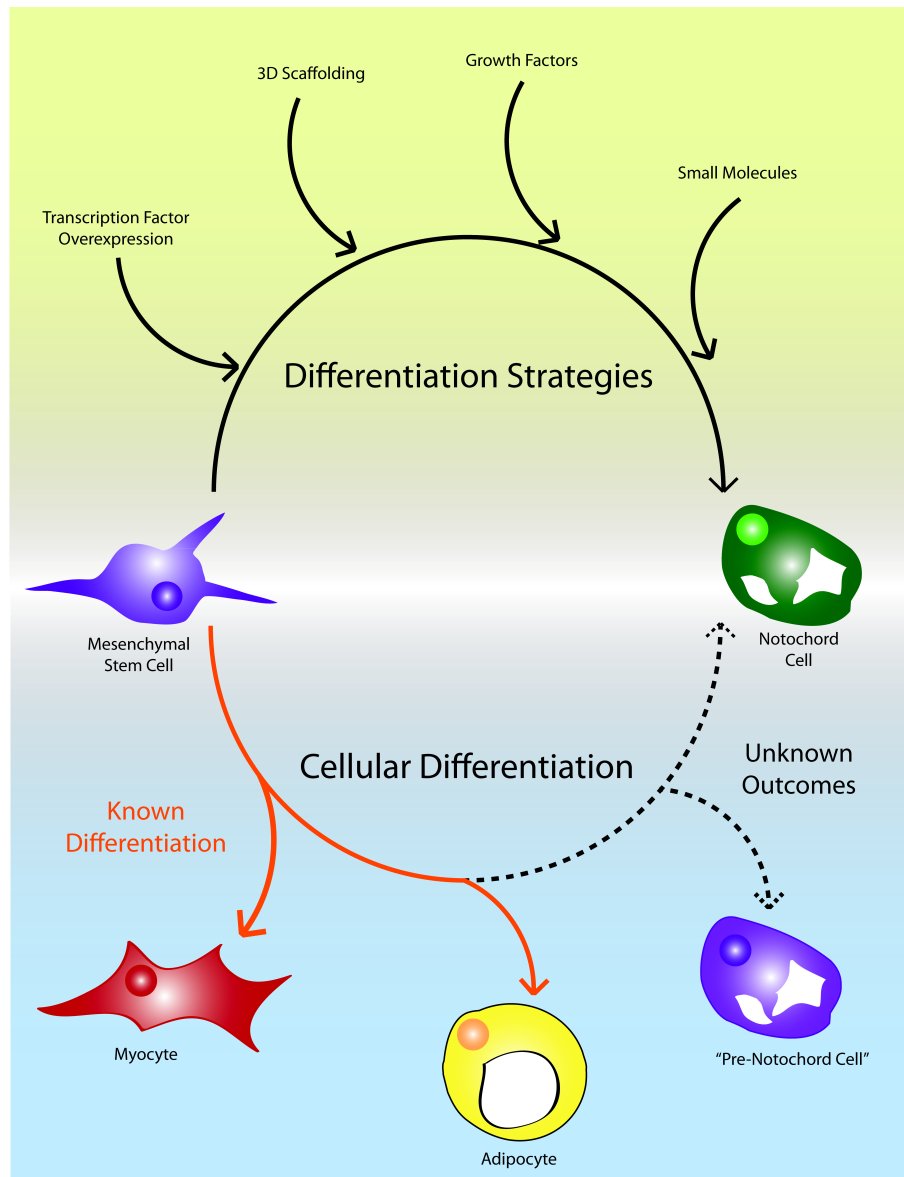


Figure 1.2 Lack of specific phenotypic markers limits strategies for notochord cell generation.

Protocols have been established for the differentiation of mesenchymal stem cells down specific lineages producing specialized cell types with known markers. This has been achieved via internal regulation (transcription factor-mediated differentiation), as well as external stimulation such as three-dimensional scaffolding and the use of growth factors and small molecules. These methods have been validated based on well-characterized cell type-specific markers, a limiting factor for the production of notochord cells. (Figure modified from (McCann et al. 2011a)).

maturation, and unless we know the molecular phenotype of the desired cell type we cannot conclusively determine what cells have been generated. Consequently, the characterization of the notochord cell phenotype throughout development should be undertaken to enable the advancement of the field of IVD biology.

1.8.4 Understanding the Phenotype of Nucleus Pulposus Cells

A clear understanding of the unique phenotype of a notochord cell in relation to that of AC, AF, CEP or differentiated NP cells is a high priority. Current strategies to distinguish notochord cells and chondrocyte-like cells in the NP is restricted to cell morphology and a limited number of notochord-specific markers (Fujita et al. 2005; Gilson et al. 2010; Minogue et al. 2010b). Many studies have used a small panel of commonly expressed markers, including *SOX9*, *COL2A1*, and *ACAN* to identify NP cells (Sive et al. 2002; Richardson et al. 2006; Tsai et al. 2007; Feng et al. 2014); however, these genes are also highly expressed in AC and CEP chondrocytes, with some overlap also detected in cells of the inner AF. The obvious morphological and physiological differences between AC and NP tissue as well as the different developmental origins of their cell types, suggest that NP and AC cells possess distinct cell phenotypes. Consequently, examining a small number of genes is likely not sufficient to differentiate between these two cell types.

Surprisingly, few attempts have been made to characterize the differences between the molecular phenotypes of NP and the surrounding IVD. Recent studies have begun to examine this question, using microarray technology to compare the gene expression profiles of NP, AF, and articular chondrocytes in rat, canine and bovine tissues

(Fujita et al. 2005; Lee et al. 2007; Sakai et al. 2009; Minogue et al. 2010b) or proteomic technology to compare bovine NP and AC cells (Gilson et al. 2010) and various cartilaginous tissues from human cadavers (Onnerfjord et al. 2012). A limited set of genes have emerged from these studies as potential NP markers. *KRT19* and *GPC3* were shown to be differentially expressed, detected in NP cells in discs from young rats but not in the AF or AC (Lee et al. 2007). *A2M*, *KRT18*, and *NCAM1* expression were reported to be elevated in canine NP cells relative to AC (Sakai et al. 2009). To date, no studies have conducted a genome-wide analysis to determine the unique phenotype of the mouse NP, which is surprising given its common use to model IVD-related pathologies.

1.9. Mechanical Loading and the Musculoskeletal System

1.9.1 Biomechanical Loading Regulates Bone Physiology

The importance of mechanical loading on the musculoskeletal system was first described for bone in 1892 by Julius Wolff who reported the adaptation of bone to mechanical stress (Wolff 1892; Brand 2010). Since this initial discovery, it has been established that osteocytes within the calcified matrix are the primary mechanosensing cells of mature bone (Bonewald 2011; Klein-Nulend et al. 2013); targeted ablation of osteocytes leads to defective mechanotransduction (Tatsumi et al. 2007). Osteocytes sense strain as increased interstitial fluid flow through the bone canalicular networks (You et al. 2001; Cowin 2002). Mechanical loading is necessary for the maintenance of bone density. The absence of mechanical load on the skeleton, due to bed rest (Leblanc et al. 1990), microgravity (LeBlanc et al. 2000) or in animal models of hind limb unloading

leads to osteoblast suppression and osteoclast (bone resorbing cells) activation (Kondo et al. 2005). Furthermore, it has been reported that weightlessness induces osteocyte apoptosis, which precedes osteoclast recruitment and bone resorption (Aguirre et al. 2006).

1.9.2 Mechanical Loading in Knee Joint Health

Mechanical loading is also critical for maintaining joint tissue homeostasis. Articular cartilage, which is the smooth lubricated connective tissue that covers the ends of bones in diarthrodial joints, allows for ease of movement between adjacent bones and facilitates the transmission of loads seen by the joint. Articular cartilage health is paramount to overall joint health and can be maintained under physiological loading (Leong et al. 2011a). Moderate physical activity has been shown to sustain cartilage health both in humans (McAlindon et al. 1999; Manninen et al. 2001) and animal studies (Leong et al. 2011b; Musumeci et al. 2014). Similar to bone, insufficient mechanical loading can lead to AC degeneration; progressive atrophy of the articular cartilage is detected in patients with paralysis when compared to healthy mobile individuals (Vanwanseele et al. 2002). Interestingly, cartilage loss can be detected relatively quickly following changes in mechanical loading. In humans, partial load bearing (contact of the sole of the foot while walking with crutches) resulted in degeneration of the AC in just 7 weeks (Hinterwimmer et al. 2004).

Mechanical overloading is perhaps the best-studied initiator of joint degeneration. Articular cartilage is highly susceptible to osteoarthritis if subjected to impact loading, either acutely (Torzilli et al. 1999; Borrelli et al. 2009) or repeatedly (Radin et al. 1978;

Ko et al. 2013). While the causes of mechanical-induced degeneration can be varied, the matrix metalloproteinase (MMPs) (Lin et al. 2004; Lee et al. 2005; Leong et al. 2010) and a disintegrin and metalloproteinase with thrombospondin motif (ADAMTS) peptidases (Fitzgerald et al. 2006) are known to be induced by mechanical loading and serve as key mediators of cartilage degeneration (Lee et al. 2005). Altered mechanical loading following injury to the knee joint, modelled in animals using surgically-induced joint destabilization (destabilization of the medial meniscus, anterior cruciate ligament transection) leads to osteoarthritis-like phenotypes (Fang and Beier 2014). Interestingly, mice lacking either *MMP3*, *MMP13*, *ADAMTS4* or *ADAMTS5* are protected, at least in part, from the loss of articular cartilage in these models (Clements et al. 2003; Majumdar et al. 2007; Wang et al. 2013).

1.9.3 Mechanical Loading and Intervertebral Disc Homeostasis

Not surprisingly, physiological loading is also required to maintain the integrity of the IVD. *In vitro* (Chen et al. 2004; Wang et al. 2007; Desmoulin et al. 2010) and *in vivo* (MacLean et al. 2003; Maclean et al. 2004; Walsh and Lotz 2004; Wuertz et al. 2009; Desmoulin et al. 2011; Iatridis et al. 2011) animal studies have shown that physiological loading promotes extracellular matrix synthesis, whereas immobilization or over-loading promotes matrix catabolism and degeneration. In humans, increased loading either through exposure to occupational hazards (Anderson et al. 1987) or recreational activities associated with increased mechanical load such as weightlifting (Videman et al. 1995) and rowing (Hosea and Hannafin 2012) are associated with disc degeneration. Similar to studies in bone, apoptosis may contribute to the response to mechanical loading in the

IVD, as caspase inhibition has been shown to protect against overload-induced disc degeneration in both an *ex vivo* and *in vitro* human models (Yamada et al. 2014).

1.10 Whole-Body Vibration as a Mechanical Stimulus

1.10.1 Whole-body Vibration on Bone

Whole-body vibration (WBV), or vibration therapy was initially used for muscle activation and strength training in athletes (**Figure 1.3**). However, following reports in animals (Rubin et al. 2001a; Rubin et al. 2001c) that showed its ability to stimulate bone formation, there has been a rapid surge in the clinical use of whole-body vibration. WBV platforms are now being marketed as fast and effective weight loss devices, marketed as capable of increasing muscle strength and tone in only 10 minutes a day. In the clinical setting, WBV was initially introduced as an adjunctive therapy for osteoporosis based on reports of bone-strengthening effects in post-menopausal and older women (Rubin et al. 2003; Rubin et al. 2004). Interestingly, no osteogenic benefit was observed in a study of young women (average age 27 yr) following WBV (Torvinen et al. 2003) or osteoporotic women treated with alendronate (Iwamoto et al. 2005), suggesting that the response of bone tissues to WBV may vary in a patient-specific manner.

Within the last decade, numerous studies have validated the use of animal models to investigate the biological effects of WBV in bone. In sheep (Rubin et al. 2001b; Rubin et al. 2002) and rodent models (Rubin et al. 2001c), studies demonstrated significant increases in bone mineral density and bone formation rates following daily exposure to WBV. Exposure to WBV was reported to normalize bone formation rates in rodent hind-limb unloading (Rubin et al. 2001c) and ovariectomy (Judex et al. 2007) models.

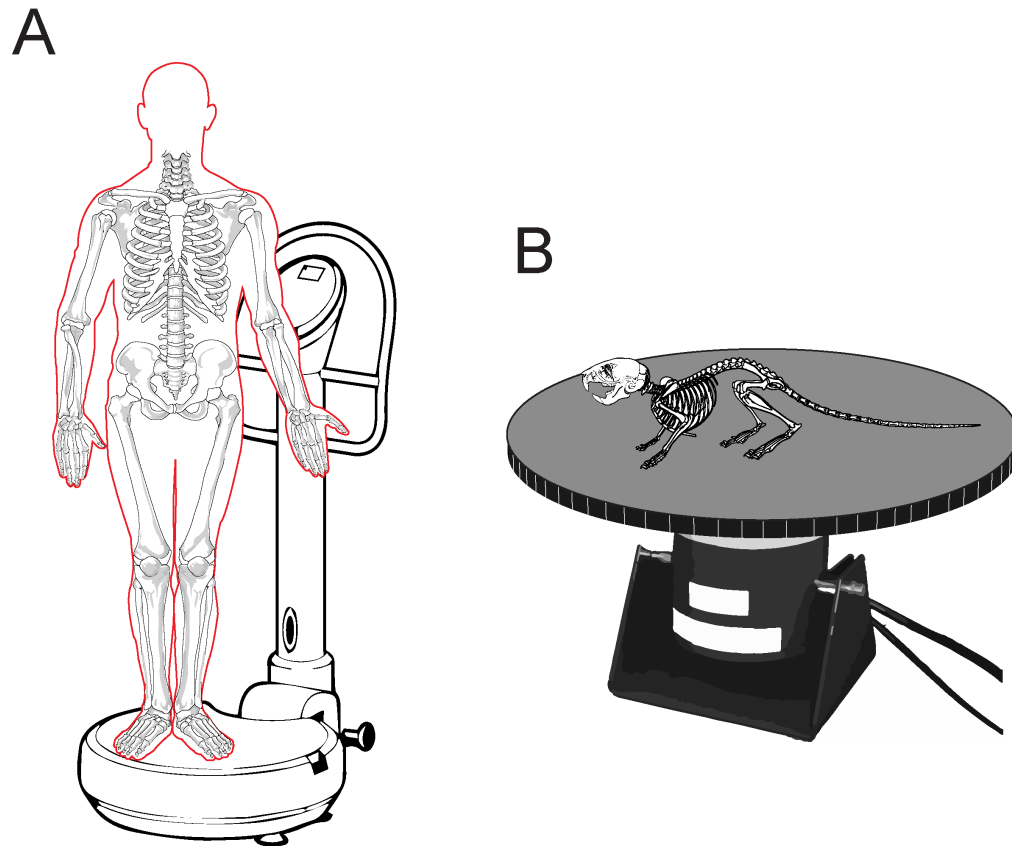


Figure 1.3 Schematic illustrations of whole-body vibration platforms

A. Illustration of a human whole-body vibration platform designed to deliver low-amplitude, high-frequency mechanical stimulation, in the form of sinusoidal vibrations, to the human body. Platforms produce vertical accelerations that are transmitted from the feet to the weight-bearing muscles, bones and joints. **B.** Illustration of a novel platform developed by our group (**Chapter 5**) that applies whole-body vibration to mice using parameters that model human platforms.

Interestingly, the effects of WBV appear to be dependent on the frequency of the applied load (Judex et al. 2007), and genetic background of animals used (Judex et al. 2002). Recent reports highlight conflicting results of the effects of WBV, both in animal models and clinical studies (Wenger et al. 2010; Slatkovska et al. 2011).

1.10.2 Whole-Body Vibration and Joint Health

While the effects of WBV on bone and muscle have been extensively studied, there are surprisingly few studies aimed at directly assessing the effects of WBV on synovial joints, surprising since the knee absorbs a great deal of the applied mechanical load. The limited studies investigating the affect of WBV on the knee joint in humans have reported alterations in knee flexibility (Karatrantou et al. 2013), knee extensor muscle strength (Roelants et al. 2004), balance and gait (Simao et al. 2012). With regards to joint health, patient self-reported pain was reported to decrease in osteoarthritis patients following WBV (Avelar et al. 2011; Salmon et al. 2012; Park et al. 2013); however, joint tissue health was not directly assessed. One study in humans reported the ability of WBV to prevent loss of cartilage thickness (determined by MRI) following prolonged immobilization of healthy male subjects (Liphardt et al. 2009).

1.10.3 Whole-body Vibration and the Intervertebral Disc

The effects of vibration on the IVD have been well studied from the standpoint of occupational exposure, where low-frequency, high-magnitude vibration (1-5 Hz, 3 g) is

an established risk factor for LBP (Matsumoto and Griffin 2002; Funakoshi et al. 2004). Interestingly, WBV platforms delivering high-frequency, low-magnitude vibration (10-60 Hz, 0.3 g) are now being used as a therapy for LBP. (Iwamoto et al. 2005; Belavy et al. 2008; del Pozo-Cruz et al. 2011). These seemingly conflicting reports highlight the need to better understand the effects of vibration on the IVD.

Recent clinical trials have reported improvements in patient self-reported back pain following WBV (Rittweger et al. 2002; del Pozo-Cruz et al. 2011); however, these studies did not assess whether improvements were due to changes in muscle strength, or changes in the IVD itself. Similarly, studies exploring the ability of WBV to prevent IVD degeneration following prolonged bed rest reported the ability of low-intensity vibration (30 Hz, 0.3 g) to reduce back pain; however, the study did not report change in disc morphology (Holguin et al. 2009; Belavy et al. 2010). There have been limited studies using *in vivo* models to study the effects of WBV on the spine. In a rat model of hindlimb unloading, WBV (15 min/day; 45 Hz, 0.3 g) did not alter IVD biochemistry, height, or volume but enhanced muscle volume (Holguin and Judex 2010). The same group subsequently reported that at a frequency of 90 Hz, vibration countered changes in IVD morphology that result from hindlimb unloading. Importantly, a recent systematic review on the use of WBV to treat back pain concluded there was no evidence for optimal treatment parameters nor evidence relating to the potential for harm and long-term effectiveness of WBV and suggested caution in applying WBV to treat back pain (Perraton et al. 2010).

1.11 Rationale, Hypotheses and Objectives

Aim 1: Fate Mapping the *Noto*^{Cre} Mouse

Rationale: The role of the notochord in NP formation and the origin of chondrocyte-like cells in mature NP was investigated using a novel notochord-specific *Noto*^{Cre} knock-in mouse, along with the *Rosa26* conditional *LacZ* reporter mouse. *Noto* is a highly conserved homeobox transcription factor whose expression is restricted to the organizer node and the nascent notochord during gastrulation and axis elongation (E7.5-12.5) where it regulates node morphogenesis, notochord ciliogenesis, and left-right patterning (Abdelkhalek et al. 2004; Yamanaka et al. 2007; Zizic Mitrecic et al. 2010). The restricted pattern of *Noto* gene expression makes it an excellent marker of the developing node and notochord and therefore was targeted to generate a notochord-specific Cre mouse strain.

Hypothesis: All cells of the embryonic and adult nucleus pulposus are derived from the embryonic notochord.

Objectives: 1) Characterize the novel *Noto*^{Cre} mouse strain. 2) Determine the embryonic origins of nucleus pulposus cells within the mouse.

Aim 2: Transcriptional Profiling to Identify Markers Associated with Nucleus Pulposus Maturation, Aging, and Degeneration.

Rationale: Studies in Aim 1 demonstrated that during embryonic development, the notochord gives rise to all cells within the mature NP and suggests this process reflects a transition from a precursor to a terminally differentiated cell. However, there is little insight as to the genes, molecular mechanisms or pathways that govern this process or the initiation of pathological disc degeneration. The use of transcriptional profiling paired with bioinformatic analysis will provide a fundamental understanding of the cell phenotype and pathways that govern NP pulposus maturation, aging and degeneration, and may in the long term lead to the identification of potential pharmaceutical targets for the treatment of back pain.

Objectives: Characterize the molecular signature associated with 1) the differentiation of notochord cells to cartilage-like NP cells, 2) aging and degeneration of the NP.

Aim 3: Define the Proteomic Signature of the Murine IVD

Rationale: The identification and classification of the proteins present within the healthy IVD is a critical step in determining the pathways and processes that are required to maintain IVD homeostasis. Although studies have reported the transcriptional profile of IVD tissues from various animal models commonly used to study intervertebral disc biology, including rat (Lee et al. 2007), bovine (Minogue et al. 2010b), canine (Sakai et al. 2009) and rabbit (Poiraudau et al. 1999), to date no global proteomic analysis has

been reported on IVD tissues from these species. Recent studies have provided detailed analysis of the extracellular matrix of multiple human cartilaginous tissues, including the IVD (Onnerfjord et al. 2012) as well as bone and cartilage tissue in the zebrafish (Kessels et al. 2014). These studies highlight the value of global proteomic analysis in establishing the composition of specialized skeletal tissues, and the need to expand this analysis to model organisms commonly used to study development, aging or disease states, such as the mouse.

Objective: Characterize the proteomic signature of the healthy murine intervertebral disc.

Aim 4: Determine the Effect of Acute Exposure to Whole-Body Vibration on the Intervertebral Disc.

Rationale: Whole-body vibration platforms are marketed as fast and low-impact exercise that claim to increase muscle and bone mass, enhance metabolism and reduce joint pain. Consequently, vibration training is being increasingly used in the fitness industry, professional sports training programs, rehabilitation clinics, and the wellness industry. These devices deliver lineal vibration to elicit a strong stretch-reflex contraction in muscle fibres that can be targeted by body position. Studies have reported beneficial effects on muscle properties in patients with multiple sclerosis, muscular dystrophy, stroke and spinal cord injury. Vibration therapy has also been integrated into physical therapy regimens for osteoporosis, fibromyalgia, back pain, and osteoarthritis. Despite its widespread use, there is an alarming lack of understanding of the effects of vibration on

joint health or how this form of mechanical stimulation influences IVD homeostasis at the cellular level.

Hypothesis: High-frequency low-amplitude vibration will modify cellular metabolism and gene expression within the IVD, specifically up-regulating the expression of anabolic genes and suppressing the expression of catabolic genes, leading to improved IVD integrity.

Objectives: 1) Determine the effects of acute exposure to high-frequency, low amplitude whole-body vibration on the intervertebral disc.

2) Assess whether the effects of whole-body vibration on the intervertebral disc are dependent on the frequency of the applied load.

3) Using an *ex vivo* organ culture system paired with *in vivo* exposure to WBV, assess if the effects of vibration on the IVD are tissue autonomous.

Aim 5: Determine the Effects of Repeated Exposure to Whole-Body Vibration on Joint Tissues

Rationale: Studies conducted in Aim 4 demonstrated beneficial effects of acute exposure to high-frequency, low amplitude WBV on the IVD. We therefore sought to determine whether these transient changes in gene expression would result in long-term beneficial effects on joint health. Given the widespread use of WBV platforms in the fitness industry and clinical setting, as well as recent reports highlighting the lack of evidence-based research associated with these devices, we aimed to assess the effects of repeated

exposure of mice to WBV using protocols that model vibration training in humans. We examined the effects of WBV on multiple skeletal tissues, including IVD, knee and long bones since there have been no studies to determine the long-term effects of WBV on joint health.

Hypothesis: Repeated exposure to high-frequency, low-amplitude whole-body vibration will be beneficial to the intervertebral disc and knee joint by increasing anabolic genes and suppressing catabolic genes, leading to overall improved joint health.

Objectives: Determine the effect of repeated exposure to high-frequency, low amplitude whole-body vibration on 1) the intervertebral disc, 2) the knee joint, and 3) long bone.

1.12 References

- Abdelkhalek HB, Beckers A, Schuster-Gossler K, Pavlova MN, Burkhardt H, Lickert H, Rossant J, Reinhardt R, Schalkwyk LC, Muller I et al. 2004. The mouse homeobox gene *Not* is required for caudal notochord development and affected by the truncate mutation. *Genes Dev* **18**: 1725-1736.
- Abe K, Araki K, Tanigawa M, Semba K, Ando T, Sato M, Sakai D, Hiyama A, Mochida J, Yamamura K. 2012. A Cre knock-in mouse line on the *Sickle tail* locus induces recombination in the notochord and intervertebral disks. *Genesis* **50**: 758-765.
- Adam M, Deyl Z. 1984. Degenerated annulus fibrosus of the intervertebral disc contains collagen type II. *Ann Rheum Dis* **43**: 258-263.
- Adams MA, Roughley PJ. 2006. What is intervertebral disc degeneration, and what causes it? *Spine (Phila Pa 1976)* **31**: 2151-2161.
- Aguiar DJ, Johnson SL, Oegema TR. 1999. Notochordal cells interact with nucleus pulposus cells: regulation of proteoglycan synthesis. *Exp Cell Res* **246**: 129-137.

- Aguirre JI, Plotkin LI, Stewart SA, Weinstein RS, Parfitt AM, Manolagas SC, Bellido T. 2006. Osteocyte apoptosis is induced by weightlessness in mice and precedes osteoclast recruitment and bone loss. *J Bone Miner Res* **21**: 605-615.
- Alini M, Eisenstein SM, Ito K, Little C, Kettler AA, Masuda K, Melrose J, Ralphs J, Stokes I, Wilke HJ. 2008. Are animal models useful for studying human disc disorders/degeneration? *Eur Spine J* **17**: 2-19.
- Allen KD, Griffin TM, Rodriguiz RM, Wetsel WC, Kraus VB, Huebner JL, Boyd LM, Setton LA. 2009. Decreased physical function and increased pain sensitivity in mice deficient for type IX collagen. *Arthritis Rheum* **60**: 2684-2693.
- Allon AA, Aurouer N, Yoo BB, Liebenberg EC, Buser Z, Lotz JC. 2010. Structured coculture of stem cells and disc cells prevent disc degeneration in a rat model. *Spine J* **10**: 1089-1097.
- Anderson JA, Otun EO, Sweetman BJ. 1987. Occupational hazards and low back pain. *Reviews on environmental health* **7**: 121-160.
- Ang SL, Rossant J. 1994. HNF-3 beta is essential for node and notochord formation in mouse development. *Cell* **78**: 561-574.
- Ang SL, Wierda A, Wong D, Stevens KA, Cascio S, Rossant J, Zaret KS. 1993. The formation and maintenance of the definitive endoderm lineage in the mouse: involvement of HNF3/forkhead proteins. *Development* **119**: 1301-1315.
- Aszodi A, Chan D, Hunziker E, Bateman JF, Fassler R. 1998. Collagen II is essential for the removal of the notochord and the formation of intervertebral discs. *J Cell Biol* **143**: 1399-1412.
- Avelar NC, Simao AP, Tossige-Gomes R, Neves CD, Rocha-Vieira E, Coimbra CC, Lacerda AC. 2011. The effect of adding whole-body vibration to squat training on the functional performance and self-report of disease status in elderly patients with knee osteoarthritis: a randomized, controlled clinical study. *J Altern Complement Med* **17**: 1149-1155.
- Babu D, Roy S. 2013. Left-right asymmetry: cilia stir up new surprises in the node. *Open biology* **3**: 130052.
- Baffi MO, Slattery E, Sohn P, Moses HL, Chytil A, Serra R. 2004. Conditional deletion of the TGF-beta type II receptor in Col2a expressing cells results in defects in the axial skeleton without alterations in chondrocyte differentiation or embryonic development of long bones. *Dev Biol* **276**: 124-142.
- Balague F, Mannion AF, Pellise F, Cedraschi C. 2012. Non-specific low back pain. *Lancet* **379**: 482-491.

- Barbir A, Godburn KE, Michalek AJ, Lai A, Monsey RD, Iatridis JC. 2011. Effects of torsion on intervertebral disc gene expression and biomechanics, using a rat tail model. *Spine (Phila Pa 1976)* **36**: 607-614.
- Barrantes IB, Elia AJ, Wunsch K, Hrabe de Angelis MH, Mak TW, Rossant J, Conlon RA, Gossler A, de la Pompa JL. 1999. Interaction between Notch signalling and Lunatic fringe during somite boundary formation in the mouse. *Current biology : CB* **9**: 470-480.
- Barrionuevo F, Taketo MM, Scherer G, Kispert A. 2006. Sox9 is required for notochord maintenance in mice. *Dev Biol* **295**: 128-140.
- Barry F, Boynton RE, Liu B, Murphy JM. 2001. Chondrogenic differentiation of mesenchymal stem cells from bone marrow: differentiation-dependent gene expression of matrix components. *Exp Cell Res* **268**: 189-200.
- Bedore J, Sha W, McCann MR, Liu S, Leask A, Seguin CA. 2013. Impaired Intervertebral Disc Development and Premature Disc Degeneration in Mice With Notochord-Specific Deletion of CCN2. *Arthritis Rheum* **65**: 2634-2644.
- Behrens A, Haigh J, Mechta-Grigoriou F, Nagy A, Yaniv M, Wagner EF. 2003. Impaired intervertebral disc formation in the absence of Jun. *Development* **130**: 103-109.
- Belavy DL, Armbrecht G, Gast U, Richardson CA, Hides JA, Felsenberg D. 2010. Countermeasures against lumbar spine deconditioning in prolonged bed rest: resistive exercise with and without whole body vibration. *J Appl Physiol* **109**: 1801-1811.
- Belavy DL, Hides JA, Wilson SJ, Stanton W, Dimeo FC, Rittweger J, Felsenberg D, Richardson CA. 2008. Resistive simulated weightbearing exercise with whole body vibration reduces lumbar spine deconditioning in bed-rest. *Spine (Phila Pa 1976)* **33**: E121-131.
- Bessho Y, Sakata R, Komatsu S, Shiota K, Yamada S, Kageyama R. 2001. Dynamic expression and essential functions of Hes7 in somite segmentation. *Genes Dev* **15**: 2642-2647.
- Bonewald LF. 2011. The amazing osteocyte. *J Bone Miner Res* **26**: 229-238.
- Boos N, Weissbach S, Rohrbach H, Weiler C, Spratt KF, Nerlich AG. 2002. Classification of age-related changes in lumbar intervertebral discs: 2002 Volvo Award in basic science. *Spine (Phila Pa 1976)* **27**: 2631-2644.
- Borrelli J, Jr., Silva MJ, Zaegel MA, Franz C, Sandell LJ. 2009. Single high-energy impact load causes posttraumatic OA in young rabbits via a decrease in cellular metabolism. *J Orthop Res* **27**: 347-352.

- Boxberger JJ, Sen S, Yerramalli CS, Elliott DM. 2006. Nucleus pulposus glycosaminoglycan content is correlated with axial mechanics in rat lumbar motion segments. *J Orthop Res* **24**: 1906-1915.
- Boyd LM, Richardson WJ, Allen KD, Flahiff C, Jing L, Li Y, Chen J, Setton LA. 2008. Early-onset degeneration of the intervertebral disc and vertebral end plate in mice deficient in type IX collagen. *Arthritis Rheum* **58**: 164-171.
- Brand RA. 2010. Biographical sketch: Julius Wolff, 1836-1902. *Clin Orthop Relat Res* **468**: 1047-1049.
- Brennan J, Norris DP, Robertson EJ. 2002. Nodal activity in the node governs left-right asymmetry. *Genes Dev* **16**: 2339-2344.
- Brent AE, Tabin CJ. 2002. Developmental regulation of somite derivatives: muscle, cartilage and tendon. *Current opinion in genetics & development* **12**: 548-557.
- Bruggeman BJ, Maier JA, Mohiuddin YS, Powers R, Lo Y, Guimaraes-Camboa N, Evans SM, Harfe BD. 2012. Avian intervertebral disc arises from rostral sclerotome and lacks a nucleus pulposus: implications for evolution of the vertebrate disc. *Dev Dyn* **241**: 675-683.
- Buckwalter JA. 1995. Aging and degeneration of the human intervertebral disc. *Spine (Phila Pa 1976)* **20**: 1307-1314.
- Bussen M, Petry M, Schuster-Gossler K, Leitges M, Gossler A, Kispert A. 2004. The T-box transcription factor Tbx18 maintains the separation of anterior and posterior somite compartments. *Genes Dev* **18**: 1209-1221.
- Cassidy JJ, Hiltner A, Baer E. 1989. Hierarchical structure of the intervertebral disc. *Connect Tissue Res* **23**: 75-88.
- Castro-Malaspina H, Gay RE, Resnick G, Kapoor N, Meyers P, Chiarieri D, McKenzie S, Broxmeyer HE, Moore MA. 1980. Characterization of human bone marrow fibroblast colony-forming cells (CFU-F) and their progeny. *Blood* **56**: 289-301.
- Chandran PL, Horkay F. 2012. Aggrecan, an unusual polyelectrolyte: review of solution behavior and physiological implications. *Acta biomaterialia* **8**: 3-12.
- Chen J, Yan W, Setton LA. 2004. Static compression induces zonal-specific changes in gene expression for extracellular matrix and cytoskeletal proteins in intervertebral disc cells in vitro. *Matrix biology : journal of the International Society for Matrix Biology* **22**: 573-583.
- Chen S, Emery SE, Pei M. 2009. Coculture of synovium-derived stem cells and nucleus pulposus cells in serum-free defined medium with supplementation of transforming growth factor-beta1: a potential application of tissue-specific stem cells in disc regeneration. *Spine (Phila Pa 1976)* **34**: 1272-1280.

- Chiang C, Litingtung Y, Lee E, Young KE, Corden JL, Westphal H, Beachy PA. 1996. Cyclopia and defective axial patterning in mice lacking Sonic hedgehog gene function. *Nature* **383**: 407-413.
- Choi KS, Cohn MJ, Harfe BD. 2008. Identification of nucleus pulposus precursor cells and notochordal remnants in the mouse: implications for disk degeneration and chordoma formation. *Dev Dyn* **237**: 3953-3958.
- Choi KS, Harfe BD. 2011. Hedgehog signaling is required for formation of the notochord sheath and patterning of nuclei pulposi within the intervertebral discs. *Proc Natl Acad Sci U S A* **108**: 9484-9489.
- Choi KS, Lee C, Harfe BD. 2012. Sonic hedgehog in the notochord is sufficient for patterning of the intervertebral discs. *Mech Dev* **129**: 255-262.
- Christ B, Wilting J. 1992. From somites to vertebral column. *Ann Anat* **174**: 23-32.
- Clements KM, Price JS, Chambers MG, Visco DM, Poole AR, Mason RM. 2003. Gene deletion of either interleukin-1beta, interleukin-1beta-converting enzyme, inducible nitric oxide synthase, or stromelysin 1 accelerates the development of knee osteoarthritis in mice after surgical transection of the medial collateral ligament and partial medial meniscectomy. *Arthritis Rheum* **48**: 3452-3463.
- Cowin SC. 2002. Mechanosensation and fluid transport in living bone. *J Musculoskelet Neuronal Interact* **2**: 256-260.
- Davidson BP, Tam PP. 2000. The node of the mouse embryo. *Current biology : CB* **10**: R617-619.
- del Pozo-Cruz B, Hernandez Mocholi MA, Adsuar JC, Parraca JA, Muro I, Gusi N. 2011. Effects of whole body vibration therapy on main outcome measures for chronic non-specific low back pain: a single-blind randomized controlled trial. *J Rehabil Med* **43**: 689-694.
- Desmoulin GT, Hewitt CR, Hunter CJ. 2011. Disc strain and resulting positive mRNA expression from application of a noninvasive treatment. *Spine (Phila Pa 1976)* **36**: E921-928.
- Desmoulin GT, Reno CR, Hunter CJ. 2010. Free axial vibrations at 0 to 200 Hz positively affect extracellular matrix messenger ribonucleic acid expression in bovine nucleus pulposi. *Spine (Phila Pa 1976)* **35**: 1437-1444.
- Driller K, Pagenstecher A, Uhl M, Omran H, Berlis A, Grunder A, Sippel AE. 2007. Nuclear factor I X deficiency causes brain malformation and severe skeletal defects. *Mol Cell Biol* **27**: 3855-3867.

- Fan CM, Tessier-Lavigne M. 1994. Patterning of mammalian somites by surface ectoderm and notochord: evidence for sclerotome induction by a hedgehog homolog. *Cell* **79**: 1175-1186.
- Fang H, Beier F. 2014. Mouse models of osteoarthritis: modelling risk factors and assessing outcomes. *Nature reviews Rheumatology* **10**: 413-421.
- Feng G, Li L, Hong Y, Liu H, Song Y, Pei F, Ma PX, Gong Q, Gupte MJ. 2014. Hypoxia promotes nucleus pulposus phenotype in 3D scaffolds in vitro and in vivo: laboratory investigation. *J Neurosurg Spine* **21**: 303-309.
- Fitzgerald JB, Jin M, Grodzinsky AJ. 2006. Shear and compression differentially regulate clusters of functionally related temporal transcription patterns in cartilage tissue. *J Biol Chem* **281**: 24095-24103.
- Flores ER, Sengupta S, Miller JB, Newman JJ, Bronson R, Crowley D, Yang A, McKeon F, Jacks T. 2005. Tumor predisposition in mice mutant for p63 and p73: evidence for broader tumor suppressor functions for the p53 family. *Cancer cell* **7**: 363-373.
- Forsberg H, Crozet F, Brown NA. 1998. Waves of mouse Lunatic fringe expression, in four-hour cycles at two-hour intervals, precede somite boundary formation. *Current biology : CB* **8**: 1027-1030.
- Friedman BW, O'Mahony S, Mulvey L, Davitt M, Choi H, Xia S, Esses D, Bijur PE, Gallagher EJ. 2012. One-week and 3-month outcomes after an emergency department visit for undifferentiated musculoskeletal low back pain. *Annals of emergency medicine* **59**: 128-133 e123.
- Fujita N, Miyamoto T, Imai J, Hosogane N, Suzuki T, Yagi M, Morita K, Ninomiya K, Miyamoto K, Takaishi H et al. 2005. CD24 is expressed specifically in the nucleus pulposus of intervertebral discs. *Biochem Biophys Res Commun* **338**: 1890-1896.
- Funakoshi M, Taoda K, Tsujimura H, Nishiyama K. 2004. Measurement of whole-body vibration in taxi drivers. *J Occup Health* **46**: 119-124.
- Furukawa T, Ito K, Nuka S, Hashimoto J, Takei H, Takahara M, Ogino T, Young MF, Shinomura T. 2009. Absence of biglycan accelerates the degenerative process in mouse intervertebral disc. *Spine (Phila Pa 1976)* **34**: E911-917.
- Furumoto TA, Miura N, Akasaka T, Mizutani-Koseki Y, Sudo H, Fukuda K, Maekawa M, Yuasa S, Fu Y, Moriya H et al. 1999. Notochord-dependent expression of MFH1 and PAX1 cooperates to maintain the proliferation of sclerotome cells during the vertebral column development. *Dev Biol* **210**: 15-29.
- Gilson A, Dreger M, Urban JP. 2010. Differential expression level of cytokeratin 8 in cells of the bovine nucleus pulposus complicates the search for specific intervertebral disc cell markers. *Arthritis Res Ther* **12**: R24.

- Gotz W, Osmers R, Herken R. 1995. Localisation of extracellular matrix components in the embryonic human notochord and axial mesenchyme. *J Anat* **186** (Pt 1): 111-121.
- Gustafsson E, Aszodi A, Ortega N, Hunziker EB, Denker HW, Werb Z, Fassler R. 2003. Role of collagen type II and perlecan in skeletal development. *Annals of the New York Academy of Sciences* **995**: 140-150.
- Haefeli M, Kalberer F, Saegesser D, Nerlich AG, Boos N, Paesold G. 2006. The course of macroscopic degeneration in the human lumbar intervertebral disc. *Spine (Phila Pa 1976)* **31**: 1522-1531.
- Harfe BD, Scherz PJ, Nissim S, Tian H, McMahon AP, Tabin CJ. 2004. Evidence for an expansion-based temporal Shh gradient in specifying vertebrate digit identities. *Cell* **118**: 517-528.
- Hayes AJ, Benjamin M, Ralphs JR. 2001. Extracellular matrix in development of the intervertebral disc. *Matrix Biol* **20**: 107-121.
- Henriksson H, Thornemo M, Karlsson C, Hagg O, Junevik K, Lindahl A, Brisby H. 2009. Identification of cell proliferation zones, progenitor cells and a potential stem cell niche in the intervertebral disc region: a study in four species. *Spine (Phila Pa 1976)* **34**: 2278-2287.
- Hinterwimmer S, Krammer M, Krotz M, Glaser C, Baumgart R, Reiser M, Eckstein F. 2004. Cartilage atrophy in the knees of patients after seven weeks of partial load bearing. *Arthritis Rheum* **50**: 2516-2520.
- Hirokawa N, Tanaka Y, Okada Y, Takeda S. 2006. Nodal flow and the generation of left-right asymmetry. *Cell* **125**: 33-45.
- Holguin N, Judex S. 2010. Rat intervertebral disc health during hindlimb unloading: brief ambulation with or without vibration. *Aviat Space Environ Med* **81**: 1078-1084.
- Holguin N, Muir J, Rubin C, Judex S. 2009. Short applications of very low-magnitude vibrations attenuate expansion of the intervertebral disc during extended bed rest. *Spine J* **9**: 470-477.
- Hosea TM, Hannafin JA. 2012. Rowing injuries. *Sports health* **4**: 236-245.
- Hoy D, Bain C, Williams G, March L, Brooks P, Blyth F, Woolf A, Vos T, Buchbinder R. 2012. A systematic review of the global prevalence of low back pain. *Arthritis Rheum* **64**: 2028-2037.
- Hunter CJ, Matyas JR, Duncan NA. 2003. The notochordal cell in the nucleus pulposus: a review in the context of tissue engineering. *Tissue Eng* **9**: 667-677.

- Hunter CJ, Matyas JR, Duncan NA. 2004. Cytomorphology of notochordal and chondrocytic cells from the nucleus pulposus: a species comparison. *J Anat* **205**: 357-362.
- Iatridis JC, Godburn K, Wuertz K, Alini M, Roughley PJ. 2011. Region-dependent aggrecan degradation patterns in the rat intervertebral disc are affected by mechanical loading in vivo. *Spine (Phila Pa 1976)* **36**: 203-209.
- Iba K, Durkin ME, Johnsen L, Hunziker E, Damgaard-Pedersen K, Zhang H, Engvall E, Albrechtsen R, Wewer UM. 2001. Mice with a targeted deletion of the tetranectin gene exhibit a spinal deformity. *Mol Cell Biol* **21**: 7817-7825.
- Iwamoto J, Takeda T, Sato Y, Uzawa M. 2005. Effect of whole-body vibration exercise on lumbar bone mineral density, bone turnover, and chronic back pain in postmenopausal osteoporotic women treated with alendronate. *Aging Clin Exp Res* **17**: 157-163.
- Jaubert J, Jaubert F, Martin N, Washburn LL, Lee BK, Eicher EM, Guenet JL. 1999. Three new allelic mouse mutations that cause skeletal overgrowth involve the natriuretic peptide receptor C gene (Npr3). *Proc Natl Acad Sci U S A* **96**: 10278-10283.
- Jiang Y, Jahagirdar BN, Reinhardt RL, Schwartz RE, Keene CD, Ortiz-Gonzalez XR, Reyes M, Lenvik T, Lund T, Blackstad M et al. 2002. Pluripotency of mesenchymal stem cells derived from adult marrow. *Nature* **418**: 41-49.
- Judex S, Donahue LR, Rubin C. 2002. Genetic predisposition to low bone mass is paralleled by an enhanced sensitivity to signals anabolic to the skeleton. *Faseb J* **16**: 1280-1282.
- Judex S, Lei X, Han D, Rubin C. 2007. Low-magnitude mechanical signals that stimulate bone formation in the ovariectomized rat are dependent on the applied frequency but not on the strain magnitude. *J Biomech* **40**: 1333-1339.
- Kaapa E, Zhang LQ, Muona P, Holm S, Vanharanta H, Peltonen J. 1994. Expression of type I, III, and VI collagen mRNAs in experimentally injured porcine intervertebral disc. *Connect Tissue Res* **30**: 203-214.
- Karatrantou K, Gerodimos V, Dipla K, Zafeiridis A. 2013. Whole-body vibration training improves flexibility, strength profile of knee flexors, and hamstrings-to-quadriceps strength ratio in females. *Journal of science and medicine in sport / Sports Medicine Australia* **16**: 477-481.
- Kessels MY, Huitema LF, Boeren S, Kranenbarg S, Schulte-Merker S, van Leeuwen JL, de Vries SC. 2014. Proteomics analysis of the zebrafish skeletal extracellular matrix. *PLoS One* **9**: e90568.

- Kim KW, Lim TH, Kim JG, Jeong ST, Masuda K, An HS. 2003. The origin of chondrocytes in the nucleus pulposus and histologic findings associated with the transition of a notochordal nucleus pulposus to a fibrocartilaginous nucleus pulposus in intact rabbit intervertebral discs. *Spine (Phila Pa 1976)* **28**: 982-990.
- Kim SK, Hebrok M, Melton DA. 1997. Notochord to endoderm signaling is required for pancreas development. *Development* **124**: 4243-4252.
- Klein-Nulend J, Bakker AD, Bacabac RG, Vatsa A, Weinbaum S. 2013. Mechanosensation and transduction in osteocytes. *Bone* **54**: 182-190.
- Ko FC, Dragomir C, Plumb DA, Goldring SR, Wright TM, Goldring MB, van der Meulen MC. 2013. In vivo cyclic compression causes cartilage degeneration and subchondral bone changes in mouse tibiae. *Arthritis Rheum* **65**: 1569-1578.
- Kondo H, Nifuji A, Takeda S, Ezura Y, Rittling SR, Denhardt DT, Nakashima K, Karsenty G, Noda M. 2005. Unloading induces osteoblastic cell suppression and osteoclastic cell activation to lead to bone loss via sympathetic nervous system. *J Biol Chem* **280**: 30192-30200.
- Korecki CL, Taboas JM, Tuan RS, Iatridis JC. 2010. Notochordal cell conditioned medium stimulates mesenchymal stem cell differentiation toward a young nucleus pulposus phenotype. *Stem Cell Res Ther* **1**: 18.
- Kraemer J, Kolditz D, Gowin R. 1985. Water and electrolyte content of human intervertebral discs under variable load. *Spine (Phila Pa 1976)* **10**: 69-71.
- Lange A, Gegg M, Burtscher I, Bengel D, Kremmer E, Lickert H. 2012. Fltp(T2AiCre): a new knock-in mouse line for conditional gene targeting in distinct mono- and multiciliated tissues. *Differentiation; research in biological diversity* **83**: S105-113.
- LeBlanc A, Schneider V, Shackelford L, West S, Oganov V, Bakulin A, Voronin L. 2000. Bone mineral and lean tissue loss after long duration space flight. *J Musculoskelet Neuronal Interact* **1**: 157-160.
- Leblanc AD, Schneider VS, Evans HJ, Engelbretson DA, Krebs JM. 1990. Bone mineral loss and recovery after 17 weeks of bed rest. *J Bone Miner Res* **5**: 843-850.
- Lee CR, Sakai D, Nakai T, Toyama K, Mochida J, Alini M, Grad S. 2007. A phenotypic comparison of intervertebral disc and articular cartilage cells in the rat. *Eur Spine J* **16**: 2174-2185.
- Lee JH, Fitzgerald JB, Dimicco MA, Grodzinsky AJ. 2005. Mechanical injury of cartilage explants causes specific time-dependent changes in chondrocyte gene expression. *Arthritis Rheum* **52**: 2386-2395.

- Leong DJ, Gu XI, Li Y, Lee JY, Laudier DM, Majeska RJ, Schaffler MB, Cardoso L, Sun HB. 2010. Matrix metalloproteinase-3 in articular cartilage is upregulated by joint immobilization and suppressed by passive joint motion. *Matrix Biol* **29**: 420-426.
- Leong DJ, Hardin JA, Cobelli NJ, Sun HB. 2011a. Mechanotransduction and cartilage integrity. *Annals of the New York Academy of Sciences* **1240**: 32-37.
- Leong DJ, Li YH, Gu XI, Sun L, Zhou Z, Nasser P, Laudier DM, Iqbal J, Majeska RJ, Schaffler MB et al. 2011b. Physiological loading of joints prevents cartilage degradation through CITED2. *FASEB J* **25**: 182-191.
- Lettice LA, Purdie LA, Carlson GJ, Kilanowski F, Dorin J, Hill RE. 1999. The mouse bagpipe gene controls development of axial skeleton, skull, and spleen. *Proc Natl Acad Sci U S A* **96**: 9695-9700.
- Li J, Liu C, Guo Q, Yang H, Li B. 2014. Regional variations in the cellular, biochemical, and biomechanical characteristics of rabbit annulus fibrosus. *PLoS One* **9**: e91799.
- Li X, Leo BM, Beck G, Balian G, Anderson GD. 2004. Collagen and proteoglycan abnormalities in the GDF-5-deficient mice and molecular changes when treating disk cells with recombinant growth factor. *Spine (Phila Pa 1976)* **29**: 2229-2234.
- Liebscher T, Haefeli M, Wuertz K, Nerlich AG, Boos N. 2010. Age-related variation in cell density of human lumbar intervertebral disc. *Spine (Phila Pa 1976)* **36**: 153-159.
- Lim KL, Jacobs P, Klarenbach S. 2006. A population-based analysis of healthcare utilization of persons with back disorders: results from the Canadian Community Health Survey 2000-2001. *Spine (Phila Pa 1976)* **31**: 212-218.
- Lin PM, Chen CT, Torzilli PA. 2004. Increased stromelysin-1 (MMP-3), proteoglycan degradation (3B3- and 7D4) and collagen damage in cyclically load-injured articular cartilage. *Osteoarthritis Cartilage* **12**: 485-496.
- Liphardt AM, Mundermann A, Koo S, Backer N, Andriacchi TP, Zange J, Mester J, Heer M. 2009. Vibration training intervention to maintain cartilage thickness and serum concentrations of cartilage oligomeric matrix protein (COMP) during immobilization. *Osteoarthritis Cartilage* **17**: 1598-1603.
- Lopez TP, Fan CM. 2013. Dynamic CREB family activity drives segmentation and posterior polarity specification in mammalian somitogenesis. *Proc Natl Acad Sci U S A* **110**: E2019-2027.
- Maclean JJ, Lee CR, Alini M, Iatridis JC. 2004. Anabolic and catabolic mRNA levels of the intervertebral disc vary with the magnitude and frequency of in vivo dynamic compression. *Journal of orthopaedic research : official publication of the Orthopaedic Research Society* **22**: 1193-1200.

- MacLean JJ, Lee CR, Grad S, Ito K, Alini M, Iatridis JC. 2003. Effects of immobilization and dynamic compression on intervertebral disc cell gene expression in vivo. *Spine* **28**: 973-981.
- Maier JA, Harfe BD. 2011. Nuclei pulposi formation from the embryonic notochord occurs normally in GDF-5-deficient mice. *Spine (Phila Pa 1976)* **36**: E1555-1561.
- Maier JA, Lo Y, Harfe BD. 2013. Foxa1 and Foxa2 are required for formation of the intervertebral discs. *PLoS One* **8**: e55528.
- Majumdar MK, Askew R, Schelling S, Stedman N, Blanchet T, Hopkins B, Morris EA, Glasson SS. 2007. Double-knockout of ADAMTS-4 and ADAMTS-5 in mice results in physiologically normal animals and prevents the progression of osteoarthritis. *Arthritis Rheum* **56**: 3670-3674.
- Majumdar MK, Thiede MA, Mosca JD, Moorman M, Gerson SL. 1998. Phenotypic and functional comparison of cultures of marrow-derived mesenchymal stem cells (MSCs) and stromal cells. *J Cell Physiol* **176**: 57-66.
- Mankoo BS, Skuntz S, Harrigan I, Grigorieva E, Candia A, Wright CV, Arnheiter H, Pachnis V. 2003. The concerted action of Meox homeobox genes is required upstream of genetic pathways essential for the formation, patterning and differentiation of somites. *Development* **130**: 4655-4664.
- Manninen P, Riihimäki H, Heliovaara M, Suomalainen O. 2001. Physical exercise and risk of severe knee osteoarthritis requiring arthroplasty. *Rheumatology* **40**: 432-437.
- Masago Y, Hosoya A, Kawasaki K, Kawano S, Nasu A, Toguchida J, Fujita K, Nakamura H, Kondoh G, Nagata K. 2012. The molecular chaperone Hsp47 is essential for cartilage and endochondral bone formation. *J Cell Sci* **125**: 1118-1128.
- Matsumoto Y, Griffin MJ. 2002. Non-linear characteristics in the dynamic responses of seated subjects exposed to vertical whole-body vibration. *J Biomech Eng* **124**: 527-532.
- Matsumura Y, Kasai Y, Obata H, Matsushima S, Inaba T, Uchida A. 2009. Changes in water content of intervertebral discs and paravertebral muscles before and after bed rest. *Journal of orthopaedic science : official journal of the Japanese Orthopaedic Association* **14**: 45-50.
- McAlinden A, Zhu Y, Sandell LJ. 2002. Expression of type II procollagens during development of the human intervertebral disc. *Biochem Soc Trans* **30**: 831-838.
- McAlindon TE, Wilson PW, Aliabadi P, Weissman B, Felson DT. 1999. Level of physical activity and the risk of radiographic and symptomatic knee osteoarthritis

- in the elderly: the Framingham study. *The American journal of medicine* **106**: 151-157.
- McCann MR, Bacher CA, Seguin CA. 2011a. Exploiting notochord cells for stem cell-based regeneration of the intervertebral disc. *J Cell Commun Signal* **5**: 39-43.
- McCann MR, Tamplin OJ, Rossant J, Seguin CA. 2011b. Tracing notochord-derived cells using a Noto-cre mouse: implications for intervertebral disc development. *Dis Model Mech*.
- Meadows SM, Fletcher PJ, Moran C, Xu K, Neufeld G, Chauvet S, Mann F, Krieg PA, Cleaver O. 2012. Integration of repulsive guidance cues generates avascular zones that shape mammalian blood vessels. *Circulation research* **110**: 34-46.
- Merceron C, Mangiavini L, Robling A, Wilson TL, Giaccia AJ, Shapiro IM, Schipani E, Risbud MV. 2014. Loss of HIF-1alpha in the Notochord Results in Cell Death and Complete Disappearance of the Nucleus Pulposus. *PLoS One* **9**: e110768.
- Millecamps M, Tajerian M, Naso L, Sage EH, Stone LS. 2012. Lumbar intervertebral disc degeneration associated with axial and radiating low back pain in ageing SPARC-null mice. *Pain* **153**: 1167-1179.
- Minogue BM, Richardson SM, Zeef LA, Freemont AJ, Hoyland JA. 2010a. Characterization of the human nucleus pulposus cell phenotype and evaluation of novel marker gene expression to define adult stem cell differentiation. *Arthritis Rheum* **62**: 3695-3705.
- Minogue BM, Richardson SM, Zeef LA, Freemont AJ, Hoyland JA. 2010b. Transcriptional profiling of bovine intervertebral disc cells: implications for identification of normal and degenerate human intervertebral disc cell phenotypes. *Arthritis Res Ther* **12**: R22.
- Mo R, Freer AM, Zinyk DL, Crackower MA, Michaud J, Heng HH, Chik KW, Shi XM, Tsui LC, Cheng SH et al. 1997. Specific and redundant functions of Gli2 and Gli3 zinc finger genes in skeletal patterning and development. *Development* **124**: 113-123.
- Moreland LW. 2003. Intra-articular hyaluronan (hyaluronic acid) and hylans for the treatment of osteoarthritis: mechanisms of action. *Arthritis Res Ther* **5**: 54-67.
- Mundy C, Yasuda T, Kinumatsu T, Yamaguchi Y, Iwamoto M, Enomoto-Iwamoto M, Koyama E, Pacifici M. 2011. Synovial joint formation requires local Ext1 expression and heparan sulfate production in developing mouse embryo limbs and spine. *Dev Biol* **351**: 70-81.
- Musumeci G, Castrogiovanni P, Trovato FM, Imbesi R, Giunta S, Szychlinska MA, Loreto C, Castorina S, Mobasher A. 2014. Physical activity ameliorates cartilage

- degeneration in a rat model of aging: A study on lubricin expression. *Scandinavian journal of medicine & science in sports*.
- Mwale F. 2014. Collagen and Other Proteins of the Nucleus Pulposus, Annulus Fibrosus, and Cartilage End Plates. in *The Intervertebral Disc*, pp. 79-92. Springer.
- Mwale F, Roughley P, Antoniou J. 2004. Distinction between the extracellular matrix of the nucleus pulposus and hyaline cartilage: a requisite for tissue engineering of intervertebral disc. *Eur Cell Mater* **8**: 58-63; discussion 63-54.
- Nagy A. 2000. Cre recombinase: the universal reagent for genome tailoring. *Genesis* **26**: 99-109.
- Nagy A, Perrimon N, Sandmeyer S, Plasterk R. 2003. Tailoring the genome: the power of genetic approaches. *Nat Genet* **33 Suppl**: 276-284.
- Nap RJ, Szleifer I. 2008. Structure and interactions of aggrecans: statistical thermodynamic approach. *Biophysical journal* **95**: 4570-4583.
- Natarajan RN, Williams JR, Andersson GB. 2006. Modeling changes in intervertebral disc mechanics with degeneration. *J Bone Joint Surg Am* **88 Suppl 2**: 36-40.
- Nilsson E, Nakamae T, Olmarker K. 2011. Pain behavior changes following disc puncture relate to nucleus pulposus rather than to the disc injury per se: an experimental study in rats. *Open Orthop J* **5**: 72-77.
- Niu CC, Yuan LJ, Lin SS, Chen LH, Chen WJ. 2009. Mesenchymal stem cell and nucleus pulposus cell coculture modulates cell profile. *Clin Orthop Relat Res* **467**: 3263-3272.
- Nonaka S, Tanaka Y, Okada Y, Takeda S, Harada A, Kanai Y, Kido M, Hirokawa N. 1998. Randomization of left-right asymmetry due to loss of nodal cilia generating leftward flow of extraembryonic fluid in mice lacking KIF3B motor protein. *Cell* **95**: 829-837.
- O'Connell GD, Guerin HL, Elliott DM. 2009. Theoretical and uniaxial experimental evaluation of human annulus fibrosus degeneration. *J Biomech Eng* **131**: 111007.
- O'Driscoll SW, Saris DB, Ito Y, Fitzimmons JS. 2001. The chondrogenic potential of periosteum decreases with age. *J Orthop Res* **19**: 95-103.
- Onnerfjord P, Khabut A, Reinholt FP, Svensson O, Heinegard D. 2012. Quantitative proteomic analysis of eight cartilaginous tissues reveals characteristic differences as well as similarities between subgroups. *J Biol Chem* **287**: 18913-18924.
- Ovchinnikov DA, Deng JM, Ogunrinu G, Behringer RR. 2000. Col2a1-directed expression of Cre recombinase in differentiating chondrocytes in transgenic mice. *Genesis* **26**: 145-146.

- Park EJ, Sun X, Nichol P, Saijoh Y, Martin JF, Moon AM. 2008. System for tamoxifen-inducible expression of cre-recombinase from the *Foxa2* locus in mice. *Dev Dyn* **237**: 447-453.
- Park YG, Kwon BS, Park JW, Cha DY, Nam KY, Sim KB, Chang J, Lee HJ. 2013. Therapeutic effect of whole body vibration on chronic knee osteoarthritis. *Annals of rehabilitation medicine* **37**: 505-515.
- Pazzaglia UE, Salisbury JR, Byers PD. 1989. Development and involution of the notochord in the human spine. *J R Soc Med* **82**: 413-415.
- Pearce RH, Grimmer BJ, Adams ME. 1987. Degeneration and the chemical composition of the human lumbar intervertebral disc. *J Orthop Res* **5**: 198-205.
- Perantoni AO, Timofeeva O, Naillat F, Richman C, Pajni-Underwood S, Wilson C, Vainio S, Dove LF, Lewandoski M. 2005. Inactivation of FGF8 in early mesoderm reveals an essential role in kidney development. *Development* **132**: 3859-3871.
- Perraton L, Machotka Z, Kumar S. 2010. Whole-body vibration to treat low back pain: fact or fad? *Physiother Can* **63**: 88-93.
- Peters H, Wilm B, Sakai N, Imai K, Maas R, Balling R. 1999. Pax1 and Pax9 synergistically regulate vertebral column development. *Development* **126**: 5399-5408.
- Pittenger MF, Mackay AM, Beck SC, Jaiswal RK, Douglas R, Mosca JD, Moorman MA, Simonetti DW, Craig S, Marshak DR. 1999. Multilineage potential of adult human mesenchymal stem cells. *Science* **284**: 143-147.
- Poiraudau S, Monteiro I, Anract P, Blanchard O, Revel M, Corvol MT. 1999. Phenotypic characteristics of rabbit intervertebral disc cells. Comparison with cartilage cells from the same animals. *Spine (Phila Pa 1976)* **24**: 837-844.
- Radin EL, Ehrlich MG, Chernack R, Abernethy P, Paul IL, Rose RM. 1978. Effect of repetitive impulsive loading on the knee joints of rabbits. *Clin Orthop Relat Res*: 288-293.
- Regnier CH, Masson R, Kedinger V, Textoris J, Stoll I, Chenard MP, Dierich A, Tomasetto C, Rio MC. 2002. Impaired neural tube closure, axial skeleton malformations, and tracheal ring disruption in TRAF4-deficient mice. *Proc Natl Acad Sci U S A* **99**: 5585-5590.
- Richardson SM, Curran JM, Chen R, Vaughan-Thomas A, Hunt JA, Freemont AJ, Hoyland JA. 2006. The differentiation of bone marrow mesenchymal stem cells into chondrocyte-like cells on poly-L-lactic acid (PLLA) scaffolds. *Biomaterials* **27**: 4069-4078.

- Risbud MV, Schaer TP, Shapiro IM. 2011. Toward an understanding of the role of notochordal cells in the adult intervertebral disc: from discord to accord. *Dev Dyn* **239**: 2141-2148.
- Rittweger J, Just K, Kautzsch K, Reeg P, Felsenberg D. 2002. Treatment of chronic lower back pain with lumbar extension and whole-body vibration exercise: a randomized controlled trial. *Spine (Phila Pa 1976)* **27**: 1829-1834.
- Roberts S. 2002. Disc morphology in health and disease. *Biochem Soc Trans* **30**: 864-869.
- Roberts S, Menage J, Duance V, Wotton SF. 1991. Type III collagen in the intervertebral disc. *Histochem J* **23**: 503-508.
- Roelants M, Delecluse C, Verschueren SM. 2004. Whole-body-vibration training increases knee-extension strength and speed of movement in older women. *Journal of the American Geriatrics Society* **52**: 901-908.
- Roughley PJ. 2004. Biology of intervertebral disc aging and degeneration: involvement of the extracellular matrix. *Spine (Phila Pa 1976)* **29**: 2691-2699.
- Roughley PJ, Lamplugh L, Lee ER, Matsumoto K, Yamaguchi Y. 2011. The role of hyaluronan produced by Has2 gene expression in development of the spine. *Spine (Phila Pa 1976)* **36**: E914-920.
- Rubin C, Pope M, Fritton JC, Magnusson M, Hansson T, McLeod K. 2003. Transmissibility of 15-hertz to 35-hertz vibrations to the human hip and lumbar spine: determining the physiologic feasibility of delivering low-level anabolic mechanical stimuli to skeletal regions at greatest risk of fracture because of osteoporosis. *Spine (Phila Pa 1976)* **28**: 2621-2627.
- Rubin C, Recker R, Cullen D, Ryaby J, McCabe J, McLeod K. 2004. Prevention of postmenopausal bone loss by a low-magnitude, high-frequency mechanical stimuli: a clinical trial assessing compliance, efficacy, and safety. *J Bone Miner Res* **19**: 343-351.
- Rubin C, Turner AS, Bain S, Mallinckrodt C, McLeod K. 2001. Anabolism: Low mechanical signals strengthen long bones. *Nature* **412**: 603-604.
- Rubin C, Turner AS, Mallinckrodt C, Jerome C, McLeod K, Bain S. 2002. Mechanical strain, induced noninvasively in the high-frequency domain, is anabolic to cancellous bone, but not cortical bone. *Bone* **30**: 445-452.
- Rubin C, Xu G, Judex S. 2001c. The anabolic activity of bone tissue, suppressed by disuse, is normalized by brief exposure to extremely low-magnitude mechanical stimuli. *FASEB J* **15**: 2225-2229.

- Saga Y, Hata N, Koseki H, Taketo MM. 1997. Mesp2: a novel mouse gene expressed in the presegmented mesoderm and essential for segmentation initiation. *Genes Dev* **11**: 1827-1839.
- Sahlman J, Inkinen R, Hirvonen T, Lammi MJ, Lammi PE, Nieminen J, Lapvetelainen T, Prockop DJ, Arita M, Li SW et al. 2001. Premature vertebral endplate ossification and mild disc degeneration in mice after inactivation of one allele belonging to the Col2a1 gene for Type II collagen. *Spine (Phila Pa 1976)* **26**: 2558-2565.
- Sakai D, Nakai T, Mochida J, Alini M, Grad S. 2009. Differential phenotype of intervertebral disc cells: microarray and immunohistochemical analysis of canine nucleus pulposus and annulus fibrosus. *Spine (Phila Pa 1976)* **34**: 1448-1456.
- Sakai D, Nakamura Y, Nakai T, Mishima T, Kato S, Grad S, Alini M, Risbud MV, Chan D, Cheah KS et al. 2012. Exhaustion of nucleus pulposus progenitor cells with ageing and degeneration of the intervertebral disc. *Nature communications* **3**: 1264.
- Sakai K, Hiripi L, Glumoff V, Brandau O, Eerola R, Vuorio E, Bosze Z, Fassler R, Aszodi A. 2001. Stage-and tissue-specific expression of a Col2a1-Cre fusion gene in transgenic mice. *Matrix Biol* **19**: 761-767.
- Salmon JR, Roper JA, Tillman MD. 2012. Does acute whole-body vibration training improve the physical performance of people with knee osteoarthritis? *Journal of strength and conditioning research / National Strength & Conditioning Association* **26**: 2983-2989.
- Sarver JJ, Elliott DM. 2004. Altered disc mechanics in mice genetically engineered for reduced type I collagen. *Spine (Phila Pa 1976)* **29**: 1094-1098.
- Schipani E, Ryan HE, Didrickson S, Kobayashi T, Knight M, Johnson RS. 2001. Hypoxia in cartilage: HIF-1alpha is essential for chondrocyte growth arrest and survival. *Genes Dev* **15**: 2865-2876.
- Semba K, Araki K, Li Z, Matsumoto K, Suzuki M, Nakagata N, Takagi K, Takeya M, Yoshinobu K, Araki M et al. 2006. A novel murine gene, Sickie tail, linked to the Danforth's short tail locus, is required for normal development of the intervertebral disc. *Genetics* **172**: 445-456.
- Sethe S, Scutt A, Stolzing A. 2006. Aging of mesenchymal stem cells. *Ageing Res Rev* **5**: 91-116.
- Setton LA, Chen J. 2006. Mechanobiology of the intervertebral disc and relevance to disc degeneration. *J Bone Joint Surg Am* **88 Suppl 2**: 52-57.
- Shim M, Foley J, Anna C, Mishina Y, Eling T. 2010. Embryonic expression of cyclooxygenase-2 causes malformations in axial skeleton. *J Biol Chem* **285**: 16206-16217.

- Simao AP, Avelar NC, Tossige-Gomes R, Neves CD, Mendonca VA, Miranda AS, Teixeira MM, Teixeira AL, Andrade AP, Coimbra CC et al. 2012. Functional performance and inflammatory cytokines after squat exercises and whole-body vibration in elderly individuals with knee osteoarthritis. *Archives of physical medicine and rehabilitation* **93**: 1692-1700.
- Sive JJ, Baird P, Jeziorski M, Watkins A, Hoyland JA, Freemont AJ. 2002. Expression of chondrocyte markers by cells of normal and degenerate intervertebral discs. *Mol Pathol* **55**: 91-97.
- Slatkowska L, Alibhai SM, Beyene J, Hu H, Demaras A, Cheung AM. 2011. Effect of 12 months of whole-body vibration therapy on bone density and structure in postmenopausal women: a randomized trial. *Annals of internal medicine* **155**: 668-679, W205.
- Smith LJ, Fazzalari NL. 2009. The elastic fibre network of the human lumbar annulus fibrosus: architecture, mechanical function and potential role in the progression of intervertebral disc degeneration. *Eur Spine J* **18**: 439-448.
- Smith LJ, Nerurkar NL, Choi KS, Harfe BD, Elliott DM. 2011. Degeneration and regeneration of the intervertebral disc: lessons from development. *Dis Model Mech* **4**: 31-41.
- Smits P, Lefebvre V. 2003. Sox5 and Sox6 are required for notochord extracellular matrix sheath formation, notochord cell survival and development of the nucleus pulposus of intervertebral discs. *Development* **130**: 1135-1148.
- Smolders LA, Meij BP, Onis D, Riemers FM, Bergknut N, Wubboldts R, Grinwis GC, Houweling M, Groot Koerkamp MJ, van Leenen D et al. 2013. Gene expression profiling of early intervertebral disc degeneration reveals a down-regulation of canonical Wnt signaling and caveolin-1 expression: implications for development of regenerative strategies. *Arthritis Res Ther* **15**: R23.
- Sobajima S, Kim JS, Gilbertson LG, Kang JD. 2004. Gene therapy for degenerative disc disease. *Gene Ther* **11**: 390-401.
- Soriano P. 1999. Generalized lacZ expression with the ROSA26 Cre reporter strain. *Nat Genet* **21**: 70-71.
- Stolzing A, Jones E, McGonagle D, Scutt A. 2008. Age-related changes in human bone marrow-derived mesenchymal stem cells: consequences for cell therapies. *Mech Ageing Dev* **129**: 163-173.
- Takagi T, Moribe H, Kondoh H, Higashi Y. 1998. DeltaEF1, a zinc finger and homeodomain transcription factor, is required for skeleton patterning in multiple lineages. *Development* **125**: 21-31.

- Tanaka Y, Okada Y, Hirokawa N. 2005. FGF-induced vesicular release of Sonic hedgehog and retinoic acid in leftward nodal flow is critical for left-right determination. *Nature* **435**: 172-177.
- Tatsumi S, Ishii K, Amizuka N, Li M, Kobayashi T, Kohno K, Ito M, Takeshita S, Ikeda K. 2007. Targeted ablation of osteocytes induces osteoporosis with defective mechanotransduction. *Cell metabolism* **5**: 464-475.
- Terpstra L, Prud'homme J, Arabian A, Takeda S, Karsenty G, Dedhar S, St-Arnaud R. 2003. Reduced chondrocyte proliferation and chondrodysplasia in mice lacking the integrin-linked kinase in chondrocytes. *J Cell Biol* **162**: 139-148.
- Torvinen S, Kannus P, Sievanen H, Jarvinen TA, Pasanen M, Kontulainen S, Nenonen A, Jarvinen TL, Paakkala T, Jarvinen M et al. 2003. Effect of 8-month vertical whole body vibration on bone, muscle performance, and body balance: a randomized controlled study. *J Bone Miner Res* **18**: 876-884.
- Torzilli PA, Grigiene R, Borrelli J, Jr., Helfet DL. 1999. Effect of impact load on articular cartilage: cell metabolism and viability, and matrix water content. *J Biomech Eng* **121**: 433-441.
- Tribioli C, Lufkin T. 1999. The murine Bapx1 homeobox gene plays a critical role in embryonic development of the axial skeleton and spleen. *Development* **126**: 5699-5711.
- Trout JJ, Buckwalter JA, Moore KC. 1982. Ultrastructure of the human intervertebral disc: II. Cells of the nucleus pulposus. *Anat Rec* **204**: 307-314.
- Tsai TT, Guttapalli A, Oguz E, Chen LH, Vaccaro AR, Albert TJ, Shapiro IM, Risbud MV. 2007. Fibroblast growth factor-2 maintains the differentiation potential of nucleus pulposus cells in vitro: implications for cell-based transplantation therapy. *Spine (Phila Pa 1976)* **32**: 495-502.
- Uetzmann L, Burtscher I, Lickert H. 2008. A mouse line expressing Foxa2-driven Cre recombinase in node, notochord, floorplate, and endoderm. *Genesis* **46**: 515-522.
- Urban JP, Smith S, Fairbank JC. 2004. Nutrition of the intervertebral disc. *Spine (Phila Pa 1976)* **29**: 2700-2709.
- Urban JPG, Roberts S, Ralphs JR. 2000. The nucleus of the intervertebral disc from development to degeneration. *American Zoologist* **40**: 53-61.
- Vadala G, Studer RK, Sowa G, Spiezia F, Iucu C, Denaro V, Gilbertson LG, Kang JD. 2008. Coculture of bone marrow mesenchymal stem cells and nucleus pulposus cells modulate gene expression profile without cell fusion. *Spine (Phila Pa 1976)* **33**: 870-876.

- Van RL, Bayliss CE, Roncari DA. 1976. Cytological and enzymological characterization of adult human adipocyte precursors in culture. *J Clin Invest* **58**: 699-704.
- Vanwanseele B, Eckstein F, Knecht H, Stussi E, Spaepen A. 2002. Knee cartilage of spinal cord-injured patients displays progressive thinning in the absence of normal joint loading and movement. *Arthritis Rheum* **46**: 2073-2078.
- Videman T, Sarna S, Battie MC, Koskinen S, Gill K, Paananen H, Gibbons L. 1995. The long-term effects of physical loading and exercise lifestyles on back-related symptoms, disability, and spinal pathology among men. *Spine (Phila Pa 1976)* **20**: 699-709.
- Vos T, Flaxman AD, Naghavi M, Lozano R, Michaud C, Ezzati M, Shibuya K, Salomon JA, Abdalla S, Aboyans V et al. 2012. Years lived with disability (YLDs) for 1160 sequelae of 289 diseases and injuries 1990-2010: a systematic analysis for the Global Burden of Disease Study 2010. *Lancet* **380**: 2163-2196.
- Vujovic S, Henderson S, Presneau N, Odell E, Jacques TS, Tirabosco R, Boshoff C, Flanagan AM. 2006. Brachyury, a crucial regulator of notochordal development, is a novel biomarker for chordomas. *J Pathol* **209**: 157-165.
- Wallin J, Wilting J, Koseki H, Fritsch R, Christ B, Balling R. 1994. The role of Pax-1 in axial skeleton development. *Development* **120**: 1109-1121.
- Walsh AJ, Lotz JC. 2004. Biological response of the intervertebral disc to dynamic loading. *J Biomech* **37**: 329-337.
- Wang DL, Jiang SD, Dai LY. 2007. Biologic response of the intervertebral disc to static and dynamic compression in vitro. *Spine (Phila Pa 1976)* **32**: 2521-2528.
- Wang M, Sampson ER, Jin H, Li J, Ke QH, Im HJ, Chen D. 2013. MMP13 is a critical target gene during the progression of osteoarthritis. *Arthritis Res Ther* **15**: R5.
- Wang M, Tang D, Shu B, Wang B, Jin H, Hao S, Dresser KA, Shen J, Im HJ, Sampson ER et al. 2012. Conditional activation of beta-catenin signaling in mice leads to severe defects in intervertebral disc tissue. *Arthritis Rheum* **64**: 2611-2623.
- Watanabe H, Nakata K, Kimata K, Nakanishi I, Yamada Y. 1997. Dwarfism and age-associated spinal degeneration of heterozygote cmd mice defective in aggrecan. *Proc Natl Acad Sci U S A* **94**: 6943-6947.
- Watanabe H, Yamada Y, Kimata K. 1998. Roles of aggrecan, a large chondroitin sulfate proteoglycan, in cartilage structure and function. *J Biochem* **124**: 687-693.
- Wenger KH, Freeman JD, Fulzele S, Immel DM, Powell BD, Molitor P, Chao YJ, Gao HS, Elsalanty M, Hamrick MW et al. 2010. Effect of whole-body vibration on bone properties in aging mice. *Bone* **47**: 746-755.

- Wilm B, Dahl E, Peters H, Balling R, Imai K. 1998. Targeted disruption of Pax1 defines its null phenotype and proves haploinsufficiency. *Proc Natl Acad Sci U S A* **95**: 8692-8697.
- Winnier GE, Hargett L, Hogan BL. 1997. The winged helix transcription factor MFH1 is required for proliferation and patterning of paraxial mesoderm in the mouse embryo. *Genes Dev* **11**: 926-940.
- Wolff J. 1892. The law of bone remodeling (Das gesetz der transformation der knochen). *Originally published by verlag von august Hirshwald, Berlin (English translation by P Maquet and R Furlong, published by Springer Verlag, Berlin, 1986).*
- Worster AA, Brower-Toland BD, Fortier LA, Bent SJ, Williams J, Nixon AJ. 2001. Chondrocytic differentiation of mesenchymal stem cells sequentially exposed to transforming growth factor-beta1 in monolayer and insulin-like growth factor-I in a three-dimensional matrix. *J Orthop Res* **19**: 738-749.
- Wuertz K, Godburn K, MacLean JJ, Barbir A, Donnelly JS, Roughley PJ, Alini M, Iatridis JC. 2009. In vivo remodeling of intervertebral discs in response to short- and long-term dynamic compression. *J Orthop Res* **27**: 1235-1242.
- Yamada K, Sudo H, Iwasaki K, Sasaki N, Higashi H, Kameda Y, Ito M, Takahata M, Abumi K, Minami A et al. 2014. Caspase 3 silencing inhibits biomechanical overload-induced intervertebral disk degeneration. *Am J Pathol* **184**: 753-764.
- Yamada T, Placzek M, Tanaka H, Dodd J, Jessell TM. 1991. Control of cell pattern in the developing nervous system: polarizing activity of the floor plate and notochord. *Cell* **64**: 635-647.
- Yamanaka Y, Tamplin OJ, Beckers A, Gossler A, Rossant J. 2007. Live imaging and genetic analysis of mouse notochord formation reveals regional morphogenetic mechanisms. *Dev Cell* **13**: 884-896.
- You L, Cowin SC, Schaffler MB, Weinbaum S. 2001. A model for strain amplification in the actin cytoskeleton of osteocytes due to fluid drag on pericellular matrix. *J Biomech* **34**: 1375-1386.
- Zakin L, De Robertis EM. 2004. Inactivation of mouse Twisted gastrulation reveals its role in promoting Bmp4 activity during forebrain development. *Development* **131**: 413-424.
- Zhang D, Jin L, Reames DL, Shen FH, Shimer AL, Li X. 2013. Intervertebral disc degeneration and ectopic bone formation in apolipoprotein E knockout mice. *J Orthop Res* **31**: 210-217.
- Zhang N, Gridley T. 1998. Defects in somite formation in lunatic fringe-deficient mice. *Nature* **394**: 374-377.

- Zhou X, Tian F, Sandzen J, Cao R, Flaberg E, Szekely L, Cao Y, Ohlsson C, Bergo MO, Boren J et al. 2007. Filamin B deficiency in mice results in skeletal malformations and impaired microvascular development. *Proc Natl Acad Sci U S A* **104**: 3919-3924.
- Zizic Mitrecic M, Mitrecic D, Pochet R, Kostovic-Knezevic L, Gajovic S. 2010. The mouse gene Noto is expressed in the tail bud and essential for its morphogenesis. *Cells Tissues Organs* **192**: 85-92.

CHAPTER TWO

TRACING NOTOCHORD-DERIVED CELLS USING A NOVEL *NOTO-CRE* MOUSE: IMPLICATIONS FOR INTERVERTEBRAL DISC DEVELOPMENT

This chapter has been reproduced with permission from:

McCann, M. R., Tamplin O.J., Rossant J., Séguin C.A. Tracing notochord-derived cells using a Noto-Cre mouse: implications for intervertebral disc development. *Disease Models & Mechanisms* 5.1 (2012): 73-82, with some modifications.

Chapter 2.1 Co-Authorship Statement

Chapter 2 is adapted from McCann, M. R., Tamplin O. J., Rossant, J., and Séguin, C.A., (2012). Tracing notochord-derived cells using a novel *Noto-Cre* mouse: implications for intervertebral disc development. *Disease Models & Mechanisms* Jan;5(1):73-82. Figures and text are reproduced with permissions from *The Company of Biologists* (Appendix X)

O. J. Tamplin generated the *Noto-Cre* mouse in the lab of Dr. J. Rossant. All other experiments were performed by M.R. McCann in the laboratory of C.A. Séguin. Manuscript was written by M.R. McCann with suggestions from Drs. O.J Tamplin, J. Rossant and C. A. Séguin. All authors were involved in study conception and design, and analysis and interpretation of the data.

2.2 Chapter Summary

Back pain related to intervertebral disc degeneration is the most common musculoskeletal problem, with a lifetime prevalence of 84%. The lack of effective treatment for this widespread problem is directly related to our limited understanding of disc development, maintenance and degeneration. The aim of this study was to determine the developmental origins of nucleus pulposus cells within the intervertebral disc using a novel notochord-specific Cre mouse. To trace the fate of notochordal cells within the intervertebral disc we derived a notochord-specific Cre mouse line by targeting the homeobox gene *Noto*. Expression of this gene is restricted to the node and the posterior notochord during gastrulation (E7.5-12.5). The *Noto-Cre* mice were crossed with a conditional lacZ reporter for visualization of notochord fate in whole mount embryos. We performed lineage-tracing experiments to examine the contribution of the notochord to spinal development from embryonic day 12.5 through to skeletally mature mice (9 months). Fate mapping studies demonstrate that following elongation and formation of the primitive axial skeleton, the notochord gives rise to the nucleus pulposus in fully formed intervertebral discs. Cellular localization of β -galactosidase and cytokeratin-8 demonstrates that both notochordal cells and chondrocyte-like nucleus pulposus cells are derived from the embryonic notochord. These studies establish conclusively that notochordal cells act as embryonic precursors to all cells found within the nucleus pulposus of the mature intervertebral disc. This suggests that notochordal cells may serve as tissue specific progenitor cells within the disc and establishes the *Noto-Cre* mouse as a unique tool to interrogate the contribution of notochordal cells to both intervertebral disc development and disc degeneration.

2.3 Introduction

Back pain accounts for the more than half of all musculoskeletal disabilities, making it one of the most prevalent and costly medical conditions (Murphy and Volinn 1999; Goetzel et al. 2003; Ramage-Morin and Gilmour 2010). The most common cause of back pain is disc degeneration, the etiology of which is poorly defined making it difficult to distinguish from the physiological processes of growth, aging or adaptive remodeling (Adams and Roughley 2006). Disc degeneration has perhaps best been defined as an aberrant, cell-mediated response to progressive structural failure (Adams and Roughley 2006): a cascade beginning with changes to the cellular microenvironment within the disc that progresses over decades resulting in structural breakdown and functional impairment (Smith et al. 2011).

Degeneration of the intervertebral disc (IVD) is characterized by increased extracellular matrix breakdown, abnormal (fibrotic) matrix synthesis, inflammation, and in-growth of nociceptive nerves and blood vessels into a typically aneural and avascular tissue. Although the exact cause(s) of disc degeneration are unclear, initiation and progression of the degenerative cascade involve multiple interdependent factors including altered mechanical loading (Ohshima et al. 1995), reduction in nutrient supply (Urban et al. 2004), altered cellular composition (Aguilar et al. 1999), and hereditary factors (Kawaguchi et al. 1999; Videman et al. 2001; Battie and Videman 2006). Currently, there is no effective treatment for individuals with this disease who develop persistent pain.

The IVD is a specialized connective tissue structure consisting of three distinct, yet interdependent tissues: the outer fibrillar annulus fibrosus (AF), the central viscous nucleus pulposus (NP), and the cartilage end-plates (CEP) that anchor the discs to the

adjacent vertebral body bones. The NP is composed of a proteoglycan and water gel held together loosely by an irregular network of type II collagen and elastin fibers. The major proteoglycan of the disc is aggrecan, which due to its highly anionic glycosaminoglycan content provides the osmotic properties enabling the NP to maintain height and turgor against compressive loads (Watanabe et al. 1998; Adams and Roughley 2006; Setton and Chen 2006). The NP contains two distinct cell types: large clusters of notochordal cells and smaller, more disperse cartilage-like cells (Roberts 2002). Interestingly, the loss of notochordal cells is associated with the onset of disc degeneration, suggesting that these cells are required for the maintenance of the NP (Aguiar et al. 1999; Boos et al. 2002; Hunter et al. 2003).

Although the role of the notochord during gastrulation has been extensively studied (Beddington and Robertson 1999), the function of the notochord during IVD formation remains relatively unknown. In the early mouse embryo, the node is formed at embryonic day (E) 7.5, and is the source of cells that will form the rod-like structure of the notochord (Yamanaka et al. 2007). The notochord is an important source of signals for patterning of the developing embryo, specifically axis determination in both dorsal/ventral and left/right planes (Johnson et al. 1994; Beddington and Robertson 1999; Beckers et al. 2007). The vertebral column is formed by aggregation of the somatic mesenchyme around the notochord, forming a continuous perichordal tube that undergoes segmentation at E13.5 forming condensed and non-condensed regions that give rise to the vertebrae and IVDs, respectively (Dagleish 1985; Urban et al. 2000). Within the IVD, notochordal cells proliferate and accumulate a gelatinous, glycosaminoglycan-rich extracellular matrix, which separates the original cell mass into a network of small cell

clusters. The NP becomes surrounded by the mesenchyme-derived AF (Christ and Wilting 1992; Eloy-Trinquet and Nicolas 2002) (**Figure 2.1**).

Beginning as early as the second decade of life in humans, notochordal cells are no longer detected within the NP, which is populated instead by smaller more dispersed cartilage-like cells (Chelberg et al. 1995; Zhou et al. 2008). Currently, identification of these two cell types is restricted to cell morphology and a limited number of notochord-specific markers (Fujita et al. 2005; Gilson et al. 2010; Minogue et al. 2010). There have historically been two conflicting hypotheses regarding the origin of the cartilage-like cells of the NP. It was originally suggested that these cells were of mesenchymal origin, a consequence of migration of cells to the NP from the surrounding CEP (Vujovic et al. 2006). During tissue formation, notochordal cells were believed to direct mesenchymal cell migration, stimulate matrix synthesis, and upon completion of their role undergo apoptosis or necrosis (Trout et al. 1982; Kim et al. 2003). Alternatively, it has been suggested that notochordal cells are progenitors for all NP cells, and undergo terminal differentiation to give rise to chondrocyte-like cells (Pazzaglia et al. 1989; Boos et al. 2002; Liebscher et al. 2010). In these two scenarios notochordal cells play distinct roles, that of organizer and tissue-specific progenitor, respectively. Recent studies sought to address this long-standing debate on the fate of notochord cells following spine formation until fate mapping using the *Shh-Cre* determined that all cells of the NP were derived from the notochord (Choi et al. 2008).

To clearly define the developmental origins of the NP, we have targeted the gene encoding the notochord-specific transcription factor *Noto*, to generate a mouse line expressing Cre recombinase specifically in the notochord. *Noto* is a highly conserved

homeobox transcription factor whose expression is restricted to the organizer node and the nascent notochord during gastrulation and axis elongation (E7.5-12.5) where it regulates node morphogenesis, notochord ciliogenesis, and left–right patterning (**Figure 2.1 A, B**) (Abdelkhalek et al. 2004; Yamanaka et al. 2007; Zizic Mitrecic et al. 2010). Expression of *Noto* is detected at E7.5 within the ventral node with the onset of primitive streak formation. Between E8.0 and E9.0, *Noto* is expressed in the node and newly formed notochord but not in the anterior node or mature notochord. *Noto* expression is restricted to the notochordal plate and posterior notochord until E12.5, after which its expression is no longer detected (Abdelkhalek et al. 2004). Using this novel notochord-specific Cre mouse, we show evidence that all cells present within the NP, from tissue formation through to skeletal maturity, are of notochord origin.

2.4 Materials and Methods

2.4.1 Generation of the Notochord-Specific *Noto-Cre* Mouse Strain

All experiments were performed under Institutional Animal Care and Use Committee guidelines at The University of Western Ontario and Toronto Centre for Phenogenomics. To generate the *Noto-Cre* knock-in mouse, the *Noto* targeting vector was amplified using long-range polymerase chain reaction (PCR) (Roche HiFi Taq polymerase) from a BAC clone that contained the *Noto* locus (RP23-417O15; library derived from female C57BL/6J tissues). PCR primers added EcoR1 and Not1 sites to the 5' and 3' homology arms, respectively (sequence provided in **Table 2.1**). The 3'

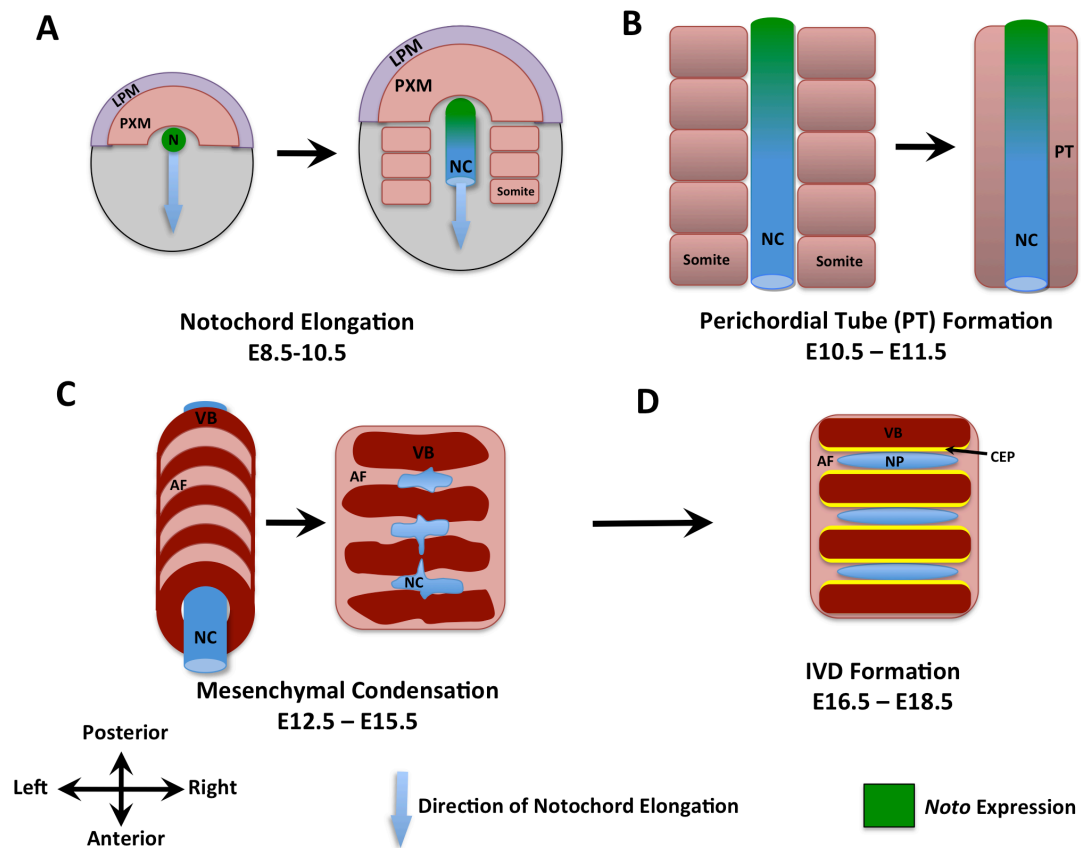


Figure 2.1 Schematic representation of the main stages in axial skeletogenesis.

A. Formation of the node and elongation of the notochord. **B.** Aggregation of the somatic mesenchyme around the notochord leads to formation of a continuous perichordal tube. Localization of *Noto* expression at these time points is indicated in green. **C.** Condensation of the axial mesenchyme leads to spine segmentation and perichordal disc formation. **D.** Formation of intervertebral discs is associated with disappearance of the notochord within the vertebral bodies, and its expansion within the IVD. AF = annulus fibrosis; CEP = cartilage end-plates; E = embryonic day; IVD = intervertebral disc; LPM = Lateral Plate Mesoderm; N = node; NC = notochord; NP = nucleus pulposus; PT = perichordal tube; PXM = Paraxial Mesoderm; Som = somites; VB = vertebral bodies.

homology arm PCR product (~3kb) was ligated into a pICN vector, and confirmed by restriction digest and sequencing. The pICN vector contains an IRES-NLS-CRE cassette (generously provided by Dr. Andras Nagy) arranged as follows: EcoR1-IRES-NLS-CRE-FRT-PGK-NEO-FRT-Not1/Sac1. The 5' homology arm PCR product (~5 kb) was digested with EcoR1, ligated into the pICN-*Noto*-3' vector, and confirmed by restriction digest and sequencing.

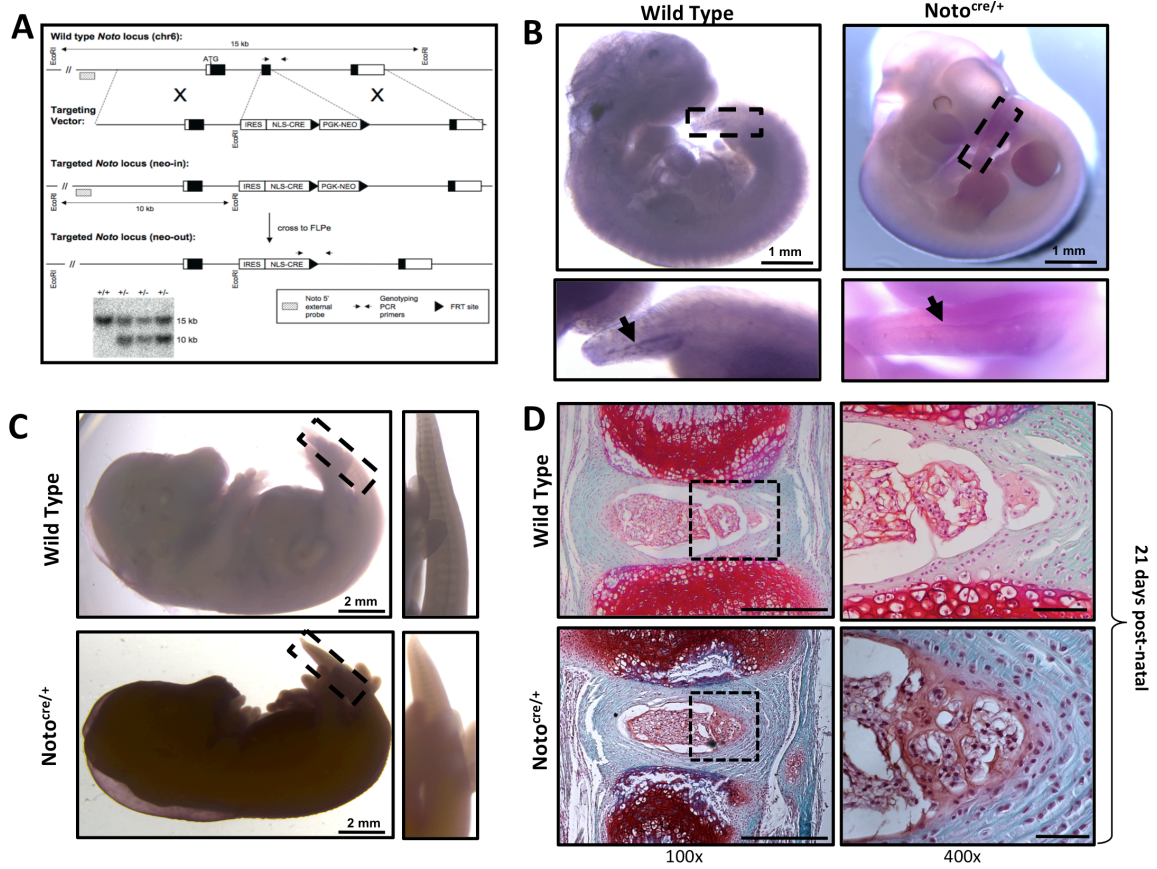
The final p*Noto*-5'-ICN-*Noto*-3' plasmid was linearized and electroporated in G4 ES cells (George et al. 2007) using standard protocols. After neomycin selection, ~170 colonies were screened by Southern blot. A 5' external probe was isolated from a plasmid generously shared by Anja Beckers and Achim Gossler (Abdelkhalek et al. 2004) and used to confirm positively targeted clones (**Figure 2.2 A**). Ten of ~120 clones were positive, giving a targeting efficiency of ~8%. Two independent positive ES cell clones were used to produce founder chimeras. Both clones produced chimeras and were crossed to CD1 (ICR) for germline transmission. Positive F1 mice were confirmed by Southern blot, and crossed to FLPe deleter strain (MGI Strain: B6;SJL-Tg(ACTFLPe)9205Dym/J) for recombination between FRT sites and removal of PGK-NEO.

2.4.2 Genotyping of Mice

Mice were genotyped by PCR analysis using tail DNA samples and *Noto-Cre* knock-in was confirmed by PCR genotyping using the *Noto* wild type (WT) and “neo-

Figure 2.2 Generation of notochord-specific Cre mouse line.

A. Targeting strategy used to generate the *Noto*^{Cre} line. An internal ribosome entry site-nuclear localization signal-cre recombinase (IRES-NLS-CRE) cassette replaced exon 2 of the *Noto* locus. Positively targeted ES cell clones were confirmed by Southern blot using an external 5' probe; the wild type allele is 15 kb and the targeted allele is 10 kb. Representative positive “neo-in” clones are shown. The positions of genotyping PCR primers for wild type and “neo-out” mice are also shown. **B.** Targeting of the *Noto*-locus does not affect its temporal regulation, as demonstrated by whole mount *in situ* hybridization at E11.5. *Noto* expression is detected in both *Noto*^{Cre/+} and wild type (*Noto*^{+/+}) littermate control embryos, localized to the posterior node in the tail region (insert and arrows). **C.** *Noto* expression is down-regulated after E12.5, confirmed by *in situ* hybridization at E15.5 showing no detectable *Noto* expression. **D.** Heterozygous inactivation of *Noto* does not disrupt notochord formation or IVD development. IVD formation and tissue architecture was examined in *Noto*^{Cre/+} mice and wild type (*Noto*^{+/+}) littermate controls using Safranin-O/fast green staining on paraffin embedded sections at postnatal day 30. Enlarged view of the nucleus pulposus and inner annulus fibrosus tissues are shown in right hand box. Scale bars = 500µm for 100x images and 50µm for 400x images.



out” primers (location indicated in **Figure 2.2 A**; sequences provided in **Table 2.1**). WT primers produce a 329 bp band and ‘neo-out’ primers produce a 415 bp band using the PCR program: for denaturing, 98°C for 30 seconds; for annealing, 60°C for 30 seconds; for extension, 72°C for 30 seconds for 39 cycles. Targeting of the ROSA26 locus in the conditional *LacZ* reporter mice, Gt(ROSA)26Sor^{tm1sor} was confirmed by genotyping using previously characterized primers (Soriano 1999) (**Table 2.1**). WT primers produce a 650 bp band and primers specific for the targeted locus produce a 340 bp band using the PCR conditions: for denaturing, 94°C for 30 sec; for annealing, 62°C for 60 sec; for extension, 72°C for 60 sec for 34 cycles.

2.4.3 Whole Mount *In Situ* Hybridization

Whole-mount *in situ* hybridization on E11.5 and E15.5 embryos was performed as previously described (Lickert et al. 2002). Briefly, embryos were fixed at the time of collection in 4% paraformaldehyde overnight at 4°C. For hybridization, embryos were rehydrated through a MeOH/PBT (PBS plus 0.1% Tween-20) (Sigma-Aldrich, St. Louis, MO, USA) series into PBT and incubated with proteinase K (10 µg/ml in PBT) for 8 min at room temperature. Digestion was stopped by washing with 2 mg/ml glycine in PBT, and embryos were postfixed in 4% paraformaldehyde with 0.2% glutaraldehyde in PBT, washed in PBT, and hybridized overnight at 70°C with 1 µg/ml of digoxigenin-labeled

Primer Name	Primer Sequence 5' → 3'
Noto 3' arm NotI FWD	GGGCGGCCCGGTGAGAGCAGGGACGAGGCTCAG
Noto 3' arm NotI REV	GGGCGGCCCGCTTAATTAAAGAGGGTCAGGAATCCAAAGTCATCC
Noto 5' arm EcoRI FWD	GGGAATTTCGGCCTGGAAC TCACTCTGTAGATCA
Noto 5' arm EcoRI REV	GGGAATTCTCTAAAGAGAAACCAAGAGCAACTTCAG
Noto WT FWD	GCTGCAAGAGTTGGAGAAAGG
Noto WT REV	ATGCACATATGCAACCCACA
Noto-Cre FWD	ATACCGGCAGATCATGCAAGC
Common Noto WT REV	*Same as Noto WT REV*
ROSA26 LacZ WT FWD	AAAGTCGCTCTGAGTTGTTAT
ROSA26 LacZ WT REV	GGAGCGGGAGAAATGGATATG
ROSA26 LacZ Mutant FWD	GCGAAGAGTTTGTCTCTCAACC
Common ROSA26 LacZ WT REV	*Same as ROSA26 LacZ WT REV*

riboprobe (Roche) in hybridization solution (50% formamide, 5× SSC [pH 4.5], 1% SDS, 50 µg/ml yeast tRNA, and 50 µg/ml heparin). Embryos were washed three times in hybridization solution for 30 min at 70°C, rinsed three times in TNT (10 mM Tris-HCl [pH 7.5], 0.5 M NaCl, and 0.1% Tween-20) for 5 min each at room temperature, and incubated for 1 hr with 100 µg/ml RNase A in TNT. After three washes in 50% formamide, 2× SSC (pH 4.5), 0.5 M NaCl, and 0.1% Tween-20 for 30 min at 65°C, followed by three washes in MAB (100 mM maleic acid [pH 7.5], 150 mM NaCl, 2 mM levamisole, and 0.1% Tween-20) for 5 min at room temperature, samples were blocked for 2 hr in 10% sheep serum in MAB/2% Roche blocking agent. Embryos were incubated overnight at 4°C with anti-digoxigenin alkaline phosphatase-coupled antibody (1:5000 diluted in MAB/2% Roche block/1% sheep serum plus 0.5 mg/ml mouse embryo powder). Following MAB washes, the embryos were washed three times in NTMT (100 mM Tris-HCl [pH 9.5], 50 mM MgCl₂, 100 mM NaCl, and 0.1% Tween-20) for 5 min each, and stained with BM purple (Roche) at room temperature. Gene expression patterns are representative of 3 or more stage-matched embryos. Imaging was done on a Leica stereo light microscope with Photon Technology International (London, ON, Can.) software.

2.4.4 Lineage Tracing and β -galactosidase Staining

Noto^{Cre/+} mice were mated with ROSA26 conditional *LacZ* reporter mice, Gt(ROSA)26Sor^{tm1sor} (Jackson Labs, Bar Harbor, ME, USA) which produces lacZ upon

Cre mediated excision of STOP sequence upstream of β -galactosidase. For timed matings, insemination was confirmed by vaginal sperm plug morning after coitus, which was counted as embryonic day 0.5. Pregnant females were sacrificed at stated embryonic time points. Genotypic analysis of embryos was done by PCR of DNA extract, using primer sets indicated in **Table 2.1**. Whole-mount β -galactosidase staining was carried out using standard protocols (Hogan 1994). Briefly, embryos were fixed for 30 min ($E < 13.5$) or 2 hr ($E > 13.5$) in 0.2% glutaraldehyde/1% formaldehyde/0.02% Nonidet P-40 in Phosphate Buffered Saline (PBS) at room temperature. Following 3 washes in PBS (10 min at room temperature), the embryos were incubated in X-gal staining solution [5 mM $K_3Fe(CN)_6$ /5 mM $K_4Fe(CN)_6$ /2 mM $MgCl_2$ /1 mg/ml X-gal in PBS] overnight at room temperature on a rocker. Embryos were then washed with PBS 3 x 10 min at room temperature and kept in PBS overnight to allow stain to develop. Whole mount embryos were imaged with a Nikon SMZ 1500 stereo microscope.

For visualization of β -galactosidase staining in embryos $>E15$, a clearing step was performed as previously described (Schatz et al. 2005). Briefly, following β -galactosidase staining embryos were cleared by a series of solutions containing decreasing potassium hydroxide and increasing glycerol concentrations; 100/0, 80/20, 50/50, 20/80 and 0/100% respectively, for 3 days each.

For analysis at postnatal day 100, spine microdissection was necessary to allow for adequate stain penetration. Following β -galactosidase staining as outlined above, tissues were post-fixed in 4% formaldehyde overnight at room temperature, embedded in

OCT (VWR, Mississauga, ON, Can.) and sagittal sections were cut at a thickness of 10 μm .

2.4.5 Histology

Whole embryos or postnatal spinal columns were isolated at indicated stages and fixed in 4% paraformaldehyde overnight at 4°C, dehydrated in a graded series of ethanol, cleared in xylene, and embedded in paraffin. Serial sections of paraffin-embedded samples sectioned sagittally at a thickness of 5 μm were stained with 0.1% Safranin-O, 0.02% fast green or Harris' hematoxylin (Sigma-Aldrich) and Eosin-Y (Sigma-Aldrich).

2.4.6 Immunohistochemistry

Paraffin-embedded sections were cut at a thickness of 5 μm using a microtome (Leica Microsystems, Concord, ON, Can.) and collected on Superfrost Plus slides (Fisher Scientific, Ottawa, ON, Can.). Sections were then de-waxed in xylene and rehydrated by successive immersion in descending concentrations of alcohol. Samples were blocked for non-specific binding by incubating sections with the corresponding species-specific serum albumin (1%) in PBS with 0.1% Tween-20 (Sigma-Aldrich) for 1 hr and then incubated with primary antibody directed against β -galactosidase (Abcam 1:500) and cytokeratin-8 (Abcam 1:200) and in a humidified chamber overnight at 4°C. After washes with PBST and incubation of goat anti-rabbit FITC and goat anti-mouse Texas Red (Jackson ImmunoResearch Laboratories Inc., West Grove, PA, USA., 1:500) for 90 min, mounting was done with Vectorasheild Mounting Medium with DAPI (Vector Labs, Burlingame,

CA, USA). Images were captured with a Leica DMRA2 fluorescence microscope and processed with Northern Eclipse (Empix, Mississauga, ON, Can.) software.

2.5 Results

2.5.1 Generation of the *Noto-Cre* Mouse Line

The *Noto-Cre* allele was created by knocking the site-specific recombinase gene *Cre* into exon 2 of the *Noto* locus (Figure 2A). Using this strategy, *Cre* is expressed in all *Noto*-expressing cells, specifically the node and posterior notochord between E7.5 and E12.5 (Yamanaka et al. 2007), and all of their descendants. To ensure that the temporal regulation of *Noto* expression was not altered in our transgenic strain, *in situ* hybridization was preformed. In both *Noto*^{Cre/+} and wild type littermate controls (*Noto*^{+/+}), *Noto* expression was detected in the posterior notochord at E11.5 (**Figure 2.2 B**) and was undetectable by E15.5 (**Figure 2.2 C**).

Previous studies demonstrated that homozygous disruption of the *Noto* gene leads to embryonic or early postnatal lethality, but heterozygous animals are viable with no reported phenotype (Abdelkhalek et al. 2004; Beckers et al. 2007; Yamanaka et al. 2007). To ensure that heterozygous inactivation of *Noto* did not alter notochord formation or IVD development spine segments from *Noto*^{Cre/+} mice were assessed by histology at postnatal day 21 and compared to wild type littermate controls (*Noto*^{+/+}). Examination of tissue architecture and joint formation by Safranin-O/fast green staining demonstrated no alterations in notochord structures or intervertebral disc formation in *Noto*^{Cre/+} mice

(**Figure 2.2 D**). Therefore all subsequent studies were conducted using the heterozygous *Noto*^{Cre/+} to interrogate intervertebral disc formation.

2.5.2 Tracing Notochord-derived Cells in the Embryonic Mouse

Through mating with the conditional R26LacZ reporter (Gt(ROSA)26Sor^{tm1so}) (Soriano 1999) fate mapping studies were conducted. Embryos carrying both the *Noto*^{Cre} allele and the R26LacZ reporter showed specific β -galactosidase expression in a subset of node and notochordal cells at E8.0, the stage at which the node is reported to undergo elongation to form the notochord (**Figure 2.3 A,B**). The mouse notochord has previously been reported to form in a non-sequential pattern with multiple organizing centers (Yamanaka et al. 2007). A discontinuous pattern of *Noto* expression was observed at E8.5, where different centers of notochord formation were seen along the rostral-caudal axis (**Figure 2.3 C,D**). These centers ultimately connected to form the solid rod-like notochord by E10.5 (**Figure 2.3 E,F**).

The segmentation of the notochord can be seen at E15.5 and E17.5 (**Figure 2.3 G-M**). Due to opacity of embryos at these later developmental stages, the staining protocol was modified to include an embryo clearing step that renders the embryo translucent while leaving the β -galactosidase stain intact (Schatz et al. 2005). β -galactosidase expression within the IVD was observed in the upper thoracic region of embryo, flanked by developing vertebrae (**Figure 2.3 L**). The formation of the nucleus pulposus through notochord condensation and segmentation was seen throughout the embryonic time

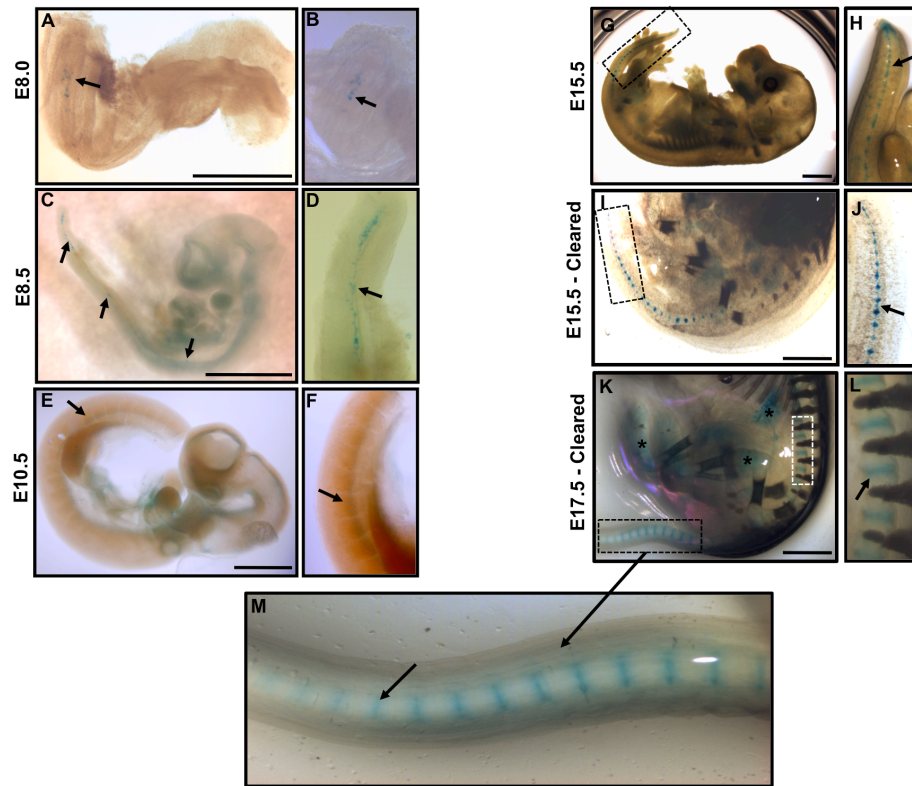


Figure 2.3 Whole mount examination of β -galactosidase staining in *Noto*^{Cre/+}; *R26*^{R/+} embryos.

A-M. Staining pattern of β -galactosidase, demonstrating the localization of notochord-derived cells throughout embryonic development (stages indicated). Higher magnification view of β -galactosidase expression at each respective time point is presented in panels to the right. **I-M.** β -galactosidase expression in E15.5 and E17.5 embryos, rendered clear to enable tissue visualization, demonstrate staining within intervertebral discs in the developing spine. Arrows denotes positive staining in the intervertebral disc. Asterisks (*) indicate non-specific background staining; specificity of Cre expression was confirmed by comparing background staining in *Noto*^{+/+} littermate controls (data not shown). Scale bars = 1 millimeter.

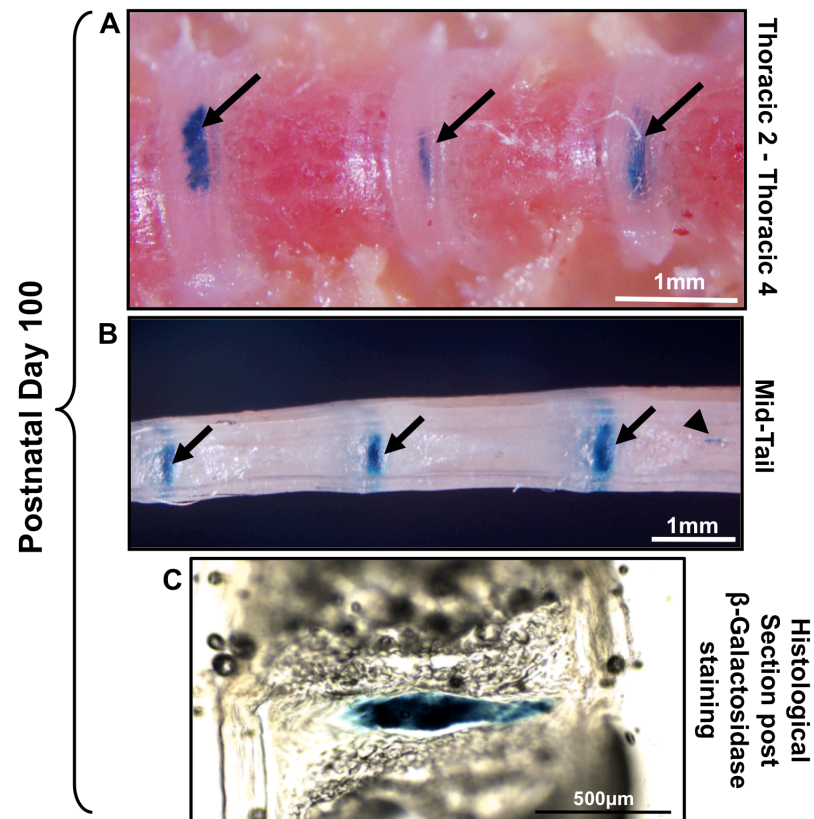


Figure 2.4 β-galactosidase staining at postnatal timepoints in *Noto^{Cre/+};R26^{R/+}* mice.

A, B. P100 skeletally mature murine spine; β-galactosidase staining was present from the tail to the upper thoracic spine. **C.** At P100, β-galactosidase staining was evident throughout the nucleus pulposus while the annulus fibrosus was negative. Representative 30-μm sagittal cyrosection of an intervertebral disc stained for LacZ is shown (Originally from tail region in B).

points, originating caudally and proceeding rostrally. This was evident in the tail region at E15.5, where the nuclei pulposi remain connected via the remaining notochord (**Figure 2.3 J, arrow**).

2.5.3 Lineage Tracing the Cells of the Adult Nucleus Pulposus

At postnatal timepoints, β -galactosidase expression was detected throughout the thoracic spine to caudal tip of the tail (**Figure 2.4**). Small clusters of notochordal cells were detected that were not incorporated into the nucleus pulposus of the intervertebral disc but appeared instead to form notochord remnants (also known as intraosseous benign notochordal cell tumors) within the vertebral bone (**Figure 2.4 B**). These notochord remnants were indiscriminately localized throughout the spine at postnatal time points, and were present in >90% of spines examined. In order to more accurately localize β -galactosidase expression to specific cellular components of the intervertebral disc, tissues were examined by histology. Cryosections were performed on skeletally mature mice (postnatal day 100) in order to preserve β -galactosidase staining. β -galactosidase was localized specifically to the nucleus pulposus, with no stain present in the surrounding annulus fibrosus or cartilage end plates (**Figure 2.4 C**).

To examine β -galactosidase expression within specific cell types of the nucleus pulposus, paraffin-embedded intervertebral disc samples were examined by immunohistochemistry for expression of β -galactosidase and cytokeratin-8, a commonly used marker of notochordal cells (Gilson et al. 2010) (**Figure 2.5**). Within the newly

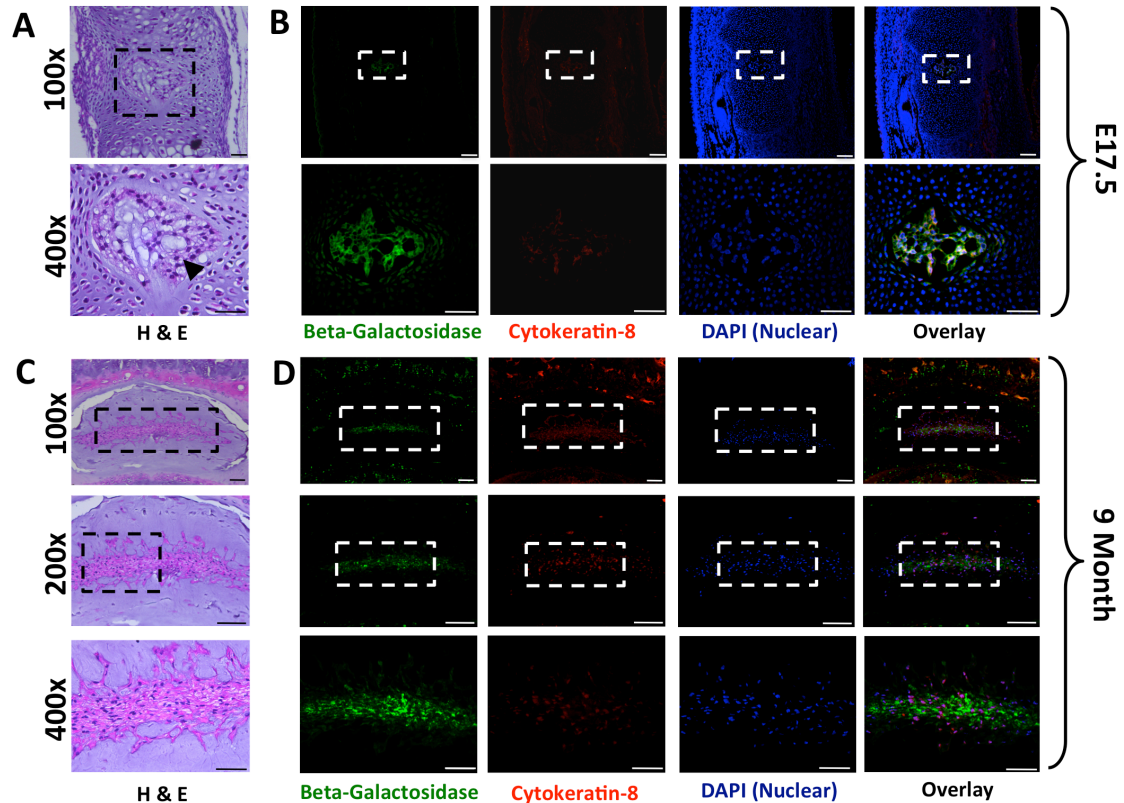


Figure 2.5 Co-localization of β -galactosidase and cytokeratin-8 in the nucleus pulposus.

A. Representative Hematoxylin and Eosin stained sections of intervertebral discs at E17.5 (tail region). Cells within the nucleus pulposus demonstrate characteristic physaliferous morphology associated with notochordal cells (*arrowhead*), and are surrounded by embryonic mesenchyme. **B.** Immunolocalization of β -galactosidase (green) and cytokeratin-8 (red) expression. No cytokeratin-8 negative cells were detected at this stage, suggesting that all cells maintain a notochord phenotype. Lower panels are a magnified view of each respective panel above. **C.** Representative Hematoxylin and Eosin stained sections of a 9 month old mouse lumbar disc demonstrates the heterogeneous cellular composition of the mature nucleus pulposus. **D.** Co-localization of β -galactosidase (green) and cytokeratin-8 (red) in serial sections demonstrates that while all cells are β -galactosidase positive, only a subset of cells maintain cytokeratin-8 expression. (100x, 200x and 400x scale bars are 100 μ m, 100 μ m and 50 μ m respectively).

formed intervertebral disc (E 15.5), cells demonstrated a physaliferous appearance characteristic of notochordal cells and expressed both β -galactosidase and cytokeratin-8 (**Figure 2.5 A,B**). In postnatal life, the nucleus pulposus undergoes a dramatic change in cellular composition and becomes progressively populated by cartilage-like NP cells which appear smaller in size than notochordal cells and are surrounded by pericellular extracellular matrix (**Figure 2.5 C**). We therefore examined the nucleus pulposus at 9 months to determine the contribution of the notochord to this heterogeneous population. At this stage, all cells were positive for β -galactosidase, while only a subset of cells maintained cytokeratin-8 co-localization (**Figure 2.5 D**). The detection of β -galactosidase in the chondrocyte-like NP cells demonstrated that they are derived from the embryonic notochord.

2.6 Discussion

Our ability to demonstrate the fate and function of notochord cells within the IVD has thus far been limited. A key tool for understanding cell function in model organisms is the Cre/loxP system for conditional mutagenesis (Lewandoski 2001). This approach can be extremely informative when carefully selected Cre recombinase lines are paired with loxP-flanked conditional reporter genes. While notochord-expressing Cre mouse lines have been generated using elements from the *Foxa2* and *Nodal* genes, Cre expression was also detected in the ventral neural tube, or floor plate, and the definitive endoderm (Stein and Kessel 1995; Uetzmann et al. 2008). In contrast, expression of the

homeobox gene *Noto* is restricted to the node and the posterior notochord during gastrulation (E7.5-12.5) and is not detected in the notochord or derivative structures after this stage (von Dassow et al. 1993; Stein and Kessel 1995; Talbot et al. 1995). Furthermore, *Noto* GFP knock-in permitted analysis of notochord formation and morphogenesis during gastrulation (Yamanaka et al. 2007). We therefore targeted the *Noto* locus to generate a Cre knockin mouse (*Noto*^{Cre/+}) and provide considerable evidence that the notochord acts as the embryonic precursor of all the cells found within the mature nucleus pulposus. We demonstrate that all cells within the NP, both the large notochordal cells as well as the smaller chondrocyte-like NP cells are of notochordal origin.

Our results are consistent with a previous study by Choi and colleagues that used an inducible *Shh-Cre*^{ERT2} system to mark the notochord during development (Choi et al. 2008). The *Shh-Cre*^{ERT2} system does have certain limitations; for example, *Shh* is expressed in the notochord as well as many other cell types in the early embryo (Bouldin et al. ; Miller et al. 2001), making it difficult to definitively track lineages at later stages. Also, the tamoxifen injected into pregnant mice for induction of *Cre*^{ERT2} *in utero* can persist for up to 48 hours, which could potentially lead to Cre induction in any *Shh*-expressing cells during that time window. Our model demonstrates that *Noto*-expressing notochordal cells give rise to all cells within the mature NP. Consistent with these findings, recent studies examining the gene expression profile of specific IVD cell populations in bovine samples reported a common gene expression signature in notochordal and NP cells that was not detected in articular chondrocytes (including *T*,

KRT8, *KRT18* and *KRT19*) and suggested this resulted from a common lineage (Minogue et al. 2010). Furthermore, studies using rabbit-derived cells demonstrated the ability of notochordal cells to undergo directed *in vitro* differentiation producing cells morphologically and phenotypically similar to chondrocyte-like NP cells (Kim et al. 2009).

Initially, the *floating head* (*flh*) gene was identified in zebrafish and was found to encode a homeodomain protein that was essential for notochord formation along the body axis (Talbot et al. 1995). Orthologs of *flh* were found in *Xenopus* and chicks and were named *Not* genes. The mammalian equivalent was identified with the report of an autosomal recessive mutation in mice that disrupted development of the caudal notochord (Abdelkhalek et al. 2004). The *Not* gene was renamed *Noto* in mammals and has been shown to be involved in axis patterning, notochord ciliogenesis, node and tail bud morphogenesis (Beckers et al. 2007; Mitrecic et al. 2010). It was the highly specific nature of *Noto* that made it an ideal tool to track the notochord, and it is for that reason that we generated a the *Noto*^{Cre/+} mouse. Given that the *Noto* transcript is detected only in the node and posterior notochord (Yamanaka et al. 2007), we initially suspected that *Noto-Cre* expression was going to be limited to the posterior region of the spine. Our results however show that *Noto-Cre* is detected in the tail but also throughout the axial spine to the upper thoracic region, thereby demonstrating the potential of this novel mouse to explore the phenotype and function of notochordal cells during development and in postnatal life, including notochord-specific targeted gene disruption.

Upon mating the *Noto*^{Cre/+} with the conditional ROSA LacZ reporter mouse, these studies have traced cells of notochord origin during the dynamic process of notochord formation, elongation, condensation and eventual formation of the NP within the IVD. We demonstrate that notochord segmentation and NP formation proceeds in the rostral to caudal direction, as can be seen in the tail region of E15.5 and E17.5. At these stages, notochord-derived cells are localized within fully formed intervertebral discs in the thoracic region, while in the tail the notochord remains connected to the condensed regions that will form the NP.

Interestingly, during the early stage of notochord formation and elongation (E8.0) *Cre* expression did not appear to be uniform throughout the notochord, and was instead detected in distinct cell clusters/centers. This heterogeneous pattern of notochord formation has previously been reported using *Noto*-driven reporters (i.e. *Noto*^{eGFP} (Abdelkhalek et al. 2004; Yamanaka et al. 2007)) as well as other node and notochord enhancer transgenics (Nishizaki et al. 2001; Sawada et al. 2005). In the current study, this patchy expression was however resolved at later stages of development (E17.5) when β -galactosidase expression was detected throughout the notochord, suggesting that the heterogeneous nature of the early notochord is not an artifact of our system. We suggest instead that the heterogeneity often observed in the notochord is biologically significant. It may be that mesodermal cells can be incorporated into the notochord and then differentiate via interaction with their neighbors. This has been observed in transplantation of zebrafish *Noto/floating head* mutant cells to wild type hosts—these cells lack a gene critical for notochord formation, yet they can still incorporate and

contribute to notochord (Amacher and Kimmel 1998). Future studies will be needed to determine the exact cause of heterogeneous expression in various notochord transgenic lines.

Speculations regarding the developmental origins of the heterogeneous population of cells that constitute the mature NP have argued that the cartilage-like cells originate either from the notochord, or from the surrounding mesenchyme following migration of cells to the nucleus pulposus from the adjacent CEP or inner AF. We present evidence that notochordal cells are the precursor cells of the NP, and undergo differentiation to generate chondrocyte-like cells during postnatal development. This transition may be induced by a variety of factors present in the extracellular environment of the intervertebral disc. Most notably, with aging the nutrient supply to the already avascular and hypoxic intervertebral disc becomes increasingly limited due to calcification of the endplates (Urban et al. 2004). The resulting changes in oxygen, glucose and lactic acid concentration within the NP may contribute to terminal notochordal cell differentiation to chondrocyte-like cells.

The lack of effective biological treatment for the widespread clinical problem of IVD degeneration is directly related to our limited understanding of the mechanisms regulating the processes of disc development, maintenance and degeneration. This gap in our knowledge is due to an incomplete understanding of the specific phenotypes of IVD cell types and the relative importance of the individual growth factors, secreted molecules and matrix components that constitute the unique extracellular environment of the IVD. Given its role in maintaining the physiological function of the IVD, a more complete

understanding of notochord and NP biology is of vital importance. The described notochord-specific Cre mouse model will be a valuable tool in future studies to interrogate the function of candidate regulatory molecules in during the processes of IVD development, homeostasis and degeneration with the eventual goal of identifying candidate biological treatments for disc degeneration.

In summary, this report provides evidence demonstrating the notochord origin of all cells within the NP and demonstrates the potential of the Noto^{cre/+} mouse in understanding IVD biology.

2.6 References

- Abdelkhalek HB, Beckers A, Schuster-Gossler K, Pavlova MN, Burkhardt H, Lickert H, Rossant J, Reinhardt R, Schalkwyk LC, Muller I et al. 2004. The mouse homeobox gene Not is required for caudal notochord development and affected by the truncate mutation. *Genes Dev* **18**: 1725-1736.
- Adams MA, Roughley PJ. 2006. What is intervertebral disc degeneration, and what causes it? *Spine (Phila Pa 1976)* **31**: 2151-2161.
- Aguiar DJ, Johnson SL, Oegema TR. 1999. Notochordal cells interact with nucleus pulposus cells: regulation of proteoglycan synthesis. *Exp Cell Res* **246**: 129-137.
- Amacher SL, Kimmel CB. 1998. Promoting notochord fate and repressing muscle development in zebrafish axial mesoderm. *Development* **125**: 1397-1406.
- Battie MC, Videman T. 2006. Lumbar disc degeneration: epidemiology and genetics. *J Bone Joint Surg Am* **88 Suppl 2**: 3-9.
- Beckers A, Alten L, Viebahn C, Andre P, Gossler A. 2007. The mouse homeobox gene Noto regulates node morphogenesis, notochordal ciliogenesis, and left right patterning. *Proc Natl Acad Sci U S A* **104**: 15765-15770.

- Beddington RS, Robertson EJ. 1999. Axis development and early asymmetry in mammals. *Cell* **96**: 195-209.
- Boos N, Weissbach S, Rohrbach H, Weiler C, Spratt KF, Nerlich AG. 2002. Classification of age-related changes in lumbar intervertebral discs: 2002 Volvo Award in basic science. *Spine (Phila Pa 1976)* **27**: 2631-2644.
- Bouldin CM, Gritli-Linde A, Ahn S, Harfe BD. Shh pathway activation is present and required within the vertebrate limb bud apical ectodermal ridge for normal autopod patterning. *Proc Natl Acad Sci U S A* **107**: 5489-5494.
- Chelberg MK, Banks GM, Geiger DF, Oegema TR, Jr. 1995. Identification of heterogeneous cell populations in normal human intervertebral disc. *J Anat* **186** (Pt 1): 43-53.
- Choi KS, Cohn MJ, Harfe BD. 2008. Identification of nucleus pulposus precursor cells and notochordal remnants in the mouse: implications for disk degeneration and chordoma formation. *Dev Dyn* **237**: 3953-3958.
- Christ B, Wilting J. 1992. From somites to vertebral column. *Ann Anat* **174**: 23-32.
- Dalgleish AE. 1985. A study of the development of thoracic vertebrae in the mouse assisted by autoradiography. *Acta Anat (Basel)* **122**: 91-98.
- Eloy-Trinquet S, Nicolas JF. 2002. Clonal separation and regionalisation during formation of the medial and lateral myotomes in the mouse embryo. *Development* **129**: 111-122.
- Fujita N, Miyamoto T, Imai J, Hosogane N, Suzuki T, Yagi M, Morita K, Ninomiya K, Miyamoto K, Takaishi H et al. 2005. CD24 is expressed specifically in the nucleus pulposus of intervertebral discs. *Biochem Biophys Res Commun* **338**: 1890-1896.
- George SH, Gertsenstein M, Vintersten K, Korets-Smith E, Murphy J, Stevens ME, Haigh JJ, Nagy A. 2007. Developmental and adult phenotyping directly from mutant embryonic stem cells. *Proc Natl Acad Sci U S A* **104**: 4455-4460.
- Gilson A, Dreger M, Urban JP. 2010. Differential expression level of cytokeratin 8 in cells of the bovine nucleus pulposus complicates the search for specific intervertebral disc cell markers. *Arthritis Res Ther* **12**: R24.
- Goetzel RZ, Hawkins K, Ozminkowski RJ, Wang S. 2003. The health and productivity cost burden of the "top 10" physical and mental health conditions affecting six large U.S. employers in 1999. *J Occup Environ Med* **45**: 5-14.

- Hogan B, Beddington, Rosa., Costantini, Frank. & Lacey, Elizabeth. 1994. Manipulating the Mouse Embryo: A Laboratory Manual 2nd edn. . *Cold Spring Harbor Press, New York*.
- Hunter CJ, Matyas JR, Duncan NA. 2003. The notochordal cell in the nucleus pulposus: a review in the context of tissue engineering. *Tissue Eng* **9**: 667-677.
- Johnson RL, Laufer E, Riddle RD, Tabin C. 1994. Ectopic expression of Sonic hedgehog alters dorsal-ventral patterning of somites. *Cell* **79**: 1165-1173.
- Kawaguchi Y, Osada R, Kanamori M, Ishihara H, Ohmori K, Matsui H, Kimura T. 1999. Association between an aggrecan gene polymorphism and lumbar disc degeneration. *Spine (Phila Pa 1976)* **24**: 2456-2460.
- Kim JH, Deasy BM, Seo HY, Studer RK, Vo NV, Georgescu HI, Sowa GA, Kang JD. 2009. Differentiation of intervertebral notochordal cells through live automated cell imaging system in vitro. *Spine (Phila Pa 1976)* **34**: 2486-2493.
- Kim KW, Lim TH, Kim JG, Jeong ST, Masuda K, An HS. 2003. The origin of chondrocytes in the nucleus pulposus and histologic findings associated with the transition of a notochordal nucleus pulposus to a fibrocartilaginous nucleus pulposus in intact rabbit intervertebral discs. *Spine (Phila Pa 1976)* **28**: 982-990.
- Lewandoski M. 2001. Conditional control of gene expression in the mouse. *Nature reviews* **2**: 743-755.
- Lickert H, Kutsch S, Kanzler B, Tamai Y, Taketo MM, Kemler R. 2002. Formation of multiple hearts in mice following deletion of beta-catenin in the embryonic endoderm. *Dev Cell* **3**: 171-181.
- Liebscher T, Haefeli M, Wuertz K, Nerlich AG, Boos N. 2010. Age-related variation in cell density of human lumbar intervertebral disc. *Spine (Phila Pa 1976)* **36**: 153-159.
- Miller LA, Wert SE, Whitsett JA. 2001. Immunolocalization of sonic hedgehog (Shh) in developing mouse lung. *J Histochem Cytochem* **49**: 1593-1604.
- Minogue BM, Richardson SM, Zeef LA, Freemont AJ, Hoyland JA. 2010. Transcriptional profiling of bovine intervertebral disc cells: implications for identification of normal and degenerate human intervertebral disc cell phenotypes. *Arthritis Res Ther* **12**: R22.
- Mitrecic MZ, Mitrecic D, Pochet R, Kostovic-Knezevic L, Gajovic S. 2010. The Mouse Gene Noto Is Expressed in the Tail Bud and Essential for Its Morphogenesis. *Cells Tissues Organs* **192**: 85-92.

- Murphy PL, Volinn E. 1999. Is occupational low back pain on the rise? *Spine (Phila Pa 1976)* **24**: 691-697.
- Nishizaki Y, Shimazu K, Kondoh H, Sasaki H. 2001. Identification of essential sequence motifs in the node/notochord enhancer of *Foxa2* (*Hnf3beta*) gene that are conserved across vertebrate species. *Mech Dev* **102**: 57-66.
- Ohshima H, Urban JP, Bergel DH. 1995. Effect of static load on matrix synthesis rates in the intervertebral disc measured in vitro by a new perfusion technique. *J Orthop Res* **13**: 22-29.
- Pazzaglia UE, Salisbury JR, Byers PD. 1989. Development and involution of the notochord in the human spine. *J R Soc Med* **82**: 413-415.
- Ramage-Morin PL, Gilmour H. 2010. Chronic pain at ages 12 to 44. *Health Rep* **21**: 53-61.
- Roberts S. 2002. Disc morphology in health and disease. *Biochem Soc Trans* **30**: 864-869.
- Sawada A, Nishizaki Y, Sato H, Yada Y, Nakayama R, Yamamoto S, Nishioka N, Kondoh H, Sasaki H. 2005. Tead proteins activate the *Foxa2* enhancer in the node in cooperation with a second factor. *Development* **132**: 4719-4729.
- Schatz O, Golenser E, Ben-Arie N. 2005. Clearing and photography of whole mount X-gal stained mouse embryos. *Biotechniques* **39**: 650, 652, 654 passim.
- Setton LA, Chen J. 2006. Mechanobiology of the intervertebral disc and relevance to disc degeneration. *J Bone Joint Surg Am* **88 Suppl 2**: 52-57.
- Smith LJ, Nerurkar NL, Choi KS, Harfe BD, Elliott DM. 2011. Degeneration and regeneration of the intervertebral disc: lessons from development. *Dis Model Mech* **4**: 31-41.
- Soriano P. 1999. Generalized lacZ expression with the ROSA26 Cre reporter strain. *Nat Genet* **21**: 70-71.
- Stein S, Kessel M. 1995. A homeobox gene involved in node, notochord and neural plate formation of chick embryos. *Mech Dev* **49**: 37-48.
- Talbot WS, Trevarrow B, Halpern ME, Melby AE, Farr G, Postlethwait JH, Jowett T, Kimmel CB, Kimelman D. 1995. A homeobox gene essential for zebrafish notochord development. *Nature* **378**: 150-157.
- Trout JJ, Buckwalter JA, Moore KC. 1982. Ultrastructure of the human intervertebral disc: II. Cells of the nucleus pulposus. *Anat Rec* **204**: 307-314.

- Uetzmann L, Burtscher I, Lickert H. 2008. A mouse line expressing Foxa2-driven Cre recombinase in node, notochord, floorplate, and endoderm. *Genesis*.
- Urban JP, Smith S, Fairbank JC. 2004. Nutrition of the intervertebral disc. *Spine (Phila Pa 1976)* **29**: 2700-2709.
- Urban JPG, Roberts S, Ralphs JR. 2000. The nucleus of the intervertebral disc from development to degeneration. *American Zoologist* **40**: 53-61.
- Videman T, Gibbons LE, Battie MC, Maravilla K, Vanninen E, Leppavuori J, Kaprio J, Peltonen L. 2001. The relative roles of intragenic polymorphisms of the vitamin d receptor gene in lumbar spine degeneration and bone density. *Spine (Phila Pa 1976)* **26**: E7-E12.
- von Dassow G, Schmidt JE, Kimelman D. 1993. Induction of the *Xenopus* organizer: expression and regulation of *Xnot*, a novel FGF and activin-regulated homeo box gene. *Genes Dev* **7**: 355-366.
- Vujovic S, Henderson S, Presneau N, Odell E, Jacques TS, Tirabosco R, Boshoff C, Flanagan AM. 2006. Brachyury, a crucial regulator of notochordal development, is a novel biomarker for chordomas. *J Pathol* **209**: 157-165.
- Watanabe H, Yamada Y, Kimata K. 1998. Roles of aggrecan, a large chondroitin sulfate proteoglycan, in cartilage structure and function. *J Biochem* **124**: 687-693.
- Yamanaka Y, Tamplin OJ, Beckers A, Gossler A, Rossant J. 2007. Live imaging and genetic analysis of mouse notochord formation reveals regional morphogenetic mechanisms. *Dev Cell* **13**: 884-896.
- Zhou GQ, Yang F, Leung VVL, Cheung KMC. 2008. Molecular and cellular biology of the intervertebral disc and the use of animal models. *Current Orthopaedics* **22**: 267-273.
- Zizic Mitrecic M, Mitrecic D, Pochet R, Kostovic-Knezevic L, Gajovic S. 2010. The mouse gene *Noto* is expressed in the tail bud and essential for its morphogenesis. *Cells Tissues Organs* **192**: 85-92.

CHAPTER THREE

ELUCIDATING THE PHENOTYPE OF NOTOCHORD AND NUCLEUS PULPOSUS CELLS; CHANGES ASSOCIATED WITH AGING AND DEGENERATION

3.1 Co-Authorship Statement

Chapter 3 is authored by McCann M.R., Carter D.E., and Séguin C.A. and is entitled Elucidating the phenotype of notochord and nucleus pulposus cells and changes associated with aging and degeneration. This study is currently in preparation for submission to *Osteoarthritis & Cartilage*. Microarray experiments were performed by D.E. Carter. All other experiments and analyses were performed by M.R. McCann in the laboratory of C.A. Séguin. Manuscript was written by M.R. McCann with suggestions from Dr. C. A. Seguin.

3.2 Chapter Summary

The role of the nucleus pulposus (NP) in the initiation and progression of intervertebral disc degeneration has been well established. However, little is known regarding the genes, molecular mechanisms or pathways associated with the initiation of degenerative changes specific to the NP. This limited understanding hinders our ability to develop disease-modifying treatments to delay or reverse disc degeneration. Transcriptional profiling paired with bioinformatic analysis will provide a deeper understanding of the cellular changes associated with notochord / NP cell maturation, aging and degeneration. To carry out this characterization, RNA was isolated from NP tissue following microdissection of spinal tissues from *Noto*^{Cre/WT}; *Rosa26*^{mTmG/+} mice at 2.5, 6, or 21 months of age. Genome-wide mRNA expression profiling was performed at each time point and bioinformatic analysis was conducted on genes with greater than a 2-fold change between time points (p value < 0.05). Our analysis indicated that the largest change in gene expression occurred between cells from the healthy mature NP (2.5 months of age) and degenerative NP (21 months of age). Surprisingly, within this time frame more genes were affected between 2.5 and 6 months of age (NP aging) than between 6 and 21 months of age (NP degeneration). Gene ontology analysis revealed that between 2.5 and 6 months of age, there was an enrichment of genes associated with mesenchymal development and chemical response. Between 6 and 21 months of age, there was an enrichment of ossification genes. Notably, compared to 2.5 months, there was an enrichment of genes associated with bone morphogenetic protein (BMP) receptor binding at 6 months of age and Wnt-pathway related genes at 21 months of age. This study has provided insight into the pathways controlling NP aging and degeneration, that

may aid in the identification of new therapeutic targets to either inhibit disc degeneration or initiate repair of the NP.

3.3 Introduction

Low back is the most common musculoskeletal disorder, with a global lifetime prevalence as high as 84% (Balague et al. 2012). The occurrence of low back pain increases with age (Andersson 1999), similar to the age-related induction of intervertebral disc (IVD) degeneration (Miller et al. 1988; Paajanen et al. 1997).

It is thought that the main contributor to back pain is degeneration of the IVD, and that the first manifestations of degenerative changes occur in the NP (Chen et al. 2006; Taher et al. 2012). The NP is a highly hydrated, gelatinous tissue that contains high levels of proteoglycans within a loose type II collagen rich extracellular matrix (ECM). Notably, the NP contains abundant aggrecan core protein, formed by multiple glycosaminoglycan side chains (chondroitin sulfate and keratan sulfate) that confer turgor to withstand compressive mechanical loading. During aging, changes in the ECM composition of the NP lead to a reduction in its ability to resist compressive forces, which are instead transferred to the surrounding annulus fibrosus (AF), leading to structural failure and degeneration of the AF (Borenstein 2013). It is hypothesized that notochord cells serve to protect the NP from degeneration and maintain the specialized extracellular matrix milieu of this avascular and aneural tissue (Cappello et al. 2006; Erwin et al. 2011). This hypothesis is consistent with the association between the loss of notochord cells in the NP within the first decade of life and the clinical appearance of disc degeneration, detected by MRI as early as the age 15 (Paajanen et al. 1997). The

mechanisms by which notochord cells serve to maintain NP health are poorly understood.

Work by our group (Bedore et al. 2013; Warraich et al. 2013) and others (Yang et al. 2009; Sakai et al. 2012) have demonstrated that the mouse is a useful model to study intervertebral disc biology. Mice are considered skeletally mature at 2.5 months of age (Poole et al. 2010), which corresponds to human ages between 10-17 (Turnbull et al. 2003). Similarly, 6-month-old and 21-month-old mice approximate 30 and 80 year old humans, respectively. One important caveat to the use of mice to study human disc biology is the fact that significant signs of degeneration are not detected until 18 months of age in mice (Bedore et al. 2013), well after the timing of degenerative changes seen in humans. This important difference is likely associated with the fact that unlike humans, notochord cells are retained throughout much of the adult life in mice (Alini et al. 2008). Work from our lab has demonstrated that notochord cells are detected in the murine NP up to 9 months of age, as demonstrated by expression of the notochord cell marker cytokeratin-8 in a subset of cells (McCann et al. 2011).

Recent studies have used bioinformatic analysis of microarray data sets to characterize changes associated with age-induced degeneration of annulus fibrosus, comparing tissue samples obtained from either degenerative or non-degenerative patients. Increased degeneration (assessed by Thompson scoring (Thompson et al. 1990)) was associated with increased expression of genes associated with membrane-bound vesicles, calcium ion binding and extracellular matrix. Furthermore, members of the Ras homologue (Rho) gene family were associated with the progression of degeneration in the AF (Chen et al. 2013a; Chen et al. 2013b). To date, there have been no studies aimed at determining the gene expression profile and changes associated with aging of the murine

NP. To study the effects of age on the phenotype of NP cells associated with the progression of disc degeneration, we analyzed gene expression by microarrays in NP cells isolated from 2.5-month-old, 6-month-old and 21 month old mice. RNA was isolated from the NP of *Noto*^{Cre/WT}; *Rosa26*^{mTmG/WT} mice in order to isolate mGFP⁺ NP cells. Using time points that demonstrate significant histological differences in NP tissue composition, we identified differences in gene expression between mature, aged and degenerative NP that might play an important role in the disease process.

3.4 Materials and Methods

3.4.1 Mice

All aspects of this study were conducted in accordance with the policies and guidelines set forth by the Canadian Council on Animal Care and were approved by the Animal Use Subcommittee of the University of Western Ontario. Mice were housed in standard cages and maintained on a 12-hour light/dark cycle, with rodent chow and water available *ad libitum*. Mice were generated by mating the notochord-specific *Noto*^{Cre/WT} mouse (McCann et al. 2011) to the conditional *ROSA26* (*R26*) *mT/mG* reporter mouse (Gt(*ROSA*)26Sor^{tm4(ACTB-tdTomato-EGFP)Luo}) (Muzumdar et al. 2007) to generate a mouse in which notochord cells and their derivatives are mGFP⁺ while all other cells types express tdTomato. Genotyping was performed as previously described (Muzumdar et al. 2007; McCann et al. 2011). At specified time points, mice were euthanized by a lethal dose of sodium pentobarbital.

3.4.2 Histology

Intact lumbar spinal segments (L1-L5) were isolated from specified time points and fixed overnight in 4% paraformaldehyde. Spinal segments were decalcified for 5 days in Shandon's TBD-2 (Thermo Scientific, Nepean, ON, Canada), washed PBS-0.2% Tween 20 (Sigma-Aldrich, St. Louis, MO, USA), processed and embedded in paraffin. Spines were sectioned sagittally at a thickness of 5 μ m using a microtome (Leica Microsystems, Concord, ON, Can.) and mounted on Superfrost plus™ slides (Fisher Scientific, Ottawa, ON, Canada). Sections were dewaxed in xylene and rehydrated by successive descending concentrations of alcohol. Slides were stained with hematoxylin and eosin (H&E) and images were acquired using a Leica DM1000 microscope. For evaluation of IVD degeneration, IVD tissues (n=2-5 IVDs/mouse, 3 mice/group) were scored according to the Thompson grading scale (Thompson et al. 1990) by 2 independent blinded observers. The Thompson grading scheme is a five-category grading system that was originally used to assess the gross morphological sections in lumbar cadaveric specimens. Each tissue compartment is graded independently and is based on the morphological features of aging and degeneration. The initial scheme had intraobserver and interobserver agreement values of greater than 85%, which was maintained when the scheme was applied across species (Bergknut et al. 2011). Our lab has used it previously used this method in mice to assess the degeneration the IVD is a NP-specific conditional knockout model (Bedore et al. 2013). In this study, a consensus was reached prior to grading by each observer and the total score were taken from each observer and averaged.

3.4.3 RNA Isolation and Purification

Lumbar and thoracic spines were dissected from 2.5, 6, or 21-month-old mice. The surrounding muscle and ligaments were removed from the vertebral column exposing the IVDs. Cleaned spinal segments were placed in sterile PBS and transferred to the Leica M165 FC stereoscope for imaging and microdissection. For each IVD, the AF was lacerated on the anterior side to expose the central gelatinous NP, containing mGFP⁺ cells, which were collected with a micropipette. During the microdissection, NP tissue was placed in RNeasy lysis buffer (Qiagen, Crawley, UK) on ice. Samples were centrifuged for 5 min at 2,500 g, RNeasy lysis buffer was aspirated and tissues were incubated in PureZOL[®] (Biorad Mississauga, ON, Can.) at -80°C pending RNA extraction using the Aurum Total RNA Fatty and Fibrous Kit (Biorad). RNA was quantified using a NanoDrop 2000 spectrophotometer (Thermo Scientific, Pittsburgh, PA, USA) and quality was verified using 2100 Bioanalyzer (Agilent Technologies Inc, Santa Clara, CA, USA). RNA samples with RIN (RNA integrity number) values greater than 7 were used for subsequent microarray analysis.

3.4.4 Global Gene Expression Analysis

Microarray analysis was performed at the London Regional Genomics Centre (Robarts Research Institute, London, ON, Can.). Briefly, biotinylated complementary RNA (cRNA) was prepared from 100 µg of total RNA according to the Affymetrix GeneChip Technical Analysis Manual 2 Cycle Protocol (Affymetrix, Santa Clara, CA, USA). Ten micrograms of labeled cRNA was hybridized to Affymetrix Mouse 430 2.0 arrays for 16 hr at 45°C. GeneChips were stained with streptavidin-PE, followed by an antibody solution and a second streptavidin-PE solution, with all liquid handling

performed with a GeneChip Fluidics Station 450. GeneChips were scanned with the Affymetrix GeneChip Scanner 3000 7G. Probe level data from the CEL files were analyzed with Partek Genomics Suite (Partek Inc, St.Louis, MO, USA) using robust multi array average-normalized values to determine fold changes. Transcripts demonstrating at least 2.0-fold change between groups with a p value < 0.05 were selected for subsequent bioinformatic analysis.

3.4.5 Gene Ontology (GO) and Kyoto Encyclopedia of Genes and Genomics (KEGG)

Pathway Analysis

Probes demonstrating a significant change between each specified time point (2.5 vs 6 months of age; 2.5 vs 21 months of age; 6 vs 21 months of age) were used for functional categorization and pathway analysis. Categories were generated based on the *Mus musculus* annotations for Gene Ontology (GO) analysis (geneontology.org) and KEGG pathway analysis (genome.ad.jp/kegg). GO terms are divided into three families: biological process, cellular component, and molecular function. Assessment of extracellular matrix genes was based on genes annotated in gene ontology for Extracellular matrix part (GO:0044420) using AmiGo2 (version 2.1.4) (Carbon et al. 2009). Cluster analysis were performed and heat maps were generated with Seurat (Gribov et al. 2010), and clustered using Euclidean distance.

3.5 RESULTS

3.5.1 Nucleus Pulposus Degeneration with Age

To examine the effects of age on the structure and morphology of the murine NP, we first performed histological assessment of intervertebral disc tissues at 2.5, 6, and 21 months of age. Using histomorphometric analysis based on the modified Thompson grading scale (Thompson et al. 1990), we detected a progressive increase in NP degeneration in the lumbar region of mice with age (**Figure 3.1**). At 2.5 months of age, the NP contained predominantly large, physaliferous notochord cells located in clusters throughout the NP (**Figure 3.1 Ai, arrowheads**). At 6 months of age, the organization of the NP was altered, demonstrating the accumulation of peripheral fibrous material in the NP and populated predominantly by smaller NP cells (**Figure 3.1 Aii**). Histological examination of IVD tissues at 21 months of age revealed marked changes in tissue architecture with clear loss of the NP-AF boundary, decrease in NP cellularity and the accumulation of fibrotic tissue throughout the NP (**Figure 3.1 Aiii**). Interestingly, at this time point the NP was populated by dispersed clusters of cells that morphologically resemble hypertrophic chondrocytes (**Figure 3.1 Aiii, arrows**). Based on the Thompson scoring system (Thompson et al. 1990) these changes resulted in significant degenerative changes in the NP and AF of mice with age (**Figure 3.1 B**)

3.5.2 Genetic Labeling and Isolation of Notochord-derived Cells

Given the changes in NP tissue structure and composition, we proceeded with the isolation of NP cells at each of these time points in order to quantify changes in global gene expression. Our strategy involved breeding the notochord-specific *Noto*^{Cre/WT} (McCann et al. 2011) mouse strain to the *Rosa26*^{mTmG/WT} double-fluorescent Cre reporter mouse (Muzumdar et al. 2007) to isolate NP cells based on fluorescent protein expression

Figure 3.1 Characterization of the nucleus pulposus composition with aging in 2.5, 6, and 21 month old mice. **A.** Representative images from hematoxylin and eosin stained lumbar IVDs demonstrate the histological appearance and cellular composition of NP with age. 2.5 month (i) mice show numerous large vacuolated notochord cells in the NP. 6 month (ii) displays an altered NP, with increased fibrotic extracellular matrix and predominant small NP cells. 21 month (iii) NP shows large degeneration with loss of tissue architecture and decreased cellularity. **B.** Thompson scores, which correspond to the stage of degeneration in all the lumbar IVDs demonstrate a significant increase in degeneration in disc with age. Values are the percentage of discs with the indicated Thompson grade. n = 3 IVDs/animal; 3 animals/timepoint (n=9). * = $p < 0.05$, ** = $p < 0.01$, *** = $p < 0.001$, **** = $p < 0.0001$

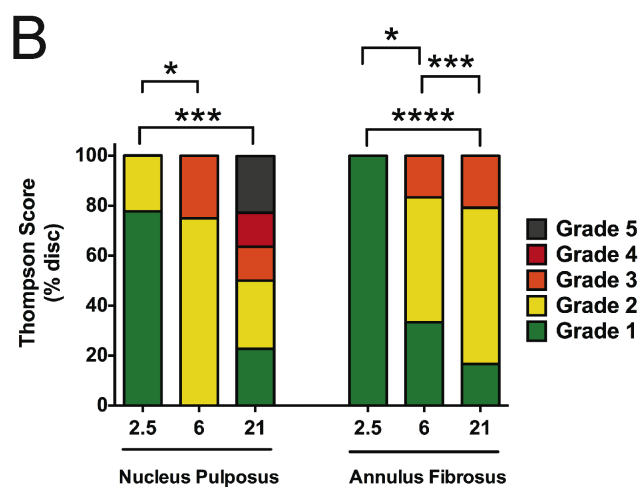
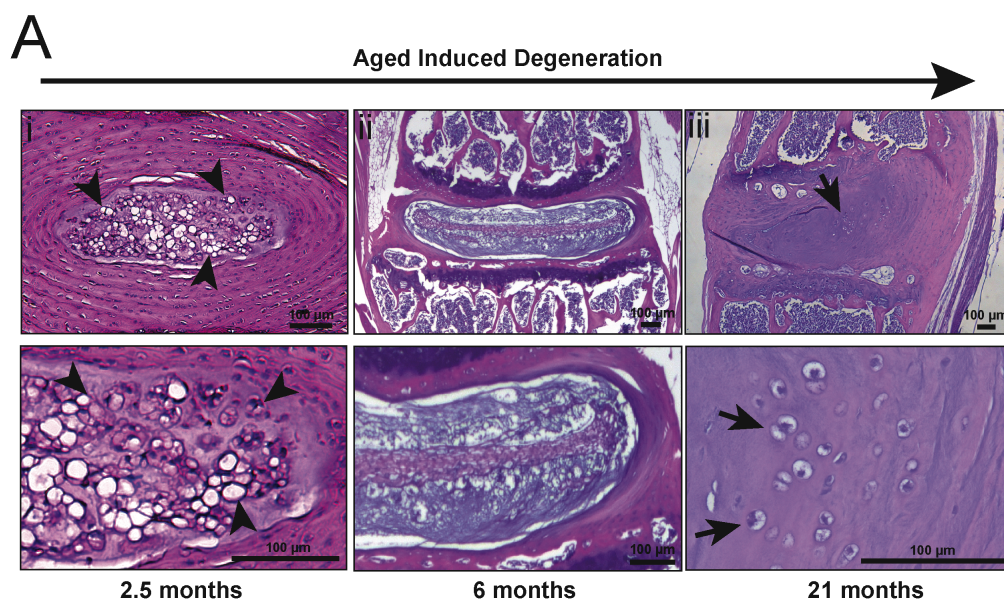


(**Figure 3.2**). The *Rosa26^{mTmG}* mouse ubiquitously expresses membrane-targeted tandem dimer Tomato (mT); following Cre-mediated excision, cells instead express membrane-targeted green fluorescent protein (mGFP). When crossed with *Noto^{Cre/WT}* mice, mGFP expression is detected uniquely in notochord and notochord-derived cells. To verify Cre-mediated recombination, we assessed fluorescence in tail segments of *Noto^{Cre/WT};Rosa26^{mTmG/WT}* mice at 2.5 months of age (**Figure 3.2 B**) and confirmed that mGFP⁺ cells were localized specifically to the NP. Furthermore, we were able to develop protocols to isolate the gelatinous mGFP⁺ NP tissue from the surrounding IVD following cutting of the AF (**Figure 3.2 B&C**).

3.5.3 Assessment of Gene Expression Profiles in Age-induced Degeneration of the Nucleus Pulposus

Using this protocol, microarray-based expression profiling was conducted on RNA isolated from mGFP⁺ NP cells from the IVD tissues of mice at 2.5, 6, or 21 months of age. Changes in gene expression were evaluated between each time point examined. There were 404 probes whose expression was significantly altered from 2.5 to 6 months of age; 260 probes significantly altered from 6 to 21 months of age; and 630 probes significantly altered from 2.5 to 21 months of age (**Figure 3.3**). Full list of probes with a $p < 0.05$ are located online in **Appendix A: www.gdriv.es/mccannmr-thesis-2014**.

Ontology analysis identified a broad spectrum of genes differentially expressed, according to biological processes, molecular function, and cellular component classifications (**Figure 3.4**). In the category of biological process, the genes associated

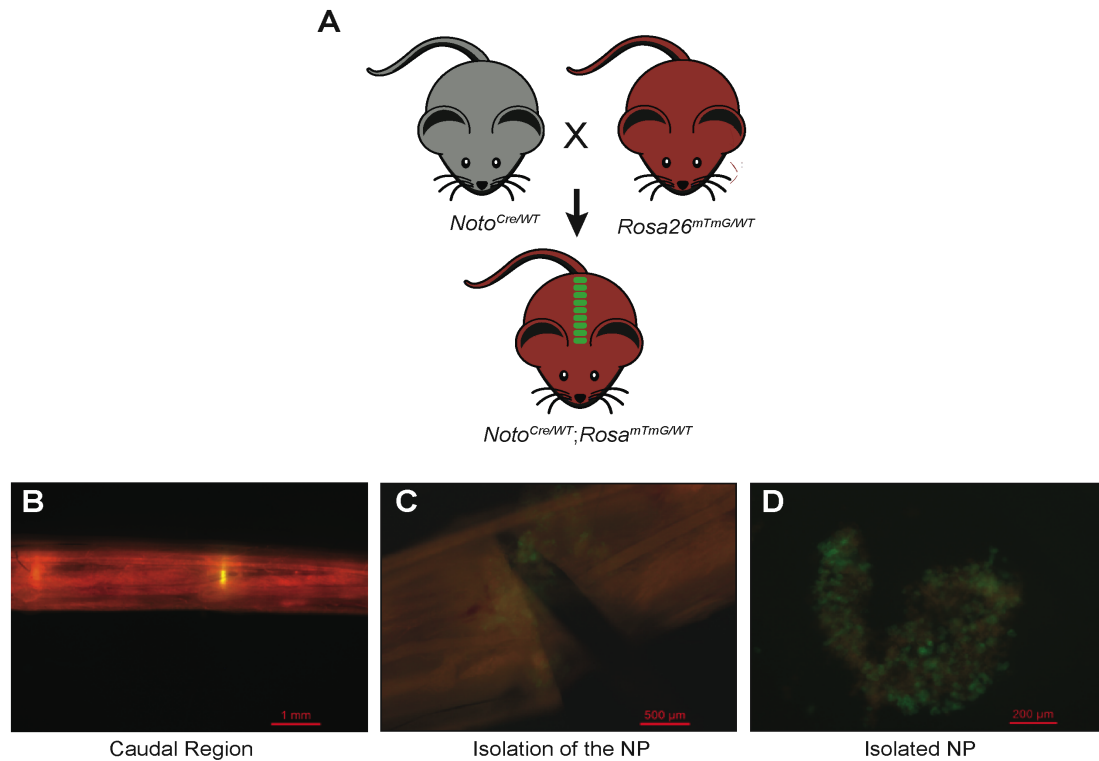
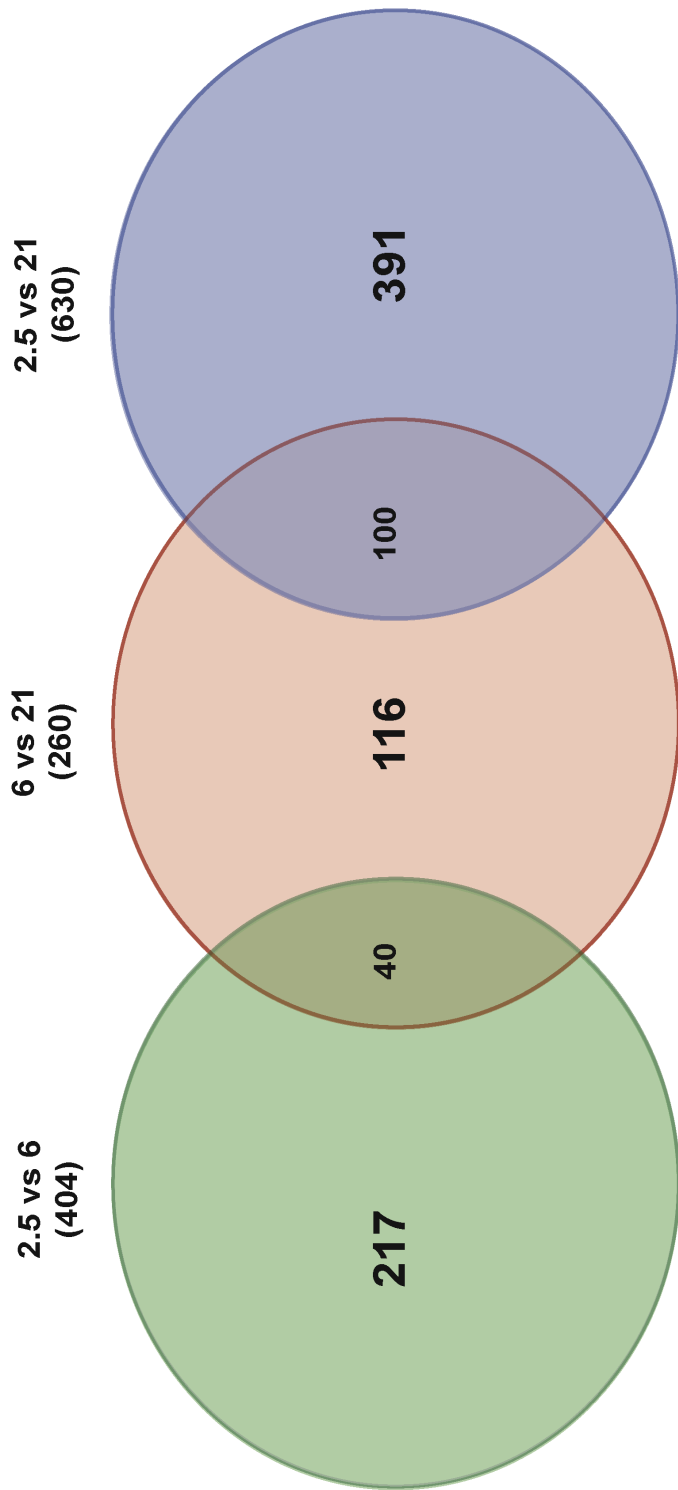


Figure 3.2 Genetic mouse model to distinguish notochord-derived cells within the intervertebral disc and nucleus pulposus microdissection.

A. Mating scheme used to cross the $Noto^{Cre/+}$ mouse to the conditional $Rosa26^{mTmG/WT}$ reporter mouse. After Cre-mediated intra-chromosomal recombination, the mT sequence is excised allowing expression of membrane-targeted enhanced green fluorescent mG protein **B.** Caudal spinal segment from a $Noto^{Cre/+}; Rosa^{mTmG/mTmG}$ mouse (skin removed) showing tdTomato and mGFP fluorescence expression. **C.** Isolated nucleus pulposus tissue demonstrates mGFP+ cells. **D.** Isolated nucleus pulposus tissue.

Figure 3.3 Phenotypic comparison of genes altered in the aging nucleus pulposus.

Venn diagram of overlapping and specific genes that were 2-fold dysregulated genes in 2.5, 6, and 21 month time points. Partial list of genes is shown along with fold change of representative probe sets. Significance was assigned with a p value < 0.05 .



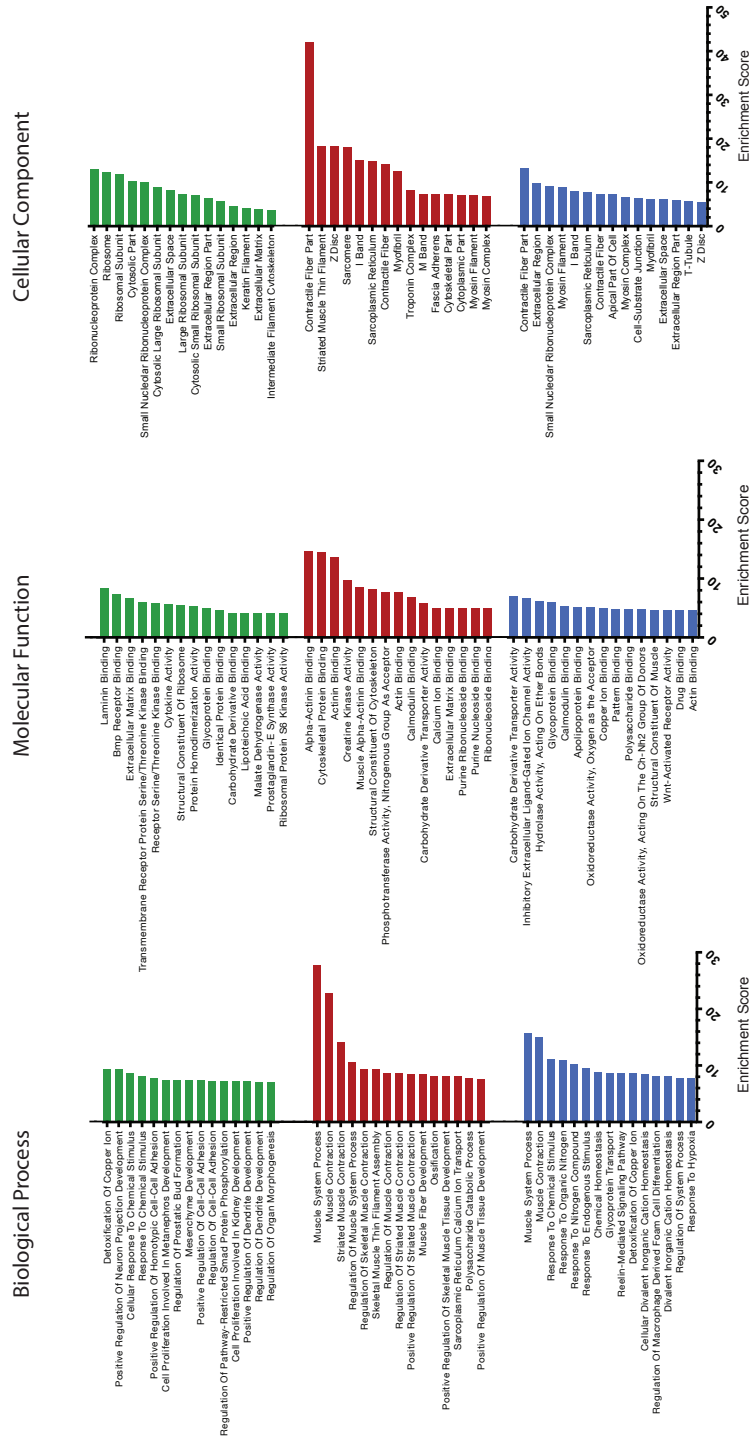
Gene Title	Gene Symbol	Fold change (6 relative to 2.5)
microRNA 703	MIR703	4.00
sonic hedgehog	SHH	3.51
secreted frizzled-related protein 5	MFRP5	3.40
secreted frizzled-related protein 4	MFRP4	3.40
solute carrier family 15, member 2	SLC15A2	-2.42
G protein-coupled receptor, class C, group 5	GPRC5A	-2.31

Gene Title	Gene Symbol	Fold change (21 relative to 2.5)
serine (or cysteine) peptidase inhibitor, clade A, member 1C	SERPINA1C	30.78
cytochrome P450, family 3, subfamily a, polypeptide 13	CYP3A13	7.18
microRNA 669h	MIR669h	-6.31
dipeptidase2	DPEP2	-3.09
foliaturin-like 4	FSL4	-2.08

Gene Title	Gene Symbol	Fold change (21 relative to 6)
proteoglycan 4	PRG4	9.52
ATPase, Ca++ transporting, cardiac muscle	ATP2A1	7.43
CD118	CD118	2.39
histone H2B	HIST1H2B	-1.90
histone cluster 1, H2bn	HIST1H2BN	-2.90
CD38	CD38	-2.27

Figure 3.4 Gene ontology enrichment analyses of differentially expressed genes.

Graphical representation of the 15 most enriched gene ontology terms based on differentially regulated genes at each time point. Categories are based on biological process, molecular function, and cellular component.



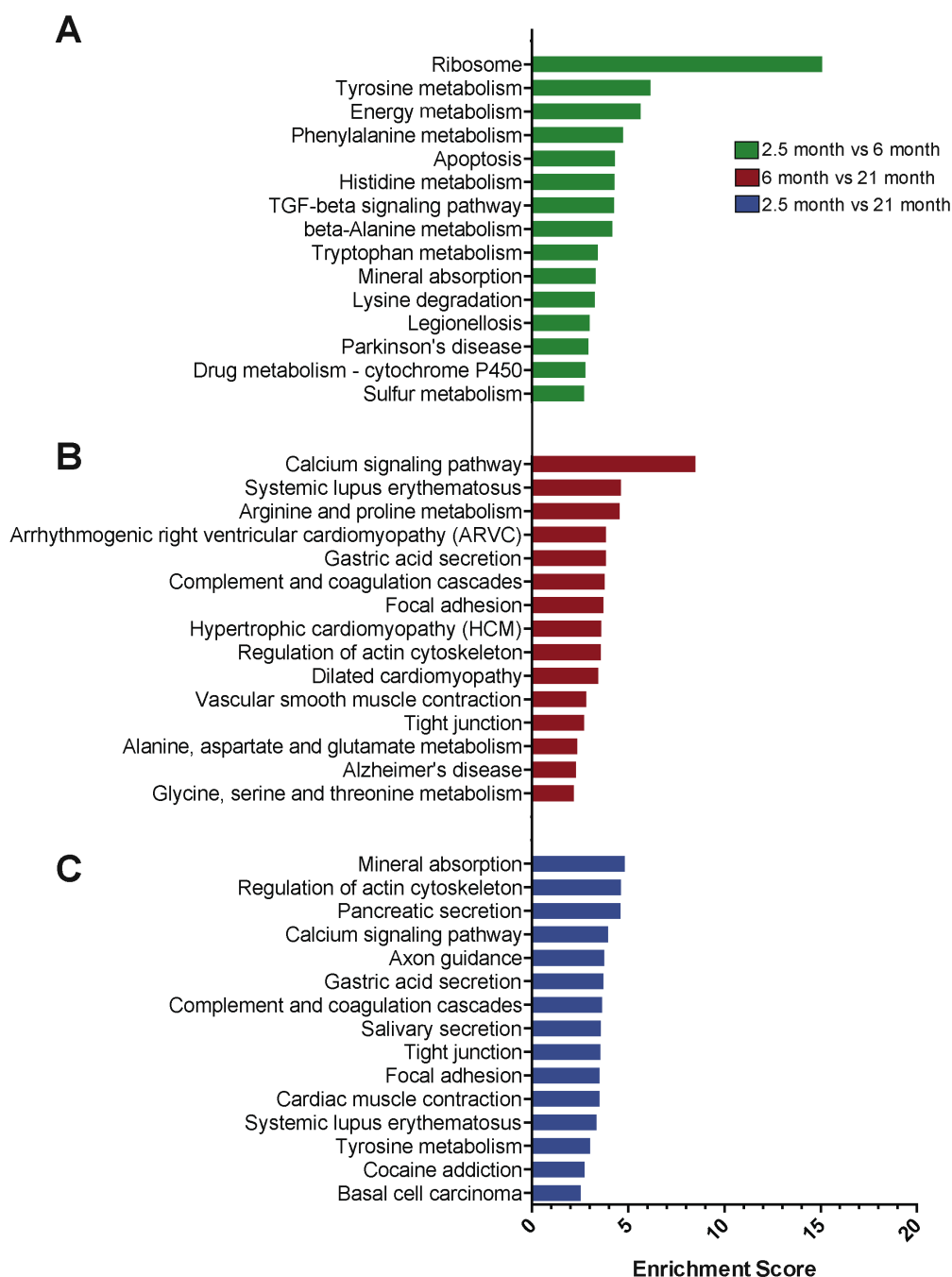
with the transition from mature to aged NP (2.5 vs 6 months of age) were categorized as being involved with adhesion and development (e.g. positive regulation of homotypic cell-cell adhesion, mesenchyme development). In the category of molecular function (2.5 vs 6 months of age) there was an enrichment of genes associated with binding (e.g. laminin binding). In the category of cellular component (2.5 vs 6 months of age), there was an enrichment of ribosomal associated genes (e.g. ribonucleoprotein complex). The transition from aged to degenerative NP (6 vs 21 months of age) was enriched for genes associated with contraction (e.g. muscle system process), cytoskeletal and calcium binding (e.g. cytoskeletal protein binding, calmodulin binding) and contractile fiber association (e.g. contractile fiber part). Finally, comparison of the young to degenerative NP (2.5 vs 21 months of age) demonstrated enrichment for genes associated with response to stimulus, binding (e.g. glycoprotein binding), contractile fiber and extracellular matrix association.

3.5.4 KEGG Pathway Analysis

We next sought to classify the gene expression profiles based on KEGG pathway analysis to provide insight into the regulatory processes involved in age-induced disc degeneration. KEGG pathway analysis indicated distinct pathways associated with either maturation or degeneration of the NP. The summary of the top 15 hits based on enrichment scores are presented (**Figure 3.5**). This analysis identified the enrichment of pathways associated with the ribosome complex, tyrosine, energy, phenylalanine metabolism, and apoptosis in the transition from mature to aged NP (2.5 vs 6 months of

Figure 3.5 KEGG pathway analyses for differentially expressed mRNA.

Graphical presentation of the 15 most enriched pathways are shown for either **A.** 2.5 month compared to 6 month, **B.** 6 month compared to 21 month, **C.** 2.5 month compared to 21 month. Length of each column represents the enrichment score for each pathway.



age) (**Figure 3.5 A**). The transition from aged to degenerative NP (6 vs 21 months of age) was enriched for TGF- β , PPAR and PI3K-AKT signaling pathways. Furthermore, this transition was enriched for calcium signaling , arginine and proline metabolism, focal adhesions and regulation of the cytoskeleton (**Figure 3.5 B**). Lastly, the transition from mature to degenerative NP (2.5 vs 21 months of age) was associated with enrichment of pathways associated with mineral absorption, actin signaling, and calcium signaling pathways as well as the PPAR and WNT signalling pathways (**Figure 3.5 C**).

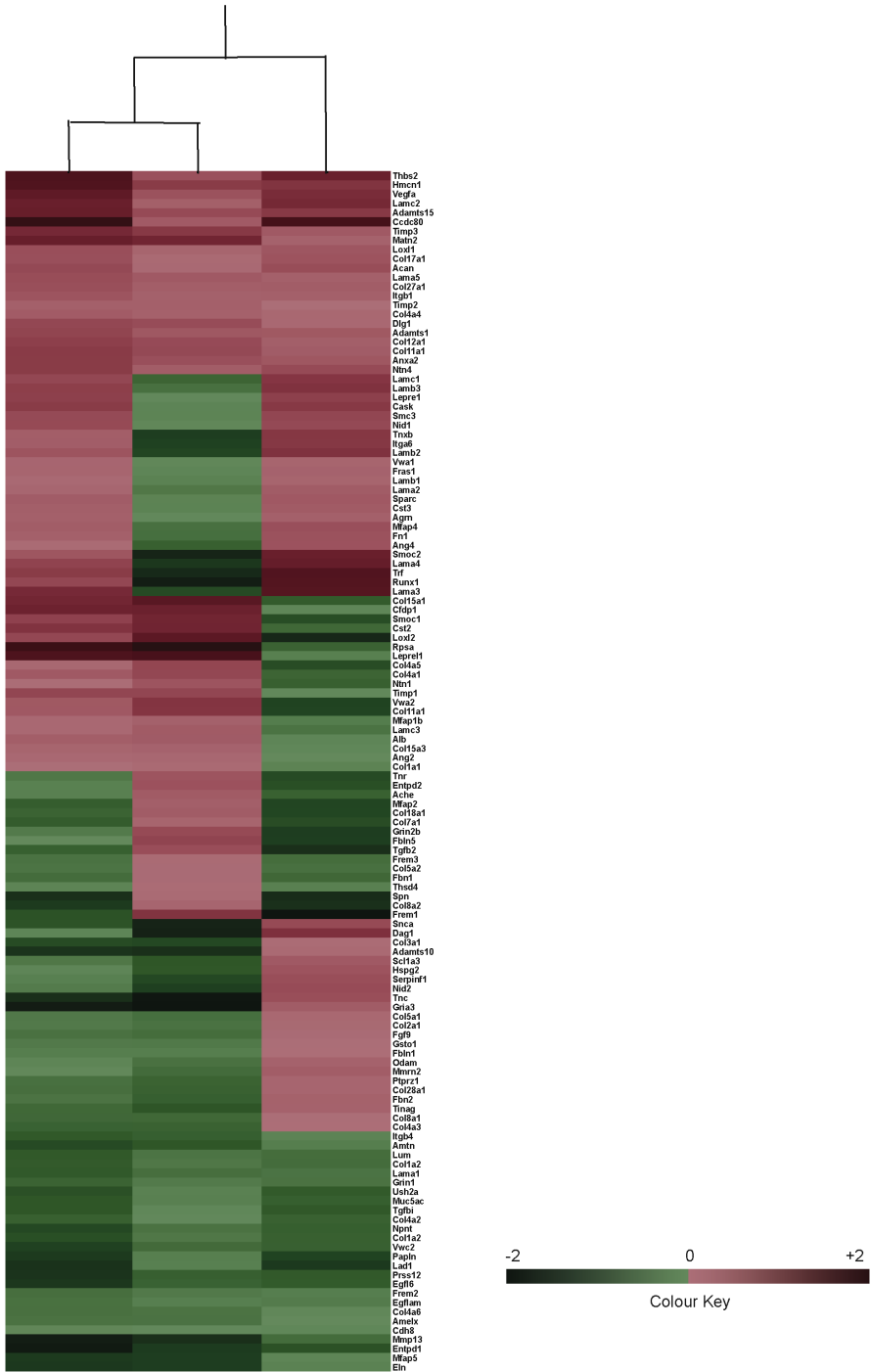
We next queried our microarray results for a list of 113 previously identified early notochord-enriched genes (Tamplin et al. 2011). We examined these markers against our dataset to determine if they were significantly altered in our comparison of mature and aged NP (**Appendix A, Table 3.1**), aged and degenerative NP (**Appendix A, Table 3.2**), or mature and degenerative NP (**Appendix A, Table 3.3**). Interestingly, we uncovered only three genes that were significantly changed in the NP with age. Expression of *Bmp7* was 2.5-fold increased in the NP at 6 months compared to 2.5 months, and demonstrated a further 2.1-fold increase in the NP at 21 months compared to 6 months. *Shh*, a key notochord signalling molecule, was expressed 3.6-fold higher at 6 months relative to 2.5 months of age. *F5* demonstrated a 2.2-fold decrease in expression at 21 months of age compared to 2.5 months of age.

3.5.5 Extracellular Matrix Cluster Analysis and Specific Gene Queries

We next determined the expression patterns of ECM genes within the NP during age induced degeneration. We conducted cluster analysis and generated heat maps using all genes annotated using the gene ontology term "Extracellular matrix". Hierarchical

Figure 3.6 Heat map and hierarchical clustering of genes annotated through Gene Ontology for extracellular matrix.

Heat map shows the results of two-way hierarchical clustering of extracellular matrix genes (rows) and differential gene expression between time-points (columns). Clustering of samples is shown on top. The color scale illustrates the relative expression level: red, high relative expression level; green, low relative expression level.



21 relative to 2.5 6 relative to 2.5 21 relative to 6

cluster analysis indicated that changes in the pattern of ECM gene expression are more from 2.5 to 6 months of age and 2.5 to 21 months of age than 6 to 21 months of age (**Figure 3.6**). However, there were specific cartilage or IVD-associated genes that were included in the ECM gene ontology term. We therefore specifically queried genes that are known regulators of cartilage homeostasis (proteoglycans, collagens, cartilage transcriptional regulators, matricellular proteins) as well as catabolic factors (matrix metalloproteinases, aggrecanases). This analysis indicated that *Dcn* was the only ECM associated gene whose expression was significantly changed in the NP, demonstrating a 2.4-fold reduction at 6 months vs 2 months of age, and a 2.8-fold induction at 21 months vs 6 months of age (**Appendix A, Table 3.4**). There was no significant change in *Dcn* expression detected between 2.5 and 21 months of age.

3.6 DISCUSSION

In the current study, transcriptional profiling paired with bioinformatic analysis allowed us to determine the molecular profile associated with the progression of NP maturation, aging and degeneration. Characterization of the morphology of the NP by histological examination demonstrated degeneration in severely aged mice. We noted the presence of large hypertrophic cells (morphologically resembling hypertrophic chondrocytes) within the degenerative NP at 21 months of age. Calcification of the IVD is associated with age related disc degeneration (Hristova et al. 2011). While the cause of calcification of the IVD is unknown, the biological processes governing this process may resemble those established for cartilage (Pitsillides and Beier 2011). Characterization of human NP degeneration (based on the Thompson score) was previously associated with a

progressive increase in hypertrophic cell differentiation localized specifically to the NP (Rutges et al. 2010). This study reported increased expression of the hypertrophic markers such as collagen type X, Runt-related transcription factor 2 (Runx2), alkaline phosphatase (ALP). In our analysis, we did not see changes in the expression of *Col10*, *Runx2* or alkaline phosphatase. However, since changes in cell morphology were noted at 21 months, these markers should be assessed in future studies using either real-time PCR or immunohistochemistry to confirm the phenotype of cells with a hypertrophic morphology.

When our dataset was assessed for genes enriched in the mouse node at E8.0 (Tamplin et al. 2011), we determined that only three of these genes demonstrated significant changes between the time points we assessed. Bone morphogenetic protein 7 (BMP7), a member of the TGF- β family (Wozney et al. 1988), is known to be expressed in the notochord where its signals, along with Shh, to affect the differentiation of neuronal cells (Dale et al. 1997). In the intervertebral disc, BMP7 is known to be anti-catabolic (Chubinskaya et al. 2007) and various animal models of disc degeneration have established that injection of BMP7 can restore the IVD height, proteoglycan content and elastic properties of the NP (Imai et al. 2003; An et al. 2005; Masuda et al. 2006). This regenerative potential might be mediated through direct regulation of ECM content, as BMP7 is known to activate the expression of the ECM molecules aggrecan and type-II collagen in cartilage (Fan et al. 2004) and inhibit the expression of MMP-13 in chondrocytes (Im et al. 2003). These findings suggest that the activation of *Bmp7* expression in aged and degenerative NP tissue may be indicative of a reparative response that might be insufficient to restore disc homeostasis and regenerate the ECM.

The composition of the extracellular matrix of the NP is well known (Melrose and Roughley 2014; Mwale 2014). Anabolic factors such aggrecan and type-II collagen are present and are targeted by aggrecanases and matrix metalloproteinases in disease states (Vo et al. 2013) (discussed in more detail in Chapter 5). Surprisingly, our analysis of ECM-associated genes indicated that *Dcn* was the only ECM gene significantly changed in our study. *Dcn* is a small leucine-rich proteoglycan that binds to type-II collagen and is thought to play an important role in tissue assembly (Vogel et al. 1984). Mice lacking expression of *Dcn* have been generated (Danielson et al. 1997) and musculoskeletal tissues were specifically assessed (Young et al. 2002); however, no phenotype in the IVD has been reported. Decorin is typically expressed by cells with a fibroblastic phenotype (Bianco et al. 1990; Gotz et al. 1997), and thus expressed in the outer AF (Melrose et al. 2001). Hence, the increases seen in the degenerative NP might reflect NP cells becoming more fibrotic with degeneration and therefore adopting a more fibroblastic-like phenotype.

Other signalling molecules are known to regulate the ECM, including PPAR signalling, which may play an important role in disc degeneration. While no studies have looked at the role of PPAR specifically in the IVD or NP, assessment in articular cartilage has revealed that both PPAR gamma (Vasheghani et al. 2013) and PPAR delta (Ratneswaran et al. 2014) are important regulators associated with the progression of osteoarthritis of the knee: PPAR gamma is known to be protective and PPAR delta is causative. The enrichment in PPAR associated genes in our analysis suggests PPAR signalling pathways as a potential targets regulating degeneration of the IVD.

The current study has provided insight into the progression of NP maturation, aging and degeneration. Identification of novel genes and molecular pathways associated with degeneration of the NP is an integral step in understanding this complex process. These molecules and pathways will provide avenues for potential new therapeutics to either inhibit progression of the disease state or activate regeneration of the NP and thus alleviate disc degeneration.

3.7 REFERENCES

- Alini M, Eisenstein SM, Ito K, Little C, Kettler AA, Masuda K, Melrose J, Ralphs J, Stokes I, Wilke HJ. 2008. Are animal models useful for studying human disc disorders/degeneration? *Eur Spine J* **17**: 2-19.
- An HS, Takegami K, Kamada H, Nguyen CM, Thonar EJ, Singh K, Andersson GB, Masuda K. 2005. Intradiscal administration of osteogenic protein-1 increases intervertebral disc height and proteoglycan content in the nucleus pulposus in normal adolescent rabbits. *Spine (Phila Pa 1976)* **30**: 25-31; discussion 31-22.
- Andersson GB. 1999. Epidemiological features of chronic low-back pain. *Lancet* **354**: 581-585.
- Balagué F, Mannion AF, Pellise F, Cedraschi C. 2012. Non-specific low back pain. *Lancet* **379**: 482-491.
- Bedore J, Sha W, McCann MR, Liu S, Leask A, Seguin CA. 2013. Impaired Intervertebral Disc Development and Premature Disc Degeneration in Mice With Notochord-Specific Deletion of CCN2. *Arthritis Rheum* **65**: 2634-2644.
- Bergknut N, Grinwis G, Pickee E, Auriemma E, Lagerstedt AS, Hagman R, Hazewinkel HA, Meij BP. 2011. Reliability of macroscopic grading of intervertebral disk degeneration in dogs by use of the Thompson system and comparison with low-field magnetic resonance imaging findings. *American journal of veterinary research* **72**: 899-904.
- Bianco P, Fisher LW, Young MF, Termine JD, Robey PG. 1990. Expression and localization of the two small proteoglycans biglycan and decorin in developing human skeletal and non-skeletal tissues. *J Histochem Cytochem* **38**: 1549-1563.
- Borenstein D. 2013. Mechanical low back pain--a rheumatologist's view. *Nature reviews Rheumatology* **9**: 643-653.

- Cappello R, Bird JL, Pfeiffer D, Bayliss MT, Dudhia J. 2006. Notochordal cell produce and assemble extracellular matrix in a distinct manner, which may be responsible for the maintenance of healthy nucleus pulposus. *Spine (Phila Pa 1976)* **31**: 873-882; discussion 883.
- Carbon S, Ireland A, Mungall CJ, Shu S, Marshall B, Lewis S, Ami GOH, Web Presence Working G. 2009. AmiGO: online access to ontology and annotation data. *Bioinformatics* **25**: 288-289.
- Chen K, Wu D, Zhu X, Ni H, Wei X, Mao N, Xie Y, Niu Y, Li M. 2013a. Gene expression profile analysis of human intervertebral disc degeneration. *Genetics and molecular biology* **36**: 448-454.
- Chen WH, Lo WC, Lee JJ, Su CH, Lin CT, Liu HY, Lin TW, Lin WC, Huang TY, Deng WP. 2006. Tissue-engineered intervertebral disc and chondrogenesis using human nucleus pulposus regulated through TGF-beta1 in platelet-rich plasma. *J Cell Physiol* **209**: 744-754.
- Chen Y, Chen K, Li M, Li C, Ma H, Bai YS, Zhu XD, Fu Q. 2013b. Genes associated with disc degeneration identified using microarray gene expression profiling and bioinformatics analysis. *Genetics and molecular research : GMR* **12**: 1431-1439.
- Chubinskaya S, Hurtig M, Rueger DC. 2007. OP-1/BMP-7 in cartilage repair. *International orthopaedics* **31**: 773-781.
- Dale JK, Vesque C, Lints TJ, Sampath TK, Furley A, Dodd J, Placzek M. 1997. Cooperation of BMP7 and SHH in the induction of forebrain ventral midline cells by prechordal mesoderm. *Cell* **90**: 257-269.
- Danielson KG, Baribault H, Holmes DF, Graham H, Kadler KE, Iozzo RV. 1997. Targeted disruption of decorin leads to abnormal collagen fibril morphology and skin fragility. *J Cell Biol* **136**: 729-743.
- Erwin WM, Islam D, Inman RD, Fehlings MG, Tsui FW. 2011. Notochordal cells protect nucleus pulposus cells from degradation and apoptosis: implications for the mechanisms of intervertebral disc degeneration. *Arthritis Res Ther* **13**: R215.
- Fan Z, Chubinskaya S, Rueger DC, Bau B, Haag J, Aigner T. 2004. Regulation of anabolic and catabolic gene expression in normal and osteoarthritic adult human articular chondrocytes by osteogenic protein-1. *Clinical and experimental rheumatology* **22**: 103-106.
- Gotz W, Barnert S, Bertagnoli R, Miosge N, Kresse H, Herken R. 1997. Immunohistochemical localization of the small proteoglycans decorin and biglycan in human intervertebral discs. *Cell Tissue Res* **289**: 185-190.

- Gribov A, Sill M, Luck S, Rucker F, Dohner K, Bullinger L, Benner A, Unwin A. 2010. SEURAT: visual analytics for the integrated analysis of microarray data. *BMC medical genomics* **3**: 21.
- Hristova GI, Jarzem P, Ouellet JA, Roughley PJ, Epure LM, Antoniou J, Mwale F. 2011. Calcification in human intervertebral disc degeneration and scoliosis. *J Orthop Res* **29**: 1888-1895.
- Im HJ, Pacione C, Chubinskaya S, Van Wijnen AJ, Sun Y, Loeser RF. 2003. Inhibitory effects of insulin-like growth factor-1 and osteogenic protein-1 on fibronectin fragment- and interleukin-1 β -stimulated matrix metalloproteinase-13 expression in human chondrocytes. *J Biol Chem* **278**: 25386-25394.
- Imai Y, An H, Thonar E, Muehleman C, Okuma M, Matsumoto T, Andersson G, Masuda K. 2003. Co-injected recombinant human osteogenic protein-1 minimizes chondroitinase ABC-induced intervertebral disc degeneration: an in vivo study using a rabbit model. *Trans Orthop Res Soc* **1143**.
- Masuda K, Imai Y, Okuma M, Muehleman C, Nakagawa K, Akeda K, Thonar E, Andersson G, An HS. 2006. Osteogenic protein-1 injection into a degenerated disc induces the restoration of disc height and structural changes in the rabbit annular puncture model. *Spine (Phila Pa 1976)* **31**: 742-754.
- McCann MR, Tamplin OJ, Rossant J, Seguin CA. 2011. Tracing notochord-derived cells using a Noto-cre mouse: implications for intervertebral disc development. *Dis Model Mech*.
- Melrose J, Ghosh P, Taylor TK. 2001. A comparative analysis of the differential spatial and temporal distributions of the large (aggrecan, versican) and small (decorin, biglycan, fibromodulin) proteoglycans of the intervertebral disc. *J Anat* **198**: 3-15.
- Melrose J, Roughley P. 2014. Proteoglycans of the intervertebral disc. in *The Intervertebral Disc*, pp. 53-77. Springer.
- Miller JA, Schmatz C, Schultz AB. 1988. Lumbar disc degeneration: correlation with age, sex, and spine level in 600 autopsy specimens. *Spine (Phila Pa 1976)* **13**: 173-178.
- Muzumdar MD, Tasic B, Miyamichi K, Li L, Luo L. 2007. A global double-fluorescent Cre reporter mouse. *Genesis* **45**: 593-605.
- Mwale F. 2014. Collagen and Other Proteins of the Nucleus Pulposus, Annulus Fibrosus, and Cartilage End Plates. in *The Intervertebral Disc*, pp. 79-92. Springer.
- Paajanen H, Erkinntalo M, Parkkola R, Salminen J, Kormanen M. 1997. Age-dependent correlation of low-back pain and lumbar disc regeneration. *Archives of orthopaedic and trauma surgery* **116**: 106-107.

- Pitsillides AA, Beier F. 2011. Cartilage biology in osteoarthritis--lessons from developmental biology. *Nature reviews Rheumatology* **7**: 654-663.
- Poole R, Blake S, Buschmann M, Goldring S, Lavery S, Lockwood S, Matyas J, McDougall J, Pritzker K, Rudolph K et al. 2010. Recommendations for the use of preclinical models in the study and treatment of osteoarthritis. *Osteoarthritis Cartilage* **18 Suppl 3**: S10-16.
- Ratneswaran A, LeBlanc EA, Walser E, Welch I, Mort JS, Borradaile N, Beier F. 2014. PPARdelta promotes progression of post-traumatic osteoarthritis. *Arthritis & rheumatology*.
- Rutges JP, Duit RA, Kummer JA, Oner FC, van Rijen MH, Verbout AJ, Castelein RM, Dhert WJ, Creemers LB. 2010. Hypertrophic differentiation and calcification during intervertebral disc degeneration. *Osteoarthritis Cartilage* **18**: 1487-1495.
- Sakai D, Nakamura Y, Nakai T, Mishima T, Kato S, Grad S, Alini M, Risbud MV, Chan D, Cheah KS et al. 2012. Exhaustion of nucleus pulposus progenitor cells with ageing and degeneration of the intervertebral disc. *Nature communications* **3**: 1264.
- Taher F, Essig D, Lebl DR, Hughes AP, Sama AA, Cammisa FP, Girardi FP. 2012. Lumbar degenerative disc disease: current and future concepts of diagnosis and management. *Advances in orthopedics* **2012**: 970752.
- Tamplin OJ, Cox BJ, Rossant J. 2011. Integrated microarray and ChIP analysis identifies multiple Foxa2 dependent target genes in the notochord. *Dev Biol* **360**: 415-425.
- Thompson JP, Pearce RH, Schechter MT, Adams ME, Tsang IK, Bishop PB. 1990. Preliminary evaluation of a scheme for grading the gross morphology of the human intervertebral disc. *Spine (Phila Pa 1976)* **15**: 411-415.
- Turnbull IR, Wlzonek JJ, Osborne D, Hotchkiss RS, Coopersmith CM, Buchman TG. 2003. Effects of age on mortality and antibiotic efficacy in cecal ligation and puncture. *Shock* **19**: 310-313.
- Vasheghani F, Monemdjou R, Fahmi H, Zhang Y, Perez G, Blati M, St-Arnaud R, Pelletier JP, Beier F, Martel-Pelletier J et al. 2013. Adult cartilage-specific peroxisome proliferator-activated receptor gamma knockout mice exhibit the spontaneous osteoarthritis phenotype. *Am J Pathol* **182**: 1099-1106.
- Vo NV, Hartman RA, Yurube T, Jacobs LJ, Sowa GA, Kang JD. 2013. Expression and regulation of metalloproteinases and their inhibitors in intervertebral disc aging and degeneration. *Spine J* **13**: 331-341.
- Vogel KG, Paulsson M, Heinegard D. 1984. Specific inhibition of type I and type II collagen fibrillogenesis by the small proteoglycan of tendon. *Biochem J* **223**: 587-597.

- Warraich S, Bone DB, Quinonez D, Ii H, Choi DS, Holdsworth DW, Drangova M, Dixon SJ, Seguin CA, Hammond JR. 2013. Loss of equilibrative nucleoside transporter 1 in mice leads to progressive ectopic mineralization of spinal tissues resembling diffuse idiopathic skeletal hyperostosis in humans. *J Bone Miner Res* **28**: 1135-1149.
- Wozney JM, Rosen V, Celeste AJ, Mitsock LM, Whitters MJ, Kriz RW, Hewick RM, Wang EA. 1988. Novel regulators of bone formation: molecular clones and activities. *Science* **242**: 1528-1534.
- Yang F, Leung VY, Luk KD, Chan D, Cheung KM. 2009. Injury-induced sequential transformation of notochordal nucleus pulposus to chondrogenic and fibrocartilaginous phenotype in the mouse. *J Pathol* **218**: 113-121.
- Young MF, Bi Y, Ameye L, Chen XD. 2002. Biglycan knockout mice: new models for musculoskeletal diseases. *Glycoconjugate journal* **19**: 257-262.

CHAPTER FOUR

PROTEOMIC SIGNATURE OF THE MURINE INTERVERTEBRAL DISC

This chapter is currently under revision at *Plos One*:

McCann, M. R., Patel P., Frimpong A., Xiao Y., Siqueira W.L., Séguin C.A.
Proteomic Signature of the Murine Intervertebral Disc.

4.1 Co-Authorship Statement

Chapter 4 is adapted from McCann, M.R., Patel P., Frimpong, A., Xiao, Y., Siqueira, W.L., and Séguin, C.A. (2014). Proteomic Signature of the Murine Interverbral Disc. Submitted to *Plos One*.

Patel P. preformed protein extraction. Xiao Y., preformed tryptic digestion, ran liquid chromatography electrospray ionization with tandem mass spectrometry. All other experiments and bioinformatic analysis was preformed by M.R. McCann in the laboratory of Dr. C.A. Séguin. Manuscript was written by M.R. McCann with suggestions from Drs. A. Frimpong, W.L. Siqueira and C.A. Séguin. All authors were involved in drafting the article or revising it critically for content, and all authors approved the final version to be published.

4.2 Chapter Summary

Low back pain is the most common musculoskeletal problem and the single most common cause of disability, often attributed to degeneration of the intervertebral disc. Lack of effective treatment is directly related to our limited understanding of the pathways responsible for maintaining disc health. While transcriptional analysis has permitted initial insights into the biology of the intervertebral disc, complete proteomic characterization is required. We therefore employed liquid chromatography electrospray ionization tandem mass spectrometry (LC-ESI-MS/MS) protein/peptide separation and mass spectrometric analyses to characterize the protein content of intervertebral discs from skeletally mature wild-type mice. A total of 1360 proteins were identified and categorized using PANTHER. Identified proteins were primarily intracellular/plasma membrane (35%), organelle (30%), macromolecular complex (10%), extracellular region (9%). Molecular function categorization resulted in three distinct categories: catalytic activity (33%), binding (molecule interactions) (29%), and structural activity (13%). To validate our list, we confirmed the presence of 14 of 20 previously identified IVD-associated markers, including matrix proteins, transcriptional regulators, and secreted proteins. Immunohistochemical analysis confirmed distinct localization patterns of select proteins with the intervertebral disc. Characterization of the protein composition of healthy intervertebral disc tissue is an important first step in identifying cellular processes and pathways disrupted during aging or disease progression.

4.3 Introduction

Non-specific low back pain has become one of the most common health problems worldwide, with recent reports indicating lifetime prevalence as high as 84% (Balague et al. 2011). According to the most recent Global Burden of Disease study ((Vos et al. 2012)) back pain is the single most common cause of disability, with a global prevalence of 23%, causing disability in approximately 12% of people (Balague et al. 2011). Alarming, while the prevalence of low back pain has increased over the past three decades (Hoy et al. 2012), current treatment options do not adequately provide improved outcomes (Friedman et al. 2012). Even though the etiology of low back pain remains unknown, the first manifestations are thought to be a result of degeneration of the intervertebral disc (IVD).

The IVD is a specialized connective tissue structure located between the vertebrae that permits flexion, extension, lateral bending, and axial rotation of the spine. The IVD consists of three interdependent tissues, the cartilage end-plates (CEP), annulus fibrosus (AF) and nucleus pulposus (NP) (McCann et al. 2011a). During aging and degeneration the IVD undergoes substantial changes in tissue composition (Urban and Roberts 2003). Biochemically, the CEP undergoes calcification (Roberts et al. 1989; Urban and Winlove 2007) thereby impeding nutrient flow to the IVD (Roberts et al. 1989). The elastin content increases in the AF (Smith and Fazzalari 2009), and increased proteoglycan degradation in the NP leads to decreased disc height and an inability to maintain turgor against compressive loading (Lyons et al. 1981).

Recent studies have reported the transcriptional profile of IVD tissues in various animal models including rat (Lee et al. 2007), bovine (Minogue et al. 2010b), canine (Sakai et al. 2009) and rabbit (Poiraudreau et al. 1999). In addition, a small panel of transcripts (Rutges et al. 2010) and microRNA (Ohrt-Nissen et al. 2013) have been associated with IVD tissue in humans, and novel genetic variants have been associated with pathological lumbar disc degeneration (Williams et al. 2012). To date however, there are limited studies using unbiased proteomic strategies to define the composition of the healthy IVD. Recent studies provided detailed compositional analysis of the extracellular matrix of multiple human cartilaginous tissues, including the IVD (Onnerfjord et al. 2012) as well as bone and cartilage tissue in the zebrafish (Kessels et al. 2014). These studies highlight the value of global proteomic analysis in establishing the composition of specialized skeletal tissues, and the need to expand this analysis to model organisms commonly used to study development, aging or disease states.

Liquid chromatography coupled with mass spectrometry has emerged as an effective tool for quantitative proteomic profiling of complex tissue extracts (Xiang et al. 2004). In the current study, we employed a mass-spectrometry approach with a label-free method to decipher the proteomic profile of the healthy murine IVD. We aimed to gain a more in-depth understanding of the proteomic signature of the IVD, including intracellular proteins (transcription factors, metabolic enzymes, etc) and secreted molecules (growth factors, cytokines and matrix components) that regulate the complex microenvironment of IVD. This characterization enables a basic understanding of IVD biology, which will ultimately contribute to the identification of targets to modulate IVD health.

4.4 Materials and Methods

4.4.1 Animals

Animal care and handling procedures were approved by the Animal Use Committee of the University of Western Ontario (AUP 2009-050) in accordance with the guidelines of the Canadian Council on Animal Care. Fourteen-week-old (skeletally mature) male CD1 mice (He et al. 2006) were sacrificed by carbon dioxide asphyxiation. Spinal columns were dissected and cleaned of surrounding tissue.

4.4.2 Intervertebral Disc Harvest, Protein Extraction and Tryptic Digestion

Intact IVDs (including NP, AF and CEP) were isolated from the thoracic and lumbar regions by microdissection by shearing the IVD from the adjacent vertebral bone. IVDs were placed in phosphate buffered saline (PBS) under a stereoscope and surrounding muscle, bone, and spinal cord tissues were removed. Four to five thoracic IVDs from each mouse were minced with a scalpel, transferred to a microcentrifuge tube and incubated in 4 M urea, 10 mM dithiothreitol and 50 mM NH_4HCO_3 (pH 8.6), for 2 h at room temperature with gentle agitation. Samples were centrifuged at 3000 g for 3 min and the supernatant was collected and total protein concentration assessed using the Micro Bicinchoninic Acid (BCA) assay (Pierce, Rockford, IL, USA). Equivalent amounts of protein (10 μg) were subjected to tryptic digest (2% trypsin per weight of protein in 50 mM NH_4HCO_3 , pH 7.8) for 18 h at 37°C.

4.4.3 Liquid Chromatography Electrospray Ionization Tandem Mass Spectrometry (LC-ESI-MS/MS)

Peptide separation and a mass spectrometric analyses were carried out with a nano-HPLC Proxeon (Thermo Scientific, San Jose, CA, USA) linked to mass spectrometer (LTQ-Velos, Thermo Scientific) using electrospray ionization in a survey scan in the range of m/z values 390-2000 tandem MS/MS (Siqueira et al. 2012). Samples were resuspended in 20 μ l of 97.5 % H₂O/2.4% acetonitrile/0.1% formic acid and then subjected to reversed-phase LC-ESI-MS/MS. The nano-flow reversed-phase HPLC was developed with linear 80 min gradient ranging from 5% to 55% of solvent B in 65 min (97.5% acetonitrile, 0.1% formic acid) at a flow rate of 300 nl/min with a maximum pressure of 280 bar. Electrospray voltage and the temperature of the ion transfer capillary were 1.8 kV and 250 °C respectively. Each survey scan (MS) was followed by automated sequential selection of seven peptides for CID, with dynamic exclusion of the previously selected ions.

The resulting MS/MS spectra were searched against mouse databases (Swiss Prot and TrEMBL, Swiss Institute of Bioinformatics, Geneva, Switzerland, <http://ca.expasy.org/sprot/>) using the SEQUEST algorithm in the Proteome Discoverer 1.3 software (Thermo Scientific, San Jose, CA, USA). Search results were filtered for a False Discovery rate of 1% employing a decoy search strategy utilizing a reverse database. An additional inclusion criterion for positive identification of proteins was the presence of at least 2 different peptides from a protein and the same protein passing the filter score from at least in four different MS analyses from a total of six MS analyses (Peng et al. 2003; Elias et al. 2005).

4.4.4 Bioinformatic Analysis

Pathway analysis, molecular function, biological processes and cellular components of proteins were obtained from GeneOntology and charts were created using the PANTHER (Protein ANalysis Through Evolutionary Relationships) (<http://pantherdb.org>; version 9.0) classification system (Mi et al. 2013). The PANTHER database allows for high throughput functional analysis of large datasets of protein sequences.

4.4.5 Validation using Previously Published IVD Markers

To validate the accuracy of the identified proteins, we specifically queried for the presence of 20 IVD associated markers (proteins or genes) that were previously reported to be expressed in the murine embryonic node (Tamplin et al. 2011), developing murine IVD (Sohn et al. 2010), or human IVD (Minogue et al. 2010a). Candidate markers were selected to include a range of protein classifications including extracellular matrix proteins, transcriptional regulators, and secreted proteins.

4.4.6 Histology and Immunohistochemistry

Caudal spines were fixed in 4% paraformaldehyde overnight at 4°C, washed in PBS, decalcified for 5 days at room temperature in Shandon's TBD-2 (Fisher Scientific, Ottawa, ON, Can), dehydrated in a graded series of ethanol, cleared in xylene and embedded in paraffin. Samples were sectioned sagittally at a thickness of 5 µm using a microtome (Leica Microsystems, Concord, ON, Can.). Sections were then de-waxed in xylene and rehydrated by successive immersion in descending concentrations of alcohol.

Serial sections were processed for immunohistochemistry following antigen retrieval with 10 mM sodium citrate for 20 min at 95°C, with the exception of sections processed for the localization of Sox9, where 1% Triton-X in PBS was used for 20 min at room temperature. Slides were then blocked with 5% donkey serum in PBS with 0.2% Tween-20 (PBST) (Sigma), for 1 h and then incubated with primary antibody directed against NFAT5 (1:50; Santa Cruz, SC-5499), versican (1:100; raised to the N-terminal 13-residue peptide sequence of human versican (Fisher et al. 1995)), Sox9 (1:200; Santa Cruz, SC17340) or BSP (1:250, Renny Franceschi, University of Michigan, Ann Arbor, USA (Foster 2012)) in a humidified chamber overnight at 4°C. Slides were washed with PBST and incubated with species-specific secondary antibody (1:200; Alexa Fluor 488, Life Technologies) for 60 min prior to mounting with Vectasheild Medium with DAPI (Vector Labs, Burlingame, CA, USA). Images were captured with a Zeiss Axio Imager.M1 fluorescence microscope and processed with Northern Eclipse (Empix, Mississauga, ON, Can.) software.

4.5 RESULTS

4.5.1 Identification of Proteins in the Mature Murine Intervertebral Disc

SEQUEST identified 1940 proteins in the tryptic digest of IVD tissues from 14-week-old, skeletally mature wild-type mice. Proteins were filtered by accession numbers and queried using the UniProt database to identify peptides that were not annotated within the database at the time of analysis (Uniprot release 2013_06) or that were considered putative uncharacterized (580), as well as any proteins that were derived from Ensembl

automatic analysis pipeline and were therefore considered preliminary (396 proteins (**Appendix B, Table 4.1**)). This initial filter reduced the list of identified proteins to 1360 proteins localized to the IVD (**Appendix B, Table 4.2**).

4.5.2 Classification of the Proteomic Signature of the Murine Intervertebral Disc

The PANTHER database was then used to classify the list of proteins into categories according to cellular component, molecular function, biological processes and protein class. Based on gene ontology terms, the identified proteins were found to be primarily associated with intracellular/plasma membrane (35%), organelle (30%), macromolecular complex (10%), and extracellular region (9%) (**Figure 4.1 A**). The list of total proteins was further classified by biological process into 12 subgroups. The most abundant subgroups were metabolic process (27%), cellular process (20%), and developmental process (10%) (**Figure 4.1 B**). Following categorization by molecular function, proteins were mostly grouped into three categories: catalytic activity (33%), binding (molecule interactions) (29%), or structural activity (13%) (**Figure 4.1 C**). Characterization based on protein class was also performed, with proteins categorized into 27 classes, with nucleic acid binding (11%) being the most common, followed by cytoskeletal proteins (11%), hydrolases (9%), enzyme modulators (9%) and receptors (7%) (**Figure 4.1 D**).

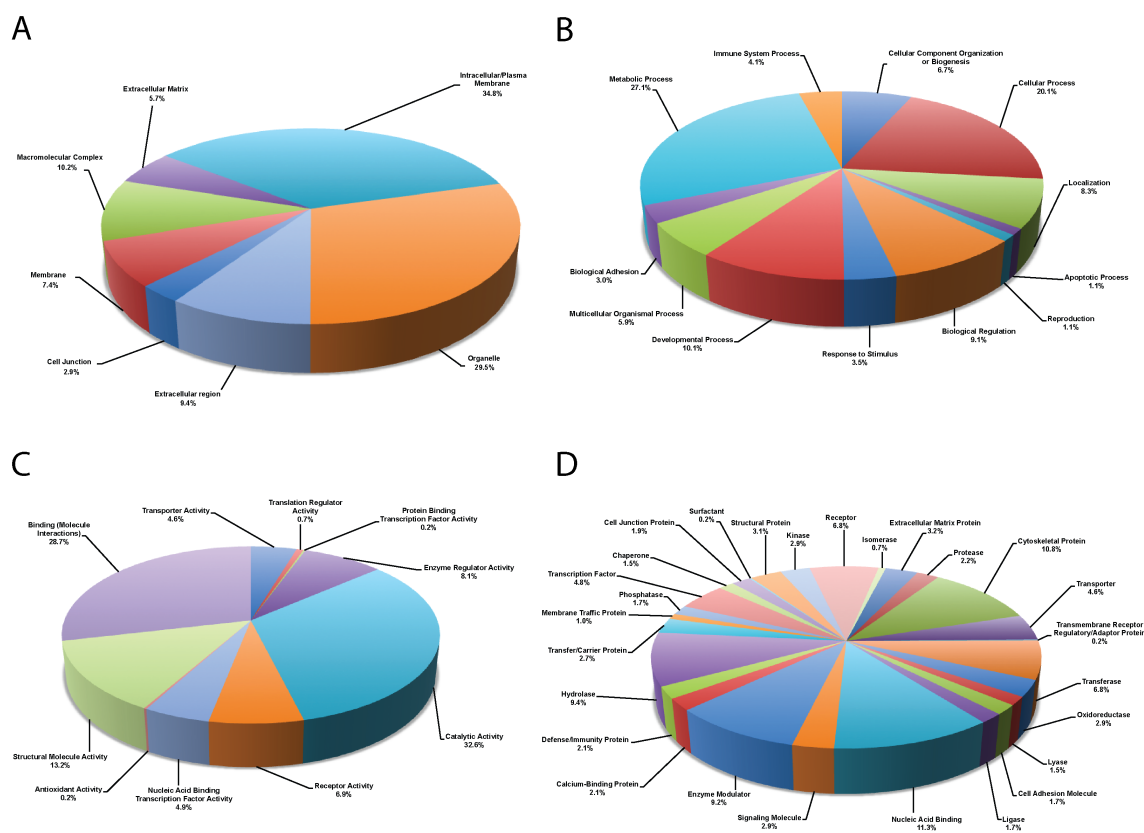


Figure 4.1 Proteomic signature of the murine intervertebral disc.

Pie chart depicting gene ontology (GO) analysis of proteins identified in the murine IVD. Representation of the distribution of proteins according to their molecular function as **A.** biological process, **B.** molecular function, **C.** cellular component, and **D.** protein class. Categorizations were based on information provided by the PANTHER classification system (www.pantherdb.org; v9.0). A total of 10 groups for molecular function, 12 groups for biological process, 7 cellular components, and 27 protein classes were detected. Further analysis of the intracellular classification revealed that the majority of proteins were characterized as cytoskeletal, followed by cytoplasmic, organelle and protein-transport ATP synthase complex.

4.5.3 Validation of identified proteins in the murine intervertebral disc

To validate the identified proteins, we queried for candidate IVD-associated genes previously identified based on transcriptional profiling and protein localization studies of the murine and human IVD (Johnstone et al. 1993; Gotz et al. 1995; Minogue et al. 2010a; Sohn et al. 2010; Tamplin et al. 2011; Bedore et al. 2013) (**Table 4.1**). Of the 20 markers selected, our proteomic approach validated expression of 14 proteins, including the extracellular matrix proteins collagen alpha-1(I), collagen alpha-2(I), and proteoglycans: aggrecan core protein, versican, decorin and biglycan. We also confirmed the presence of both keratin, type I cytoskeletal 8 (cytokeratin 8) and keratin, type I cytoskeletal 19 (cytokeratin 19) within the IVD, established as markers of notochord cells. Members of the Sox family of transcriptional regulators known to be important for cartilage development (Smits et al. 2001) were screened, with both of SOX 5 and 9 detected within the IVD. However, the secreted matricellular proteins CCN2 (CTGF) and CCN1 (Cyr61) were not identified. While TGF- β 2 was not identified, TGF- β 3 a related member of the TGF- β superfamily was detected.

Immunohistochemical analysis was performed to further confirm expression and tissue-specific localization of a subset of IVD proteins (**Figure 4.2**). NFAT5 was localized to NP and CEP cells, with the expected nuclear and perinuclear subcellular localization. Versican staining was detected throughout the disc with high levels detected in the pericellular matrix of fibrocartilagenous cells of the outer annulus. As expected, Sox 9 was detected in NP, CEP, and inner AF but was absent from cells of the outer AF. In contrast to previous reports (Minogue et al. 2010b) detection of Bone sialoprotein (BSP) was limited to the CEP, localized to the pericellular matrix.

Table 4.1: Validation using previously identified genes and proteins in the intervertebral disc.

UniProtKB Accession no.	Gene [†]	Name [†]	Presence/ Absence	Reference
Q61838	A2M	Alpha-2-macroglobulin	+	Minogue <i>et al.</i> 2010a
Q61282	Acan	Aggrecan core protein	+	Minogue <i>et al.</i> 2010a
P28653	Bgn	Biglycan	+	Johnstone <i>et al.</i>
Q6ZQ08	Cnot1	CCR4-NOT transcription complex subunit 1	+	Tamplin <i>et al.</i>
P29268	Ccn2	Connective tissue growth factor	-	Bedore <i>et al.</i>
P11087	Col1a	Collagen alpha-1(I) chain	+	Minogue <i>et al.</i> 2010a
Q01149	Col2a	Collagen alpha-2(I) chain	+	Minogue <i>et al.</i> 2010a
P28654	Dcn	Decorin	+	Johnstone <i>et al.</i>
Q61221	Hif-1a	Hypoxia-inducible factor 1-alpha	+	Minogue <i>et al.</i> 2010a
Q3TRM5	Ibsp	Integrin-binding Sialoprotein	-	Minogue <i>et al.</i> 2010a
P11679	Krt8	Keratin, type I cytoskeletal 8	+	Minogue <i>et al.</i> 2010a
P19001	Krt19	Keratin, type I cytoskeletal 19	+	Minogue <i>et al.</i> 2010a
Q14BI5	Myom2	Myomesin 2	+	Tamplin <i>et al.</i>
O88942	NFATc1	Nuclear factor of activated T-cells, cytoplasmic 1	-	Sohn <i>et al.</i>
P09084	Pax1	Paired box protein Pax-1	-	Sohn <i>et al.</i>
P35710	Sox5	Transcription Factor Sox-5	-	Smits <i>et al.</i>
Q8BSS6	Sox6	Transcription Factor Sox-6	+	Minogue <i>et al.</i> 2010a
Q04887	Sox9	Transcription Factor Sox-9	+	Minogue <i>et al.</i> 2010a
P27090	Tgfb2	Transforming growth factor beta-2	-	Sohn <i>et al.</i>
Q62059	Vcan	Versican core protein	+	Sohn <i>et al.</i>

[†]Details obtained from Uniprot database (www.uniprot.org/)

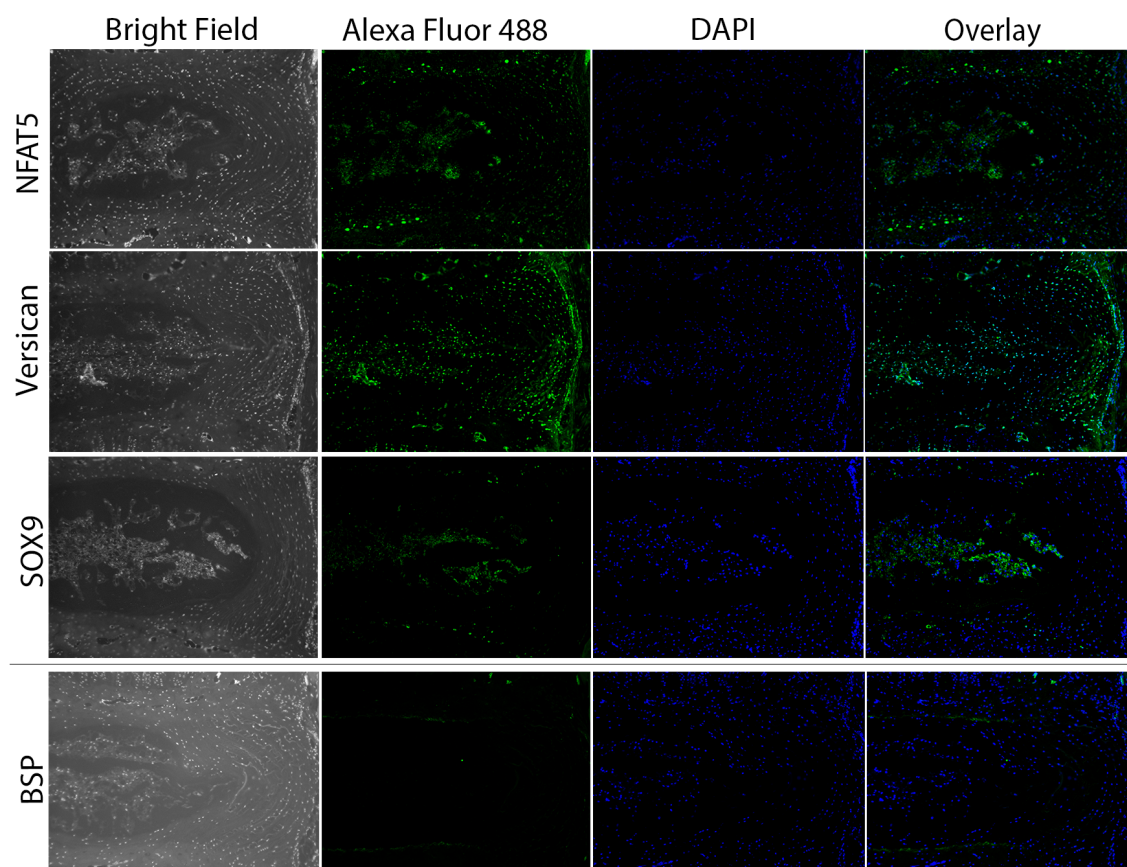


Figure 4.2 Immunohistochemical staining validating the localization of proteins in the murine intervertebral disc.

Representative images demonstrating the immunolocalization of NFAT5, versican, Sox 9, and BSP within the murine IVD. Each protein demonstrates a distinct pattern of localization within specific compartments of the disc. NFAT5 is localized to the NP and CEP, versican is present throughout the disc with high levels detected in the outer annulus, Sox 9 is present in NP and CEP and BSP is only detected in the CEP. For each protein-specific antibody, sections corresponding to 3 IVDs were assessed for each animal; n=3 mice. Scale bar = 100 μ m.

4.6 DISCUSSION

In this study, we employed a shotgun proteomic approach to determine the proteomic signature of the healthy murine IVD. Our findings provide a comprehensive and efficient resource for understanding the pathways responsible for maintaining disc homeostasis.

To validate the proteomic characterization of the IVD, we employed a candidate approach to specifically query IVD-associated genes previously identified by transcriptional analysis of murine (Sohn et al. 2010; Tamplin et al. 2011), and human disc tissues (Minogue et al. 2010a). This analysis identified 14 of 20 candidate genes, and furthermore identified numerous additional peptides belonging to related protein superfamilies. Specific examples include WISP1, DUSP1 and NFAT5 identified in our proteomic study which are related to WISP2, DUSP27 and NFATC1, respectively, which were previously identified at the level of gene expression in the developing mouse IVD (Sohn et al. 2010). This interesting trend may reflect temporal changes in expression of related proteins associated with skeletal development and maturity, or the co-expression of multiple related proteins within the IVD and differences in the resolution or sensitivity of transcriptional and proteomic analysis. To further validate the list of proteins identified in the current study, we compared our findings to recent datasets generated from the proteomic analysis of human cartilaginous tissues, which included both NP and AF (Onnerfjord et al. 2012). Similar to the analysis of human IVD tissues, we identified well-characterized ECM proteins (aggrecan, decorin, versican, lumican, type-I and type-II collagen) as well as intracellular proteins such as phospholipase A₂ and protein S100-A9. However, some discrepancies were also noted. For example, high levels of lubricin

expression were reported in human NP tissues; however, lubricin was not identified in the murine IVD. These discrepancies highlight the need for further investigation, specifically aimed at examining the proteomic signature of human and murine tissues at similar ages or stages of disc disease to more thoroughly assess conservation between species relevant to the use of mouse models to study human disc disease (Kislinger and Gramolini 2010).

Our analysis also detected the expression of proteins previously found to be enriched in the murine developing node at embryonic day E8.5, including CNOT1, MYOM1 and CA3. These findings validate studies by our lab and others that used lineage tracing to demonstrate that the murine NP of the IVD is derived from the embryonic notochord (Choi et al. 2008; McCann et al. 2011b). Our previous studies detected the presence of notochord cells within the mouse NP up to 9 months of age, therefore we anticipate that a population of notochord cells would be present in the NP at the time point examined in this study. The detection of notochord-specific markers in our analysis validates our ability to capture the multiple cell types that constitute the mature IVD. Further suggesting that our analysis included a significant proportion of notochord or notochord-derived cells was the identification of proteins annotated to the protein-transport ATP synthase complex. Recent studies in the developing zebrafish demonstrated that vacuolated notochord cells require acidification, in the form of ATP/H⁺ complex to form and maintain vacuoles (Ellis et al. 2013).

It is interesting to note that several proteins identified by our screen are associated with IVD-specific or skeletal phenotypes in mutant mice, such as SPARC (secreted protein, acidic, and rich in cysteine) (Gruber et al. 2005; Millecamps et al. 2012) and NPR3 (natriuretic peptide receptor C) (Jaubert et al. 1999). SPARC is a matricellular

protein important for modulating interactions between cells and their ECM, including collagen deposition and remodeling, and growth factor efficacy. Targeted deletion of SPARC alters the cellular content and ECM composition/organization of the AF, and results in disc wedging, endplate calcification, and sclerosis (Gruber et al. 2005), which lead to an increase in the detection of back pain-associated behavior (Millecamps et al. 2012). Similarly, mutation of NPR3 resulted in thin or absent NP with calcification of the dorsal AF in mice at postnatal day 21 (Jaubert et al. 1999). Inactivation of two paralogous genes is often required to observe a developmental phenotype in mutant mice, as is the case with SOX5 and SOX6 (Smits and Lefebvre 2003; Lefebvre 2010). Mice lacking expression of both *Sox5* and *Sox6* demonstrated defects in notochord sheath formation, leading to notochord cell apoptosis and the absence of NP within the IVD. We also detected IVD-enriched proteins such as *FOXA2/HNF-3 β* , which has been implicated in notochord development in other model organisms (Olsen and Jeffery 1997). Other proteins detected in our study, such as TGF- β , have reported general disruptions in skeletal development in knockout mouse models (Spagnoli et al. 2007). This further exemplifies that our proteomic characterization of the IVD provides insight into the homeostasis of the murine IVD and a list of candidate proteins that can be further explored to determine their role within the IVD.

This study provides the first proteome database of IVD tissue from healthy, skeletally mature mouse. The identification and classification of the proteins present within the healthy IVD is a critical first step in determining the pathways and processes that are required to maintain IVD homeostasis. Such data will establish a solid foundation for better understanding the complex microenvironment of the IVD, and provide a

starting point from which to identify and ultimately target the pathways that are altered during the process of disc degeneration that contribute to back pain.

4.7 REFERENCES

- Balague F, Mannion AF, Pellise F, Cedraschi C. 2011. Non-specific low back pain. *Lancet*.
- Bedore J, Sha W, McCann MR, Liu S, Leask A, Seguin CA. 2013. Impaired Intervertebral Disc Development and Premature Disc Degeneration in Mice With Notochord-Specific Deletion of Ccn2. *Arthritis Rheum* **65**: 2634-2644.
- Choi KS, Cohn MJ, Harfe BD. 2008. Identification of nucleus pulposus precursor cells and notochordal remnants in the mouse: implications for disk degeneration and chordoma formation. *Dev Dyn* **237**: 3953-3958.
- Elias JE, Haas W, Faherty BK, Gygi SP. 2005. Comparative evaluation of mass spectrometry platforms used in large-scale proteomics investigations. *Nature methods* **2**: 667-675.
- Ellis K, Bagwell J, Bagnat M. 2013. Notochord vacuoles are lysosome-related organelles that function in axis and spine morphogenesis. *J Cell Biol* **200**: 667-679.
- Fisher LW, Stubbs JT, 3rd, Young MF. 1995. Antisera and cDNA probes to human and certain animal model bone matrix noncollagenous proteins. *Acta orthopaedica Scandinavica Supplementum* **266**: 61-65.
- Foster BL. 2012. Methods for studying tooth root cementum by light microscopy. *International journal of oral science* **4**: 119-128.
- Friedman BW, O'Mahony S, Mulvey L, Davitt M, Choi H, Xia S, Esses D, Bijur PE, Gallagher EJ. 2012. One-week and 3-month outcomes after an emergency department visit for undifferentiated musculoskeletal low back pain. *Annals of emergency medicine* **59**: 128-133 e123.
- Gotz W, Kasper M, Fischer G, Herken R. 1995. Intermediate filament typing of the human embryonic and fetal notochord. *Cell Tissue Res* **280**: 455-462.
- Gruber HE, Sage EH, Norton HJ, Funk S, Ingram J, Hanley EN, Jr. 2005. Targeted deletion of the SPARC gene accelerates disc degeneration in the aging mouse. *J Histochem Cytochem* **53**: 1131-1138.

- He J, Rosen CJ, Adams DJ, Kream BE. 2006. Postnatal growth and bone mass in mice with IGF-I haploinsufficiency. *Bone* **38**: 826-835.
- Hoy D, Bain C, Williams G, March L, Brooks P, Blyth F, Woolf A, Vos T, Buchbinder R. 2012. A systematic review of the global prevalence of low back pain. *Arthritis Rheum* **64**: 2028-2037.
- Jaubert J, Jaubert F, Martin N, Washburn LL, Lee BK, Eicher EM, Guenet JL. 1999. Three new allelic mouse mutations that cause skeletal overgrowth involve the natriuretic peptide receptor C gene (Npr3). *Proc Natl Acad Sci U S A* **96**: 10278-10283.
- Johnstone B, Markopoulos M, Neame P, Caterson B. 1993. Identification and characterization of glycanated and non-glycanated forms of biglycan and decorin in the human intervertebral disc. *Biochem J* **292** (Pt 3): 661-666.
- Kessels MY, Huitema LF, Boeren S, Kranenbarg S, Schulte-Merker S, van Leeuwen JL, de Vries SC. 2014. Proteomics analysis of the zebrafish skeletal extracellular matrix. *PLoS One* **9**: e90568.
- Kislinger T, Gramolini AO. 2010. Proteome analysis of mouse model systems: A tool to model human disease and for the investigation of tissue-specific biology. *Journal of proteomics* **73**: 2205-2218.
- Lee CR, Sakai D, Nakai T, Toyama K, Mochida J, Alini M, Grad S. 2007. A phenotypic comparison of intervertebral disc and articular cartilage cells in the rat. *Eur Spine J* **16**: 2174-2185.
- Lefebvre V. 2010. The SoxD transcription factors--Sox5, Sox6, and Sox13--are key cell fate modulators. *The international journal of biochemistry & cell biology* **42**: 429-432.
- Lyons G, Eisenstein SM, Sweet MB. 1981. Biochemical changes in intervertebral disc degeneration. *Biochimica et biophysica acta* **673**: 443-453.
- McCann MR, Bacher CA, Seguin CA. 2011a. Exploiting notochord cells for stem cell-based regeneration of the intervertebral disc. *J Cell Commun Signal* **5**: 39-43.
- McCann MR, Tamplin OJ, Rossant J, Seguin CA. 2011b. Tracing notochord-derived cells using a Noto-cre mouse: implications for intervertebral disc development. *Dis Model Mech*.
- Mi H, Muruganujan A, Thomas PD. 2013. PANTHER in 2013: modeling the evolution of gene function, and other gene attributes, in the context of phylogenetic trees. *Nucleic Acids Res* **41**: D377-386.

- Millecamps M, Tajerian M, Naso L, Sage EH, Stone LS. 2012. Lumbar intervertebral disc degeneration associated with axial and radiating low back pain in ageing SPARC-null mice. *Pain* **153**: 1167-1179.
- Minogue BM, Richardson SM, Zeef LA, Freemont AJ, Hoyland JA. 2010a. Characterization of the human nucleus pulposus cell phenotype and evaluation of novel marker gene expression to define adult stem cell differentiation. *Arthritis Rheum* **62**: 3695-3705.
- Minogue BM, Richardson SM, Zeef LA, Freemont AJ, Hoyland JA. 2010b. Transcriptional profiling of bovine intervertebral disc cells: implications for identification of normal and degenerate human intervertebral disc cell phenotypes. *Arthritis Res Ther* **12**: R22.
- Ohrh-Nissen S, Dossing KB, Rossing M, Lajer C, Vikesa J, Nielsen FC, Friis-Hansen L, Dahl B. 2013. Characterization of miRNA Expression in Human Degenerative Lumbar Disks. *Connect Tissue Res* **54**: 197-203.
- Olsen CL, Jeffery WR. 1997. A forkhead gene related to HNF-3beta is required for gastrulation and axis formation in the ascidian embryo. *Development* **124**: 3609-3619.
- Onnerfjord P, Khabut A, Reinholt FP, Svensson O, Heinegard D. 2012. Quantitative proteomic analysis of eight cartilaginous tissues reveals characteristic differences as well as similarities between subgroups. *J Biol Chem* **287**: 18913-18924.
- Peng J, Elias JE, Thoreen CC, Licklider LJ, Gygi SP. 2003. Evaluation of multidimensional chromatography coupled with tandem mass spectrometry (LC/LC-MS/MS) for large-scale protein analysis: the yeast proteome. *J Proteome Res* **2**: 43-50.
- Poiraudeau S, Monteiro I, Anract P, Blanchard O, Revel M, Corvol MT. 1999. Phenotypic characteristics of rabbit intervertebral disc cells. Comparison with cartilage cells from the same animals. *Spine (Phila Pa 1976)* **24**: 837-844.
- Roberts S, Menage J, Urban JP. 1989. Biochemical and structural properties of the cartilage end-plate and its relation to the intervertebral disc. *Spine (Phila Pa 1976)* **14**: 166-174.
- Rutges J, Creemers LB, Dhert W, Milz S, Sakai D, Mochida J, Alini M, Grad S. 2010. Variations in gene and protein expression in human nucleus pulposus in comparison with annulus fibrosus and cartilage cells: potential associations with aging and degeneration. *Osteoarthritis Cartilage* **18**: 416-423.

- Sakai D, Nakai T, Mochida J, Alini M, Grad S. 2009. Differential phenotype of intervertebral disc cells: microarray and immunohistochemical analysis of canine nucleus pulposus and anulus fibrosus. *Spine (Phila Pa 1976)* **34**: 1448-1456.
- Siqueira WL, Bakkal M, Xiao Y, Sutton JN, Mendes FM. 2012. Quantitative proteomic analysis of the effect of fluoride on the acquired enamel pellicle. *PLoS One* **7**: e42204.
- Smith LJ, Fazzalari NL. 2009. The elastic fibre network of the human lumbar anulus fibrosus: architecture, mechanical function and potential role in the progression of intervertebral disc degeneration. *Eur Spine J* **18**: 439-448.
- Smits P, Lefebvre V. 2003. Sox5 and Sox6 are required for notochord extracellular matrix sheath formation, notochord cell survival and development of the nucleus pulposus of intervertebral discs. *Development* **130**: 1135-1148.
- Smits P, Li P, Mandel J, Zhang Z, Deng JM, Behringer RR, de Crombrughe B, Lefebvre V. 2001. The transcription factors L-Sox5 and Sox6 are essential for cartilage formation. *Dev Cell* **1**: 277-290.
- Sohn P, Cox M, Chen D, Serra R. 2010. Molecular profiling of the developing mouse axial skeleton: a role for Tgfr2 in the development of the intervertebral disc. *BMC Dev Biol* **10**: 29.
- Spagnoli A, O'Rear L, Chandler RL, Granero-Molto F, Mortlock DP, Gorska AE, Weis JA, Longobardi L, Chytil A, Shimer K et al. 2007. TGF-beta signaling is essential for joint morphogenesis. *J Cell Biol* **177**: 1105-1117.
- Tamplin OJ, Cox BJ, Rossant J. 2011. Integrated microarray and ChIP analysis identifies multiple Foxa2 dependent target genes in the notochord. *Dev Biol* **360**: 415-425.
- Urban JP, Roberts S. 2003. Degeneration of the intervertebral disc. *Arthritis Res Ther* **5**: 120-130.
- Urban JP, Winlove CP. 2007. Pathophysiology of the intervertebral disc and the challenges for MRI. *Journal of magnetic resonance imaging : JMRI* **25**: 419-432.
- Vos T, Flaxman AD, Naghavi M, Lozano R, Michaud C, Ezzati M, Shibuya K, Salomon JA, Abdalla S, Aboyans V et al. 2012. Years lived with disability (YLDs) for 1160 sequelae of 289 diseases and injuries 1990-2010: a systematic analysis for the Global Burden of Disease Study 2010. *Lancet* **380**: 2163-2196.
- Williams FM, Bansal AT, van Meurs JB, Bell JT, Meulenbelt I, Suri P, Rivadeneira F, Sambrook PN, Hofman A, Bierma-Zeinstra S et al. 2012. Novel genetic variants associated with lumbar disc degeneration in northern Europeans: a meta-analysis of 4600 subjects. *Ann Rheum Dis*.

Xiang R, Shi Y, Dillon DA, Negin B, Horvath C, Wilkins JA. 2004. 2D LC/MS analysis of membrane proteins from breast cancer cell lines MCF7 and BT474. *J Proteome Res* **3**: 1278-1283.

CHAPTER FIVE

ACUTE VIBRATION INDUCES TRANSIENT EXPRESSION OF ANABOLIC
GENES IN THE MURINE INTERVERTEBRAL DISC

This chapter has been reproduced with permission from:

McCann M.R.*, Patel P.*, Beaucage K.L, Xiao Y., Bacher C.A., Siqueira W.L., Holdsworth D.W., Dixon S.J, Séguin C.A. Acute vibration induces transient expression of anabolic genes in the intervertebral disc in a frequency dependent manner. *Arthritis and Rheumatism*. 2013 Jul;65(7):1853-64, with some modifications. *Equal first author contribution.

5.1 Co-Authorship Statement

Chapter 5 is adapted from McCann, M.R., Patel P., Beaucage, K.L., Xiao, Y., Bacher, C.A. Siqueira, W.L., Holdsworth, D.W., Dixon S.J., and Séguin, C.A. (2013). Acute Vibration Induces Transient Expression of Anabolic Genes in the Murine Intervertebral Disc. *Arthritis & Rheumatism* Jul;65(7):1853-1864. Figures and text are reproduced with permission from *Arthritis & Rheumatism* (Appendix X).

P. Patel preformed real-time PCR. K.L. Beaucage assisted in project development and help run the *ex vivo* and *in vivo* vibration apparatus. C.A Bacher assisted in project development and preformed initial *ex vivo* vibration. Y. Xiao preformed tryptic digestion and ran liquid chromatography electrospray ionization with tandem mass spectrometry. All other experiments were preformed by M.R. McCann in the laboratory of Dr. C.A. Séguin. All authors were involved in drafting the article or revising it critically for important intellectual content, and all authors approved the final version to be published. Manuscript was written by M.R. McCann with suggestions from Drs. W.L. Siqueira, D.W. Holdsworth, S.J. Dixon and C.A. Séguin.

5.2 Chapter Summary

Low-amplitude whole body vibration has been adopted for the treatment of back pain and spinal disorders. However, there is limited knowledge of the impact of vibration on the intervertebral disc. This study was undertaken to examine the effects of acute vibration on anabolic and catabolic pathways in the intervertebral disc and to characterize the dependence of these changes on time and frequency. Custom-designed platforms were developed to apply acute vibration to *ex vivo* and *in vivo* mouse models. Spinal segments (*ex vivo*) or mice (*in vivo*) were subjected to vibration (for 30 minutes at 15–90 Hz with peak acceleration at 0.3 g), and intervertebral discs were examined at specific time points after vibration. Gene expression was quantified using real-time polymerase chain reaction, and protein levels were examined by quantitative mass spectrometry and immunofluorescence. In the *ex vivo* model, acute vibration at 15 Hz induced expression of anabolic genes (aggrecan, biglycan, decorin, type I collagen, and *Sox9*) and suppressed expression of *Mmp13*, with the most pronounced changes detected 6 hours following vibration. These beneficial effects were frequency dependent and were no longer evident between 45 and 90 Hz. *In vivo*, the effects on anabolic gene expression were even more robust and were accompanied by decreased expression of *Adamts4*, *Adamts5*, and *Mmp3*. Moreover, significant increases in the protein levels of aggrecan, biglycan, decorin, and type I collagen were detected *in vivo*. These findings demonstrate dramatic anabolic effects of acute vibration on intervertebral disc tissue, responses that are dependent on frequency. The similarity of the *in vivo* and *ex vivo* responses indicates that at least some effects of vibration are tissue autonomous.

5.3 Introduction

Back pain is the second most common chronic condition, with a reported lifetime incidence of 84% in industrialized countries (Balague et al. 2011). Degenerative disc disease is a major cause of back pain and results from changes in the composition of the extracellular matrix (ECM) within the intervertebral disc (IVD) (Buckwalter et al. 1994). The IVD is maintained by specialized cell types that adjust their metabolism, and subsequently ECM composition, in response to external factors including nutritional, genetic, and biomechanical influences (Roughley 2004). The annulus fibrosus (AF) is composed of concentric lamellae formed by parallel bundles of type I collagen fibers, which provide tensile strength. In contrast, the central nucleus pulposus (NP) is composed of an irregular network of type II collagen (Humzah and Soames 1988), large aggregating proteoglycans (aggrecan), versican, and small proteoglycans (decorin and biglycan), which establish an osmotic swelling pressure by attracting water (Urban and Roberts 2003). The high water content allows the spine to withstand mechanical loading. Decreased expression of matrix molecules and increased expression of catabolic enzymes, such as matrix metalloproteinases (MMPs) and members of the ADAMTS family, have been associated with IVD degeneration (Crean et al. 1997; Pockert et al. 2009).

Mechanical loading contributes to IVD homeostasis and maintenance of the ECM. *In vitro* (Chen et al. 2004; Wang et al. 2007; Desmoulin et al. 2010) and *in vivo* (MacLean et al. 2003; Maclean et al. 2004; Walsh and Lotz 2004; Wuertz et al. 2009; Desmoulin et al. 2011; Iatridis et al. 2011) studies have shown that physiologic loading promotes matrix anabolism, whereas nonphysiologic loading (i.e., immobilization or

overloading) promotes matrix catabolism and degeneration. Static compression of the IVD is associated with down-regulation of anabolic genes (collagens and aggrecans), whereas dynamic compression stimulates anabolic gene expression (Wang et al. 2007). The application of dynamic compression *in vivo* stimulates anabolic gene expression (aggrecan and collagens) with minimal changes in catabolic gene expression (ADAMTS and MMPs), promoting an overall increase in glycosaminoglycan content within the NP (Wuertz et al. 2009). Regional differences in the response of the NP and AF to mechanical loading have been reported, with responses dependent on frequency in the NP and both frequency and magnitude in the AF (Maclean et al. 2004). Moreover, dynamic overloading *in vivo* increases levels of aggrecan degradation products in both the AF and the NP (Iatridis et al. 2011). Although these studies have begun to elucidate responses of IVD cells to mechanical stimulation, they are limited in their ability to distinguish the direct effects (i.e., tissue autonomous) from indirect effects (i.e., secondary to muscle activation, altered blood flow, or endocrine or neural signaling) on disc homeostasis.

It is well established that physiologic loading is required to maintain IVD integrity, since prolonged bed rest and microgravity alter disc composition and decrease IVD height (Sayson and Hargens 2008; Belavy et al. 2011). However, specific parameters of physiologic loading critical to maintain disc health have yet to be established. Recent studies have explored the ability of WBV to regulate disc health and homeostasis. In fact, vibration therapy is becoming a common clinical treatment for spine-related disorders, including nonspecific back pain (Belavy et al. 2008; del Pozo-Cruz et al. 2011), fibromyalgia (Alentorn-Geli et al. 2008), and ankylosing spondylitis (Chaplin 2010). For instance, recent studies have described the ability of acute exposure to low-intensity

vibration (30 Hz for 10 minutes per day) to reduce the detrimental changes in disc morphology and incidence of back pain induced by prolonged bed rest (Holguin et al. 2009).

There are several theories regarding the mechanism through which whole-body vibration (WBV) alleviates back pain. First, WBV may strengthen core muscles, improving posture and reducing strain on the spine (Rittweger et al. 2002). Second, WBV may relax back muscles, leading to reduced back pain (Rittweger et al. 2003). Third, WBV may stimulate the expression of anabolic genes, while suppressing the expression of catabolic genes in the IVD, improving disc integrity (Henchoz and Kai-Lik So 2008). In contrast, exposure to excessive vibration, such as that associated with operating heavy machinery, increases the prevalence of lower back pain (Kuisma et al. 2007; Tiemessen et al. 2008). This dichotomy demonstrates that maintenance of IVD health through mechanical loading or vibration therapy requires an optimized amplitude and frequency of the applied load.

Despite the clinical use of vibration therapy, there have been few studies undertaken to investigate the optimal parameters of vibration and, moreover, how this form of mechanical stimulation influences IVD homeostasis at the cellular level. Using a spine organ culture system paired with an *in vivo* system for the application of WBV, we examined the effects of acute vibration on murine IVD homeostasis. We hypothesized that high-frequency low-amplitude vibration would modify cellular metabolism and gene expression within the IVD, up-regulating the expression of anabolic genes and suppressing the expression of catabolic genes, leading to improved IVD integrity.

5.4 MATERIALS AND METHODS

5.4.1 *Ex Vivo* Spine Organ Culture

All procedures were approved by the Council on Animal Care at The University of Western Ontario and were conducted in accordance with the guidelines of the Canadian Council on Animal Care. Ten-week-old male CD-1 mice were euthanized by CO₂ asphyxiation. Spinal columns from the first cervical vertebrae to the fourth caudal vertebrae were dissected and cleaned of surrounding tissue. Isolated spines were incubated in 0.25% trypsin-EDTA (Gibco, Burlington, ON, Can.) for 15 minutes at 37°C with gentle rotation. Following incubation, spines were washed with phosphate buffered saline (PBS) and then incubated in 2 mg/ml of type II collagenase (Worthington Biochemical Corporation, Lakewood, NJ, USA) in Dulbecco's modified Eagle's medium (DMEM; Gibco) at 37°C for 45 minutes with rotation to remove surrounding musculature, while retaining the anterior and posterior longitudinal ligaments (**Figure 5.1**). Isolated spinal columns were then vigorously shaken in PBS 3 times. Each vertebral column was separated into 3 segments; these segments were affixed to 35-mm cell culture dishes by attachment of the dorsal spinal processes using cyanoacrylate adhesive (**Figure 5.2 A**). Tissues were submerged in DMEM-F-12 with 10% fetal bovine serum and 1X penicillin-streptomycin (Gibco). Following vibration, the medium was replaced for incubation.

5.4.2. *Ex Vivo* Vibration Apparatus

An *ex vivo* vibration platform was developed in house. This apparatus produced

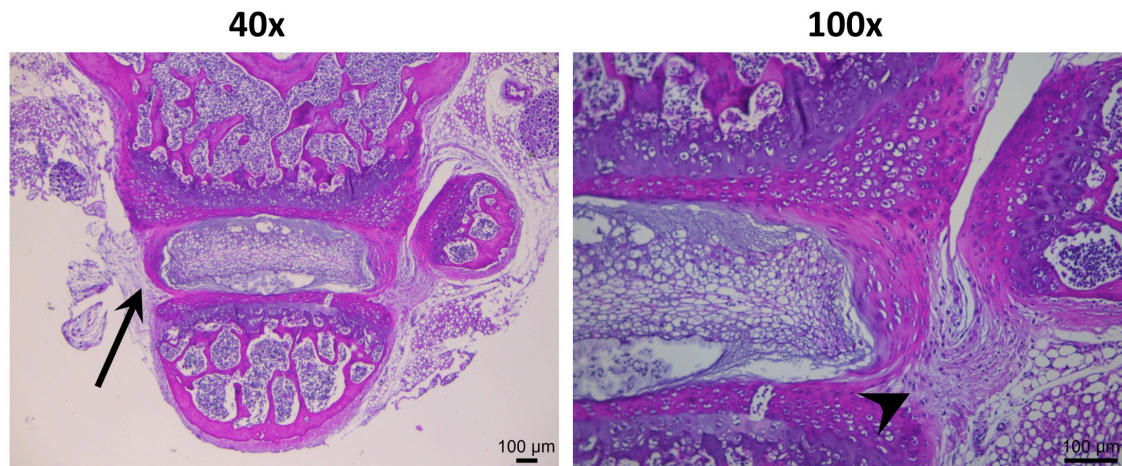


Figure 5.1 Histological appearance of murine spinal segments used in *ex vivo* organ culture model.

Representative images demonstrating the composition of spinal segments used for *ex vivo* organ culture experiments (sections stained with hematoxylin and eosin). Histological sections from cervical region of the spine demonstrated that following isolation, the musculature and soft tissues were removed and the disc and surrounding supportive ligaments remained intact (arrow indicates anterior longitudinal ligament, arrowhead indicates intra-articular ligament). Sections corresponding to 4-6 intervertebral discs were assessed for each animal from $n = 3$ mice.

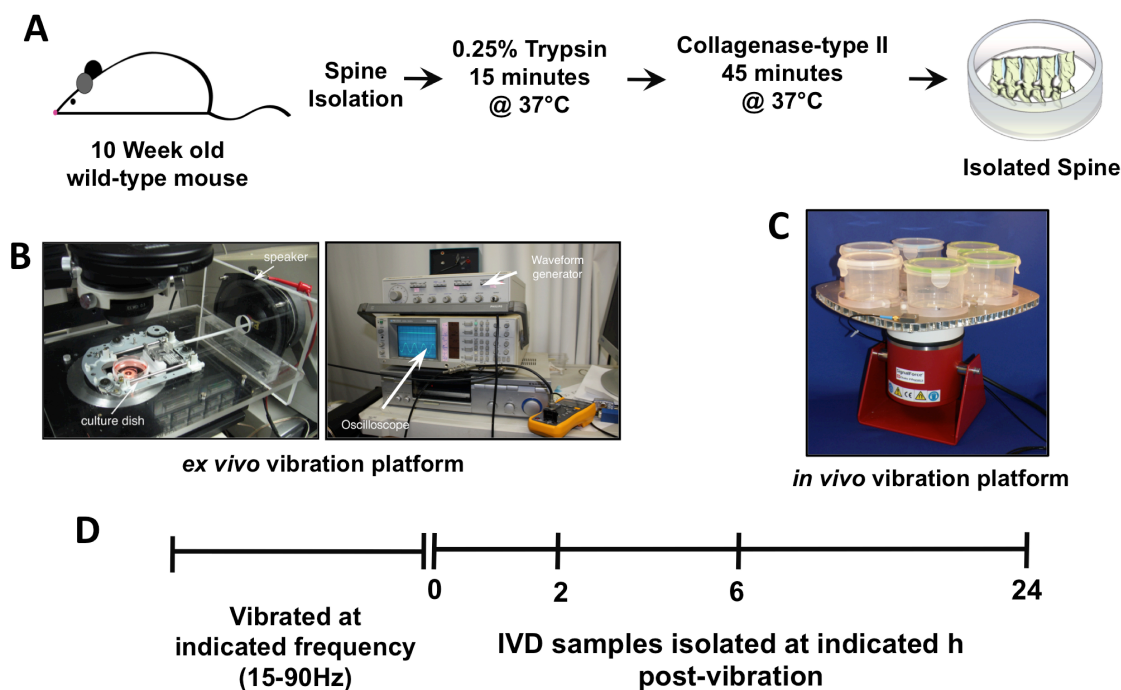


Figure 5.2 Experimental design and platforms developed for *ex vivo* and *in vivo* studies of the effects of vibration on murine intervertebral discs.

A. Schematic representation of the protocol used for the mouse spine organ culture model. **B.** *Ex vivo* vibration platform designed for the delivery of 10–90 Hz, 0.01–0.33 mm peak-to-peak displacement. Amplitudes were adjusted to maintain the peak acceleration at 0.3 g at all frequencies tested. **C.** WBV platform developed for *in vivo* studies. Vibrations were produced by an electromagnetic shaker regulated by an open-loop controller allowing for vibration at frequencies ranging from 10 to 90 Hz. During vibration, animals were housed in individual affixed chambers without bedding. Signals from the waveform generator and those detected by the accelerometer were acquired throughout each experiment. Waveforms from both the generator and the accelerometer were confirmed to be sinusoidal. **D.** Schematic representation of the experimental procedures used in *ex vivo* organ culture and *in vivo* models.

vibrations over the following ranges: peak acceleration 0.2–0.6 g (1.96–5.88 meters second²), frequency 10–90 Hz, and peak-to-peak displacement 0.01–0.33 mm. Sinusoidal, horizontal vibrations were applied to 35 mm cell culture dishes, controlled through a voice coil (model W54; Pyramid Pro 150W) driven at the desired frequency and amplitude (**Figure 5.2 B**). The dish was placed in a plastic cradle, supported by a custom-designed carriage, with vibration motion waveforms transmitted through a thin-walled plastic tube. The carriage assembly incorporates a small amount of metal ballast to eliminate unwanted mechanical resonance. Acceleration was monitored using a miniature accelerometer (model 7521A1; Dytran Instruments, Chatsworth, CA, USA) attached to the cradle. The voice coil was driven by an AC-coupled audio-frequency amplifier (model DCR 100; Sanyo), with input from a function generator (model PM 5135; Fluke and Philips, Mississauga, ON, Can.) that provides the desired amplitude and frequency. Waveform shape was monitored by an oscilloscope (PM3350A; Fluke and Philips) to ensure that a sinusoidal waveform was maintained.

The apparatus was set to vibrate samples horizontally (along the long axis of the spinal segments) at frequencies of up to 90 Hz and peak acceleration of 0.3 g (2.94 meters second²). Experimental parameters for vibration (15, 45, 60, and 90 Hz) were selected based on previous literature (Prisby et al. 2008). Sham control segments were adhered to dishes and placed beside the vibration platform to maintain identical environmental factors. Following 30 minutes of vibration, the sham and vibration groups were either immediately processed for RNA extraction (0 hours) or incubated at 37°C and 5% CO₂ for 2, 6, or 24 hours (**Figure 5.2 D**).

5.4.3 *In Vivo* Vibration

A low-amplitude high-frequency vibration platform was designed in house for WBV of mice (**Figure 5.2 C**). The platform was constructed using a 12-mm-thick commercial grade aluminum-core honey- comb (model PCGA-XR13003; Plascore, Zeeland, MI, USA) affixed to an electromagnetic shaker (Signal Force V20; Data Physics, San Jose, CA, USA) producing sinusoidal vertical vibrations regulated by a scalar open-loop controller (a model 148A Wavetek Waveform Generator and a Data Physics model PA100E Power Amplifier). Acceleration was monitored using a precision piezoelectric accelerometer affixed to the platform (model 7500A1; Dytran Instruments), and the motion waveform was verified using a high-speed digital camera (Casio Ex-F1, Casio, Markham, ON, Can.). The system operated with user-variable parameters of load (balanced and unbalanced weight distribution of up to 6 mice), acceleration (0.1–0.3g), amplitude (10–100 μm), and frequency (10–90 Hz). Voltage and sinusoidal waveforms were confirmed prior to and throughout the experiments using a multimeter (model 115 True RMS; Fluke Corporation) and a Powerlab data acquisition system (Powerlab/4SP; ADInstruments, Colorado Springs, CO, USA) with Chart5 software version 5.0.1 for real-time waveform patterns (ADInstruments) (**Figure 5.3**).

Based on previous reports of optimized parameters of WBV for tissue including muscle and bone (Oxlund et al. 2003; Verschueren et al. 2004) with a peak-to-peak amplitude of 74 μm , and 0.3 g acceleration for 30 minutes. Age- and sex-matched controls were housed in chambers on a sham platform throughout the experiment to maintain identical handling and environmental conditions. During vibration, mice were housed in individual chambers without bedding to prevent damping of the vibration.

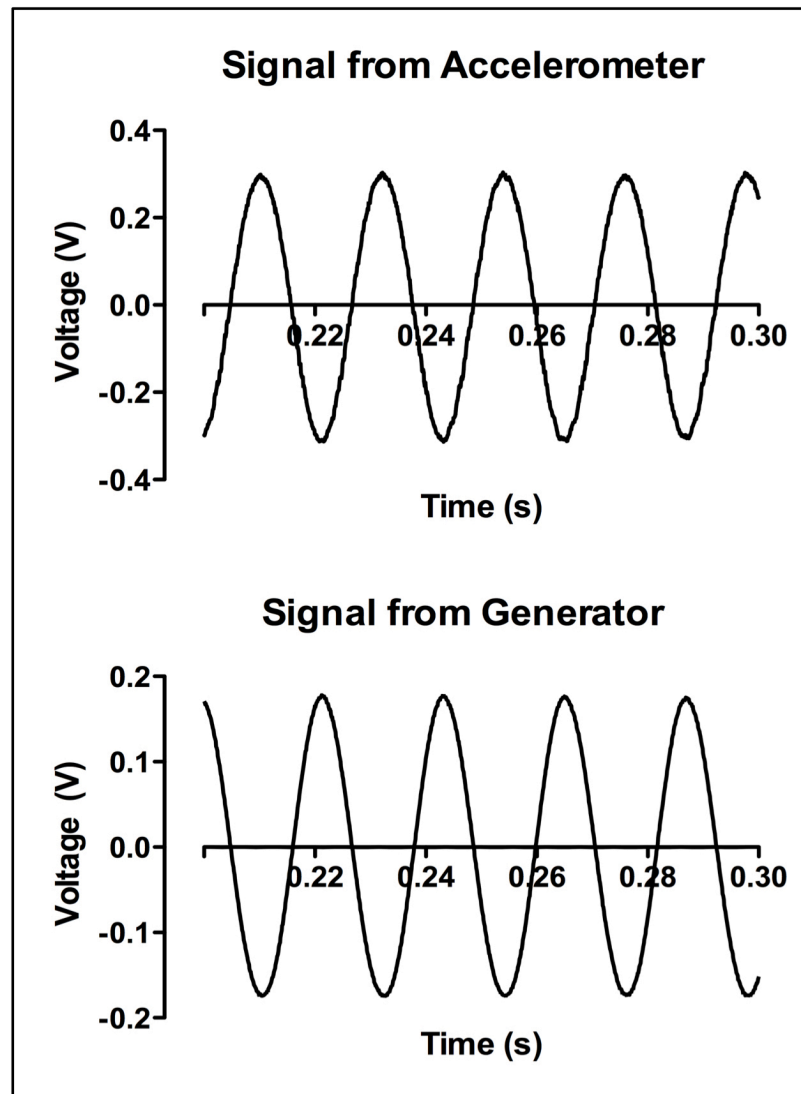


Figure 5.3 Representative graphs illustrate the waveform generated during *in vivo* vibration.

Prior to, during and after each experimental run, waveforms from both the generator and the accelerometer were monitored and recorded. Output signals shown are a representative excerpt of data obtained from vibration at 45 Hz, 0.3 g acceleration, validating the output as consistently sinusoidal. Graph is a representative image of 3 runs.

Following stimulation, mice were returned to normal housing and monitored, and no abnormal behavior was displayed. Six and 24 hours after vibration, mice were euthanized by CO₂ asphyxiation, and their spines were isolated by dissection (**Figure 5.2 D**).

5.4.4 Harvesting of Murine IVDs and RNA Extraction

At specified times post-vibration, intact IVDs (including NP, AF, and cartilage end-plates) from each treatment group were isolated by microdissection by shearing the IVD from the adjacent vertebral bone. The IVDs from each treatment group were pooled into 1 ml of TRIzol reagent (Life Technologies, Burlington, ON, Can.). Tissues were homogenized using a PRO250 tissue homogenizer (PRO Scientific, Oxford, CT, USA), and RNA was extracted according to the manufacturer's instructions. RNA was quantified using a NanoDrop 2000 spectrophotometer (Thermo Scientific, Burlington, ON, Can.), and 1 µg was reverse transcribed into complementary DNA (cDNA) using an iScript cDNA Synthesis kit (Bio-Rad, Mississauga, ON, Can.).

5.4.5. Real-time Polymerase Chain Reaction (PCR).

Gene expression was assessed by real-time PCR using a Bio-Rad CFX384 RT-PCR system. PCR reactions were run in triplicate, using 120 ng of cDNA per reaction and 25 µM forward and reverse primers with 2x SsoFast EvaGreen Supermix (Bio-Rad). The PCR parameters consisted of an initial 2 minutes of denaturing at 95°C, followed by 40 cycles of 10 seconds of denaturing at 95°C, and 20 seconds of annealing/ elongation (Table 5.1). Relative gene expression was calculated using the $\Delta\Delta C_t$ method, normalized for input using hypoxanthine guanine phosphoribosyltransferase (Seol et al. 2011) and expressed relative to non-vibrated sham controls at each time point.

Table 5.1 Primers for real-time PCR

NCBI Gene Symbol	Primer Sequence 5' → 3'
<i>Hprt</i> Fwd*	CAGGCCAGACTTTGTTGGAT
<i>Hprt</i> Rev*	TTGCGCTCATCTTAGGCTTT
<i>Adamts4</i> Fwd*	GAGGAGGAGATCGTGTTTCCAG
<i>Adamts4</i> Rev*	CAAACCCTCTACCTGCACCC
<i>Adamts5</i> Fwd*	GGAGCGAGGCCATTTACAAC
<i>Adamts5</i> Rev*	GCGTAGACAAGGTAGCCCACTTT
<i>Acan</i> Fwd*	CTGGGATCTACCGCTGTGAAG
<i>Acan</i> Rev*	GTGTGGAAATAGCTCTGTAGTGGA
<i>Bgn</i> Fwd ⁺	ACGAATCCATGACAACCGTATC
<i>Bgn</i> Rev ⁺	GCTCCTGGTTCAAAGCCACT
<i>Colla1</i> Fwd*	CTGGCGGTTTCAGGTCCAAT
<i>Colla1</i> Rev*	TCCAGGCAATCCAGGAGC
<i>Col2a1</i> Fwd*	GCACATCTGGTTTGGAGAGACC
<i>Col2a1</i> Rev*	TAGCGGTGTTGGGAGCCA
<i>Ctgf</i> Fwd*	GGGCCTCTTCTGCGATTTC
<i>Ctgf</i> Rev*	ATCCAGGCAAGTGCATTGGTA
<i>Dcn</i> Fwd ⁺	TCTTGGGCTGGACCATTGAA
<i>Dcn</i> Rev ⁺	CATCGGTAGGGGCACATAGA
<i>Hif1a</i> Fwd*	ACCTTCATCGGAAACTCCAAAG
<i>Hif1a</i> Rev*	CTGTTAGGCTGGGAAAAGTTA
<i>Mmp3</i> Fwd*	TTGTCCCGTTTCCATCTCTCTC
<i>Mmp3</i> Rev*	TTGGTGATGTCTCAGGTTCCAG
<i>Mmp7</i> Fwd*	GCCAGGGAACACTCTAGGTCAT
<i>Mmp7</i> Rev*	CTGCGTCCTCACCATCAGTC
<i>Mmp8</i> Fwd*	GATCTTCCTCCACACACAGCTTG
<i>Mmp8</i> Rev*	CTGCAACCATCGTGGCATT
<i>Mmp12</i> Fwd*	GCTTACCCCAAGCTGATTTCC
<i>Mmp12</i> Rev*	ATGTTTTGGTGACACGACGGA
<i>Mmp13</i> Fwd*	CTTCTTCTTGTTGAGCTGGAAGTC
<i>Mmp13</i> Rev*	CTCTGTGGACCTCACTGTAGACT
<i>Timp1</i> Fwd*	CTTGGTTCCCTGGCGTACTC
<i>Timp1</i> Rev*	ACCTGATCCGTCCACAAACAG
<i>Sox6</i> Fwd*	GGTCATGTTTCCCACCCACA
<i>Sox6</i> Rev*	TTCAGAGGGGTCCAAATTCCT
<i>Sox9</i> Fwd*	AGTACCCGCATCTGCACAAC
<i>Sox9</i> Rev*	TACTTGTAATCGGGGTGGTCTT
<i>Vcan</i> Fwd ⁺	TTTTACCCGAGTTACCAGACTC
<i>Vcan</i> Rev ⁺	GGAGTAGTTGTTACATCCGTTG

Annealing Temperatures: *60°C degree; + = 58°C degrees

Relative gene expression was determined for type I and type II collagens (*Colla1* and *Col2a1*); the proteoglycans aggrecan, versican, biglycan, and decorin; the anabolic regulatory genes *Sox6* and *Sox9*, tissue inhibitor of metalloproteinases 1 (*Timp1*), connective tissue growth factor (*Ctgf*), and hypoxia-inducible factor 1- α (*Hif1 α*); and the matrix-degrading enzymes MMPs (*Mmp3*, *Mmp7*, *Mmp8*, *Mmp12*, and *Mmp13*) and ADAMTS (*Adamts4* and *Adamts5*) (Table 5.1). Standard curves were generated to control for primer efficiency, and the specificity of the primers was determined by melt curve analysis (0.5°C/5 seconds).

5.4.6 Protein Extraction and Trypsin Digestion

At 6 hours post-vibration, intact murine IVDs were isolated from the lower thoracic and lumbar regions by microdissection, minced with a scalpel, and incubated in 4M urea, 10 mM dithiothreitol, and 50 mM ammonium bicarbonate for 2 hours at room temperature with gentle agitation. The supernatant was collected, and total protein concentration was assessed using a Micro Bicinchoninic Acid assay (Pierce, Burlington, ON, Can.). Equivalent amounts of protein (10 μ g) from experimental and control groups (n = 3 each) were subjected to tryptic digest (2% trypsin per weight of protein in 50 mM ammonium bicarbonate, pH 7.8) for 18 hours at 37°C.

5.4.7 Liquid Chromatography Electrospray Ionization Tandem Mass Spectrometry (LC-ESI-MS/MS)

Peptide separation and mass spectrometric analyses were carried out with a Proxeon nano-high-performance liquid chromatography systems (Thermo Scientific) linked to a mass spectrometer (LTQ-Velos; Thermo Scientific) using electrospray

ionization in a survey scan with mass/charge values ranging from 390 to 2,000 in tandem MS/MS (Siqueira et al. 2012). The MS/MS spectra obtained were searched against a customized mouse database (including aggrecan, biglycan, type I collagen, decorin, and GAPDH) to query specific ECM proteins using the Sequest algorithm in Proteome Discoverer software version 1.3 (Thermo Scientific). Search results were filtered for a false discovery rate of 1% using a decoy search strategy utilizing a reverse database. The inclusion criterion for positive identification of proteins was the presence of 2 or more different peptides from the same protein.

For mass spectrometry-based quantitative proteomics analysis, 3 MS raw files from each sample (n = 3 mice per group) were analyzed using Sieve software, version 2.0 (Thermo Scientific) as previously described (Siqueira et al. 2012). Peptide peak integration was performed for each tryptic peptide related to the customized mouse protein database, and these values were used for statistical analysis. An area under the curve value was calculated for each peptide peak. Peptide sequences obtained from the database search described above were then imported into Sieve and mapped.

5.4.8 Histologic Analysis

Murine spinal columns were fixed in 4% paraformaldehyde overnight at 4°C, washed in PBS, decalcified for 5 days at room temperature in Shandon TBD-2 (Fisher Scientific), dehydrated in a graded series of ethanol, cleared in xylene, and embedded in paraffin. Samples were sectioned sagittally at a thickness of 5 µm using a microtome (Leica Microsystems, Concord, ON, Can.). Sections were then dewaxed in xylene and rehydrated by successive immersion in descending concentrations of alcohol. Serial

sections were processed with either 0.1% Safranin-O/0.02% fast green for sulfated glycosaminoglycans or picosirius red for collagen and imaged on a Leica DM1000 microscope with Leica Application Suite. For each staining protocol, sections corresponding to 4–6 IVDs were assessed for each animal ($n = 4$ mice per group).

5.4.9 Immunofluorescence Analysis

Samples were sectioned and processed as described above. Antigen retrieval was performed with 10 mM sodium citrate for 12 minutes at 95°C. Slides were then blocked with 5% donkey serum in PBS–0.2% Tween 20 (PBST) (Sigma-Aldrich, St. Louis, MO, USA) for 1 hour and then incubated with primary antibody directed against aggrecan (1:50) (SC-25674; Santa Cruz) in a humidified chamber overnight at 4°C. Slides were washed with PBST and incubated with goat anti-rabbit IgG (Alexa Fluor 488; Life Technologies) for 60 minutes prior to mounting with Vectashield medium containing DAPI (Vector Labs, Burlingame, CA, USA). Images were captured with a Leica DMRA2 fluorescence microscope and processed with Northern Eclipse software (Empix, Mississauga, ON, Can.). Staining and imaging parameters were kept constant to enable comparisons of labeling intensities. Quantification of the fluorescence signal was performed using sections corresponding to 4–6 IVDs for each animal ($n = 4$ mice per group), using ImageJ software (National Institutes of Health, Bethesda, MD, USA), and is presented as mean pixel intensity per unit area.

5.4.10 Statistical Analysis

Gene expression levels in IVD tissue exposed to vibration at varying frequencies were compared to non-vibrated sham controls at each time point using one-way analysis

of variance (ANOVA) with Dunnett's post-hoc test. For each gene, differences in expression values between vibrated IVD tissues harvested at specific time points post-vibration were compared using a one-way ANOVA with Tukey's post hoc test. Similarly, for each gene, differences in expression values between IVD tissues subjected to stimulation at varying frequencies were compared using a one-way ANOVA with Tukey's post hoc test. Aggrecan immunofluorescence (measured as mean pixel intensity per IVD area) was compared between samples subjected to vibration and sham controls using Student's *t*-test. For all analyses, *P* values less than 0.05 were considered significant.

For statistical analyses of protein abundance, peak integrations were summarized into protein-level annotation in Sieve using a weighted average of intensities of LC-ESI-MS/MS of a protein by run, where the weights are inversely proportional to the between-run variance of the peaks. In addition, a statistical model based on an ANOVA framework with Tukey's post hoc test was carried out as previously described (Clough et al. 2009). The relative abundance level of an individual protein from the experimental vibration group was considered significantly different from the sham control group when the values observed were < 0.75 for decreased abundance or > 1.25 for increased abundance with a *P* value of less than 0.05.

5.5 Results

5.5.1 Acute *Ex Vivo* High-Frequency, Low-Amplitude Vibration Affects on the Intervertebral disc.

To determine the effect of acute vibration on IVD gene expression, we developed an organ culture system to subject intact murine spinal segments to high-frequency low-amplitude vibration. Based on previous reports describing beneficial responses of skeletal tissues to WBV (Prisby et al. 2008), spines were subjected to 30 minutes of vibration at 15 Hz (sinusoidal signal, 0.3g peak acceleration). Gene expression was assessed at 0, 2, 6, and 24 hours following vibration (**Figure 5.2 D**).

To investigate immediate cellular responses, murine IVDs were harvested after vibration for real-time PCR analysis (0 hours post-vibration). Immediately following vibration, there was a general trend toward down-regulation of both anabolic (**Figure 5.4 A**) and catabolic (**Figure 5.4 B**) genes, with a significant decrease in *Mmp3* and *Adamts4* compared to sham controls. At 2 hours post-vibration, expression levels of both anabolic and catabolic genes returned to basal (SHAM) levels, with the exception of the mechanosensitive gene *Mmp8*, which was significantly induced (**Figure 5.4 B**). The most pronounced effect on gene expression was observed at 6 hours post-vibration. At this time point, a significant induction of anabolic genes was observed, with a 15-fold increase in type I collagen, 3.8-fold increase in aggrecan, 2.9-fold increase in *Sox9*, 3.2-fold increase in biglycan, 2.2-fold increase in decorin, 5.6-fold increase in *Ctgf*, and 2.6-fold increase in *Hif1 α* (**Figure 5.4 A**). In contrast, catabolic genes remained at basal levels with the exception of *Mmp13*, which was significantly down-regulated, and *Mmp8*, which

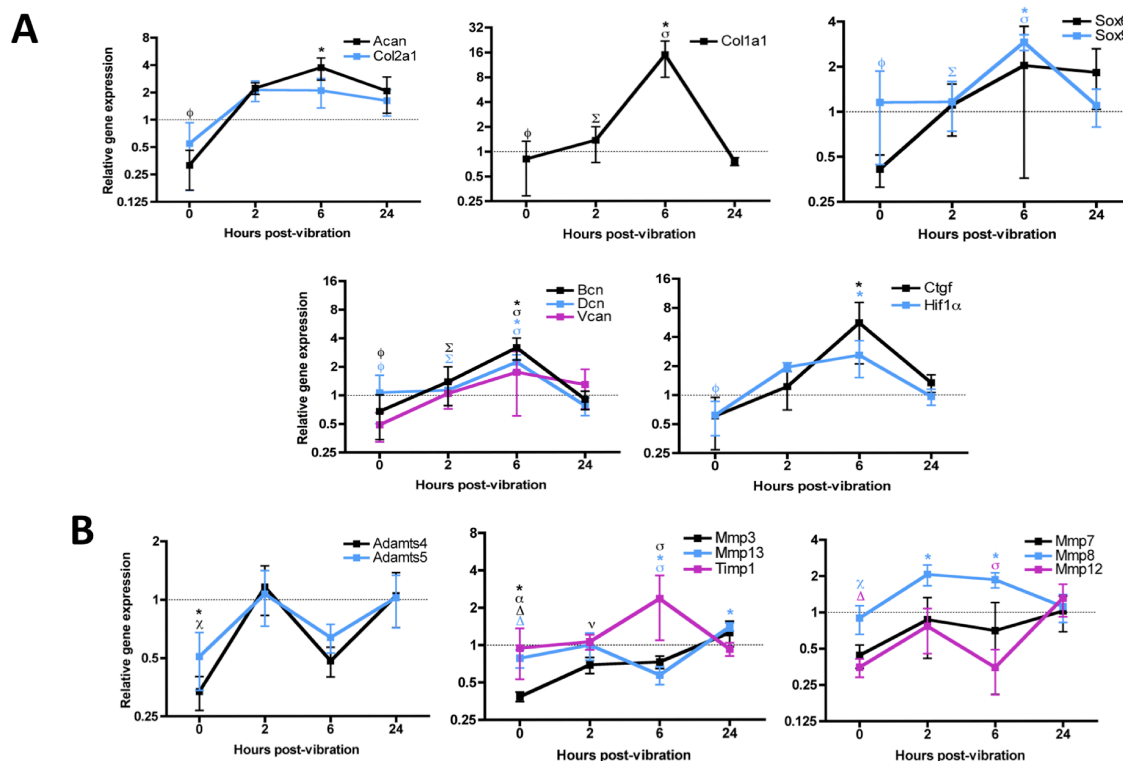


Figure 5.4 Transient effects of acute vibration on anabolic and catabolic gene expression in the murine intervertebral disc *ex vivo*.

Murine spinal segments were subjected to acute vibration for 30 minutes at 15 Hz and 0.3g and then incubated for up to 24 hours prior to SYBR-based real-time polymerase chain reaction (PCR) analysis of IVD gene expression. Expression of **A.** anabolic genes and **B.** catabolic genes was determined relative to the expression of the housekeeping gene *Hprt* and normalized to that of non-vibrated sham controls at the same time point (set to 1; broken lines). Values are the mean \pm SEM of triplicate PCR experiments ($n = 5$ mice per group). * = $P < 0.05$ versus sham controls at the same time point; $\chi = P < 0.05$ versus the same gene at 2 hours; ϕ and $\Sigma = P < 0.05$ versus the same gene at 6 hours; Δ , ν , and $\sigma = P < 0.05$ versus the same gene at 24 hours. The colors of the symbols correspond to the genes, as indicated in the key for each graph. Acan = aggrecan; Bcn = biglycan; Dcn = decorin; Vcan = versican; Ctgf = connective tissue growth factor; Hif1 α = hypoxia-inducible factor 1 α ; Mmp = matrix metalloproteinase; Timp1 = tissue inhibitor of metalloproteinases 1.

remained up-regulated (**Figure 5.4 B**). Analysis of gene expression 24 hours post-vibration demonstrated the transient nature of the response, as anabolic and catabolic factors returned to basal levels, with the exception of *Mmp13*, which was significantly increased compared to sham controls.

5.5.2 Affect of Frequency of Vibration on the IVD

Having established that significant changes in gene expression were detected 6 hours following vibration, this time point was used to assess the effect of vibration frequency on murine IVD gene expression. The induction of anabolic gene expression by acute vibration was frequency dependent, with no significant changes in gene expression detected compared to sham controls at frequencies of 45 Hz or greater (**Figure 5.5 A**). In fact, when compared to the induction observed at 15 Hz, there was a significant decrease in the expression of type I collagen, biglycan, and decorin at 60 Hz. The expression of catabolic genes was likewise examined following vibration at frequencies up to 90 Hz; however, no significant changes were observed (**Figure 5.5 B**). These data suggest that acute vibration induces optimal effects on IVD gene expression at a frequency of 15 Hz.

5.5.3 High-Frequency, Low-Amplitude Whole-body Vibration *In Vivo* Model

In parallel to vibration of isolated spinal segments, we subjected 10-week-old mice to WBV *in vivo*. Based on previous reports (Judex et al. 2007; Holguin et al. 2011), animals were subjected to 30 minutes of vibration at 45 Hz (sinusoidal signal, 0.3g peak

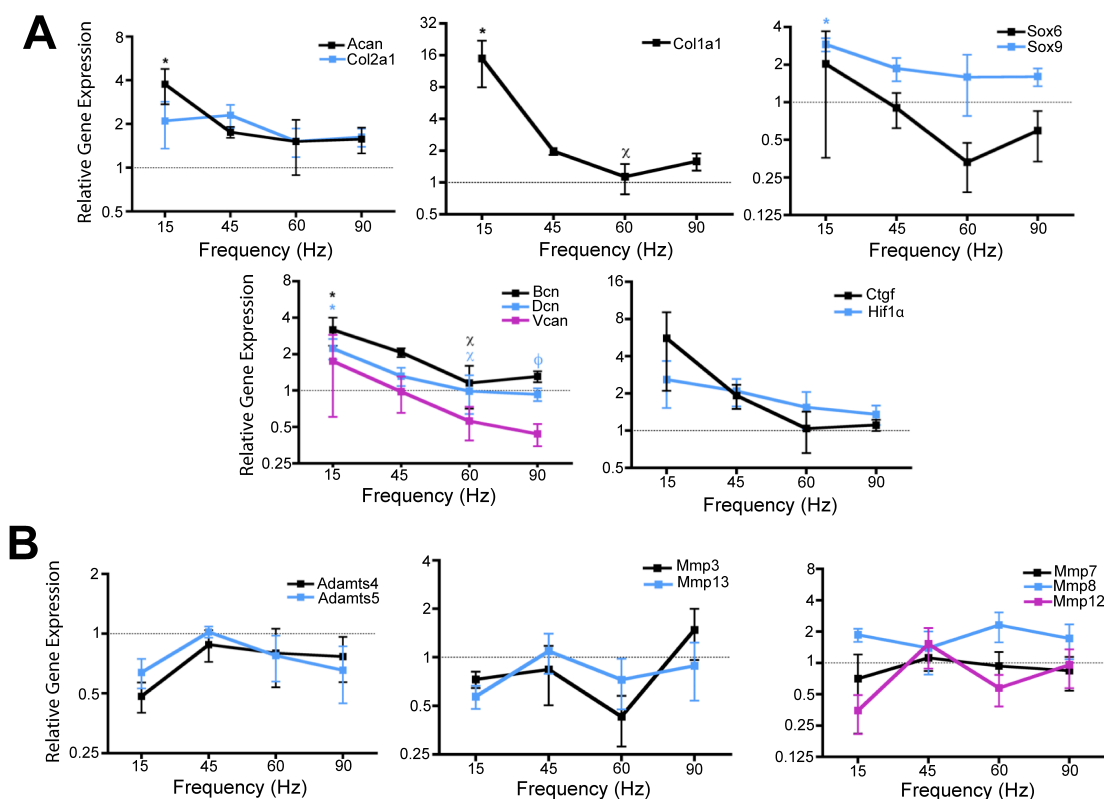


Figure 5.5 Frequency-dependent effects of acute vibration on anabolic and catabolic gene expression in the murine IVD *ex vivo*.

Murine spinal segments were subjected to acute vibration for 30 minutes at 15, 45, 60, or 90 Hz (with peak acceleration constant at 0.3g) and then incubated for 6 hours prior to SYBR-based real-time PCR analysis of IVD gene expression. Expression of **A.** anabolic genes and **B.** catabolic genes was determined relative to the expression of the housekeeping gene *Hprt* and normalized to that of non-vibrated sham controls (set to 1; broken lines). Values are the mean \pm SEM of triplicate PCR experiments ($n = 3$ mice per group). * = $P < 0.05$ versus sham at the same frequency; χ and ϕ = $P < 0.05$ versus the same gene at 15 Hz. The colors of the symbols correspond to the genes, as indicated in the key for each graph. See **Figure 5.4** for definitions.

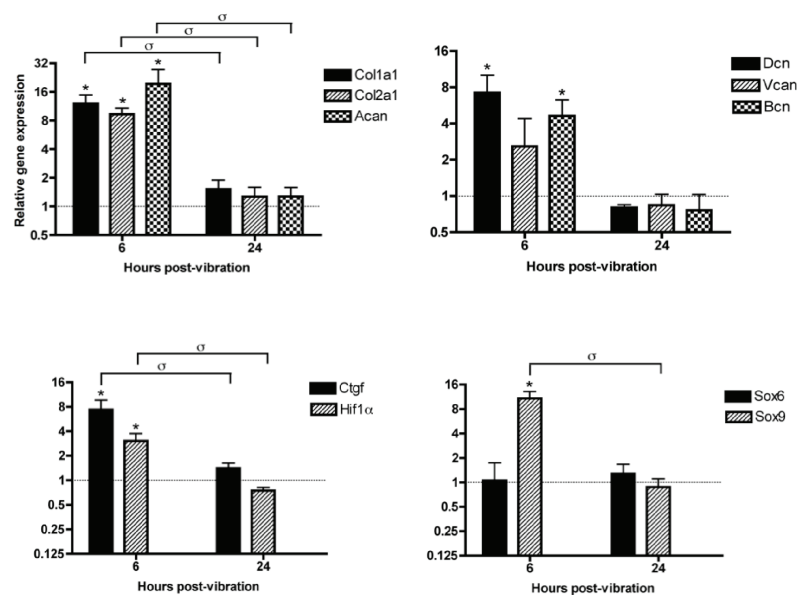
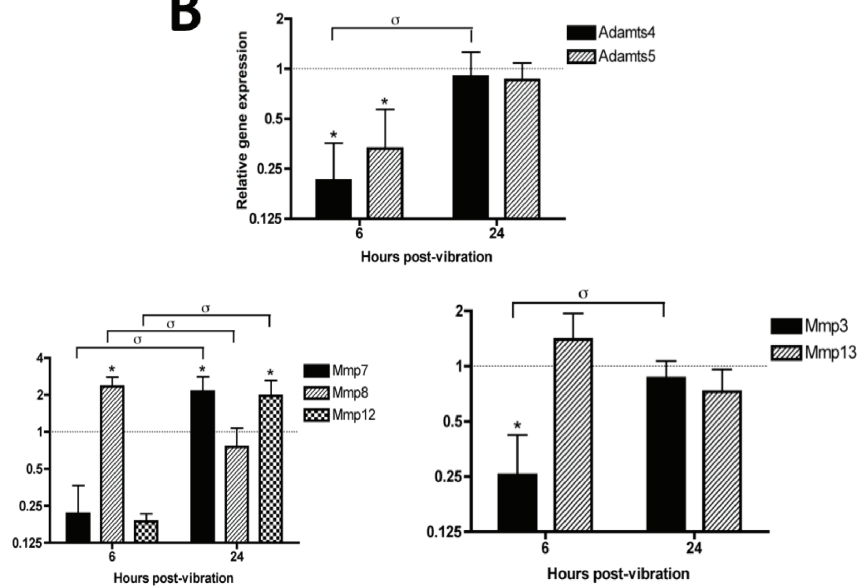
acceleration) and assessed at either 6 hours or 24 hours post-vibration (**Figure 5.2 D**). Interestingly, the beneficial effects observed *ex vivo* were even more robust when vibration was applied *in vivo*, and a greater number of genes were significantly altered (**Figure 5.6**). At 6 hours, significant induction of anabolic gene expression was observed, with a 12.1-fold increase in type I collagen, 9.3-fold increase in type II collagen, 19.4-fold increase in aggrecan, 4.6-fold increase in biglycan, 7.2-fold increase in decorin, 7.4-fold increase in *Ctgf*, 3.1-fold increase in *Hif1 α* , and 10.8-fold increase in *Sox9* (**Figure 5.6 A**). The more pronounced effect of acute vibration *in vivo* was further exemplified by significant down-regulation of the expression of *Adamts4*, *Adamts5*, and *Mmp3* (**Figure 5.6 B**). The induction of *Mmp8* expression detected *ex vivo* was likewise detected 6 hours following stimulation *in vivo* (2.3-fold). Similar to the response demonstrated in organ culture, the induction of anabolic gene expression was transient following acute vibration *in vivo*, with expression of most genes returning to basal (SHAM) levels within 24 hours, with the exception of *Mmp7* and *Mmp12*, which were significantly increased at this time point compared to sham controls.

5.5.4 High-Frequency, Low-amplitude Whole-body Vibration Affect on Protein Abundance in the IVD

We next determined whether changes in murine IVD gene expression following acute vibration *in vivo* were accompanied by changes in protein abundance. Thoracic and lumbar IVDs were isolated, and protein content was assessed by liquid chromatography tandem mass spectrometry at 6 hours post-vibration. A quantitative proteomics-based

Figure 5.6 Effect of acute WBV *in vivo* on anabolic and catabolic gene expression in the murine IVD.

Animals were subjected to acute vibration for 30 minutes at 45 Hz and 0.3g, and IVD tissues were isolated by microdissection after 6 hours or 24 hours for SYBR-based real-time PCR analysis of gene expression. Expression of **A.** anabolic genes and **B.** catabolic genes was determined relative to the expression of the housekeeping gene *Hprt* and normalized to that of non-vibrated sham controls at the same time point (set to 1; broken lines). Values are the mean \pm SEM of triplicate PCR experiments (n = 4 mice per group). * $< P = 0.05$ versus sham at the same time point; $\sigma = P < 0.05$. See **Figure 5.4** for definitions.

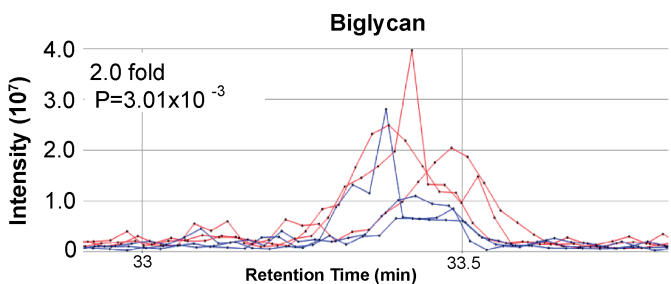
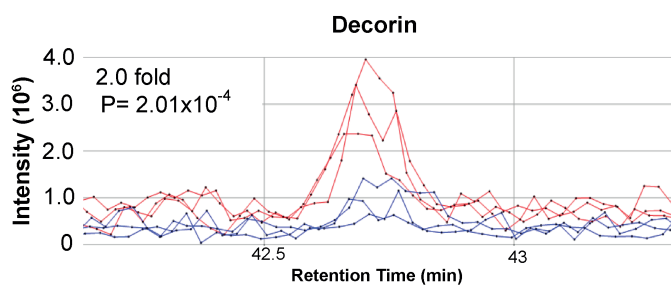
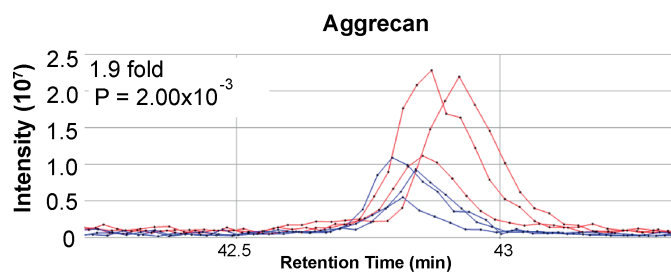
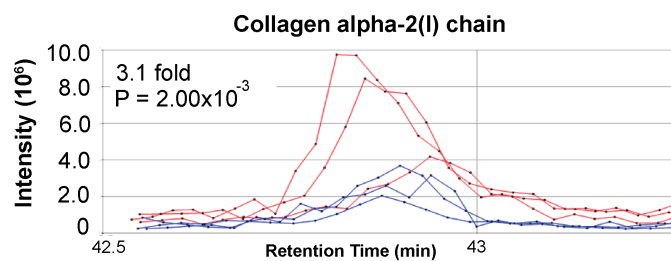
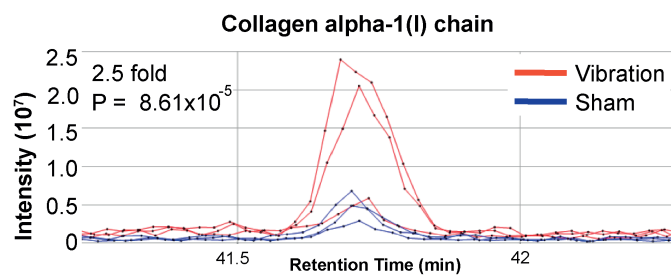
A**B**

mass spectrometry approach was used to compare the relative abundance of candidate ECM proteins, selected based on gene expression data, in the vibration and sham control groups. Alignment base-peak chromatograms revealed marked increases in the abundance of representative peptides from specific ECM proteins (**Figure 5.7**). Differences were quantified by calculating the areas under the peaks of all identified peptides from each specific protein. Relative abundances were expressed as a ratio of the mean values for the vibrated samples divided by the values for the non-vibrated (SHAM) control samples. Interestingly, at 6 hours post-vibration, significant differences in murine IVD protein levels were detected. Relative to non-vibrated sham controls, disc tissue from animals subjected to vibration demonstrated a significant 2.5-fold increase in abundance of type I collagen $\alpha 1$ chain, 3.1-fold increase in abundance of type I collagen $\alpha 2$ chain, 1.9-fold increase in abundance of aggrecan, and 2.0-fold increases in abundance of both decorin and biglycan. In contrast, no significant differences were detected in the abundance of GAPDH in IVD tissue from animals subjected to vibration compared to non- vibrated sham controls (ratio of vibrated samples to sham samples 1.04; $P = 0.97$).

To localize ECM changes within specific IVD tissue types, intact mouse thoracic and lumbar spinal segments were examined histologically using picrosirius red or Safranin O/fast green to detect collagens and proteoglycans, respectively. Collagen staining appeared more intense within the inner AF in samples from animals subjected to vibration than in sham controls (**Figure 5.8 A**). Safranin-O staining was more intense within the NP and inner AF in vibrated samples than in sham controls (**Figure 5.8 A**). Antibody staining suggested that vibration caused increased aggrecan immunoreactivity within the NP when compared to sham controls (**Figure 5.8 B**). Aggrecan

Figure 5.7 Effect of acute WBV *in vivo* on the abundance of extracellular matrix proteins in the murine intervertebral disc.

Mice were subjected to acute vibration for 30 minutes at 45 Hz and 0.3g, and IVD tissues were isolated from the lower thoracic and lumbar regions by microdissection 6 hours post-vibration. IVDs were minced, and total protein was extracted from tissue sections for liquid chromatography electrospray ionization tandem mass spectrometry. Chromatograms depict the integration peaks of a representative tryptic peptide for each protein of interest. The fold change is the average of 2–5 peptides per protein compared to non-vibrated sham controls (n = 3 animals per group with triplicate mass spectrometry runs for each animal).



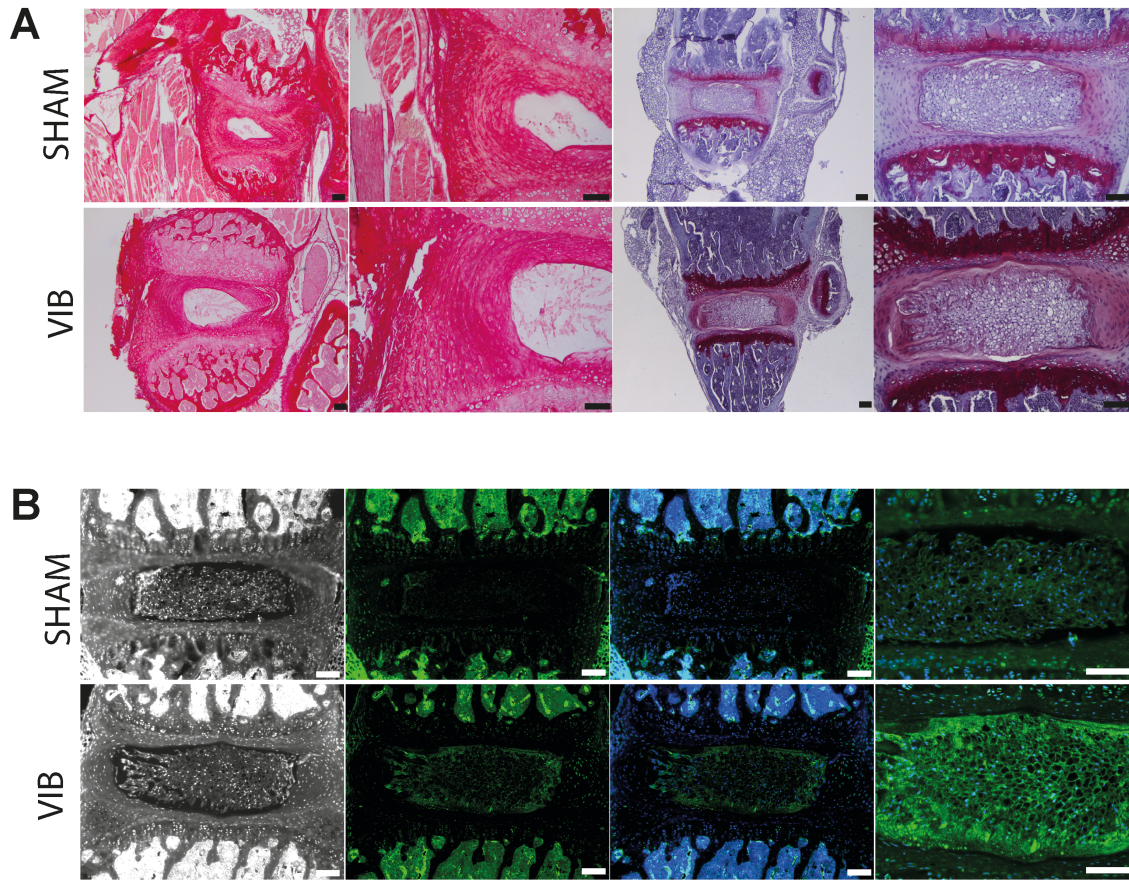


Figure 5.8 Effect of acute WBV *in vivo* on histologic features of the murine intervertebral disc.

A. Picrosirius red staining for collagen (left) and Safranin-O/fast green staining for sulfated glycosaminoglycans (right) in serial spinal sections from mice subjected to vibration (VIB) and non-vibrated controls (SHAM). Mice were subjected to acute vibration for 30 minutes at 45 Hz and 0.3 g, and intact spinal columns were isolated 6 hours after vibration and processed for histologic analysis. **B.** Representative images demonstrating the immunolocalization of aggrecan within the murine IVD. Aggrecan immunoreactivity was increased within the nucleus pulposus 6 hours after vibration compared to non-vibrated sham controls. For each staining protocol, sections corresponding to 4–6 IVDs were assessed for each animal ($n = 4$ mice per group). Bars = 100 μm .

immunofluorescence within the murine IVD was quantified by measuring the mean pixel intensity per unit area. The fluorescence signal was 4-fold greater in vibrated samples than in sham control samples at 6 hours (mean \pm SEM 0.15 ± 0.08 in sham control samples versus 0.60 ± 0.08 in samples subjected to vibration; $P = 0.0042$).

5.6 DISCUSSION

Using both *ex vivo* and *in vivo* mouse models, we analyzed the effect of acute exposure to vibration on IVD homeostasis. We demonstrated that a single exposure to high-frequency low-amplitude vibration induces the expression of anabolic genes, while promoting the down-regulation of catabolic gene expression *in vivo*. Changes in gene expression detected *in vivo* were accompanied by significant alterations in ECM content, including increased levels of type I collagen, aggrecan, decorin, and biglycan. We showed that acute vibration has a transient effect at the level of gene expression, with the greatest changes occurring at 6 hours post-vibration. *Ex vivo* experiments revealed that the effects were frequency dependent. Recapitulation in organ culture of changes observed *in vivo* indicates that induction of anabolic gene expression in the murine IVD is mediated, at least in part, by activation of mechanosensitive pathways intrinsic to spinal tissue.

WBV platforms are currently used in clinical settings, initially introduced for the treatment of osteoporosis to increase the bone mineral density of vertebral bones (Rubin et al. 2003). In addition, these platforms are marketed for use in exercise regimens owing to their reported ability to increase muscle strength and tone. However, the widespread

application of this form of mechanical stimulation is countered by reports that exposure to vibration *in vivo* can cause back pain (Perraton et al. 2011). This dichotomy highlights the need to investigate and establish optimized parameters for vibration therapy to promote spine health, while minimizing harmful changes (Perraton et al. 2011). The present study demonstrates that murine IVD cells are mechanosensitive with frequency-dependent responses. However, there is clearly a need for additional preclinical studies before WBV can be applied safely and effectively for the prevention and/or treatment of spinal disorders in humans.

To our knowledge, this study is the first to correlate *in vivo* and *ex vivo* findings, enabling us to distinguish direct (tissue autonomous) and indirect effects of vibration on IVD homeostasis. The changes in gene expression observed *in vivo* were greater than those seen *ex vivo*. These findings are consistent with the complexity of spinal loading *in vivo*, which includes constant mechanical compression due to weight bearing (Wilke et al. 1999), the stimulation of muscle-induced mechanical compression (Judex and Rubin 2010), and the resultant shear forces experienced by IVD cells (Hwang et al. 2012). The effects of vibration *in vivo* are also likely influenced by secondary factors, including enhanced transport and systemic changes in the endocrine, neural, or cardiovascular systems.

Others have proposed several physical mechanisms through which vibration may interact with cells (Jacobs et al. 2010). These include direct mechanical acceleration of the cell or subcellular components, fluid shear, and compression. Although multiple physical stimuli were likely at play in the *in vivo* system, our study was not designed to distinguish among these potential mechanisms. In the *ex vivo* model, however, spinal

segments were affixed to the dish and therefore unlikely to be subjected to compressive load along the axis of the spine. Moreover, it is not likely that *ex vivo* samples experienced significant fluid shear (Lau et al. 2010), and they could not have been influenced by muscle contraction or perfusion changes. It should also be noted that, in both models, the amplitude of mechanical stimulus at the cellular level would be less than that of the applied stimulus due to damping. As such, the mechanical acceleration experienced by IVD cells likely differs between the two models, and future studies are needed to address this issue.

Furthermore, during vibration *in vivo*, mice were free to move and alternated between quadrupedal and bipedal postures. Previous studies have demonstrated that in both situations the spine experiences loading (via muscle contraction and ligament tension) (Wilke et al. 2003); however, differences in the direction of the applied acceleration in our mouse model may limit its ability to accurately mimic the effects of WBV platforms in humans. Nonetheless, the fact that significant changes in anabolic activity were observed in both *ex vivo* and *in vivo* murine systems indicates that at least some effects were due to mechanical acceleration acting directly on IVD tissue.

In the present study, samples were isolated from intact murine IVDs (NP, AF, and cartilage end-plates) to assess the effects of vibration. Although this approach permits global analysis of disc health at the messenger RNA (mRNA) and protein levels, it is limited since we cannot specify which of the component cell types are responsible for the changes detected. We predicted that increased expression of collagens and proteoglycans in response to acute vibration would occur in a cell type-specific pattern. Consistent with the results of our proteomic analysis, histologic examination of murine IVD tissue at 6

hours post-vibration suggested increased collagen staining in the inner AF and increased sulfated glycosaminoglycan staining in the NP and inner AF. Moreover, increased aggrecan immunoreactivity within the NP was detected. The increase in ECM proteins that was detected by mass spectrometry within the IVD following WBV may involve increased synthesis and/or decreased degradation. Further studies are needed to characterize the mechanisms underlying these relatively rapid changes in protein levels.

Interestingly, recent studies have demonstrated that aggrecan degradation products exhibit a regionally specific pattern across the IVD and are increased by the application of dynamic compressive loading above physiologic levels (Iatridis et al. 2011). Furthermore, increased levels of ADAMTS proteins in human NP tissue have been reported following dynamic compressive loading (Huang et al. 2012). Although examination of matrix-degrading enzymes in the present study was limited to gene expression analysis, alterations in *Adamts* and *Mmp* expression suggest that regulation of catabolic pathways within the IVD is dependent on the magnitude of the mechanical stimulus.

Our study demonstrates that acute vibration induces a transient, yet significant increase in anabolic gene expression 6 hours after treatment, accompanied *in vivo* by a significant decrease in catabolic gene expression. Our results build on previous studies, which examined the expression of ECM genes using an *ex vivo* bovine model (Desmoulin et al. 2011), by including an analysis of matrix-degrading enzymes and IVD-associated regulatory molecules such as *Sox6*, *Sox9*, *Ctgf*, and *Hif1 α* . Wang et al observed a similar increase in the expression of *Colla1*, *Col2a1*, and aggrecan following dynamic compression of bovine IVDs (Wang et al. 2007). Previous studies evaluating the kinetics of IVD mRNA expression following a single compressive loading event demonstrated

similar anabolic changes, including the up-regulation of *Timp1* at 8 and 24 hours post-vibration (Wang et al. 2007). Similar to the effects of vibration, others have also demonstrated that changes in IVD gene expression in response to mechanical compression are dependent on both amplitude and frequency (Lotz and Chin 2000; Maclean et al. 2004). Furthermore, the duration of vibration may be an important factor, since previous studies showed that exposure of IVDs to static compressive loading for prolonged periods was associated with increased apoptosis (Lotz and Chin 2000). Repeated exposure of IVD tissue to vibration, which mimics exposures experienced during vibration therapies, may also alter the nature or magnitude of the cellular response, features that will be examined in future studies.

It is important to note that WBV is being used in clinical applications, often with patients of advanced age, who exhibit degenerative changes in the IVD. Consequently, in these patients, IVD cells may not demonstrate the same potential for anabolic responses since the cellular composition of IVD changes with age and degeneration (Clouet et al. 2011). In this regard, it has been established that human cells derived from degenerated IVDs do not have the same capacity to respond to tensile or compressive mechanical loads as cells derived from younger non-degenerated discs (Gilbert et al. 2010). These findings suggest a potential limitation of the present study, which was conducted using skeletally mature 10-week-old mice, which typically do not demonstrate degenerative changes in the IVD. Further study is needed to determine whether the anabolic response observed in healthy IVDs is recapitulated in degenerated IVDs.

Despite the paucity of preclinical data describing the effects of vibration on IVD homeostasis, clinical studies are being performed using vibration therapies to treat

patients with back pain and have shown positive outcomes in pain reduction (Fontana et al. 2005). However, these benefits may result from changes in the musculature or nervous system and not directly from changes in IVD integrity. Interpretation is further hampered by the small patient populations and lack of methodologic information provided. Therefore, further studies are needed to identify parameters of mechanical vibration that promote long-term beneficial effects on IVD integrity. The present study used a combination of *ex vivo* and *in vivo* mouse models to investigate changes in gene expression and protein levels within the IVD following a single exposure to vibration, an approach that cannot be undertaken with human samples. We demonstrated a transient, but significant induction of anabolic gene expression that was dependent on the frequency of vibration. Furthermore, the beneficial effects of vibration were more pronounced *in vivo* than *ex vivo*, suggesting that appropriate animal models are necessary to comprehensively model the response of IVD cell types to WBV.

5.7 References

- Alentorn-Geli E, Padilla J, Moras G, Lazaro Haro C, Fernandez-Sola J. 2008. Six weeks of whole-body vibration exercise improves pain and fatigue in women with fibromyalgia. *J Altern Complement Med* **14**: 975-981.
- Balague F, Mannion AF, Pellise F, Cedraschi C. 2011. Non-specific low back pain. *Lancet*.
- Belavy DL, Bansmann PM, Bohme G, Frings-Meuthen P, Heer M, Rittweger J, Zange J, Felsenberg D. 2011. Changes in intervertebral disc morphology persist 5 mo after 21-day bed rest. *J Appl Physiol* **111**: 1304-1314.
- Belavy DL, Hides JA, Wilson SJ, Stanton W, Dimeo FC, Rittweger J, Felsenberg D, Richardson CA. 2008. Resistive simulated weightbearing exercise with whole

- body vibration reduces lumbar spine deconditioning in bed-rest. *Spine (Phila Pa 1976)* **33**: E121-131.
- Buckwalter JA, Roughley PJ, Rosenberg LC. 1994. Age-related changes in cartilage proteoglycans: quantitative electron microscopic studies. *Microsc Res Tech* **28**: 398-408.
- Chaplin R. 2010. The effect of whole body vibration training on patients with Ankylosing Spondylitis. *Journal of Sports Therapy* **3**: 18-22.
- Chen J, Yan W, Setton LA. 2004. Static compression induces zonal-specific changes in gene expression for extracellular matrix and cytoskeletal proteins in intervertebral disc cells in vitro. *Matrix Biol* **22**: 573-583.
- Clouet J, Pot-Vaucel M, Grimandi G, Masson M, Lesoeur J, Fellah BH, Gauthier O, Fusellier M, Cherel Y, Maugars Y et al. 2011. Characterization of the age-dependent intervertebral disc changes in rabbit by correlation between MRI, histology and gene expression. *BMC Musculoskelet Disord* **12**: 147.
- Clough T, Key M, Ott I, Ragg S, Schadow G, Vitek O. 2009. Protein quantification in label-free LC-MS experiments. *J Proteome Res* **8**: 5275-5284.
- Crean JK, Roberts S, Jaffray DC, Eisenstein SM, Duance VC. 1997. Matrix metalloproteinases in the human intervertebral disc: role in disc degeneration and scoliosis. *Spine (Phila Pa 1976)* **22**: 2877-2884.
- del Pozo-Cruz B, Hernandez Mocholi MA, Adsuar JC, Parraca JA, Muro I, Gusi N. 2011. Effects of whole body vibration therapy on main outcome measures for chronic non-specific low back pain: a single-blind randomized controlled trial. *J Rehabil Med* **43**: 689-694.
- Desmoulin GT, Hewitt CR, Hunter CJ. 2011. Disc strain and resulting positive mRNA expression from application of a noninvasive treatment. *Spine (Phila Pa 1976)* **36**: E921-928.
- Desmoulin GT, Reno CR, Hunter CJ. 2010. Free axial vibrations at 0 to 200 Hz positively affect extracellular matrix messenger ribonucleic acid expression in bovine nucleus pulposi. *Spine (Phila Pa 1976)* **35**: 1437-1444.
- Fontana TL, Richardson CA, Stanton WR. 2005. The effect of weight-bearing exercise with low frequency, whole body vibration on lumbosacral proprioception: a pilot study on normal subjects. *Aust J Physiother* **51**: 259-263.
- Gilbert HT, Hoyland JA, Millward-Sadler SJ. 2010. The response of human annulus fibrosus cells to cyclic tensile strain is frequency-dependent and altered with disc degeneration. *Arthritis Rheum* **62**: 3385-3394.

- Henchoz Y, Kai-Lik So A. 2008. Exercise and nonspecific low back pain: a literature review. *Joint Bone Spine* **75**: 533-539.
- Holguin N, Muir J, Rubin C, Judex S. 2009. Short applications of very low-magnitude vibrations attenuate expansion of the intervertebral disc during extended bed rest. *Spine J* **9**: 470-477.
- Holguin N, Uzer G, Chiang FP, Rubin C, Judex S. 2011. Brief daily exposure to low-intensity vibration mitigates the degradation of the intervertebral disc in a frequency-specific manner. *J Appl Physiol* **111**: 1846-1853.
- Huang M, Wang HQ, Zhang Q, Yan XD, Hao M, Luo ZJ. 2012. Alterations of ADAMTSs and TIMP-3 in human nucleus pulposus cells subjected to compressive load: Implications in the pathogenesis of human intervertebral disc degeneration. *J Orthop Res* **30**: 267-273.
- Humzah MD, Soames RW. 1988. Human intervertebral disc: structure and function. *Anat Rec* **220**: 337-356.
- Hwang D, Gabai AS, Yu M, Yew AG, Hsieh AH. 2012. Role of load history in intervertebral disc mechanics and intradiscal pressure generation. *Biomech Model Mechanobiol* **11**: 95-106.
- Iatridis JC, Godburn K, Wuertz K, Alini M, Roughley PJ. 2011. Region-dependent aggrecan degradation patterns in the rat intervertebral disc are affected by mechanical loading in vivo. *Spine (Phila Pa 1976)* **36**: 203-209.
- Jacobs CR, Temiyasathit S, Castillo AB. 2010. Osteocyte mechanobiology and pericellular mechanics. *Annu Rev Biomed Eng* **12**: 369-400.
- Judex S, Lei X, Han D, Rubin C. 2007. Low-magnitude mechanical signals that stimulate bone formation in the ovariectomized rat are dependent on the applied frequency but not on the strain magnitude. *J Biomech* **40**: 1333-1339.
- Judex S, Rubin CT. 2010. Is bone formation induced by high-frequency mechanical signals modulated by muscle activity? *J Musculoskelet Neuronal Interact* **10**: 3-11.
- Kuisma M, Karppinen J, Niinimäki J, Ojala R, Haapea M, Heliovaara M, Korpelainen R, Taimela S, Natri A, Tervonen O. 2007. Modic changes in endplates of lumbar vertebral bodies: prevalence and association with low back and sciatic pain among middle-aged male workers. *Spine (Phila Pa 1976)* **32**: 1116-1122.

- Lau E, Al-Dujaili S, Guenther A, Liu D, Wang L, You L. 2010. Effect of low-magnitude, high-frequency vibration on osteocytes in the regulation of osteoclasts. *Bone* **46**: 1508-1515.
- Lotz JC, Chin JR. 2000. Intervertebral disc cell death is dependent on the magnitude and duration of spinal loading. *Spine (Phila Pa 1976)* **25**: 1477-1483.
- Maclean JJ, Lee CR, Alini M, Iatridis JC. 2004. Anabolic and catabolic mRNA levels of the intervertebral disc vary with the magnitude and frequency of in vivo dynamic compression. *J Orthop Res* **22**: 1193-1200.
- MacLean JJ, Lee CR, Grad S, Ito K, Alini M, Iatridis JC. 2003. Effects of immobilization and dynamic compression on intervertebral disc cell gene expression in vivo. *Spine (Phila Pa 1976)* **28**: 973-981.
- Oxlund BS, Ortoft G, Andreassen TT, Oxlund H. 2003. Low-intensity, high-frequency vibration appears to prevent the decrease in strength of the femur and tibia associated with ovariectomy of adult rats. *Bone* **32**: 69-77.
- Perraton L, Machotka Z, Kumar S. 2011. Whole-body vibration to treat low back pain: fact or fad? *Physiother Can* **63**: 88-93.
- Pockert AJ, Richardson SM, Le Maitre CL, Lyon M, Deakin JA, Buttle DJ, Freemont AJ, Hoyland JA. 2009. Modified expression of the ADAMTS enzymes and tissue inhibitor of metalloproteinases 3 during human intervertebral disc degeneration. *Arthritis Rheum* **60**: 482-491.
- Prisby RD, Lafage-Proust MH, Malaval L, Belli A, Vico L. 2008. Effects of whole body vibration on the skeleton and other organ systems in man and animal models: what we know and what we need to know. *Ageing Res Rev* **7**: 319-329.
- Rittweger J, Just K, Kautzsch K, Reeg P, Felsenberg D. 2002. Treatment of chronic lower back pain with lumbar extension and whole-body vibration exercise: a randomized controlled trial. *Spine (Phila Pa 1976)* **27**: 1829-1834.
- Rittweger J, Mutschelknauss M, Felsenberg D. 2003. Acute changes in neuromuscular excitability after exhaustive whole body vibration exercise as compared to exhaustion by squatting exercise. *Clin Physiol Funct Imaging* **23**: 81-86.
- Roughley PJ. 2004. Biology of intervertebral disc aging and degeneration: involvement of the extracellular matrix. *Spine (Phila Pa 1976)* **29**: 2691-2699.
- Rubin C, Pope M, Fritton JC, Magnusson M, Hansson T, McLeod K. 2003. Transmissibility of 15-hertz to 35-hertz vibrations to the human hip and lumbar spine: determining the physiologic feasibility of delivering low-level

- anabolic mechanical stimuli to skeletal regions at greatest risk of fracture because of osteoporosis. *Spine (Phila Pa 1976)* **28**: 2621-2627.
- Sayson JV, Hargens AR. 2008. Pathophysiology of low back pain during exposure to microgravity. *Aviat Space Environ Med* **79**: 365-373.
- Seol D, Choe H, Zheng H, Jang K, Ramakrishnan PS, Lim TH, Martin JA. 2011. Selection of reference genes for normalization of quantitative real-time PCR in organ culture of the rat and rabbit intervertebral disc. *BMC Res Notes* **4**: 162.
- Siqueira WL, Bakkal M, Xiao Y, Sutton JN, Mendes FM. 2012. Quantitative proteomic analysis of the effect of fluoride on the acquired enamel pellicle. *PLoS One* **7**: e42204.
- Tiemessen IJ, Hulshof CT, Frings-Dresen MH. 2008. Low back pain in drivers exposed to whole body vibration: analysis of a dose-response pattern. *Occup Environ Med* **65**: 667-675.
- Urban JP, Roberts S. 2003. Degeneration of the intervertebral disc. *Arthritis Res Ther* **5**: 120-130.
- Verschueren SM, Roelants M, Delecluse C, Swinnen S, Vanderschueren D, Boonen S. 2004. Effect of 6-month whole body vibration training on hip density, muscle strength, and postural control in postmenopausal women: a randomized controlled pilot study. *J Bone Miner Res* **19**: 352-359.
- Walsh AJ, Lotz JC. 2004. Biological response of the intervertebral disc to dynamic loading. *J Biomech* **37**: 329-337.
- Wang DL, Jiang SD, Dai LY. 2007. Biologic response of the intervertebral disc to static and dynamic compression in vitro. *Spine (Phila Pa 1976)* **32**: 2521-2528.
- Wilke HJ, Neef P, Caimi M, Hoogland T, Claes LE. 1999. New in vivo measurements of pressures in the intervertebral disc in daily life. *Spine (Phila Pa 1976)* **24**: 755-762.
- Wilke HJ, Rohlmann A, Neller S, Graichen F, Claes L, Bergmann G. 2003. ISSLS prize winner: A novel approach to determine trunk muscle forces during flexion and extension: a comparison of data from an in vitro experiment and in vivo measurements. *Spine (Phila Pa 1976)* **28**: 2585-2593.
- Wuertz K, Godburn K, MacLean JJ, Barbir A, Donnelly JS, Roughley PJ, Alini M, Iatridis JC. 2009. In vivo remodeling of intervertebral discs in response to short- and long-term dynamic compression. *J Orthop Res* **27**: 1235-1242.

CHAPTER SIX

REPEATED EXPOSURE TO HIGH-FREQUENCY LOW-AMPLITUDE VIBRATION
INDUCES DEGENERATION OF INTERVERTEBRAL DISC AND KNEE JOINTS
IN A MURINE MODEL

This Chapter has is currently under review at *Arthritis and Rheumatism*:

McCann M.R., Patel P., Pest M.A., Ratneswaran A., Kamphuis M.P., Esmail Z., Lee J., Barbalinardo M., Beaucage K.L, Holdsworth D.W., Beier F., Dixon S.J, Séguin C.A. Repeated exposure to high-frequency low-amplitude vibration induce degeneration of intervertebral disc and knee joint in a murine model.

6.1 Co-Authorship Statement

Chapter 6 is adapted from McCann, M.R., Patel, P., Pest, M.A., Ratneswaran A., Lalli, G., Beaucage K.L., Backler, G., Kamphuis M.P., Esmail Z., Lee, J., Barbalinardo, M., Mort, J., Holdsworth, D.W., Beier, F., Dixon S.J., and Séguin, C.A. Repeated exposure to high-frequency low-amplitude vibration induces degeneration of intervertebral disc and knee joints. Submitted to *Arthritis & Rheumatism*.

P. Patel and G. Lalli performed real-time PCR. M.A. Pest and A. Ratneswaran isolated knees, articular cartilage and performed histology. K.L. Beaucage and G. Backler performed micro-CT analysis. M.P. Kamphuis, Z. Esmail, J. Lee, and M. Barbalinardo assisted with *in vivo* vibration. Dr. J. Mort contributed reagents. All other experiments were performed by M.R. McCann in the laboratory of Dr. C.A. Séguin. Manuscript was written by M.R. McCann with suggestions from Drs. D.W. Holdsworth, F. Beier., S.J. Dixon and C.A. Séguin.

6.2 Chapter Summary

High-frequency, low-amplitude whole-body vibration (WBV) is being used to treat a range of musculoskeletal disorders; however, there is surprisingly limited knowledge of the effect(s) on joint tissues. An *in vivo* mouse model was used to study the effects of repeated exposure to WBV on bone and joint tissues. Ten-week-old male mice were subjected to vertical sinusoidal vibration (45 Hz, 0.3 g peak acceleration, 30 min/day, 5 days/week), conditions that mimic those used clinically in humans. Following WBV, skeletal tissues were examined by micro-computed tomography, histology and immunohistochemistry, and gene expression was quantified using real-time PCR. Following 4 weeks of WBV, intervertebral discs displayed histological hallmarks of degeneration in the annulus fibrosus, disruption of collagen organization and increased cell death. Mice exposed to WBV demonstrated greater *Mmp3* expression in the intervertebral disc, accompanied by enhanced collagen and aggrecan degradation. Examination of the knee joints after 4 weeks WBV revealed meniscal tears and focal damage to the articular cartilage, changes resembling osteoarthritis. Moreover, mice exposed to WBV demonstrated greater *Mmp13* gene expression and enhanced MMP-mediated collagen and aggrecan degradation in the articular cartilage compared to controls. No changes in trabecular bone microarchitecture or density were detected in the proximal tibia. These experiments reveal significant negative effects of WBV on joint tissues; findings that suggest the need for caution in the use of WBV pending further studies examining joint health in humans following WBV.

6.3 Introduction

Whole-body vibration (WBV) platforms, designed to deliver low-amplitude high-frequency mechanical stimulation in the form of sinusoidal vibrations, have emerged as a popular trend in the fitness industry. Within the last decade, the use of WBV as a clinical therapy for musculoskeletal disorders has expanded from its original use as an adjunctive therapy for osteoporosis (Rubin et al. 2003; Rubin et al. 2004), and is now being used to treat a wide range of conditions including stroke (Pang et al. 2013), spinal cord injury (Herrero et al. 2011), and multiple sclerosis (Claerbout et al. 2012). Furthermore, clinical trials have investigated WBV as an adjunctive or stand-alone therapy for non-specific back pain (Rittweger et al. 2002) and osteoarthritis (Park et al. 2013). A recent review of WBV as a treatment for back pain raised concerns based on the authors' view that integration of WBV into clinical practice has not been founded on rigorous research-based evidence of efficacy and safety (Perraton et al. 2010). In fact, the widespread use of WBV in the fitness industry as well as the aggressive marketing of these devices for home gyms, has raised concern within the scientific community (Muir et al. 2013).

WBV was implemented in the clinical setting as a therapy for osteoporosis based on reports of bone-strengthening effects in post-menopausal women (Rubin et al. 2003; Rubin et al. 2004). Within the last ten years, numerous studies have validated the use of mouse models to investigate the biological effects of WBV and recent studies demonstrated that WBV induces local effects that differ based on the anatomical site (e.g. tibia, femur, vertebrae) (Pasqualini et al. 2013).

Of concern is the fact that the effects of WBV on joint tissues have not been thoroughly evaluated. In the IVD, vibration poses an intriguing dichotomy: at amplitudes and frequencies associated with operation of heavy machinery, vibration is an established risk factor for back pain (Matsumoto and Griffin 2002; Funakoshi et al. 2004); however, WBV platforms are being used to treat back pain (Iwamoto et al. 2005; Belavy et al. 2008; del Pozo-Cruz et al. 2011). In clinical trials, WBV (30 Hz, 10 min/day) was reported to reduce the incidence of self-reported back pain following prolonged bed rest, however conflicting results were provided regarding measurable changes in disc morphology (Holguin et al. 2009; Belavy et al. 2010). In a rat model of hindlimb unloading, WBV (15 min/day; 45 Hz, 0.3 g) did not alter IVD biochemistry or morphology but enhanced muscle volume (Holguin and Judex 2010); however, changes in IVD morphology resulting from hindlimb unloading were ameliorated when the frequency of vibration was increased to 90 Hz (Holguin et al. 2013). In contrast, a recent study reported increased neurotrophins in cervical IVDs following exposure of rats to WBV (15 Hz, 30 min/day) (Karthi et al. 2014).

Similarly, there are few studies that directly assess the effects of WBV on synovial joints. Patient-reported pain in osteoarthritis was shown to decrease following WBV (Salmon et al. 2012; Park et al. 2013); however the studies did not directly assess joint health. One study in humans reported the ability of WBV to prevent loss of cartilage thickness resulting from prolonged immobilization of healthy male subjects (Liphardt et al. 2009). The overall lack of research demonstrates the urgent need to investigate the specific effects of WBV on joint tissues, given the increasing use of these platforms in both clinical practice and the fitness industry.

Our recent study using mouse models demonstrated anabolic effects of a single exposure to WBV on the IVD (McCann et al. 2013). We therefore sought to determine whether the transient changes previously reported would result in long-term beneficial effects on joint health. The current study was designed to assess the effects of repeated exposure of mice to WBV, using protocols that model vibration training in humans. We examined the effects of WBV on multiple skeletal tissues, including IVD, knee and long bones. Our findings point to deleterious responses of joint tissues to WBV in mice, highlighting the critical need to determine the safety of WBV for joint health in humans.

6.4 Materials and Methods

6.4.1 *In Vivo* Vibration

All procedures were approved by the Council on Animal Care at The University of Western Ontario, in accordance with the guidelines of the Canadian Council on Animal Care. Based on parameters of WBV used in clinical protocols, 10-week-old male CD-1 mice were subjected to vertical sinusoidal vibration at a frequency of 45 Hz, peak-to-peak amplitude of 74 μm and 0.3 g peak acceleration for 30 min/day, 5 days/week for 2 or 4 weeks, using a previously described vibration platform (McCann et al. 2013). Age-matched controls were housed in identical chambers on a sham (non-vibrated) platform to replicate handling and environmental conditions. Following WBV, mice were returned to conventional housing and monitored daily. At specified time points, mice were euthanized by a lethal dose of sodium pentobarbital.

6.4.2 Tissue Harvest and RNA Extraction

Twenty-four hours after the final exposure to WBV, thoracic IVDs (T10-T15) from each mouse were isolated by microdissection. Articular cartilage was isolated from the tibial plateau and femoral condyles (1 knee/mouse). One femur/mouse was isolated and flushed with sterile PBS to remove bone marrow. Tissues were immediately placed in TRIzol[®] Reagent (Life Technologies, Burlington, ON, Can.) and homogenized using a PRO250 tissue homogenizer (PRO Scientific, Oxford, CT, USA). RNA was extracted according to the manufacturer's instructions, quantified using a NanoDrop 2000 spectrophotometer (Thermo Scientific, Burlington, ON, Can.) and 0.5 µg was reverse transcribed into cDNA (iScript, Bio-Rad, Mississauga, ON, Can.).

6.4.3 Quantitative Polymerase Chain Reaction (qPCR)

Gene expression was assessed by real-time PCR using the BioRad CFX384. PCR reactions were run in triplicate, using 120 ng of cDNA per reaction and 25 µM forward and reverse primers with 2X SsoFast EvaGreen Supermix (Bio-Rad). The PCR program was: initial 2 min at 95°C denaturing; 10 sec at 95°C denaturing; and 10 sec annealing/elongation for a total of 40 cycles (primer details in **Table 6.1**). Transcript levels were calculated using $\Delta\Delta C_t$, normalized for input based on hypoxanthine-guanine phosphoribosyltransferase (*Hprt*) (Oxlund et al. 2003), and expressed relative to non-vibrated sham controls at each time point.

Table 6.1 Primers for real-time PCR

NCBI Gene Symbol	Primer Sequence 5' → 3'
<i>Hprt</i> Fwd	CAGGCCAGACTTTGTTGGAT
<i>Hprt</i> Rev	TTGCGCTCATCTTAGGCTTT
<i>Adamts4</i> Fwd	GAGGAGGAGATCGTGTTTCCAG
<i>Adamts4</i> Rev	CAAACCCTCTACCTGCACCC
<i>Adamts5</i> Fwd	GGAGCGAGGCCATTTACAAC
<i>Adamts5</i> Rev	GCGTAGACAAGGTAGCCCACTTT
<i>Acan</i> Fwd	CTGGGATCTACCGCTGTGAAG
<i>Acan</i> Rev	GTGTGGAAATAGCTCTGTAGTGGAA
<i>Colla1</i> Fwd	CTGGCGGTTTCAGGTCCAAT
<i>Colla1</i> Rev	TCCAGGCAATCCAGGAGC
<i>Col2a1</i> Fwd	GCACATCTGGTTTGGAGAGACC
<i>Col2a1</i> Rev	TAGCGGTGTTGGGAGCCA
<i>Dmp1</i> Fwd	CTGAAGAGAGGACGGGTGATT
<i>Dmp1</i> Rev	CGTGTGGTCACTATTTGCCTG
<i>Ibsp</i> Fwd	ACGGCGATAGTTCCGAAGAG
<i>Ibsp</i> Rev	CTAGCTGTTACACCCGAGAGT
<i>Mmp3</i> Fwd	TTGTCCCGTTTCCATCTCTCTC
<i>Mmp3</i> Rev	TTGGTGATGTCTCAGGTTCAG
<i>Mmp13</i> Fwd	CTTCTTCTTGTTGAGCTGGAATC
<i>Mmp13</i> Rev	CTCTGTGGACCTCACTGTAGACT
<i>RANK</i> Fwd	CCAGGAGAGGCATTATGAGCA
<i>RANK</i> Rev	ACTGTCGGAGGTAGGAGTGC
<i>Sox9</i> Fwd	AGTACCCGCATCTGCACAAC
<i>Sox9</i> Rev	TACTTGTAATCGGGGTGGTCTT
<i>Wnt10b</i> Fwd	CGGACTGAGTAAGCGACAGC
<i>Wnt10b</i> Rev	ACTCGTGAACGGCGATGTG

Annealing Temperature: 60°C degree

6.4.4 Histology

Intact lumbar spinal segments (L1-L5) and right knee (with joint capsule intact) were isolated and fixed in 4% paraformaldehyde. Spinal columns were decalcified for 5 days in Shandon's TBD-2 (Fisher Scientific) and knee joints were decalcified for 10 days in 5% EDTA in PBS (pH 7.0). Tissues were processed and embedded in paraffin. Spines were sectioned sagittally and knees sectioned coronally, at a thickness of 5 μ m using a microtome (Leica Microsystems, Concord, ON, Can.). Using established protocols (McCann et al. 2013; Pest et al. 2014), serial sections were stained with either 0.1% Safranin-O/0.02% fast green for sulfated glycosaminoglycans or 1.3% picric acid and 0.1% Direct red 80 (Sigma-Aldrich, St. Louis, MO, USA) for collagen. Sections were imaged on a Leica DM1000 microscope (equipped with polarizing filter (#11505087) and analyzer (#11555045)), with Leica Application Suite (Leica Microsystems).

6.4.5 Immunohistochemistry

Antigen retrieval was performed with 0.1% Triton X-100 in PBS for 20 min at room temperature and tissue sections were blocked with 5% goat serum/5% Bovine Serum Albumin for 1 hr at room temperature. Tissue sections were incubated with rabbit primary antibodies against the products of ADAMTS-mediated aggrecan cleavage (NITEGE), MMP-mediated aggrecan cleavage (DIPEN) (Sztrolovics et al. 1997), or MMP-mediated collagen cleavage (C1,2C) (Billinghurst et al. 1997) overnight at 4°C. Goat anti-rabbit secondary antibody conjugated to horseradish peroxidase (Santa Cruz Biotechnology, Dallas, TX, USA) was used in conjunction with DAB+ chromogen (Dako

Canada, Burlington, ON, Can.) for colorimetric detection of antibody binding. Secondary only controls were performed in parallel. Sections were counterstained using 0.5% methyl green and imaged on a Leica DM1000 microscope.

6.4.6 Cell Death Assay

Spinal sections were assessed for *in situ* cell death using the terminal nucleotidyl transferase-mediated nick end labeling (TUNEL) staining kit (Roche, Mississauga, ON, Can), according to the manufacturer's instructions. Sections were mounted using VECTASHIELD Medium with DAPI (Vector Labs, Burlingame, CA, USA) and imaged with a Leica DMI6000B inverted microscope with Leica Application Suite. Images were scored by two independent blinded observers, and TUNEL-positive cells were counted within each IVD compartment (NP and AF) and expressed as a percentage of the total cells. Pretreatment with DNase I (Roche) and omission of labeling solution served as positive and negative controls, respectively.

6.4.7 Micro-computed tomography (micro-CT)

Right hindlimbs (mid-femur to ankle, with knee joint capsule intact) were isolated and fixed in 4% paraformaldehyde. To avoid motion during scanning, specimens were fixed in 50 mL tubes containing 1% agarose in PBS. Individual tubes were mounted onto the bed of the GE eXplore Locus micro-CT scanner (GE Healthcare Biosciences, Piscataway, NJ, USA) with calibrators for air, water and bone-mimicking epoxy with a

mineral value of 1.1 g/cm³ (SB3, Gammex RMI). The scanning protocol included 900 projection images at a 0.4 degree angle increment, obtained over a 165-min gantry rotation. The X-ray tube potential was 80 kVp with 450 μ A tube current, 4500 ms exposure and 2 frames per view angle averaged. Images were reconstructed into 3D volumes with 20 μ m isotropic voxel size and linearly rescaled into Hounsfield Units (HU) using internal calibration standards.

Using MicroView (GE Healthcare Biosciences), full volumes were cropped to contain only the tibia and fibula, and reoriented to the same axes. To determine trabecular bone morphometry, a standardized region of interest (ROI) was selected in the proximal tibia using the largest dimensions possible to capture trabecular bone and excluding cortical bone in all scans. The ROI was an elliptic cylinder (41 pixels (x-axis) x 42 (y-axis) x 48 (z-axis) positioned 50 μ m distal to the growth plate, to measure the secondary spongiosa. Bone morphometry was quantified using the Bone Analysis tool in MicroView, as previously reported (Ulici et al. 2009).

6.4.8 Statistical Analyses

Data are presented from experiments conducted in 2 independent trials, each with 4-6 mice per treatment group. Parameters from mice exposed to WBV were compared to those from non-vibrated sham controls at the same time point using a parametric, two-tailed, unpaired t-test with a Welch's correction. $P < 0.05$ was considered significant.

6.5 Results

To examine the effects of repeated exposure to WBV on joint tissues, wild-type mice (10 weeks of age) were exposed to daily protocols of vertical sinusoidal WBV based on those currently used in clinical and exercise protocols (45 Hz, 0.3 g peak acceleration, 30 min/day, 5 days/week) for 2 or 4 weeks. Skeletal tissues, including a synovial joint (knee), cartilaginous joints (IVDs) and bone (tibia) were assessed and compared to those of age-matched control mice.

6.5.1 Effects of Repeated Exposure to WBV on the Intervertebral Disc

We first assessed lumbar IVD health. No discernible differences were detected in the IVD following 2 weeks of WBV. However, following 4 weeks, Safranin-O/fast-green staining demonstrated loss of the distinct NP-AF boundary, greater mucinous material leading to enhanced glycosaminoglycan staining in the intra-lamellar matrix of the AF, and focal disruptions in the AF lamellae in mice exposed to WBV compared to sham controls (**Figure 6.1 A**). Evaluation of the histological appearance using the modified Thompson scoring system (Thompson et al. 1990) indicated significant degenerative changes in the AF of mice exposed to WBV compared to sham controls (**Figure 6.1 B**). Collagen content and organization within the IVD was examined using picrosirius-red staining, which showed no discernible differences between mice exposed to 4 weeks WBV and sham controls, in either the NP or the AF (**Figure 6.1 C**). However, examination of sections by polarized light microscopy revealed disrupted collagen organization with breaks within the collagen lamellae in the inner AF of mice exposed to

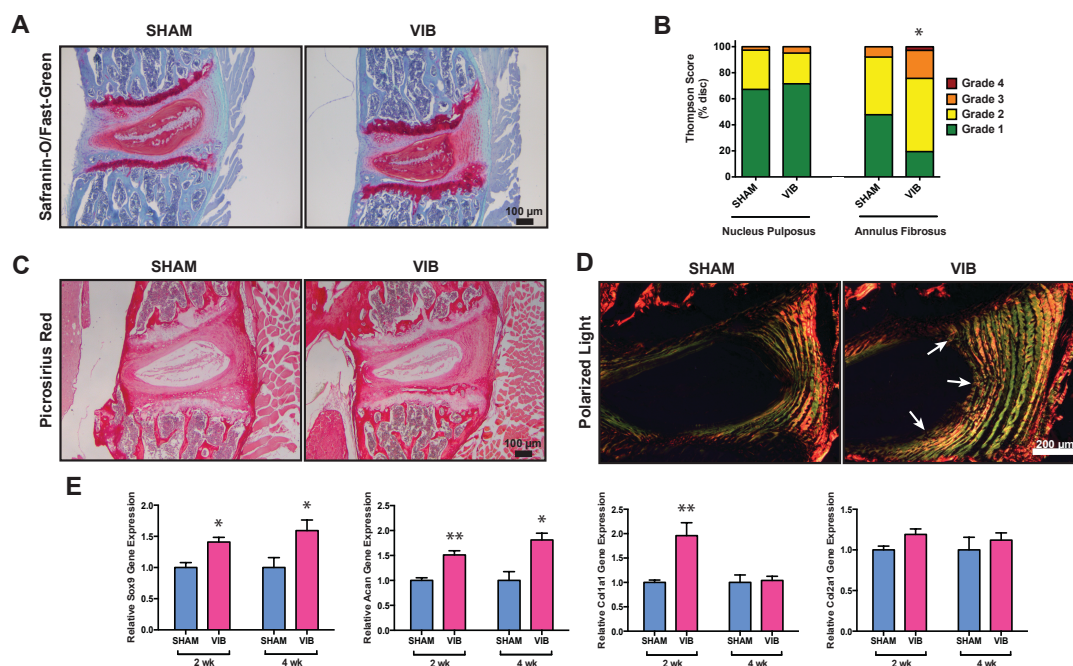


Figure 6.1 Repeated exposure to whole-body vibration negatively affects the lumbar intervertebral disc.

A. Representative histological sections of the lumbar spine stained with Safranin O/fast green from mice exposed to WBV (30 min/day; 45 Hz, 0.3 g; 4 weeks vibration) and non-vibrated sham controls. Images are oriented with rostral on top and dorsal on the right. **B.** Evaluation of the morphologic grade of tissue degeneration (using the Thompson score) demonstrates a significant increase in tissue degeneration in the annulus fibrosus of mice subjected to WBV. * $p < 0.05$; $n = 3$ IVDs/animal; 5 animals/group ($n = 15$). **C.** Picrosirius red stain for collagen content imaged by polarized light (presented in D.) for collagen structure revealed disrupted collagen organization (arrows) **E.** SYBR-based real-time PCR analysis of intervertebral disc gene expression. Expression of anabolic genes was determined relative to the expression of the housekeeping gene *Hprt* and normalized to non-vibrated (sham) controls at each time point. Data are presented as the mean \pm SEM, from 5 pooled IVDs per mouse, 4-5 mice/group, run in technical triplicate; * = $p < 0.05$, ** = $p < 0.01$.

WBV, changes not observed in sham controls (**Figure 6.1 D**, *arrows*). Interestingly, degenerative changes induced by WBV in lumbar IVDs were also detected in the caudal spine (**Figure 6.2**). To investigate the cellular response to repeated exposure to WBV, we performed real-time PCR on whole-disc RNA (**Figure 6.1 E**). IVD tissues from mice exposed to WBV demonstrated a significant increase in the expression of *Sox9* (1.4-fold increase at 2 weeks, 1.6-fold increase at 4 weeks). This was accompanied by increased expression of aggrecan (1.5-fold increase at 2 weeks, 1.8-fold increase at 4 weeks) and a 2.0-fold increase in type I collagen expression after 2 weeks WBV. In contrast, no significant change in type II collagen expression was detected at either time point following WBV.

We further investigated WBV-induced disc degeneration by examining the accumulation of matrix degradation fragments. Immunohistochemical staining revealed that 4 week exposure of mice to WBV resulted in increased MMP-mediated aggrecan cleavage in the outer AF, as evidenced by increased detection of the DIPEN cleavage product (**Figure 6.3 A**, *arrows*). In contrast, no changes in aggrecanase activity were detected following exposure of mice to WBV, as detected by NITEGE staining (**Figure 6.3 B**). We next labeled C1,2C neoepitopes, which correspond to type I and/or type II collagen cleavage by MMPs (Billinghurst et al. 1997). Similar to aggrecan, we detected greater accumulation of MMP-mediated collagen cleavage products in the outer AF of mice exposed to WBV compared to sham controls (**Figure 6.3 C**, *arrows*). No differences in staining were detected in either the inner AF or NP between mice exposed to WBV and sham controls. Increased matrix cleavage in mice exposed to WBV was accompanied by a significant increase in the expression of *Mmp3* (1.5-fold induction at 2

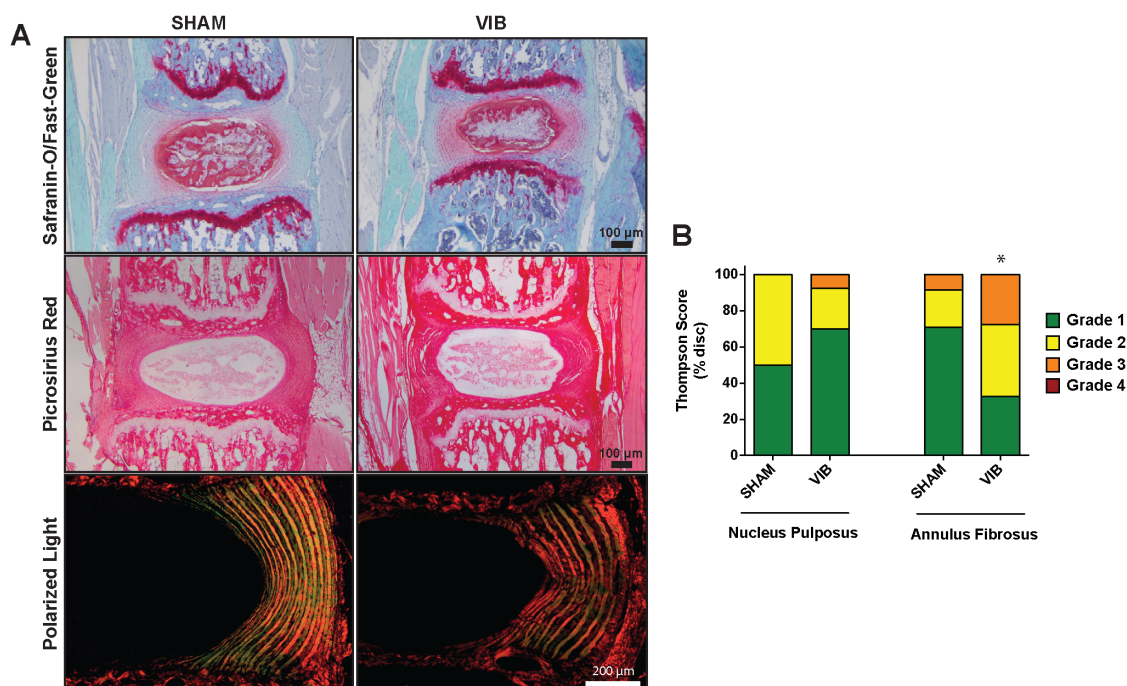
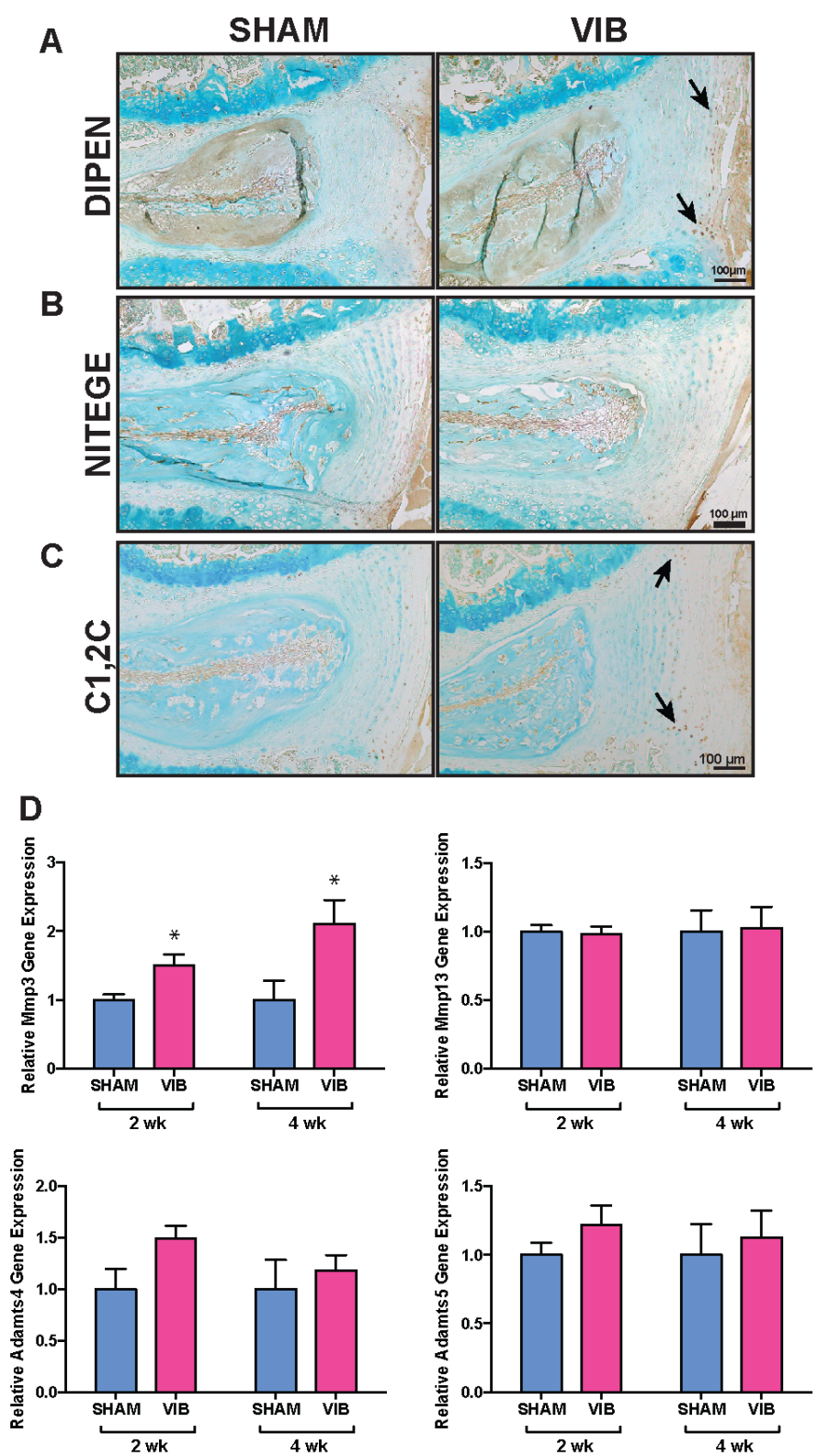


Figure 6.2 Repeated exposure to whole-body vibration negatively affects the caudal intervertebral disc.

A. Representative histological sections from the caudal spine stained with Safranin-O/fast green for glycosaminoglycans, picrosirius red for collagen content, and picrosirius red imaged with polarized light for collagen organization, in mice exposed to 4 weeks WBV (30 min/day; 45 Hz, 0.3 g) or non-vibrated sham controls. **B.** Evaluation of the morphologic grade of tissue degeneration (using the Thompson score) demonstrated a significant increase in tissue degeneration in the annulus fibrosus of mice subjected to WBV compared to sham controls. Data are presented as the mean \pm SEM, based on 3 IVDs per animal, 4-5 animals/group ($n = 15$), * = $p < 0.05$.

Figure 6.3 Matrix degradation in mouse intervertebral discs following whole-body vibration.

A-C. Representative sagittal sections of intervertebral discs from mice subjected to 4 weeks WBV or non-vibrated sham controls, stained for DIPEN (MMP cleaved aggrecan neoepitope), NITEGE (ADAMTS 4/5 cleaved aggrecan neoepitope) and C1,2C (MMP cleaved collagen neoepitope) and counterstained with methyl green. **D.** SYBR-based real-time PCR analysis of IVD gene expression. Expression of catabolic genes was determined relative to the expression of the housekeeping gene *Hprt* and normalized to non-vibrated (SHAM) controls at each time point. Data are presented as the mean \pm SEM, from 5 pooled IVDs per mouse, 4-5 mice/group, run in technical triplicate; * = $p < 0.05$.



weeks, 2.1-fold induction at 4 weeks over sham controls) (**Figure 6.3 D**). In contrast, exposure of mice to WBV did not alter the expression of *Mmp-13*, *Adamts-4* or *Adamts-5* in IVD tissues compared to non-vibrated sham controls.

To determine if WBV altered cell viability in the IVD, TUNEL staining was performed on lumbar IVDs following 4 weeks of WBV. Mice exposed to WBV demonstrated a greater percentage of TUNEL-positive cells when compared to sham controls (**Figure 6.4 3A**) in the NP and, to a greater extent, in the AF (**Figure 6.4 B**).

6.5.2 Effects of Repeated Exposure to WBV on the Knee Joint

We next sought to determine whether the deleterious changes detected within the IVD also occurred within synovial joints such as the knee. Histological examination revealed tears in the medial meniscus of mice exposed to 2 weeks WBV (3 of 4 mice; **Figure 6.5 Aii & iii, arrows**), changes that were not detected in the sham controls. No alterations in the articular cartilage were detected following 2 week exposure to WBV. Signs of early osteophyte formation were observed on the medial tibial plateau of one mouse following 2 week exposure to daily WBV (**Figure 6.5 Aiii, asterisk**), the animal demonstrating the most severe meniscal damage at this time point.

Assessment of knee joint tissues after 4 weeks of WBV revealed meniscal tears in 4 out of the 5 mice exposed to WBV (**Figure 6.5 Av & vi, arrows**), changes not detected in the sham controls. The extent of meniscal damage was greater following 4 weeks of WBV compared to that detected after 2 weeks, and was likewise accompanied by

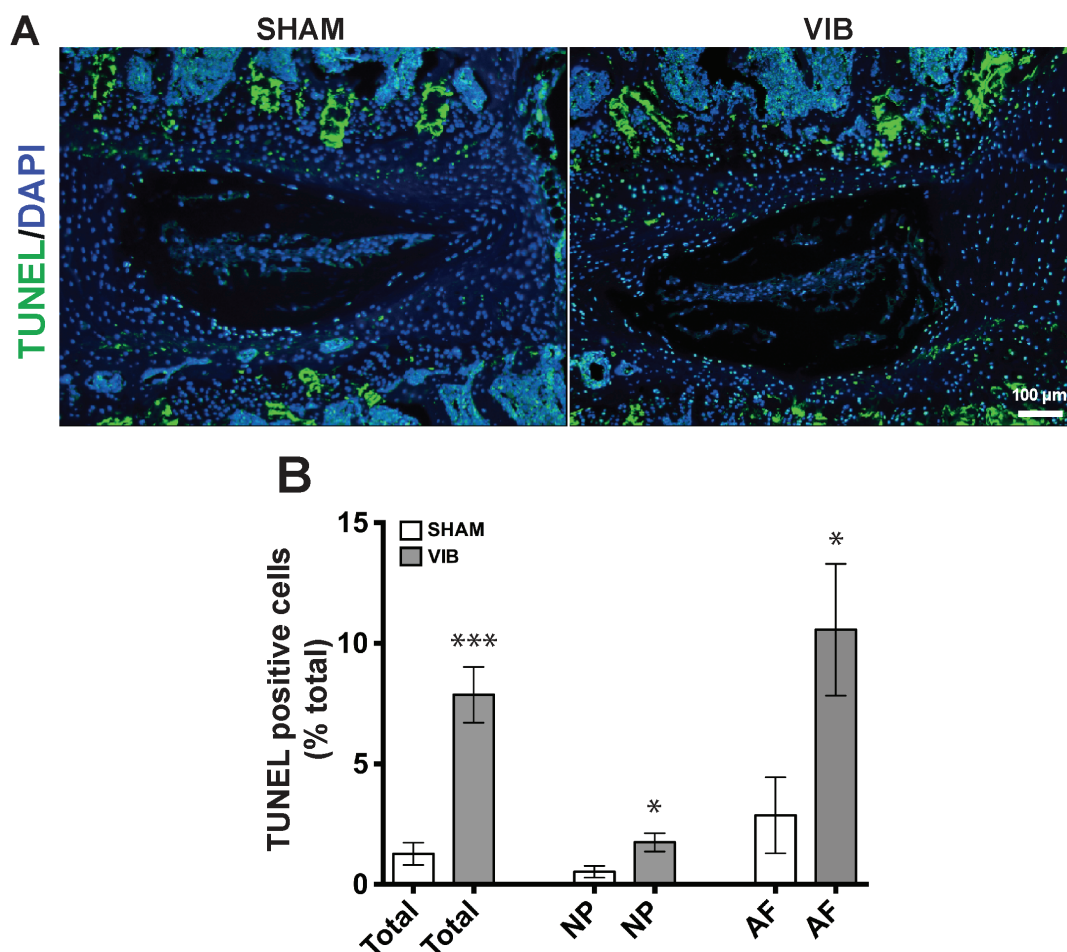


Figure 6.4 TUNEL staining of intervertebral discs after repeated exposure to whole-body vibration.

A. Representative sections of lumbar IVDs stained with TUNEL to detect DNA fragmentation and counterstained with DAPI. **B.** Percentage of TUNEL-positive cells was determined for specific regions (NP, AF) within the IVD. Vibration induced a significant increase in cell death within IVD when compared to non-vibrated sham controls, specifically within the NP and AF. Data are presented as the mean \pm SEM, based on 3 IVDs per mouse, 4-5 mice/group (n=15). * = $p < 0.05$, *** = $p < 0.001$. NP = Nucleus Pulposus, AF = Annulus Fibrosus

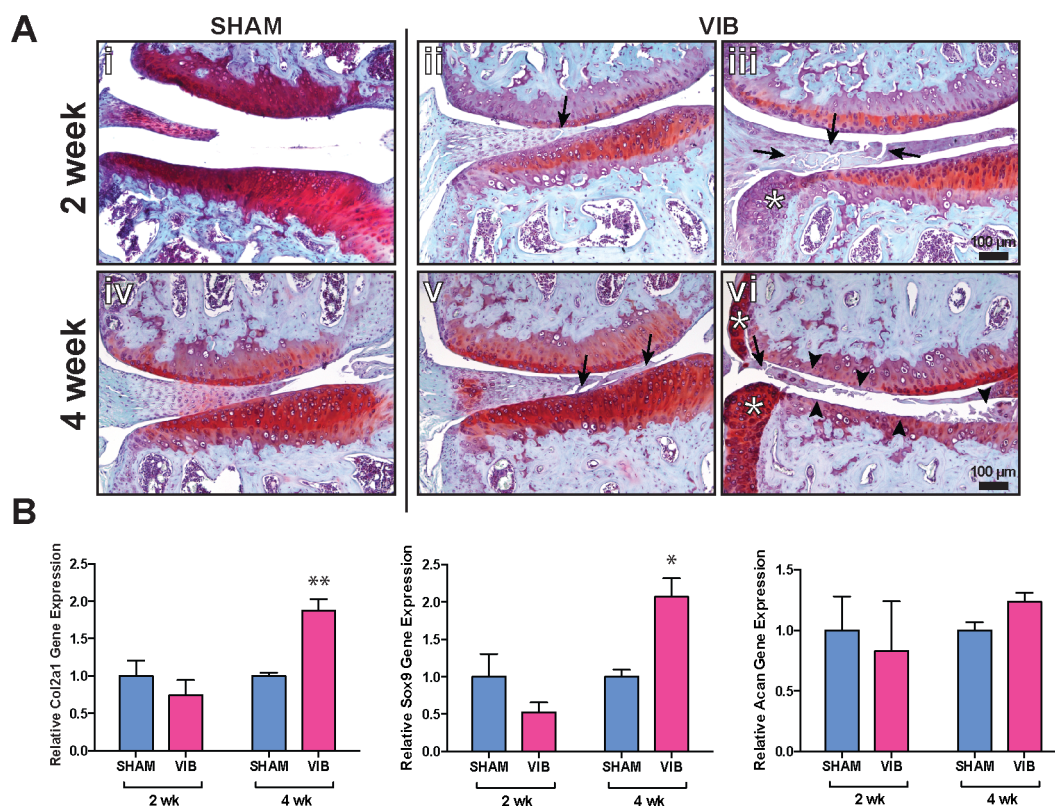


Figure 6.5 Histological sections of mouse medial knee joint after exposure to whole-body vibration.

A. Coronal sections of knee joints from 1 control and 2 mice exposed to WBV at each time point stained with Safranin-O/fast green to detect sulfated glycosaminoglycans. Images are oriented with medial meniscus on the left, femoral condyle on top and tibial plateau beneath. Arrows indicate microfissures detected within the medial meniscus in 3 of 4 mice at 2-weeks (ii,iii) and 4 of 5 mice at 4 weeks (v,vi) subjected to WBV. No meniscal damage was detected in non-vibrated sham controls (i,iv). Arrowheads indicate severe degeneration of the articular cartilage on the medial quadrants of both the tibia and the femur (vi). High levels of degeneration were detected in 2 of the 5 mice subjected to WBV as seen in (iv). No articular cartilage degeneration was detected in the non-vibrated sham controls. Asterisks depict osteophytes. **B.** SYBR based real-time PCR analysis of articular cartilage gene expression. Expression of anabolic genes was determined relative to the expression of the housekeeping gene *Hprt* and normalized to non-vibrated (sham) controls at each time point. Data are presented as the mean \pm SEM, 4-5 animals/group, run in technical triplicate; * = $p < 0.05$, ** = $p < 0.01$.

osteophyte formation in one mouse (**Figure 6.5 Av**, *asterisk*). Extensive articular cartilage damage was observed in 2 of the 5 mice exposed to 4 weeks WBV, with loss of the superficial zone cartilage extending to the calcified cartilage zone of both the tibial and femoral heads (**Figure 6.5 Av**, *arrowheads*). Notably, focal damage to the articular surface was limited to the medial joint compartment; no defects were detected in the articular cartilage of the lateral joint compartment (**Figure 6.6**). No apparent changes in the organization or abundance of collagen fibres were detected in the medial joint following WBV (**Figure 6.7**).

To investigate the cellular response of articular chondrocytes to WBV, real-time gene expression analysis was following 2 or 4 weeks WBV (**Figure 6.5 B**). While no significant changes were detected following 2 weeks WBV, significant induction of both *Sox9* and *Col2a1* gene expression was detected in articular chondrocytes following exposure to 4 weeks of WBV (2.1-fold and 1.9-fold increase, respectively). No significant change in the expression of *Acan* was detected following WBV when compared to controls (**Figure 6.6**).

To assess articular cartilage breakdown, we performed neopeptide staining to detect matrix breakdown fragments within the joint compartment. In contrast to non-vibrated sham controls, diffuse extracellular DIPEN staining was detected in the superficial articular cartilage fibrillations on the tibial plateau as well as the meniscus (**Figure 6.8 A**, *arrows*). Mice exposed to 4 weeks of WBV also demonstrated increased DIPEN staining associated with the chondrocytes of the calcified cartilage, compared to sham controls (**Figure 6.8 5 A**, *arrowheads*). Due to the loss of the superficial articular cartilage in the medial joint compartment following 4 weeks WBV, we examined the

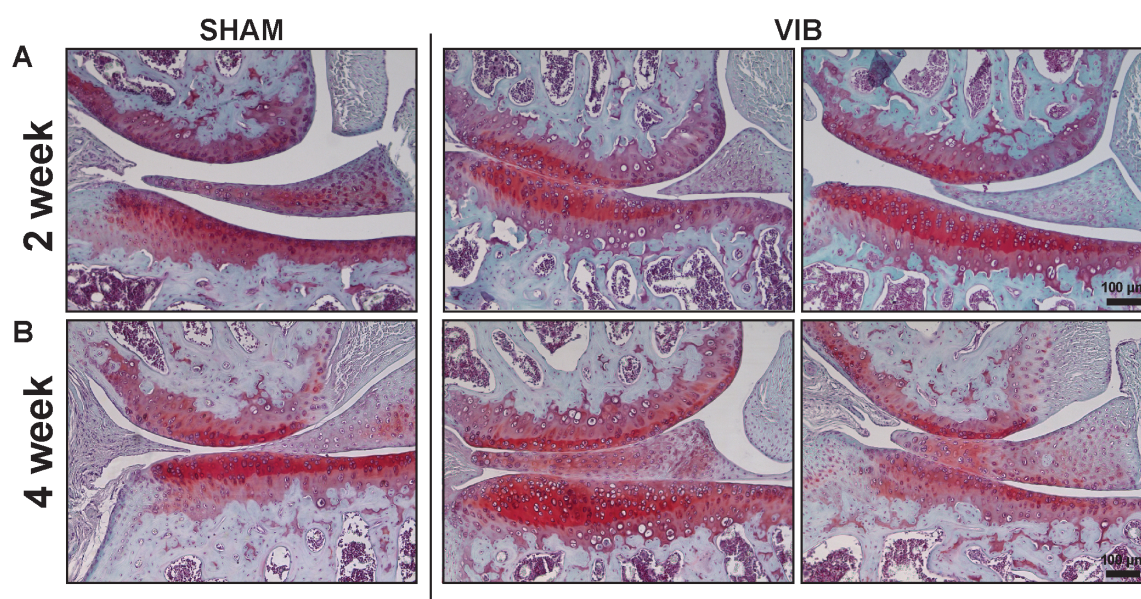


Figure 6.6 Histological sections of the lateral compartment of the mouse knee joint after exposure to whole-body vibration.

Representative coronal sections of the knee joint from 1 control and 2 mice exposed to WBV at each time point stained with Safranin-O/fast green to detect sulfated glycosaminoglycans. No meniscal or articular cartilage damage was detected in the lateral knee joint compartment in mice from either group at A. 2 weeks or B. 4 weeks.

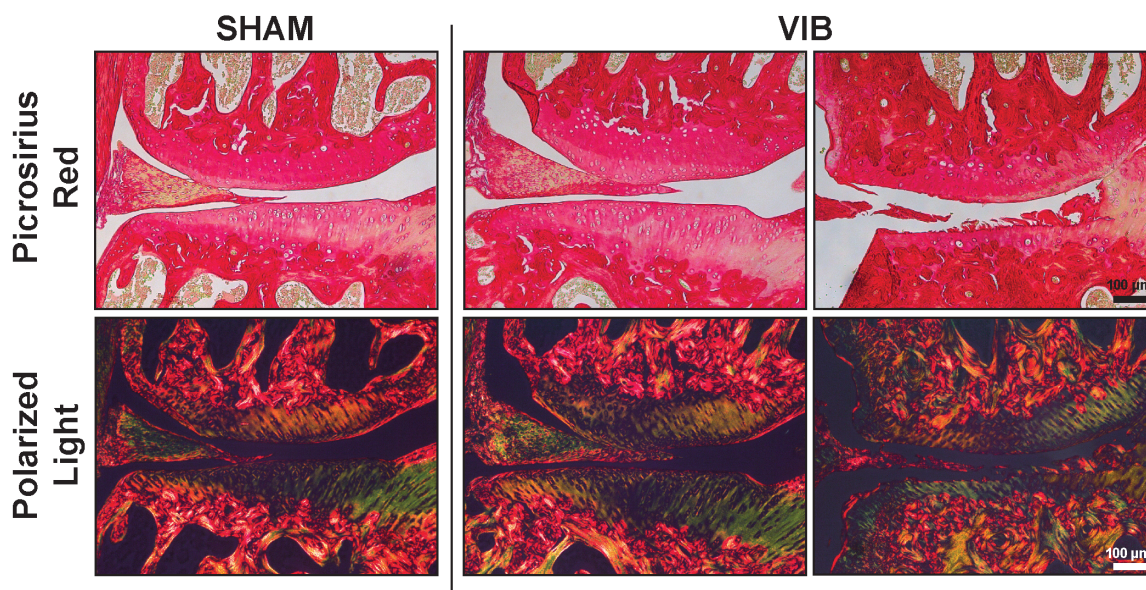


Figure 6.7 Histological sections of mouse medial knee joint after 4 weeks of exposure to whole-body vibration.

Representative coronal sections of the knee joint from 1 sham and 2 mice exposed to WBV stained with picrosirius red to detect collagen content and imaged with polarized light. Images are oriented with medial meniscus on the left, femoral condyle on top and tibial plateau beneath. No apparent changes were seen in the organization or abundance of collagen following WBV.

Figure 6.8 Matrix degradation in mouse medial knee joint compartment following whole-body vibration.

A. Representative sections of medial knee joint from mice subjected to 4-weeks WBF or sham controls stained by immunohistochemistry for DIPEN (MMP cleaved aggrecan neoepitope), NITEGE (ADAMTS cleaved aggrecan neoepitope) or C1,2C (MMP-cleaved collagen neoepitope) and counterstained with methyl green. **B.** SYBR-based real-time PCR analysis of articular cartilage gene expression. Expression of catabolic genes was determined relative to the expression of the housekeeping gene *Hprt* and normalized to non-vibrated (sham) controls at each time point. Data are presented as the mean \pm SEM, 4-5 animals/group, run in technical triplicate; * = $p < 0.05$.

lateral joint compartments for matrix degradation. Pericellular DIPEN staining was detected more uniformly throughout the meniscus in mice exposed to WBV than in sham controls (**Figure 6.9**). Furthermore, increased pericellular DIPEN staining was detected within the superficial zone of the tibial and femoral articular cartilage in mice following 4 weeks WBV compared to sham controls (**Figure 6.9 A**, *arrows*). In contrast, no overt change in NITEGE staining was detected in the articular cartilage of either the medial or lateral knee joint compartments (**Figure 6.8B**, **Figure 6.9 B**). Greater pericellular NITEGE staining was however detected in the meniscus within the lateral joint compartment of mice exposed to WBV than in sham controls (**Figure 6.9 B**).

The presence of collagen breakdown fragments was likewise assessed following 4 weeks WBV. Greater diffuse C1,2C neopeptide staining was detected in the fibrillated articular cartilage of the tibial plateau as well as the meniscus of mice exposed to WBV, compared to sham controls (**Figure 6.8 C**). The lateral joint compartments of the same mice demonstrated a similar increase in C1,2C staining in the ECM of the meniscus, as well as pericellular staining throughout the superficial zone of the articular cartilage (**Figure 6.9 C**).

Real-time gene expression analysis of articular cartilage RNA demonstrated that, whereas no significant changes were detected in *Mmp3* expression, exposure of mice to 4 weeks WBV induced a significant increase in *Mmp13* expression (1.5-fold increase over sham controls) (**Figure 6.8 D**). Similar to the IVD, no change was detected in expression of *Adamts-4* or *Adamts-5* in articular cartilage following exposure of mice to WBV.

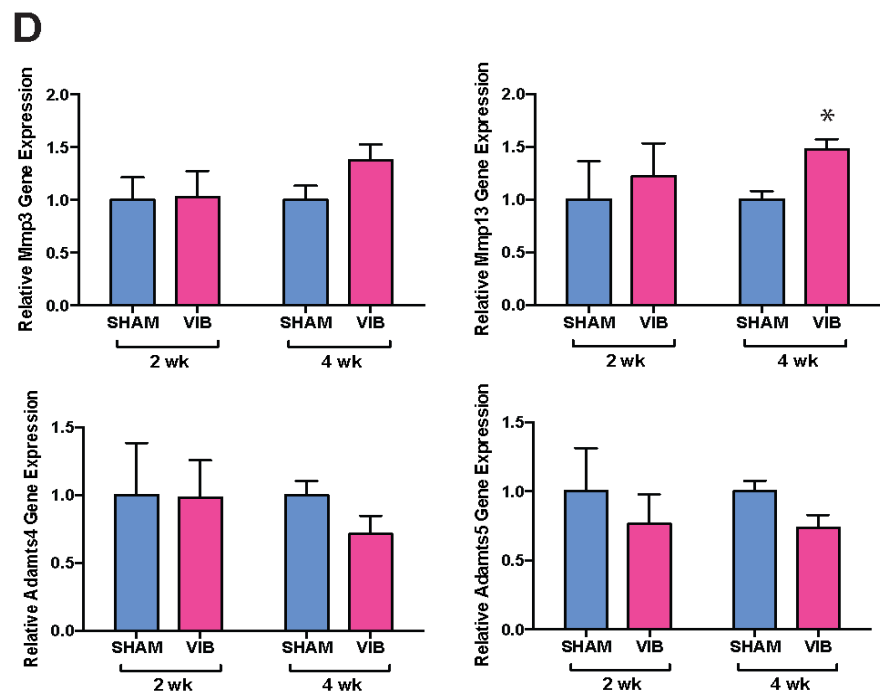
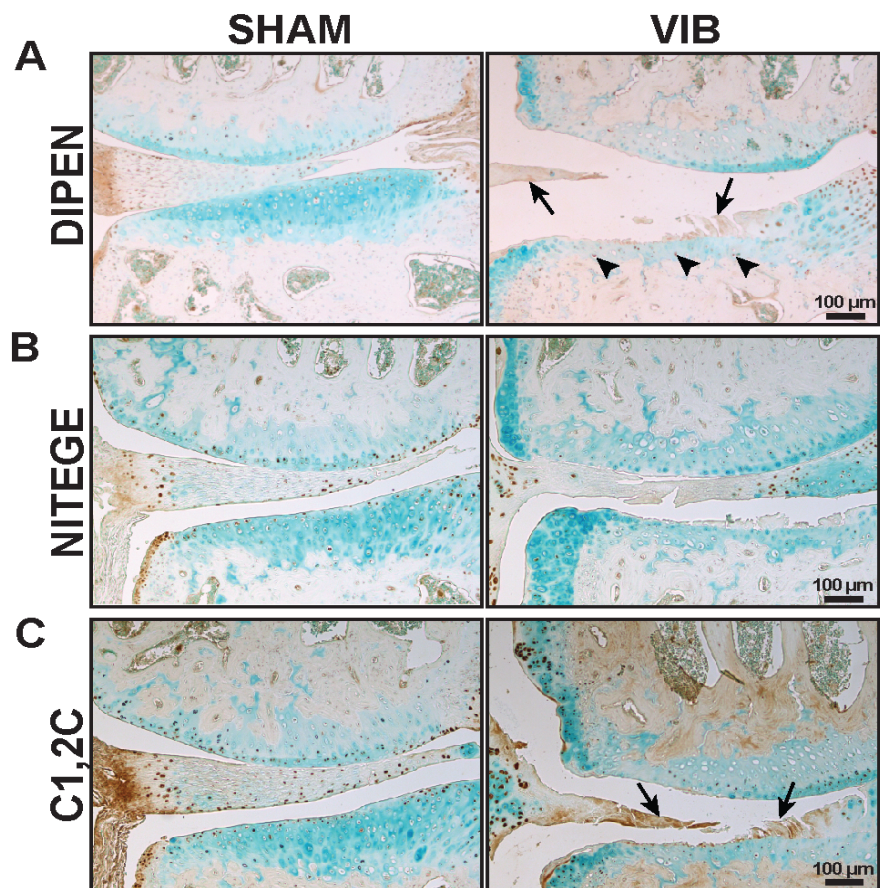
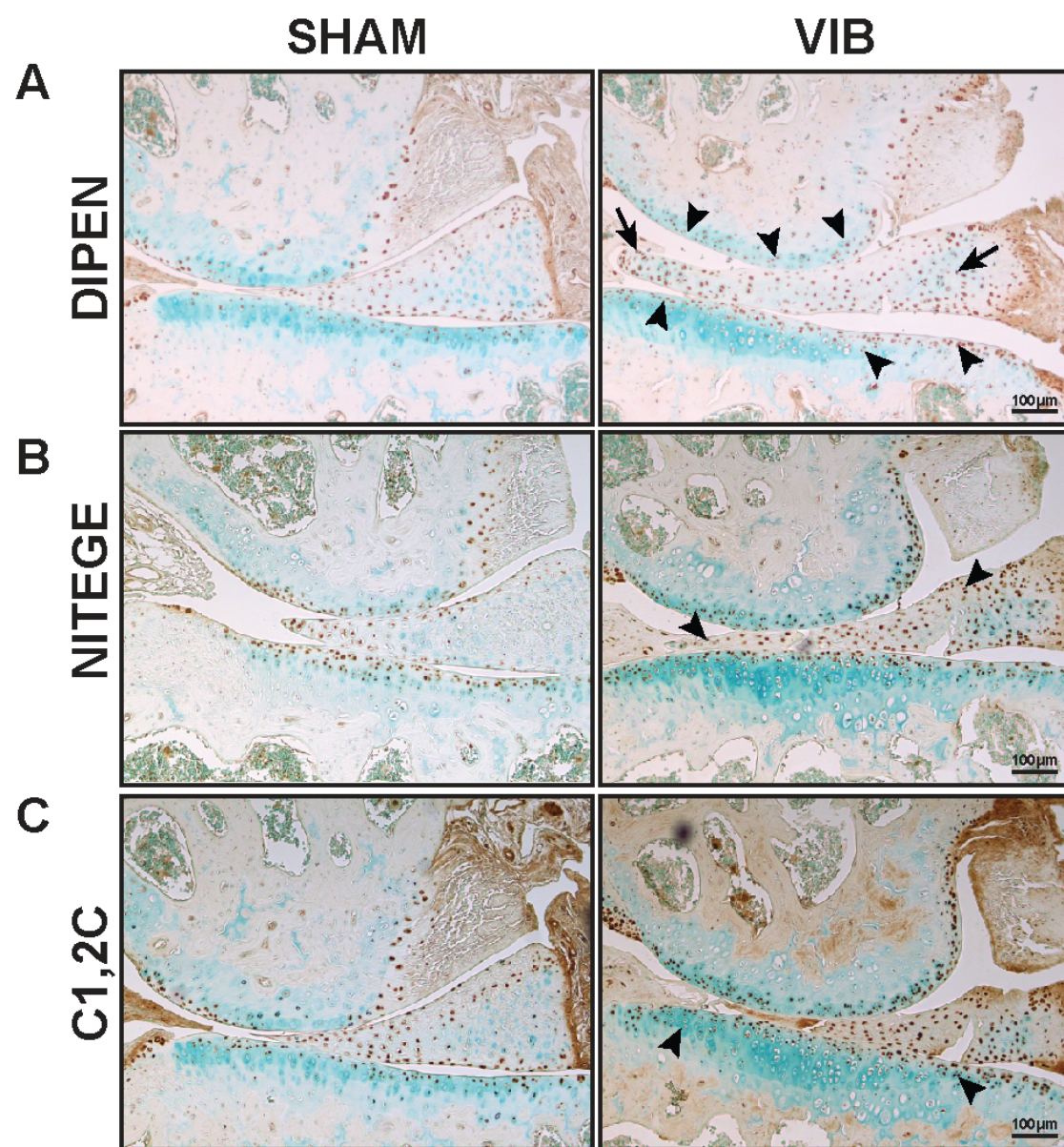


Figure 6.9 Catabolic activities in lateral mouse knee joints following whole-body vibration.

A. Representative images of lateral knee joint sections in mice subjected to 4 weeks WBV or sham controls stained by immunohistochemistry for DIPEN (ADAMTS cleaved aggrecan neoepitope), **B.** NITEGE (MMP cleaved aggrecan neoepitope) and **C.** C1,2C (MMP cleaved collagen neoepitope) and counterstained with methyl green.



6.5.3 Repeated Exposure to WBV did not Alter Bone Morphometry

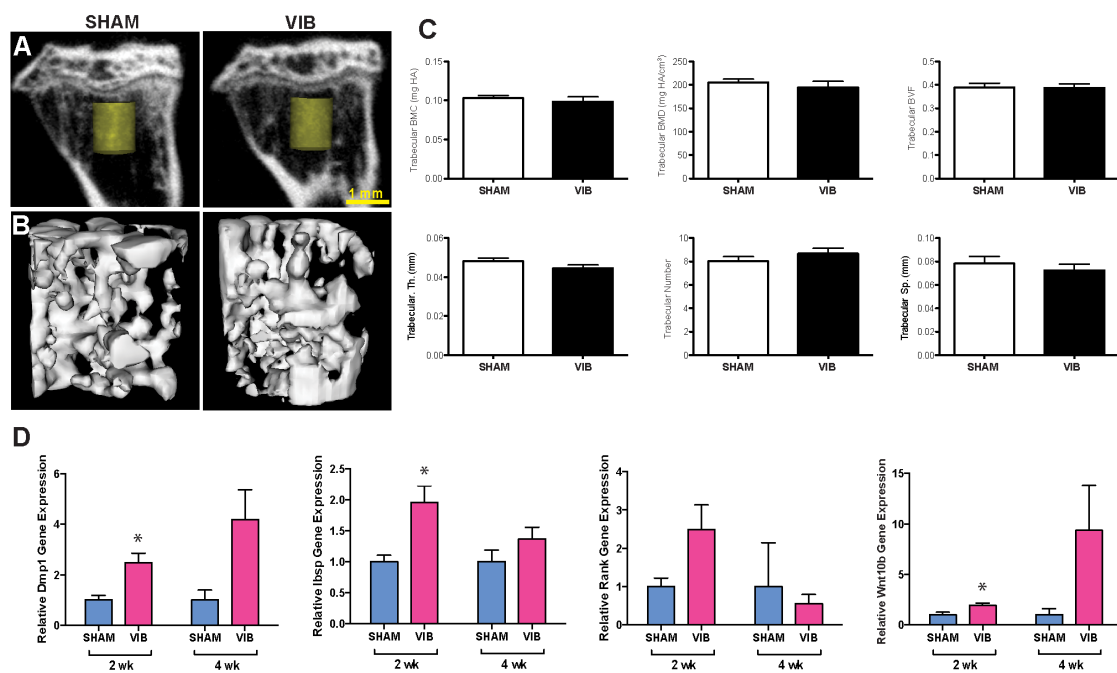
We employed high-resolution micro-CT to determine whether exposure of mice to 2 or 4 weeks of daily WBV altered bone microarchitecture. Volumetric analysis was conducted within a region of interest localized to the secondary spongiosa of the tibia (**Figure 6.10 A & B**). No significant differences in bone mineral density (BMD), bone mineral content (BMC), bone volume fraction (BVF), trabecular thickness (Tb.Th), trabecular number (Tb.N) or trabecular separation (Tb.Sp) were observed between mice following 4 weeks WBV and sham controls (**Figure 6.10 C**). To investigate cellular responses within bone to WBV, we performed real-time PCR on RNA isolated from the femur. Following 2 weeks WBV, significantly greater expression of markers of the osteoblast lineage *Dmp1* (2.5 fold) and *Ibsp* (2.0 fold) were detected compared to sham controls (**Figure 6.10 D**). Similarly, exposure of mice to WBV promoted increased expression of *Wnt10b* (1.9 fold over sham controls), a secreted molecule implicated as an effector of bone mechanotransduction (Hou et al. 2011). No significant change was detected in expression of the osteoclast receptor *Rank* following exposure of mice to WBV at either time point.

6.6 Discussion

WBV has recently been incorporated as an adjuvant or stand-alone treatment for a wide range of diseases, ranging from stroke to chronic-obstructive pulmonary disease. Most notably, WBV is being used to treat musculoskeletal disorders including osteoporosis (Rubin et al. 2004), back pain (del Pozo-Cruz et al. 2011), and osteoarthritis

Figure 6.10 Analysis of bone microarchitecture and gene expression following whole-body vibration.

A. Hind limbs from mice following 4 weeks WBV (VIB) and non-vibrated controls (SHAM) were isolated post-mortem and prepared for micro-CT scanning at 20 μm resolution. Representative coronal plane X-ray images of the proximal tibia are depicted. A standardized region of interest (ROI – indicated in yellow) was selected in the proximal tibia to assess trabecular bone and exclude cortical bone. The ROI was an elliptic cylinder (41 pixels (x-axis) x 42 (y-axis) x 48 (z-axis)) positioned 50 μm distal to the growth plate, to measure the secondary spongiosa. **B.** Isosurface image of ROI indicated in A from SHAM and VIB specimens. **C.** Histograms illustrate bone mineral density (BMD), bone mineral content (BMC), bone volume fraction (BVF, ratio), trabecular thickness (Tb.Th), trabecular number (Tb.N) and trabecular spacing (Tb.Sp). No significant differences were observed in bone density, mineral content or microarchitectural parameters. Data are presented as the mean \pm SEM, 4-6 animals/group. Differences between sham and vibration groups were assessed using unpaired two-tailed *t* tests. **D.** SYBR-based real-time PCR analysis of femur gene expression. Gene expression was determined relative to levels of the housekeeping gene *Hprt* and normalized to non-vibrated (sham) controls at each time point. Data are presented as the mean \pm SEM, from 6 animals/group, run in technical triplicate; * = $p < 0.05$.



(Park et al. 2013). However, recent reports highlight conflicting results following exposure to WBV, both in animal models and clinical studies (Wenger et al. 2010; Slatkowska et al. 2011). Further confounding their interpretation, many clinical studies of WBV are based on patient-reported pain, and not quantitative assessment of tissue health (del Pozo-Cruz et al. 2011; Park et al. 2013). Surprisingly, to our knowledge no studies have examined the cellular changes in soft joint tissues following exposure to WBV, in either animal models or humans. As such, the current study was designed to simultaneously examine the effects of repeated exposure to WBV on musculoskeletal tissues including the IVD and knee joints, using an *in vivo* mouse model.

The parameters of WBV used in the current study were chosen to introduce specific values of peak acceleration (in $\text{m}\cdot\text{s}^{-2}$) and frequency (in Hz). The combination of acceleration and frequency uniquely determines the amplitude of the platform displacement (in mm). Perhaps surprisingly, these parameters are essentially the same for animal and human studies, especially from the perspective of individual cells that are the functional units responding to the stimulus. Thus, the parameters for WBV are the same for animal and human subjects to produce similar levels of strain and deformation within the tissues. Importantly, the parameters of WBV used in this study (45 Hz, peak-to-peak amplitude of 74 μm and 0.3 g peak acceleration) were selected based on previous studies which reported beneficial effects of WBV on muscle and bone (Oxlund et al. 2003). While there is currently no consensus as to the relative importance of specific parameters of WBV (i.e. magnitude, frequency, acceleration), it is generally accepted that low-amplitude high-frequency loading promotes adaptive bone formation (Torcasio et al. 2008). Importantly, while the frequency values are comparable, the acceleration

experienced by mice in the current study is an order of magnitude less than experienced by humans using clinical WBV protocols, which reported beneficial effects on bone (Verschuere et al. 2004).

Our previous work used *ex vivo* and *in vitro* mouse models to examine the acute response of IVD tissues to WBV. These studies established that a single exposure to WBV resulted in a transient decrease in the expression of catabolic genes (*Adamts4*, *Adamts5*, *Mmp3*) and increase in the expression of anabolic genes (*Acan*, *Bgn*, *Dcn*, *Colla1*, *Col2a1*), with significant increases in matrix proteins detected in the IVD 6-hours post-vibration (McCann et al. 2013). We therefore sought to establish if repeated exposure to WBV would result in a net beneficial effect to the IVD and cartilaginous tissues of the knee joint. To our surprise, the current study demonstrates that 4 week exposure of 10-week-old wild-type mice to WBV leads to degeneration of the IVD. A recent study demonstrated that exposure of excised annular lamellae to vibration resulted in alterations in the deformation magnitude of the tissue, which the authors postulate was caused by damage to the intra-lamellar matrix (Gregory and Callaghan 2012). Our findings are in keeping with the characterized effects of dynamic loading on the IVD, which has been shown to increase AF degeneration (Walsh and Lotz 2004), and promote cell apoptosis associated with the progression of degeneration (Lotz and Chin 2000).

In the present study, changes in the histological appearance of the IVD induced by WBV were accompanied by increased MMP activity, as evidenced by the accumulation of matrix degradation fragments and increased expression of *Mmp3*. Interestingly, single nucleotide polymorphisms of the *MMP3* locus are associated with degenerative lumbar

spinal stenosis (Omair et al. 2013), correlate with the radiographic progression of lumbar disc degeneration (Omair et al. 2013), and confer an increased risk for disc degeneration following occupational exposure to vibration (Yuan et al. 2010). Our previous work demonstrated a transient decrease in *Mmp3* expression in the IVD following acute exposure to vibration (McCann et al. 2013), in keeping with data demonstrating a similar decrease in *MMP3* expression by AF cells following acute exposure to cyclic tensile strain (Gilbert et al. 2011). Taken together, these findings suggest that MMPs are regulated by mechanosensitive pathways in IVD tissues, dependent upon parameters of mechanical stimulation such as the cumulative exposure to the applied load.

In the synovial joint of the knee, we detected meniscal damage and focal articular cartilage erosion in the medial joint compartment after 4 weeks of WBV, damage that resembles osteoarthritis. These results were surprising given the young age of the mice, since spontaneous osteoarthritis has been reported to present between 17-20 months of age in mice (Wilhelmi and Faust 1976). We noted increased MMP-mediated extracellular matrix degradation within the joint tissues following 4 weeks of WBV, accompanied by increased *Mmp13* expression. We also noted increased *Col2a1* expression in the articular cartilage after 4 weeks WBV, a change that has been associated with the osteoarthritis phenotype *in vivo* (Brew et al. 2010). Although *SOX9* expression is typically downregulated in cartilage during late stage osteoarthritis (Brew et al. 2010), mechanical loading has been shown to both induce *SOX9* and type-II collagen in cells of the meniscus (Kanazawa et al. 2012). These increases in *Sox9* and *Col2a1* expression may represent cellular attempts to maintain cartilage integrity that are ultimately unsuccessful because of the overwhelming induction of catabolic factors.

As with the IVD, there are surprisingly few studies aimed at assessing the effect of WBV on synovial joints such as the knee. Recent studies in rodent models examined the effects of WBV on articular cartilage in a model of osteoporosis induced by prednisolone (Musumeci et al. 2013) and a surgical model of osteoarthritis (Qin et al. 2014); however in both studies cartilage was not examined in animals subjected to WBV alone. Our findings are consistent with the later study, which reported increased cartilage degradation and functional deterioration of osteoarthritis-affected joints following WBV (Qin et al. 2014). While the extensive damage to the knee joint caused by WBV in our mouse model was unexpected, several mechanisms may underlie the observed changes. First, we noted that WBV-induced meniscus damage preceded damage to the articular surface, suggesting that destabilization of the joint may contribute to cartilage degeneration. While mechanisms responsible for initiation of meniscal damage are yet unknown, removal or damage to the meniscus is known to increase focal point stress on the articular cartilage surface of the tibial plateau (Kurosawa et al. 1980), a pattern that mirrors focal damage induced by WBV in our study. In fact, surgical destabilization of the medial meniscus is routinely used to induce an osteoarthritis-like pathology in animal models (Welch et al. 2009). Alternatively, articular cartilage damage may result from changes to the subchondral bone resulting from repeated exposure to WBV. Increased mechanical load on the articular surface has been shown to increase subchondral bone thickness (Hwang et al. 2008), thereby altering joint biomechanics leading to increased loading of the articular surface (Anderson-MacKenzie et al. 2005) and altering cartilage biology by regulating the activity and availability of growth factors and cytokines within the tissue, promoting osteoarthritis progression (Burr and Gallant

2012). The cellular pathways responsible for the initiation of tissue degradation in response to WBV in the meniscus and articular cartilage require further examination.

Taken together, the current study demonstrates that repeated exposure to WBV leads to degeneration of both the intervertebral discs and knee joints in a mouse model. These findings raise concern due to the clinical use of these platforms for the treatment of various conditions, as well as the increasing use of vibration platforms by the general population in daily exercise regimens. Further studies are required to determine if WBV is safe effective for the treatment of human conditions and to specifically address potential negative effects on joint health.

6.7 References

- Anderson-MacKenzie JM, Quasnicka HL, Starr RL, Lewis EJ, Billingham ME, Bailey AJ. 2005. Fundamental subchondral bone changes in spontaneous knee osteoarthritis. *The international journal of biochemistry & cell biology* **37**: 224-236.
- Belavy DL, Armbrecht G, Gast U, Richardson CA, Hides JA, Felsenberg D. 2010. Countermeasures against lumbar spine deconditioning in prolonged bed rest: resistive exercise with and without whole body vibration. *J Appl Physiol* **109**: 1801-1811.
- Belavy DL, Hides JA, Wilson SJ, Stanton W, Dimeo FC, Rittweger J, Felsenberg D, Richardson CA. 2008. Resistive simulated weightbearing exercise with whole body vibration reduces lumbar spine deconditioning in bed-rest. *Spine (Phila Pa 1976)* **33**: E121-131.
- Billingham RC, Dahlberg L, Ionescu M, Reiner A, Bourne R, Rorabeck C, Mitchell P, Hambor J, Diekmann O, Tschesche H et al. 1997. Enhanced cleavage of type II collagen by collagenases in osteoarthritic articular cartilage. *J Clin Invest* **99**: 1534-1545.

- Brew CJ, Clegg PD, Boot-Handford RP, Andrew JG, Hardingham T. 2010. Gene expression in human chondrocytes in late osteoarthritis is changed in both fibrillated and intact cartilage without evidence of generalised chondrocyte hypertrophy. *Ann Rheum Dis* **69**: 234-240.
- Burr DB, Gallant MA. 2012. Bone remodelling in osteoarthritis. *Nature reviews Rheumatology* **8**: 665-673.
- Claerbout M, Gebara B, Ilsbrouckx S, Verschueren S, Peers K, Van Asch P, Feys P. 2012. Effects of 3 weeks' whole body vibration training on muscle strength and functional mobility in hospitalized persons with multiple sclerosis. *Mult Scler* **18**: 498-505.
- del Pozo-Cruz B, Hernandez Mocholi MA, Adsuar JC, Parraca JA, Muro I, Gusi N. 2011. Effects of whole body vibration therapy on main outcome measures for chronic non-specific low back pain: a single-blind randomized controlled trial. *J Rehabil Med* **43**: 689-694.
- Funakoshi M, Taoda K, Tsujimura H, Nishiyama K. 2004. Measurement of whole-body vibration in taxi drivers. *J Occup Health* **46**: 119-124.
- Gilbert HT, Hoyland JA, Freemont AJ, Millward-Sadler SJ. 2011. The involvement of interleukin-1 and interleukin-4 in the response of human annulus fibrosus cells to cyclic tensile strain: an altered mechanotransduction pathway with degeneration. *Arthritis Res Ther* **13**: R8.
- Gregory DE, Callaghan JP. 2012. An examination of the mechanical properties of the annulus fibrosus: the effect of vibration on the intra-lamellar matrix strength. *Medical engineering & physics* **34**: 472-477.
- Herrero AJ, Menendez H, Gil L, Martin J, Martin T, Garcia-Lopez D, Gil-Agudo A, Marin PJ. 2011. Effects of whole-body vibration on blood flow and neuromuscular activity in spinal cord injury. *Spinal cord* **49**: 554-559.
- Holguin N, Judex S. 2010. Rat intervertebral disc health during hindlimb unloading: brief ambulation with or without vibration. *Aviat Space Environ Med* **81**: 1078-1084.
- Holguin N, Martin JT, Elliott DM, Judex S. 2013. Low-intensity vibrations partially maintain intervertebral disc mechanics and spinal muscle area during deconditioning. *Spine J* **13**: 428-436.
- Holguin N, Muir J, Rubin C, Judex S. 2009. Short applications of very low-magnitude vibrations attenuate expansion of the intervertebral disc during extended bed rest. *Spine J* **9**: 470-477.
- Hou WW, Zhu ZL, Zhou Y, Zhang CX, Yu HY. 2011. Involvement of Wnt activation in the micromechanical vibration-enhanced osteogenic response of osteoblasts.

Journal of orthopaedic science : official journal of the Japanese Orthopaedic Association **16**: 598-605.

- Hwang J, Bae WC, Shieu W, Lewis CW, Bugbee WD, Sah RL. 2008. Increased hydraulic conductance of human articular cartilage and subchondral bone plate with progression of osteoarthritis. *Arthritis Rheum* **58**: 3831-3842.
- Iwamoto J, Takeda T, Sato Y, Uzawa M. 2005. Effect of whole-body vibration exercise on lumbar bone mineral density, bone turnover, and chronic back pain in post-menopausal osteoporotic women treated with alendronate. *Aging Clin Exp Res* **17**: 157-163.
- Kanazawa T, Furumatsu T, Hachioji M, Oohashi T, Ninomiya Y, Ozaki T. 2012. Mechanical stretch enhances COL2A1 expression on chromatin by inducing SOX9 nuclear translocalization in inner meniscus cells. *J Orthop Res* **30**: 468-474.
- Kartha S, Zeeman ME, Baig HA, Guarino BB, Winkelstein BA. 2014. Upregulation of BDNF & NGF in Cervical Intervertebral Discs Exposed to Painful Whole Body Vibration. *Spine (Phila Pa 1976)*.
- Kurosawa H, Fukubayashi T, Nakajima H. 1980. Load-bearing mode of the knee joint: physical behavior of the knee joint with or without menisci. *Clin Orthop Relat Res*: 283-290.
- Liphardt AM, Mundermann A, Koo S, Backer N, Andriacchi TP, Zange J, Mester J, Heer M. 2009. Vibration training intervention to maintain cartilage thickness and serum concentrations of cartilage oligometric matrix protein (COMP) during immobilization. *Osteoarthritis Cartilage* **17**: 1598-1603.
- Lotz JC, Chin JR. 2000. Intervertebral disc cell death is dependent on the magnitude and duration of spinal loading. *Spine (Phila Pa 1976)* **25**: 1477-1483.
- Matsumoto Y, Griffin MJ. 2002. Non-linear characteristics in the dynamic responses of seated subjects exposed to vertical whole-body vibration. *J Biomech Eng* **124**: 527-532.
- McCann MR, Patel P, Beaucage KL, Xiao Y, Bacher C, Siqueira WL, Holdsworth DW, Dixon SJ, Seguin CA. 2013. Acute vibration induces transient expression of anabolic genes in the murine intervertebral disc. *Arthritis Rheum* **65**: 1853-1864.
- Muir J, Kiel DP, Rubin CT. 2013. Safety and severity of accelerations delivered from whole body vibration exercise devices to standing adults. *Journal of science and medicine in sport / Sports Medicine Australia* **16**: 526-531.
- Musumeci G, Loreto C, Leonardi R, Castorina S, Giunta S, Carnazza ML, Trovato FM, Pichler K, Weinberg AM. 2013. The effects of physical activity on apoptosis and

- lubricin expression in articular cartilage in rats with glucocorticoid-induced osteoporosis. *J Bone Miner Metab* **31**: 274-284.
- Omair A, Holden M, Lie BA, Reikeras O, Brox JI. 2013. Treatment outcome of chronic low back pain and radiographic lumbar disc degeneration are associated with inflammatory and matrix degrading gene variants: a prospective genetic association study. *BMC Musculoskelet Disord* **14**: 105.
- Oxlund BS, Ortoft G, Andreassen TT, Oxlund H. 2003. Low-intensity, high-frequency vibration appears to prevent the decrease in strength of the femur and tibia associated with ovariectomy of adult rats. *Bone* **32**: 69-77.
- Pang MY, Lau RW, Yip SP. 2013. The effects of whole-body vibration therapy on bone turnover, muscle strength, motor function, and spasticity in chronic stroke: a randomized controlled trial. *European journal of physical and rehabilitation medicine* **49**: 439-450.
- Park YG, Kwon BS, Park JW, Cha DY, Nam KY, Sim KB, Chang J, Lee HJ. 2013. Therapeutic effect of whole body vibration on chronic knee osteoarthritis. *Annals of rehabilitation medicine* **37**: 505-515.
- Pasqualini M, Lavet C, Elbadaoui M, Vanden-Bossche A, Laroche N, Gnyubkin V, Vico L. 2013. Skeletal site-specific effects of whole body vibration in mature rats: from deleterious to beneficial frequency-dependent effects. *Bone* **55**: 69-77.
- Perraton L, Machotka Z, Kumar S. 2010. Whole-body vibration to treat low back pain: fact or fad? *Physiother Can* **63**: 88-93.
- Pest MA, Russell BA, Zhang YW, Jeong JW, Beier F. 2014. Loss of mitogen-Inducible gene 6 results in disturbed cartilage and joint homeostasis. *Arthritis & rheumatology*.
- Qin J, Chow SK, Guo A, Wong WN, Leung KS, Cheung WH. 2014. Low magnitude high frequency vibration accelerated cartilage degeneration but improved epiphyseal bone formation in anterior cruciate ligament transect induced osteoarthritis rat model. *Osteoarthritis Cartilage* **22**: 1061-1067.
- Rittweger J, Just K, Kautzsch K, Reeg P, Felsenberg D. 2002. Treatment of chronic lower back pain with lumbar extension and whole-body vibration exercise: a randomized controlled trial. *Spine (Phila Pa 1976)* **27**: 1829-1834.
- Rubin C, Pope M, Fritton JC, Magnusson M, Hansson T, McLeod K. 2003. Transmissibility of 15-hertz to 35-hertz vibrations to the human hip and lumbar spine: determining the physiologic feasibility of delivering low-level anabolic mechanical stimuli to skeletal regions at greatest risk of fracture because of osteoporosis. *Spine (Phila Pa 1976)* **28**: 2621-2627.

- Rubin C, Recker R, Cullen D, Ryaby J, McCabe J, McLeod K. 2004. Prevention of postmenopausal bone loss by a low-magnitude, high-frequency mechanical stimuli: a clinical trial assessing compliance, efficacy, and safety. *J Bone Miner Res* **19**: 343-351.
- Salmon JR, Roper JA, Tillman MD. 2012. Does acute whole-body vibration training improve the physical performance of people with knee osteoarthritis? *Journal of strength and conditioning research / National Strength & Conditioning Association* **26**: 2983-2989.
- Slatkovska L, Alibhai SM, Beyene J, Hu H, Demaras A, Cheung AM. 2011. Effect of 12 months of whole-body vibration therapy on bone density and structure in postmenopausal women: a randomized trial. *Annals of internal medicine* **155**: 668-679, W205.
- Sztrolovics R, Alini M, Roughley PJ, Mort JS. 1997. Aggrecan degradation in human intervertebral disc and articular cartilage. *Biochem J* **326 (Pt 1)**: 235-241.
- Thompson JP, Pearce RH, Schechter MT, Adams ME, Tsang IK, Bishop PB. 1990. Preliminary evaluation of a scheme for grading the gross morphology of the human intervertebral disc. *Spine (Phila Pa 1976)* **15**: 411-415.
- Torcasio A, van Lenthe GH, Van Oosterwyck H. 2008. The importance of loading frequency, rate and vibration for enhancing bone adaptation and implant osseointegration. *Eur Cell Mater* **16**: 56-68.
- Ulici V, Hoenselaar KD, Agoston H, McErlain DD, Umoh J, Chakrabarti S, Holdsworth DW, Beier F. 2009. The role of Akt1 in terminal stages of endochondral bone formation: angiogenesis and ossification. *Bone* **45**: 1133-1145.
- Verschueren SM, Roelants M, Delecluse C, Swinnen S, Vanderschueren D, Boonen S. 2004. Effect of 6-month whole body vibration training on hip density, muscle strength, and postural control in postmenopausal women: a randomized controlled pilot study. *J Bone Miner Res* **19**: 352-359.
- Walsh AJ, Lotz JC. 2004. Biological response of the intervertebral disc to dynamic loading. *J Biomech* **37**: 329-337.
- Welch ID, Cowan MF, Beier F, Underhill TM. 2009. The retinoic acid binding protein CRABP2 is increased in murine models of degenerative joint disease. *Arthritis Res Ther* **11**: R14.
- Wenger KH, Freeman JD, Fulzele S, Immel DM, Powell BD, Molitor P, Chao YJ, Gao HS, Elsalanty M, Hamrick MW et al. 2010. Effect of whole-body vibration on bone properties in aging mice. *Bone* **47**: 746-755.

- Wilhelmi G, Faust R. 1976. Suitability of the C57 black mouse as an experimental animal for the study of skeletal changes due to ageing, with special reference to osteoarthrosis and its response to tribenoside. *Pharmacology* **14**: 289-296.
- Yuan HY, Tang Y, Liang YX, Lei L, Xiao GB, Wang S, Xia ZL. 2010. Matrix metalloproteinase-3 and vitamin d receptor genetic polymorphisms, and their interactions with occupational exposure in lumbar disc degeneration. *Journal of occupational health* **52**: 23-30.

APPENDIX A

Gene tables from Chapter 2

Table 3.1: Fold change in expression of genes known to be enriched in the early node notochord (E8.0) in the aged (6 month) lumbar nucleus pulposus relative to the young (2.5 month) lumbar nucleus pulposus tissues

Gene Symbol	Fold Change	p-value
1600029D21Rik	1.0345	0.8266
1700007G11Rik	-1.0586	0.1825
1700009P17Rik	-1.4778	0.1822
1700027A23Rik	-1.1883	0.0530
2410066E13Rik	-1.0038	0.9898
Adcy8	-1.1933	0.1497
Alcam	1.2957	0.1162
Anxa4	1.6024	0.1323
Arhgef16	1.4290	0.1250
Atp9a	1.2998	0.3226
Bicc1	1.0344	0.7623
Bmp7	2.5075	0.0423
Btg1	-1.3442	0.0784
Calca	1.0908	0.3621
Capsl	-1.7532	0.1458
Car3	1.1682	0.5542
Cdo1	1.2999	0.5717
Cfc1	1.0307	0.8633
Chl1	-1.0565	0.3954
Chrd	1.1226	0.4531
Clu	1.3647	0.3018
Cobl	1.0447	0.6704
Col9a3	1.1515	0.1928
Ctgf	1.0742	0.8460
Cthrc1	1.0454	0.0903
Cyb561	1.0165	0.9013
Dand5	1.1991	0.3467
Ddo	-1.1332	0.5840
Dmgdh	1.0515	0.7004
Dnahc11	-1.1734	0.4445
Dnahc5	1.0059	0.9572
Dpyd	-1.1834	0.0700
Dync2li1	1.1577	0.5266
Dynlrb2	-1.2370	0.2811
Epha2	-1.1787	0.2845
F5	-1.8169	0.4054
Flrt3	-1.1189	0.6475
Foxa1	-1.1044	0.5065

Foxa2	1.3505	0.0014
Foxd1	1.1773	0.4771
Foxd4	1.0066	0.9607
Foxj1	-1.4343	0.2621
Furin	-1.2854	0.0381
Gal	1.3152	0.0668
Gdf3	1.1244	0.3687
Glis3	-1.0275	0.8828
Gsc	-1.1549	0.1626
Gsn	1.0886	0.6386
Gstm5	1.3670	0.2543
Hdc	-1.4959	0.5298
Htra1	-1.1357	0.4550
Ift57	1.3148	0.2616
Ift88	1.1720	0.3386
Igfbp5	-1.0652	0.8106
Josd2	1.0336	0.8094
Kbtbd4	1.2235	0.2035
Kdelr3	1.5551	0.2070
Klhl6	-1.5505	0.4144
Krt19	1.2375	0.3959
Lhx1	1.0615	0.6561
Lypd6b	-1.6798	0.0948
Mlf1	-1.1460	0.1840
Mmp15	1.0871	0.5407
Mnx1	1.0874	0.2226
Moxd1	1.0690	0.8209
Nav3	-1.3115	0.4497
Ndrgr1	1.1526	0.5263
Nodal	-1.0139	0.9254
Nog	1.1455	0.4686
Noto	1.0431	0.8244
Nphp3	1.0838	0.7042
Pim1	1.1084	0.3320
Pkd11l	1.0852	0.4227
Prickle2	-1.0874	0.3677
Prnd	1.0969	0.5878
Prox1	-1.0561	0.5117
Rassf9	-1.0309	0.8619
Rfx3	1.3983	0.0978
Ripk4	1.0226	0.8618
Scara3	-1.0599	0.7288
Sepp1	-1.0823	0.6888

Shh	3.5134	0.0032
Six1	1.2534	0.3834
Slc39a8	1.0180	0.9651
Slit2	1.1883	0.2696
Smoc1	1.4866	0.1749
Sostdc1	1.0459	0.8513
Sp5	1.1040	0.3405
Spink3	-1.0175	0.8760
St8sia6	1.1849	0.3986
Sulf1	1.1628	0.0927
T	1.0389	0.6732
Tctn1	-1.0694	0.5778
Tgm2	1.7879	0.0568
Tmem176a	1.8183	0.1047
Tmem176b	1.9218	0.1466
Tmprss2	-1.2883	0.2232
Ttll6	-1.0653	0.7224
Upk3a	1.2183	0.1587
Vtn	1.0565	0.7557
Wif1	1.3498	0.2313
Wnt11	-1.0568	0.4377
Zic3	-1.1079	0.6361

Table 3.2: Fold change in expression of genes known to be enriched in the early node notochord (E8.0) in the degenerative (21 month) lumbar nucleus pulposus relative to the aged (6 month) lumbar nucleus pulposus tissues.

Gene Symbol	Fold-Change	p-value
1600029D21Rik	1.1520	0.3792
1700007G11Rik	-1.1814	0.0062
1700009P17Rik	1.7438	0.0786
1700027A23Rik	1.0629	0.4130
2410066E13Rik	-1.0371	0.9011
Adcy8	1.0406	0.7173
Alcam	1.1758	0.2887
Anxa4	-1.0416	0.8825
Arhgef16	-1.0429	0.8369
Atp9a	1.2659	0.3693
Bicc1	1.1573	0.2254
Bmp7	-1.1963	0.6199
Btg1	1.3113	0.0992
Calca	-1.1166	0.2591
Capsl	1.2717	0.4942
Car3	-1.3753	0.2507
Cdo1	1.0388	0.9334
Cfc1	-1.0524	0.7718
Chl1	1.0950	0.1856
Chrd	1.0447	0.7707
Clu	1.0901	0.7624
Cobl	1.1078	0.3390
Col9a3	1.0411	0.6851
Ctgf	1.3103	0.4747
Cthrc1	-1.0721	0.0217
Cyb561	-1.0483	0.7225
Dand5	-1.0304	0.8708
Ddo	1.1852	0.4629
Dmgdh	-1.2245	0.1608
Dnahc11	1.3697	0.1635
Dnahc5	-1.0894	0.4448
Dpyd	1.3492	0.0095
Dync2li1	1.1039	0.6654
Dynlrb2	1.2536	0.2556
Epha2	1.3908	0.0613
F5	-1.2108	0.7828
Flrt3	1.4166	0.1921
Foxa1	-1.0296	0.8422

Foxa2	-1.2596	0.0044
Foxd1	1.4452	0.1437
Foxd4	-1.1798	0.2466
Foxj1	1.4673	0.2370
Furin	1.2211	0.0766
Gal	-1.2937	0.0796
Gdf3	-1.2956	0.0809
Glis3	1.1659	0.4197
Gsc	-1.0582	0.5487
Gsn	1.8362	0.0160
Gstm5	1.0296	0.9090
Hdc	-1.1959	0.7764
Htra1	1.0846	0.6276
Ift57	1.1149	0.6365
Ift88	1.0537	0.7415
Igfbp5	1.6632	0.0974
Josd2	1.0124	0.9283
Kbtbd4	1.0826	0.5900
Kdelr3	-1.4529	0.2747
Klhl6	-1.2068	0.7186
Krt19	1.0484	0.8450
Lhx1	-1.1575	0.2986
Lypd6b	1.5490	0.1432
Mlf1	1.2239	0.0712
Mmp15	-1.1179	0.4210
Mnx1	1.0592	0.3834
Moxd1	1.1805	0.5787
Nav3	1.6967	0.1709
Ndrgr1	1.4093	0.1610
Nodal	-1.0496	0.7437
Nog	-1.2270	0.2908
Noto	1.0015	0.9937
Nphp3	1.1319	0.5628
Pim1	-1.1898	0.1295
Pkd11l	-1.0088	0.9292
Prickle2	-1.0110	0.9025
Prnd	-1.4649	0.0625
Prox1	1.0802	0.3642
Rassf9	-1.0147	0.9334
Rfx3	1.1727	0.3784
Ripk4	-1.0926	0.4996
Scara3	-1.0076	0.9640
Sepp1	-1.0084	0.9659

Shh	-3.2288	0.0043
Six1	-1.0303	0.9045
Slc39a8	1.0507	0.9038
Slit2	1.1953	0.2556
Smoc1	-1.1847	0.5293
Sostdc1	-1.3261	0.2695
Sp5	-1.1512	0.1941
Spink3	-1.0071	0.9490
St8sia6	-1.2461	0.2852
Sulf1	-1.1128	0.2015
T	-1.0663	0.4858
Tctn1	1.0581	0.6382
Tgm2	-1.2220	0.4336
Tmem176a	-1.5046	0.2342
Tmem176b	-1.4776	0.3518
Tmprss2	1.4055	0.1208
Ttll6	1.0120	0.9463
Upk3a	-1.1658	0.2548
Vtn	-1.2421	0.2513
Wif1	-1.3031	0.2830
Wnt11	1.0405	0.5711
Zic3	1.1667	0.4827

Table 3.3: Fold change in expression of genes known to be enriched in the early node notochord (E8.0) in the degenerative (21 month) lumbar nucleus pulposus relative to the mature (2.5 month) lumbar nucleus pulposus tissues.

Gene Symbol	Fold Change	p-value
1600029D21Rik	1.1917	0.2391
1700007G11Rik	-1.2507	0.0011
1700009P17Rik	1.1800	0.4961
1700027A23Rik	-1.1179	0.1280
2410066E13Rik	-1.0410	0.8782
Adcy8	-1.1467	0.2007
Alcam	1.5236	0.0183
Anxa4	1.5384	0.1259
Arhgef16	1.3701	0.1291
Atp9a	1.6454	0.0673
Bicc1	1.1971	0.1154
Bmp7	2.0959	0.0588
Btg1	-1.0252	0.8440
Calca	-1.0237	0.7750
Capsl	-1.3786	0.3212
Car3	-1.1773	0.4906
Cdo1	1.3504	0.4737
Cfc1	-1.0211	0.8943
Chl1	1.0364	0.5290
Chrd	1.1728	0.2656
Clu	1.4876	0.1611
Cobl	1.1573	0.1525
Col9a3	1.1989	0.0829
Ctgf	1.4075	0.3245
Cthrc1	-1.0256	0.2393
Cyb561	-1.0313	0.7949
Dand5	1.1638	0.3768
Ddo	1.0459	0.8240
Dmgdh	-1.1646	0.2249
Dnahc11	1.1673	0.4105
Dnahc5	-1.0831	0.4272
Dpyd	1.1401	0.1019
Dync2li1	1.2780	0.2588
Dynlrb2	1.0134	0.9360
Epha2	1.1800	0.2354
F5	-2.1998	0.2377
Flrt3	1.2661	0.3053
Foxa1	-1.1371	0.3485

Foxa2	1.0721	0.1580
Foxd1	1.7014	0.0382
Foxd4	-1.1722	0.2180
Foxj1	1.0230	0.9326
Furin	-1.0526	0.5509
Gal	1.0166	0.8817
Gdf3	-1.1523	0.2393
Glis3	1.1347	0.4551
Gsc	-1.2221	0.0513
Gsn	1.9989	0.0061
Gstm5	1.4075	0.1764
Hdc	-1.7890	0.3256
Htra1	-1.0472	0.7564
Ift57	1.4659	0.1051
Ift88	1.2349	0.1766
Igfbp5	1.5615	0.1027
Josd2	1.0463	0.7125
Kbtbd4	1.3246	0.0717
Kdelr3	1.0703	0.8130
Klhl6	-1.8711	0.2146
Krt19	1.2974	0.2606
Lhx1	-1.0904	0.4775
Lypd6b	-1.0845	0.7339
Myf1	1.0679	0.4440
Mmp15	-1.0284	0.8155
Mnx1	1.1517	0.0468
Moxd1	1.2620	0.3949
Nav3	1.2938	0.4238
Ndr1	1.6244	0.0483
Nodal	-1.0641	0.6406
Nog	-1.0712	0.6759
Noto	1.0447	0.7974
Nphp3	1.2268	0.3051
Pim1	-1.0735	0.4458
Pkd11l1	1.0757	0.4235
Prickle2	-1.0993	0.2663
Prnd	-1.3355	0.0989
Prox1	1.0228	0.7574
Rassf9	-1.0460	0.7741
Rfx3	1.6398	0.0203
Ripk4	-1.0685	0.5696
Scara3	-1.0679	0.6628
Sepp1	-1.0914	0.6220

Shh	1.0882	0.7070
Six1	1.2166	0.3966
Slc39a8	1.0696	0.8542
Slit2	1.4204	0.0370
Smoc1	1.2548	0.3582
Sostdc1	-1.2679	0.2957
Sp5	-1.0428	0.6390
Spink3	-1.0247	0.8061
St8sia6	-1.0517	0.7718
Sulf1	1.0450	0.5289
T	-1.0263	0.7472
Tctn1	-1.0107	0.9198
Tgm2	1.4630	0.1308
Tmem176a	1.2085	0.5146
Tmem176b	1.3006	0.4747
Tmprss2	1.0909	0.6163
Ttll6	-1.0527	0.7468
Upk3a	1.0451	0.6967
Vtn	-1.1757	0.3285
Wif1	1.0358	0.8653
Wnt11	-1.0157	0.8015
Zic3	1.0531	0.7874

Table 3.4 Gene associated with extracellular matrix synthesis, regulation or catabolism. Gene expression results based on indicated relative fold-change.

Gene Symbol	Fold Change (6 relative to 2.5)		Fold Change (21 relative to 6)		Fold Change (21 relative to 2.5)	
		p-value		p-value		p-value
Acan	1.0222	0.8838	1.1759	0.3073	1.2019	0.2088
Adam1a	-1.0002	0.9979	1.0952	0.2013	1.0950	0.1616
Adam1b	-1.0091	0.9492	-1.0148	0.9178	-1.0240	0.8522
Adam2	-1.1329	0.1238	1.1253	0.1409	-1.0068	0.9147
Adam3	1.0718	0.7386	1.2459	0.3141	1.3354	0.1608
Adam4	1.5635	0.0507	-1.3815	0.1234	1.1317	0.4641
Adam5	-1.0481	0.1664	1.1061	0.0177	1.0553	0.0926
Adam6a	1.0664	0.3631	-1.0158	0.8169	1.0498	0.4365
Adam6b	-1.0924	0.1095	1.0002	0.9960	-1.0921	0.0824
Adam7	-1.0488	0.4725	-1.0272	0.6798	-1.0774	0.2326
Adam8	-1.7903	0.4538	1.0321	0.9666	-1.7346	0.4299
Adam9	-1.2918	0.2593	1.4801	0.1089	1.1458	0.4837
Adam10	-1.2889	0.1902	1.1993	0.3275	-1.0747	0.6508
Adam11	1.2374	0.1708	-1.2411	0.1659	-1.0030	0.9810
Adam12	-1.0282	0.5737	1.0017	0.9719	-1.0264	0.5556
Adam15	1.0723	0.4137	-1.2124	0.0574	-1.1306	0.1403
Adam15	-1.1113	0.3775	1.1320	0.3070	1.0186	0.8576
Adam17	-1.3793	0.0201	1.3656	0.0225	-1.0101	0.9115
Adam18	-1.0988	0.3738	1.0865	0.4292	-1.0113	0.9014
Adam19	-1.1122	0.1571	1.1725	0.0552	1.0542	0.3982
Adam19	-1.4373	0.3671	-1.0257	0.9473	-1.4743	0.2889
Adam21	-1.0378	0.7663	-1.0461	0.7185	-1.0855	0.4721
Adam22	-1.1117	0.2070	1.1698	0.0846	1.0523	0.4709
Adam23	1.0775	0.3665	1.0810	0.3481	1.1647	0.0727
Adam24	-1.1333	0.5017	1.0417	0.8224	-1.0879	0.6094
Adam25	-1.2292	0.1102	1.3755	0.0303	1.1190	0.2905
Adam26a	-1.1714	0.4230	1.1565	0.4593	-1.0129	0.9399
Adam26b	-1.1688	0.4056	1.2156	0.3073	1.0401	0.8083
Adam28	1.0870	0.4814	-1.2473	0.1001	-1.1475	0.2200
Adam29	1.0193	0.8336	-1.0152	0.8683	1.0040	0.9603
Adam30	-1.0237	0.6994	-1.0737	0.2692	-1.0992	0.1241
Adam32	1.0998	0.5573	1.0605	0.7141	1.1663	0.3074
Adam33	-1.1276	0.3390	1.0076	0.9495	-1.1191	0.3187
Adam34	-1.5141	0.2347	1.1777	0.6171	-1.2857	0.4022
Adam39	-1.0261	0.8149	-1.0700	0.5451	-1.0979	0.3627
Adamdec1	1.0311	0.5677	-1.1330	0.0551	-1.0988	0.0896

Adamts1	1.1123	0.4405	1.1082	0.4555	1.2326	0.1251
Adamts2	1.1079	0.5652	1.3488	0.1323	1.4943	0.0429
Adamts3	1.0468	0.5187	-1.1497	0.0879	-1.0983	0.1725
Adamts4	-1.0461	0.7515	-1.3862	0.0597	-1.4501	0.0273
Adamts5	-1.4995	0.2913	1.6352	0.2117	1.0905	0.7893
Adamts6	-1.2399	0.2772	1.1400	0.4910	-1.0876	0.6172
Adamts7	-1.1810	0.6214	-1.1928	0.6013	-1.4087	0.2799
Adamts8	1.0555	0.3240	-1.1017	0.1073	-1.0437	0.3774
Adamts8	1.0585	0.7228	1.0424	0.7952	1.1033	0.5005
Adamts9	1.0594	0.6532	-1.2066	0.1810	-1.1389	0.2829
Adamts10	-1.3166	0.1929	1.0187	0.9231	-1.2924	0.1776
Adamts12	-1.2067	0.4944	-1.0415	0.8797	-1.2567	0.3625
Adamts13	1.1909	0.2429	-1.0495	0.7293	1.1348	0.3332
Adamts14	1.0996	0.0812	-1.2017	0.0083	-1.0929	0.0716
Adamts14	-1.1491	0.4100	-1.0532	0.7513	-1.2102	0.2264
Adamts15	-1.0522	0.3144	-1.1132	0.0650	-1.1712	0.0116
Adamts16	1.1173	0.5019	-1.3534	0.1055	-1.2113	0.2211
Adamts17	-1.1918	0.2059	-1.0073	0.9545	-1.2005	0.1515
Adamts18	-1.0590	0.5171	-1.1117	0.2548	-1.1773	0.0775
Adamts19	1.0662	0.4132	1.0141	0.8535	1.0811	0.2787
Adamts20	-1.5915	0.0229	-1.0295	0.8472	-1.6385	0.0120
Adamtsl1	-1.3828	0.1349	1.9912	0.0128	1.4400	0.0751
Adamtsl2	1.0002	0.9982	1.0108	0.9127	1.0110	0.9005
Adamtsl3	-1.1582	0.0632	1.0308	0.6440	-1.1236	0.0886
Adamtsl4	-1.0881	0.3357	-1.1584	0.1227	-1.2604	0.0223
Adamtsl5	1.1954	0.2929	1.3201	0.1271	1.5780	0.0202
Bgn	-1.0610	0.8419	1.0904	0.7710	1.0278	0.9177
Col1a1	1.0206	0.8886	-1.0182	0.9014	1.0024	0.9856
Col1a2	-1.0517	0.7190	-1.0854	0.5630	-1.1415	0.3144
Col1a2	-1.0517	0.8149	-1.1230	0.5948	-1.1810	0.4042
Col2a1	-1.0670	0.6996	1.0210	0.9007	-1.0450	0.7688
Col3a1	-1.2028	0.3519	1.0105	0.9560	-1.1903	0.3285
Col4a1	1.2162	0.1445	-1.1064	0.4129	1.0993	0.3931
Col4a2	-1.0024	0.9787	-1.1199	0.2495	-1.1226	0.1970
Col4a3	-1.1169	0.4611	1.0006	0.9966	-1.1162	0.4156
Col4a3bp	-1.0341	0.7749	1.3627	0.0386	1.3178	0.0390
Col4a4	1.0596	0.6820	1.0280	0.8441	1.0893	0.5053
Col4a5	1.2240	0.1669	-1.1869	0.2289	1.0313	0.7942
Col4a6	-1.0642	0.3827	-1.0070	0.9188	-1.0717	0.2877
Col5a1	1.0536	0.6487	-1.2160	0.1296	-1.1541	0.1975
Col5a1	-1.0770	0.6408	1.0285	0.8583	-1.0471	0.7444
Col5a2	1.0125	0.9013	-1.0735	0.4888	-1.0603	0.5214
Col5a3	1.0504	0.7891	-1.0058	0.9746	1.0443	0.7921

Col6a1	1.8673	0.0096	-1.3194	0.1303	1.4153	0.0523
Col6a1	1.5852	0.2575	-1.3096	0.4882	1.2105	0.5795
Col6a1	-1.0125	0.9344	-1.0185	0.9036	-1.0313	0.8205
Col6a2	1.1775	0.3733	-1.0342	0.8483	1.1385	0.4254
Col6a3	-1.1464	0.4136	1.1484	0.4081	1.0017	0.9904
Col6a4	1.0556	0.6121	-1.0793	0.4807	-1.0224	0.8146
Col6a5	1.3559	0.1246	-1.5420	0.0470	-1.1372	0.4239
Col6a6	1.0396	0.7072	-1.1405	0.2361	-1.0970	0.3375
Col7a1	1.0433	0.7288	-1.1857	0.2008	-1.1365	0.2711
Col8a1	-1.0974	0.7385	1.0014	0.9959	-1.0959	0.7136
Col8a2	1.0385	0.8350	-1.3085	0.1794	-1.2600	0.1940
Col9a1	1.2701	0.0923	-1.0856	0.5074	1.1700	0.1876
Col9a2	1.0711	0.6344	-1.1141	0.4622	-1.0402	0.7589
Col9a3	1.1515	0.1928	1.0411	0.6851	1.1989	0.0829
Col10a1	-1.0998	0.6911	1.1919	0.4722	1.0838	0.7069
Col11a1	1.3431	0.2648	-1.2147	0.4456	1.1058	0.6526
Col11a2	1.2015	0.1741	1.0844	0.5158	1.3028	0.0511
Col12a1	1.1900	0.4427	1.0706	0.7572	1.2740	0.2513
Col13a1	1.0652	0.6774	-1.1993	0.2600	-1.1259	0.3968
Col14a1	-1.1961	0.3745	-1.0923	0.6511	-1.3066	0.1647
Col15a1	1.6842	0.0055	-1.1396	0.2952	1.4778	0.0113
Col16a1	1.1198	0.1902	1.0237	0.7665	1.1463	0.0963
Col17a1	1.0198	0.8585	1.1365	0.2743	1.1590	0.1745
Col18a1	1.0877	0.5155	-1.2098	0.1739	-1.1123	0.3678
Col19a1	1.0465	0.5089	-1.1521	0.0775	-1.1009	0.1532
Col20a1	1.3676	0.0172	-1.4079	0.0123	-1.0295	0.7312
Col22a1	1.1125	0.3516	-1.0588	0.6057	1.0507	0.6171
Col23a1	1.0108	0.8514	-1.0262	0.6546	-1.0152	0.7685
Col24a1	-1.1666	0.0998	-1.0485	0.5624	-1.2232	0.0320
Col25a1	1.0289	0.7644	-1.0624	0.5307	-1.0326	0.7066
Col27a1	1.0765	0.4724	1.0819	0.4446	1.1647	0.1325
Col28a1	-1.1195	0.3645	1.0390	0.7495	-1.0776	0.4939
Comp	-1.1381	0.6404	1.7030	0.0963	1.4963	0.1441
Dcn	-2.4427	0.2565	2.8153	0.1979	1.1525	0.8290
Mmp1a	1.0697	0.3485	-1.1695	0.0613	-1.0933	0.1862
Mmp1b	-1.1724	0.2410	1.0690	0.6012	-1.0968	0.4274
Mmp2	-1.1342	0.5231	1.2167	0.3340	1.0727	0.6868
Mmp3	-1.1448	0.3576	1.3312	0.0850	1.1628	0.2622
Mmp7	-1.0730	0.3303	1.0515	0.4772	-1.0205	0.7429
Mmp7	-1.0197	0.8939	1.0461	0.7585	1.0259	0.8448
Mmp8	1.3269	0.8245	-1.5210	0.7432	-1.1463	0.9046
Mmp9	-1.5689	0.6788	-1.1951	0.8688	-1.8751	0.5235
Mmp10	-1.1819	0.2047	-1.1107	0.4019	-1.3128	0.0452

Mmp11	1.1708	0.0789	1.1197	0.1752	1.3109	0.0083
Mmp11	1.0548	0.5552	-1.0077	0.9315	1.0468	0.5712
Mmp12	-1.1714	0.1726	-1.0773	0.4878	-1.2619	0.0474
Mmp13	-1.3149	0.4289	-1.0857	0.8064	-1.4275	0.2663
Mmp14	-1.3345	0.2537	1.2560	0.3552	-1.0625	0.7741
Mmp15	1.0871	0.5407	-1.1179	0.4210	-1.0284	0.8155
Mmp16	1.0301	0.6093	-1.1750	0.0316	-1.1406	0.0428
Mmp17	1.0999	0.4528	-1.0290	0.8166	1.0689	0.5525
Mmp19	1.2334	0.0280	1.2584	0.0202	1.5521	0.0008
Mmp20	1.0219	0.8525	-1.0988	0.4338	-1.0752	0.4969
Mmp21	-1.0868	0.3964	-1.1125	0.2886	-1.2091	0.0645
Mmp23	-1.0089	0.9606	-1.2335	0.2716	-1.2444	0.2096
Mmp24	-1.0888	0.4126	-1.0934	0.3916	-1.1905	0.0960
Mmp24	-1.1360	0.2890	-1.0306	0.7906	-1.1707	0.1622
Mmp25	-1.5532	0.5101	-1.1098	0.8734	-1.7237	0.3721
Mmp27	-1.0414	0.7337	-1.1082	0.4042	-1.1540	0.2147
Mmp28	1.1509	0.5506	-1.0131	0.9552	1.1360	0.5449
Sox5	1.4580	0.0994	-1.0516	0.7983	1.3864	0.1077
Sox6	1.2295	0.2383	1.2044	0.2820	1.4808	0.0361
Sox9	1.0434	0.8285	-1.3340	0.1819	-1.2786	0.1996
Sparc	-1.0182	0.8046	1.1042	0.2105	1.0845	0.2460
Timp1	1.2225	0.5984	-1.0037	0.9921	1.2179	0.5645
Timp2	1.0654	0.6520	1.0029	0.9832	1.0685	0.5993
Timp3	1.3193	0.2894	1.0997	0.7014	1.4508	0.1355
Timp4	1.6351	0.0762	1.2288	0.3931	2.0092	0.0166
Vcan	1.1246	0.8094	1.1509	0.7731	1.2943	0.5596

APPENDIX B

Characterized Proteins from Chapter 4

Table 4.1: Proteins from the murine intervertebral disc that were unidentified or classified as preliminary according to Uniprot analysis.

List of identified proteins from a skeletally mature CD-1 mouse IVD that were not annotated within the database at the time of analysis or that were considered putative uncharacterized (578), as well as any proteins that were derived from Ensembl automatic analysis pipeline and were therefore considered preliminary (396 proteins).

Uniprot Accession No.	Protein Name	% Coverage	No. Different Peptides
A2AAU3	Probable helicase with zinc finger domain	88.89	2
E9QM04	Fc receptor-like protein 6	77.78	2
D3Z184	Ropporin-1	68.85	3
E9Q7C4	Proline rich 14-like	68.85	3
A2AJH3	Glycylpeptide N-tetradecanoyltransferase 2	68.69	3
D3YTR0	Adenomatous polyposis coli protein 2	65.82	2
E9PZH6	WW domain-containing adapter protein with coiled-coil	65.82	2
E9PZ84	Tetratricopeptide repeat protein 16	60.86	2
D6Q0F7	Cytoplasmic dynein intermediate chain 2 isoform 2.5	57.01	2
D3YTN4	GTPase IMAP family member 4	53.62	4
E9PZ97	Bloom syndrome protein homolog	53.62	3
B1AQ57	Copper-transporting ATPase 2	48.82	2
D3YTR2	Receptor expression-enhancing protein 6	46.10	4
E9PZJ8	Activating signal cointegrator 1 complex subunit 3	46.10	2
E0CXJ6	Tubulin-specific chaperone E	45.00	2
E9QMU1	Kinesin-like protein KIF7	45.00	2
D3YUE4	Family with sequence similarity 151, member B	41.51	3
E2QRQ3	Double-stranded RNA-binding protein Staufin homolog 2	40.25	2
E9QNR8	4930432K21Rik	40.25	2
B1B1B8	Phosphatase and actin regulator 1	39.07	2
D3YUX1	Pogo transposable element with ZNF domain	38.26	4
E9Q1E1	Trophinin	38.26	4
D3YTT4	Isobutyryl-CoA dehydrogenase, mitochondrial	35.46	4
E9PZS7	Olfactory receptor 287	35.46	4
E9Q8P0	Troponin C, slow skeletal and cardiac muscles	35.04	2
D3YYQ4	Carbonic anhydrase 1	34.29	3
E9Q4S3	Ninein	34.29	3

E9PYJ9	LIM domain-binding protein 3	34.09	2
D3YUE7	GRAM domain-containing protein 4	33.67	3
E9PZX1	Gm17384	33.43	7
D3YTT9	ZZ-type zinc finger-containing protein 3	32.88	6
E9PXF0	Protocadherin 17	29.89	2
D3YTU3	Mina	29.68	5
E9PZW8	Unconventional myosin-IXb	29.68	5
D6RFP6	Dual-specificity testis-specific protein kinase 1	27.83	2
E9QLK3	BRCA1-associated ATM activator 1	27.83	2
E9PV45	Ubiquitin carboxyl-terminal hydrolase	27.27	2
E9Q2N7	Interferon-induced guanylate-binding protein 2	26.19	3
E9PW85	Inactive serine/threonine-protein kinase VRK3	24.82	2
D3Z7R1	Pyridoxal kinase	24.75	2
D3Z5P0	Serine/threonine-protein kinase BRSK1	24.42	2
E9QAF1	Spata31d1c	24.42	2
E9PUV9	Caspase recruitment domain-containing protein 10	24.32	2
D3YWN6	Protein downstream neighbor of Son	24.11	3
D3YYS9	Acid-sensing ion channel 4	23.81	2
E9Q4Z5	Gm6729	23.81	2
D3YX57	Fanconi anemia group I protein homolog	23.47	3
E9Q3G8	Nucleoporin 153	23.47	3
D3YWA6	Serine/threonine-protein kinase 33	22.69	2
E9Q2Z1	Cat eye syndrome chromosome region, candidate 2	22.69	2
B1AUY3	Rho GTPase activating protein 4	22.45	2
E9PYB0	AHNAK nucleoprotein 2	22.02	2
D3Z3A9	Reticulocalbin-3	20.28	3
E9Q8I5	Zinc finger protein 108	20.28	3
E0CY73	1700112E06Rik	20.21	2
E9QN41	Striatin-interacting proteins 2	20.21	2
D3YWY5	Mth938 domain-containing protein	18.71	4
E9Q3D6	Heat shock protein HSP 90-beta	18.71	4
D3YTR7	Adenylyl cyclase-associated protein	18.63	3
E9PZM4	Chromodomain helicase DNA binding protein 2	18.63	2
D3Z5N5	1-phosphatidylinositol 3-phosphate 5-kinase	18.49	3
E9QAE4	Nsd1	18.49	3
E9QKK1	Centromere-associated protein E	17.74	2
E9Q072	Selection and upkeep of intraepithelial T-cells protein 5	17.67	9
D3Z678	Gm15448	17.50	2
E9Q7D5	Rho guanine nucleotide exchange factor (GEF) 5	17.23	2

D3YUF9	UDP-glucuronic acid decarboxylase 1	16.76	3
D3Z0D4	DNA-binding protein Rfx5	16.67	2
E9Q6C7	Latrophilin-2	16.67	2
E0CYZ9	E3 ubiquitin-protein ligase RNF6	15.93	2
D3YYQ8	Dynein, axonemal, heavy chain 10	15.44	2
E9PXP7	Stonin-2	14.88	2
D3Z2Q3	Diablo homolog, mitochondrial	14.22	2
E9Q8A3	Phosphatidylinositol 4-kinase beta	14.22	2
D3Z7J9	60 kDa heat shock protein, mitochondrial	14.11	2
E9PXX8	Macc1	13.89	2
D3YX99	Subunit 5, mitochondrial	13.51	5
D6REH1	Peroxisomal membrane protein 2	13.44	2
E9QLA5	Inverted formin-2	13.44	2
B1AUY7	N-alpha-acetyltransferase 10	13.39	2
D3Z7F0	L-lactate dehydrogenase	13.32	2
A2AF47	Dedicator of cytokinesis protein 11	13.22	2
D3YYD9	Gfpt1	13.16	3
E9Q4F8	Ankyrin repeat domain 11	13.16	3
D3Z1N2	RING finger protein 10	13.15	2
E9Q7R9	WD repeat domain 96	13.15	2
D3Z7D5	Collagen alpha-2(VI) chain	12.64	2
D3YYI9	Gm7347	12.54	3
E9Q4H1	Adenomatous polyposis coli protein	12.54	3
E0CYH7	Filamin A-interacting protein 1-like	12.17	2
D3YYK2	Beta-defensin 30	11.80	3
D3Z2G7	Histone deacetylase 11	11.76	2
E9Q813	Ras-GEF domain-containing family member 1B	11.76	2
D3YVJ8	Retinol dehydrogenase 13	11.70	2
D3Z460	Gm1330	11.66	2
D3YU67	Vacuolar protein sorting-associated protein 8 homolog	11.61	3
E9Q0W7	cAMP-specific 3',5'-cyclic phosphodiesterase 7B	11.61	3
E9PWQ6	Serine/threonine-protein kinase 31	11.58	2
E0CY56	SUMO-interacting motifs containing 1	11.54	2
E9Q7G0	Nuclear mitotic apparatus protein 1	11.38	3
Q003Y8	Uncharacterized protein KIAA2022	11.37	4
D3YYY8	Rho guanine nucleotide exchange factor (GEF) 26	11.13	2
E9Q512	Thyroid hormone receptor interactor 11	11.13	4
B1AV28	Gm14862	11.07	2
D3Z2E7	AI607873	11.07	3

E0CXG4	Greb1	10.72	2
D6RH44	NMDA receptor-regulated protein 2	10.61	2
D3YZ06	Heat shock protein beta-1	10.59	3
E0CYV9	Protein 1110002E22Rik	10.09	2
D3YX91	Gm7682	10.02	2
D3Z061	Ubiquitin-like modifier-activating enzyme 6	9.93	3
E9Q640	RNA-binding protein 26	9.93	3
E9QM06	Telomeric repeat-binding factor 2	9.91	2
A2AQA7	Intron-binding protein aquarius	9.88	2
D6RH34	Phosphatidate phosphatase LPIN2	9.82	2
E9PX70	Collagen alpha-1(XII) chain	9.62	2
D3Z7F6	Cytochrome P450, family 2, subfamily t, polypeptide 4	9.57	2
E0CY67	Sodium/hydrogen exchanger 9B1	9.49	2
E9QN32	LIM/homeobox protein Lhx6	9.49	2
D3Z4T1	CUGBP, Elav-like family member 5	9.45	2
E9Q9S8	Glutamine repeat protein 1	9.45	2
E9Q1N6	RasGEF domain family, member 1A	9.41	2
D3Z0Q6	Glycogen [starch] synthase, muscle	9.40	2
E9Q7C3	Plekhg4	9.39	2
D3Z7I5	RAD51-associated protein 1	9.38	2
E9QKX5	Vacuolar protein sorting-associated protein 13B	9.38	2
E9QMF5	Neuron navigator 3	9.31	2
D3YVP6	Glutathione S-transferase Mu 7	9.27	2
E9Q264	Myosin, heavy chain 15	9.27	2
D3Z6W2	Tyrosine-protein phosphatase non-receptor type	9.25	2
E9PV87	TALPID3	9.24	2
E9PVY8	Microtubule-actin cross-linking factor 1	9.18	2
E9PWK2	Vomerolnasal 1 receptor 224	9.16	2
D3YUE0	Three prime repair exonuclease 1	9.10	2
A2AJG1	Acyl-CoA-binding domain-containing protein 7	9.08	2
D3YXJ0	Diacylglycerol kinase, eta	9.05	4
E9PZ36	Polycystic kidney and hepatic disease 1	8.90	2
D6RH66	Transmembrane and TPR repeat-containing protein 4	8.82	2
E9Q7K7	Janus kinase and microtubule-interacting protein 3	8.65	3
E9QLT6	Aryl hydrocarbon receptor nuclear translocator	8.60	2
D3Z757	WD repeat domain 86	8.50	2
D3Z2A3	Histone demethylase UTY	8.47	2
D3Z6Z5	Family with sequence similarity 189, member	8.47	3

	A1		
E9Q7Y3	Uncharacterized protein ENSP00000471857 homolog	8.47	2
E9QKE4	Rab3 GTPase-activating protein non-catalytic subunit	8.47	3
E9Q9F1	Kcnq5	8.45	2
D6RFA3	Hexokinase-3	8.42	2
E0CYB9	Mitochondrial fission factor	8.38	2
E9QN53	Lebercilin-like protein	8.38	2
D6RCW6	V-type proton ATPase subunit C 2	8.34	2
A2AHD2	Protein Kcnk15	8.32	2
D6RGU3	Dedicator of cytokinesis protein 2	8.29	2
E9QLW6	Microtubule-associated serine/threonine-protein kinase 2	8.29	2
D6RH37	Serine/threonine-protein kinase N1	8.25	2
D3Z795	Proteasome assembly chaperone 1	8.13	2
E9PWI6	GRIP and coiled-coil domain-containing protein 2	8.13	2
E9QKS6	Synaptotagmin-like protein 2	8.13	2
D6RG93	Probable tubulin polyglutamylase TTLL9	8.08	2
A2AF67	Dedicator of cytokinesis protein 11	7.82	2
E9Q357	Gm17673	7.82	3
D3YVM5	60S acidic ribosomal protein P0	7.77	3
D3Z3N9	Nyap2	7.77	3
E9Q8N1	Titin	7.77	3
E9PY76	Gm4868	7.53	2
D3Z2W1	Diacylglycerol kinase, iota	7.27	2
E9Q8E3	ABI gene family, member 3 (NESH) binding protein	7.27	2
D3YWG0	11-cis retinol dehydrogenase	7.21	2
E9Q309	Centrosomal protein 350	7.21	2
D3Z5Q9	Tropomodulin-4	7.16	2
D3Z3F0	Lateral-signaling target protein 2 homolog	7.12	2
A2AM74	Kinesin-like protein KIF17	7.09	2
D3Z2B6	Vomer nasal 2, receptor 35	7.02	2
E9Q804	Ankyrin repeat domain-containing protein 17	7.02	2
E9PUU8	Fibrocystin-L	7.00	2
D6RFS3	Chloride channel protein 2	6.99	2
E9PYI8	Ubiquitin specific peptidase 14	6.91	2
D3Z4D4	1700064H15Rik	6.88	2
E0CY47	Plch1	6.75	2
D3YVU7	Lysine-specific demethylase 2B	6.74	4
E9Q2H1	E3 ubiquitin-protein ligase UBR5	6.74	4
B1AVN8	Phosphatase and actin regulator 2	6.60	2

D3Z440	COP9 signalosome complex subunit 7a	6.60	2
D6RGL4	Ankyrin repeat domain-containing protein 16	6.60	2
E9Q8Y0	Myl2	6.60	2
D3Z709	Disks large-associated protein 1	6.47	2
D3Z1M7	Synaptojanin-1	6.33	2
E9Q7Q0	Mucin-4	6.33	2
A2AP83	Fibronectin type III domain containing 3C2	6.32	2
E9QAU4	Sickle tail protein	6.28	3
A2ANY6	Midasin	6.24	2
D3Z0B2	Nuclear-interacting partner of ALK	6.20	2
E9Q6C1	Oxysterol-binding protein	6.20	2
D3Z0I9	Rnft2	6.16	4
E9Q6J4	Ceacam3	6.16	4
D3YXG0	Hemicentin 1	6.11	2
E9PVU7	cAMP-specific 3',5'-cyclic phosphodiesterase 4D	6.08	2
E9QQ17	Lipid phosphate phosphatase-related protein type 2	6.08	2
E0CZ72	Kinesin-like protein KIF2A	6.06	2
B1AUX2	Host cell factor 1	5.89	2
D3Z784	Probable UDP-sugar transporter protein SLC35A5	5.84	2
E9QKK8	Probable phospholipid-transporting ATPase 11C	5.84	2
A2AGR6	DNA damage-binding protein 2	5.83	2
D6RGN2	Plcd4	5.76	2
D3YXQ5	Probable phospholipid-transporting ATPase ID	5.75	2
D3Z6W1	Microtubule-associated protein 6	5.75	2
E9Q423	Dysferlin	5.75	2
E9QKD1	Nucleolar protein 8	5.75	2
D3YV10	Coiled-coil domain containing 13	5.61	2
E9Q1N0	4932431P20Rik	5.61	2
D3Z7A8	WD40 repeat domain 95	5.57	2
D3YXM6	Yip1 domain family, member 3	5.53	2
E9Q3Z5	Supervillin	5.53	2
D6RFN6	Caspase 2, apoptosis-related cysteine peptidase	5.46	2
E9QLJ0	Cardiomyopathy-associated protein 5	5.46	2
D3Z0R4	Tubby-related protein 2	5.35	3
D3Z576	Filamin-C	5.27	2
E9QA45	GTP-binding protein 2	5.27	2
E9Q4N3	E3 ubiquitin-protein ligase LNX	5.21	3
E9QPZ3	Filaggrin-2	5.19	2
D3YZ35	Neurofilament medium polypeptide	5.17	2

D3Z3M7	CAP-Gly domain-containing linker protein 1	5.03	3
E9Q8M8	Mineralocorticoid receptor	5.03	3
D3Z041	Long-chain-fatty-acid--CoA ligase 1	5.01	3
E0CYG5	Transmembrane protein 191C	4.99	2
E9QN87	Plectin	4.99	2
E9PXR3	Sestrin-1	4.97	2
E9Q8S5	Microtubule-associated serine/threonine-protein kinase 3	4.96	3
D3Z7A7	Formin-like protein 3	4.93	2
E9PZ38	Serine/threonine-protein kinase WNK4	4.93	2
E0CYY1	Anamorsin	4.86	2
D3Z0Z4	ATP-binding cassette sub-family G member 3	4.84	2
E9Q793	4931429I11Rik	4.84	2
D3YWI1	Fructose-bisphosphate aldolase	4.77	2
D3Z736	L-lactate dehydrogenase	4.74	2
A2AHW8	GTPase-activating Rap/Ran-GAP domain-like protein 3	4.71	2
D3Z4K0	Ankyrin repeat domain 36	4.70	2
E9PX39	Adams14	4.67	2
D3Z7F5	NACHT, LRR and PYD domains-containing protein 9A	4.65	3
E9QKV8	Nrde-2	4.65	3
E9QMD3	Zinc finger homeobox protein 3	4.65	2
E9PYK6	Olfactory receptor 1410	4.62	2
E9PZ41	Trafficking protein particle complex subunit 9	4.59	2
E9Q8N4	Microtubule-associated tumor suppressor 1 homolog	4.52	2
E0CXW4	Histone-lysine N-methyltransferase SUV420H2	4.50	2
E0CZF7	Homeobox protein prophet of Pit-1	4.49	2
D3YU01	Plekha1	4.46	4
D3YXX8	TP53RK-binding protein	4.40	2
D3YZW1	SLIT-ROBO Rho GTPase-activating protein 1	4.40	5
E9Q448	Tropomyosin alpha-1 chain	4.40	2
A8DUV1	Hemoglobin alpha, adult chain 1	4.38	2
E9PWB8	Tubulin polyglutamylase TTLL7	4.38	2
D3YXL0	Coiled-coil domain containing 170	4.35	2
E9Q3Y8	Gm6811	4.35	2
D3YUC3	1700026D08Rik	4.32	8
E9QNY8	Sacsin	4.31	2
E9PWG4	Myosin light chain 1/3, skeletal muscle isoform	4.27	2
D6RG56	Round spermatid basic protein 1	4.26	2
D6RIK9	Rpgrip1-like	4.24	2

A2AEP5	ATP-binding cassette sub-family A member 5	4.23	2
D3YVU6	Partner and localizer of BRCA2	4.20	2
D3YX59	Nicotinamide N-methyltransferase	4.18	2
E9Q3H7	Dynein, axonemal, heavy chain 6	4.18	2
D3YXI6	N-lysine methyltransferase SETD8	4.15	4
D3YVM9	Setd8	4.12	2
E0CY48	Tetratricopeptide repeat protein 39B	4.12	2
E9Q1W3	Nebulin	4.12	2
D3YTW9	Wnt5b	4.10	2
E9Q455	Tropomyosin alpha-1 chain	4.10	2
D3YXH8	Integrin beta 2-like	4.09	2
E9Q3U6	Killer cell lectin-like receptor subfamily B member 1C	4.09	2
E0CXJ0	Slco6d1	4.03	2
D3YZH8	Transducin beta-like protein 2	4.00	2
E0CXX5	Coiled-coil domain containing 19	4.00	2
E9Q5D9	Insulin-like growth factor-binding protein 7	4.00	2
D3Z5G8	Disco-interacting protein 2 homolog B	3.98	3
E9QAD4	Coiled-coil domain-containing protein 93	3.98	3
E9QPR6	Transmembrane protease serine 13	3.96	2
A2ANT9	Ankyrin repeat and SAM domain-containing protein 6	3.90	2
D6REH6	BCL-6 corepressor-like protein 1	3.90	2
E9PU96	Nucleolar pre-ribosomal-associated protein 1	3.90	2
E9QP09	Cullin-9	3.90	2
E9PX79	March10	3.88	2
D3YUU6	Cornulin	3.75	2
D3Z5G3	Anion exchange protein 2	3.75	3
E9QNW4	Piezo-type mechanosensitive ion channel component 2	3.72	2
A2AHQ2	G-protein-coupled receptor 64	3.58	2
D3Z5T8	4930407I10Rik	3.57	2
E9QAX1	Balap2l2	3.57	2
D3Z0L7	SUN domain-containing protein 1	3.55	2
E9Q6J5	Biorientation of chromosomes in cell division 1-like	3.55	2
D3Z0G8	MAGUK p55 subfamily member 4	3.47	2
E9Q6D8	Complement component 6	3.47	2
D3Z4T0	Interleukin-17 receptor B	3.46	3
E9PYT0	Rho GTPase-activating protein 5	3.36	2
D3Z4U7	Testis-expressed sequence 35 protein	3.35	3
E0CZ30	Myosin light chain 1/3, skeletal muscle isoform	3.30	2
E9PW83	Fam184a:family with sequence similarity 184, member A	3.30	2

E9QNG1	Intersectin-2	3.30	2
D3YZR0	Gm15737	3.28	2
D3Z4D9	C2 domain-containing protein 3	3.28	2
E9Q9B2	NEDD4 binding protein 2	3.28	2
D3YUZ4	CREB/ATF bZIP transcription factor	3.27	2
D6REG6	PX domain-containing protein 1	3.26	2
E9QPI5	Sister chromatid cohesion protein PDS5 homolog A	3.26	2
D3Z5W6	Fatty acyl-CoA reductase 1	3.21	2
E9QAZ9	Vomerolnasal 2, receptor 100	3.21	2
A2AG09	RNA-binding protein 41	3.17	2
E9Q6T9	BTB/POZ domain-containing protein KCTD1	3.16	2
D3YYR3	2210418O10Rik	3.11	2
E9PUJ6	Probable E3 ubiquitin-protein ligase MYCBP2	3.10	2
E9QPG2	Polycystic kidney disease protein 1-like 2	3.10	2
E9QL22	TatD DNase domain containing 3	3.04	2
E9PVU0	Unconventional myosin-VI	3.03	2
E9PXA7	Cytosolic carboxypeptidase 1	3.01	2
D3YY55	Histone deacetylase complex subunit SAP18	2.98	3
E9Q456	Tropomyosin alpha-1 chain	2.98	3
E9PYP7	Trehalase	2.86	2
D3YYC3	Histone-lysine N-methyltransferase SETDB1	2.85	3
E9PUA3	IQ motif and SEC7 domain-containing protein 1	2.83	2
E9QP46	Nesprin-2	2.83	2
A2ALV5	Protein AI481877	2.76	2
E9PYD7	Kelch repeat and BTB (POZ) domain containing 6	2.76	2
D3YXT2	Ribosomal protein L10A, pseudogene 2	2.72	2
E9Q444	Zinc finger and BTB domain containing 21	2.72	2
E0CZA1	T-complex protein 1 subunit epsilon	2.68	2
D3Z4N8	Vomerolnasal 2, receptor 72	2.66	2
E9Q9M0	Centrosomal protein of 290 kDa	2.66	2
E9PW44	YTH domain containing 1	2.60	2
E9PUV7	Gm872	2.56	2
E9Q616	AHNAK nucleoprotein (desmoyokin)	2.56	4
D3Z3X6	Latrophilin-3	2.49	4
D3YYD6	Aquaporin-9	2.47	2
E9Q489	Calsequestrin	2.47	2
D3YZZ5	Tmed7	2.40	2
E9Q5L3	Acadsb	2.40	2
D3YZE8	Cdca2	2.35	3
E9PUL4	Pde8b	2.35	2

E9Q559	Sarcoplasmic/endoplasmic reticulum calcium ATPase 3	2.35	3
D3YY08	Tubulin polyglutamylase TTLL4	2.32	2
E9Q452	Tropomyosin alpha-1 chain	2.32	2
E9PWG6	Non-SMC condensin I complex, subunit G	2.30	2
E9QP99	Golgin subfamily A member 3	2.26	2
E9Q9D8	ankyrin repeat domain 35	2.24	3
D3Z2J3	Putative ATP-dependent RNA helicase DHX30	2.23	2
E9Q7S1	Zinc finger protein 106	2.23	3
D3Z3B2	V-type proton ATPase 16 kDa proteolipid subunit	2.22	2
D6RIM8	Harmonin	2.16	2
A2AE98	WD and tetratricopeptide repeats protein 1	2.12	2
E9Q7E2	AT rich interactive domain 2 (ARID, RFX-like)	2.11	3
D3YWV3	Differentially-expressed in FDCP 8	2.09	4
E9Q390	Myoferlin	2.09	7
D3Z2L1	General transcription factor 3C polypeptide 2	2.08	2
E9Q892	Lrch3	2.08	2
D3Z6N0	BB014433	2.06	3
E9Q1K1	4933411K20Rik	1.87	2
B1ASL6	Tumor necrosis factor receptor superfamily member 18	1.85	2
E9PZ74	Vomeroneasal 2, receptor 7	1.85	2
D3Z030	Leucine-rich repeat-containing protein 16A	1.82	2
D3Z007	Interleukin-1 receptor-associated kinase 3	1.81	3
E9Q5M6	WD repeat domain 52	1.81	3
E9QQ10	A-kinase anchor protein 9	1.80	2
E9QML5	Zinc finger protein 638	1.76	2
E9Q0D4	SET binding factor 2	1.75	2
D3Z5A7	Peroxisome biogenesis factor 1	1.62	3
E9QAC0	StAR-related lipid transfer protein 9	1.62	3
D3Z0T2	Dimethylaniline monooxygenase [N-oxide-forming] 1	1.60	2
E9Q6Y8	Ubiquitin specific peptidase 31	1.60	2
D3Z0I5	Tripartite motif-containing protein 59	1.53	2
D3Z5R8	40S ribosomal protein S19	1.48	3
E9QAH1	Golgi autoantigen, golgin subfamily b, macrogolgin 1	1.48	3
E0CZ42	Fer-1-like 6 (C. elegans)	1.44	2
E9PUJ2	DNA repair protein RAD50	1.44	2
D3Z1X5	Rho GTPase-activating protein 26	1.42	2
E9Q7S8	Vomeroneasal 2, receptor 22	1.42	2
D3YU32	Gm362	1.40	3

D3Z533	Galnt15	1.40	3
E9Q0A4	Kinesin-like protein KIF21B	1.40	3
E9QA22	Xinc finger protein 644	1.40	3
D3Z2S4	Enolase	1.38	3
E9Q8C5	Family with sequence similarity 3, member C	1.38	3
A2AEC2	Transcription elongation factor A protein-like 3	1.24	2
D3Z4B5	Family with sequence similarity 210, member A	1.24	3
E9QKH0	CLIP-associating protein 1	1.23	2
D6RFE3	Transmembrane protein 180	1.19	2
E9Q555	E3 ubiquitin-protein ligase RNF213	1.17	5
D6RFR7	DCC-interacting protein 13-beta	0.98	2
E9Q7N9	Dynein, axonemal, heavy chain 11	0.98	2
E9QLK7	Transformation/transcription domain-associated protein	0.98	2
D3Z6P9	DEAD (Asp-Glu-Ala-Asp) box polypeptide 43	0.91	2
E9QK83	Small subunit processome component 20 homolog	0.91	2
D3Z4A4	Peroxiredoxin-2	0.88	2
D3YV81	Sarcolemmal membrane-associated protein	0.86	2
D3Z667	Dynein heavy chain 2, axonemal	0.86	2
D3Z6P1	Multifunctional protein ADE2	0.74	2
E9QK82	Myelin protein P0	0.74	2
D3YVW2	Golgi integral membrane protein 4	0.30	5

Table 4.2: Proteins identified in the murine intervertebral disc.

List of identified proteins using the LC-ESI-MS/MS strategy from the IVD of skeletally mature (14 week old) wild-type CD-1 mice .

Uniprot Accession No.	Protein Name	% Coverage	No. Different Peptides
B2RXU7	Chondroitin sulfate synthase 3	97.87	2
B9EI21	Zinc finger matrin type 3	82.61	2
B9EKB8	Insulin-like growth factor 2 receptor	65.82	4
P46660	Alpha-internexin	65.82	2
Q9JIH4	Nuclear factor of activated T cells 5	63.37	2
Q8BSS6	Transcription factor SOX-6	57.69	3
Q91VH3	Tropomyosin 2, beta	57.36	3
D6Q0F7	Cytoplasmic dynein intermediate chain 2 isoform 2.5	57.01	2
Q64343	ATP-binding cassette sub-family G member 1	57.01	2
Q8C0Q3	Tetratricopeptide repeat domain 34	50.81	2
B1AXJ0	5-azacytidine-induced protein 1	50.00	2
Q505F0	Asap1	49.28	2
P59528	Taste receptor type 2 member 123	49.28	2
P61164	Alpha-centractin	49.06	2
Q6P8J7	Creatine kinase S-type, mitochondrial	46.94	2
A4Q9E4	Probable tubulin polyglutamylase TTL2	46.43	2
E9PZJ8	Activating signal cointegrator 1 complex subunit 3	46.10	2
Q8BYN3	Inositol-tetrakisphosphate 1-kinase	45.95	2
P31725	Protein S100-A9	44.03	13
P63101	14-3-3 protein zeta/delta	41.51	3
B2RRF6	Zinc finger protein 518A	40.94	2
B7ZND3	Avian erythroblastosis virus E-26 (v-ets) oncogene related	40.41	4
Q7TQ48	Sarcalumenin	40.11	4
P40142	Transketolase	39.73	12
Q5U440	Maternal embryonic leucine zipper kinase	39.72	2
Q8K0Z9	Probable G-protein coupled receptor 153	38.60	2
Q6PAJ3	GRB2-associated and regulator of MAPK protein-like	38.46	2
Q0VBN2	Dermatan-sulfate epimerase-like protein	38.16	2
Q9DCC3	Coiled-coil domain-containing protein 107	37.50	2
B2RSN6	REST corepressor 3	37.41	2
A6ZI46	Fructose-bisphosphate aldolase	37.06	2

E9QMK7	Arap3	37.06	2
D9HP81	Regulating synaptic membrane exocytosis 2	37.06	2
Q9D6J4	N-terminal EF-hand calcium-binding protein 3	36.42	2
P10639	Thioredoxin	34.09	2
A2RSS2	Carbohydrate sulfotransferase 10	33.95	2
E9Q165	Trpm8	33.67	3
Q02242	Programmed cell death protein 1	33.17	3
Q8CGY6	Protein unc-45 homolog B	31.71	3
Q9WV42	Nuclear receptor coactivator 4	31.06	2
P60879	Synaptosomal-associated protein 25	30.57	2
Q9D5R3	Centrosomal protein of 83 kDa	30.09	2
P07759	Serine protease inhibitor A3K	29.89	2
A2A864	Integrin Beta 4	29.26	2
Q14B66	Potassium voltage-gated channel, subfamily Q, member 3	29.25	2
Q9DAM4	Citrate synthase like	29.25	2
P97864	Caspase-7	29.17	2
Q5F4S6	Trpm3	29.02	2
Q8K2Y2	Receptor-interacting serine-threonine kinase 3	28.87	3
Q9WVM2	Dematin	28.57	2
Q8R4D4	Signal transducer and activator of transcription 6	27.22	3
D3YU07	RAD50 interactor 1, isoform CRA f	26.60	6
D3YW52	Alpha-2-macroglobulin	26.19	3
Q5FWH3	Grainyhead-like protein 3 homolog	26.10	5
A6H694	Leucine-rich repeat-containing protein 63	26.09	2
O70343	PPAR-gamma coactivator 1-alpha	26.09	2
A2A9Z0	Dystrophin	25.93	2
Q0P661	Proline rich Gla (G-carboxyglutamic acid) 1	25.38	2
C6EQG1	Ubiquitin carboxyl-terminal hydrolase 29	25.12	2
O54949	Serine/threonine-protein kinase NLK	24.82	2
E9QL17	Serine/threonine-protein kinase MARK1	24.75	2
Q8BH44	Coronin-2B	24.71	2
Q9WV02	RNA-binding motif protein, X chromosome	24.67	2
Q4FK59	Enolase 3, beta muscle	24.66	3
O55226	Chondroadherin	24.24	2
Q9DCM0	Persulfide dioxygenase ETHE1, mitochondrial	24.22	2
P08249	Malate dehydrogenase, mitochondrial	24.16	2
A2A791	Zinc finger MYM_type protein 4	24.11	2
Q3KNG4	Neuropeptide FF-amide peptide precursor	24.09	2
B2RWR1	Protocadherin 20	23.97	2
Q2KHI9	DNA helicase MCM9	23.28	2
Q00898	Alpha-1-antitrypsin 1-5	23.08	2
Q9D5U0	Lysophosphatidylcholine acyltransferase 2B	22.90	2

Q3UGP9	Leucine-rich repeat-containing protein 58	22.89	2
B2RY08	Dedicator of cytokinesis 9	22.64	2
P80316	T-complex protein 1 subunit epsilon	22.61	2
P80316	T-complex protein 1 subunit epsilon	22.61	2
Q8VDD5	Myosin-9	22.45	2
Q45VK6	Interleukin enhancer binding factor 3	22.06	2
P70270	DNA repair and recombination protein RAD54-like	22.04	2
Q80XH2	Interphotoreceptor matrix proteoglycan 2	22.03	2
P09411	Phosphoglycerate kinase 1	22.02	2
A7TU71	Shroom2	21.60	2
A2ARV4	Low-density lipoprotein receptor-related protein 2	21.54	2
Q80U35	Rho guanine nucleotide exchange factor (GEF) 17	21.16	4
Q9ESP5	Fez family zinc finger protein 2	20.89	2
Q04887	Transcription factor SOX-9	20.75	3
Q80ZE2	Sialic acid-binding Ig-like lectin 5	20.63	2
P99027	60S acidic ribosomal protein P2	20.38	2
A0JNY8	RE1-Silencing Transcription Factor	20.20	2
Q7TPD5	Ribosomal protein S6 kinase	20.19	2
B1AVI6	Sushi-repeat-containing protein, X-linked 2	20.00	3
Q2EY15	Protogenin	19.88	2
Q5SDA5	Retinal guanylyl cyclase 2	19.76	2
B7ZMQ1	CD84	19.52	2
A2ABQ3	Centrosomal protein of 112 kDa	19.46	2
Q8CCJ3	E3 UFM1-protein ligase 1	19.35	2
Q5VCS6	Tudor domain-containing protein 5	19.19	2
Q3TXI6	Secreted acidic cysteine rich glycoprotein	19.14	2
Q99MX7	Cat eye syndrome critical region protein 6 homolog	18.53	2
B7ZN98	Otoferlin	18.49	2
B2RPU9	Neuromedin U receptor 2	18.47	2
Q4FJU1	Serine (or cysteine) peptidase inhibitor, clade E, member 2	18.44	3
Q8CIA8	Uaca	18.18	2
Q61785	ORF2	17.99	2
D3Z750	Maestro heat-like repeat-containing protein family member 2A	17.74	2
E9QJR6	Polycystin-1	17.73	2
D3YU22	LIM and calponin homology domains-containing protein 1	17.67	2
D3YU22	LIM and calponin homology domains-containing protein 1	17.67	2
E9QK00	Tight junction protein ZO-1	17.50	2
Q9EP71	Ankyrin	17.35	2

Q6DR98	Neuregulin-1 type I beta1-a	17.24	5
B2RQL1	Coiled-coil domain containing 158	17.22	2
Q9Z285	Tektin 1	17.21	2
Q3U186	Probable arginine--tRNA ligase, mitochondrial	17.15	2
Q99K08	6-phosphofructokinase	17.13	3
Q3U1F0	Ligase III, DNA, ATP-dependent	17.09	2
Q9D738	Ankyrin repeat and SOCS box protein 12	16.93	2
B2RX00	RB1-inducible coiled-coil 1	16.87	2
Q9D5T7	HORMA domain-containing protein 1	16.81	2
Q6NZC3	Solute carrier family 30 (zinc transporter), member 3	16.67	2
Q7TN79	A-kinase anchor protein 7 isoform gamma	16.64	3
Q9QWT9	Kinesin-like protein KIFC1	16.62	2
Q6NZR2	Myb/SANT-like DNA-binding domain-containing protein 2	16.55	2
B2RWR3	Coiled-coil domain containing 73	16.38	2
Q5FW75	Actinin alpha 2	16.31	2
Q5PR68	Centrosomal protein of 112 kDa	16.19	2
Q9WU03	Kunitz-type protease inhibitor 2	16.19	2
Q7TSV6	Putative aspartate aminotransferase, cytoplasmic 2	16.18	3
Q7TRL9	Olfactory receptor 745	15.79	2
B9EKQ3	PR domain containing 2, with ZNF domain	15.63	2
A2A7Z8	Arylacetamide deacetylase-like 3	15.61	2
Q71LX8	Heat shock protein 84b	15.54	2
P56480	ATP synthase subunit beta, mitochondrial	15.28	2
P58873	Rhomboid-related protein 3	15.28	2
Q3KPE4	Phospholipase C, zeta 1	15.20	2
A0JP62	F-box and WD-40 domain protein 13	15.14	2
B2BBR8	Xin actin-binding repeat containing 2	15.10	2
Q148R9	Regulator of G-protein signaling 9-binding protein	15.04	2
Q7TPV4	Myb-binding protein 1A	15.02	2
Q9EQ38	Vomeroneasal receptor V1RC5	15.01	2
Q8CEH8	Profilin	14.96	2
Q9CQL5	39S ribosomal protein L18, mitochondrial	14.94	2
Q9D3P1	Trichohyalin-like protein 1	14.94	2
Q3TGF2	Family with sequence similarity 107, member B	14.93	2
Q14DL3	Leucine-rich repeat and IQ domain-containing protein 3	14.90	3
P08553	Neurofilament medium polypeptide	14.88	2
Q14AV0	Myosin binding protein H	14.84	2
Q91YT9	6-phosphogluconate dehydrogenase, decarboxylating	14.76	3
Q9D9J3	Actin-related protein T1	14.73	2

Q9CZA6	Nuclear distribution protein nudE homolog 1	14.71	2
Q9DBA6	Peroxisomal leader peptide-processing protease	14.64	2
B2RWW8	Myosin, heavy polypeptide 8, skeletal muscle, perinatal	14.64	2
Q80VZ1	Calpain 6	14.49	2
Q3UHI0	Serine-rich coiled-coil domain-containing protein 2	14.22	2
Q8R554	OTU domain-containing protein 7A	14.20	2
A2AHD1	WNT1 inducible signaling pathway protein 2, isoform CRA_a	14.11	2
Q640N8	Major intrinsic protein of eye lens fiber	14.00	2
A1X3U7	Beta growth arrest specific protein 11	13.98	2
P09036	Serine protease inhibitor Kazal-type 3	13.89	2
Q9Z0U9	Sphingosine 1-phosphate receptor 3	13.87	2
A2AQP0	Myosin-7B	13.75	2
A8C756	Thyroid adenoma-associated protein homolog	13.72	2
A2A6J1	Troponin T, fast skeletal muscle	13.65	2
Q9CYU9	PRP18 pre-mRNA processing factor 18 homolog (yeast)	13.64	2
B2RU94	Olfactory receptor 1115	13.63	2
Q80UL7	Heart and neural crest derivatives expressed transcript 1	13.60	4
Q8BI29	Specifically androgen-regulated gene protein	13.56	4
Q6T707	Stearoyl-coenzyme A desaturase 4	13.55	6
Q8BJF9	Charged multivesicular body protein 2b	13.53	3
Q14AY4	Mitogen-activated protein kinase kinase kinase 5	13.50	2
Q8R5B7	General transcription factor IIF subunit 1	13.47	3
Q8R480	Nuclear pore complex protein Nup85	13.45	2
Q78KN5	Leucine rich repeat containing 40	13.38	2
A2AFF9	Plexin-B3	13.35	3
Q80UF7	TIR domain-containing adapter molecule 1	13.25	4
Q8BW94	Dynein heavy chain 3, axonemal	13.23	2
A2AF47	Dedicator of cytokinesis protein 11	13.22	2
Q99KR8	Plasma alpha-L-fucosidase	13.16	2
B2RU58	G-protein-coupled receptor 115	13.11	2
Q6XBG3	ATP-binding cassette transporter sub-family A member 14	13.05	2
Q9JI67	Beta-1,3-galactosyltransferase 5	12.92	2
Q9D881	Cytochrome c oxidase subunit 5B, mitochondrial	12.90	2
Q9CRY7	Gdpd1	12.88	2
Q3TE63	Peptidyl-prolyl cis-trans isomerase A	12.85	2
Q8BKU8	Transcription factor HES-7	12.84	4
Q9QXE7	F-box-like/WD repeat-containing protein TBL1X	12.77	2
B1AU57	Envoplakin	12.73	2

Q8BG58	Transmembrane prolyl 4-hydroxylase	12.72	5
Q6PGB9	A kinase (PRKA) anchor protein 6	12.68	2
E9QKU0	Intraflagellar transport protein 88 homolog	12.64	2
P42859	Huntingtin	12.59	2
Q9Z218	Dipeptidyl aminopeptidase-like protein 6	12.55	2
Q923C5	Centromere protein B	12.53	2
Q8VFI0	Olfactory receptor 788	12.52	3
A2AAA9	C-type mannose receptor 2	12.50	2
D7RXM0	GPR155 variant 4	12.50	2
A3K GK3	Fer-1-like protein 4	12.41	2
Q9QZS8	SH2 domain-containing protein 3C	12.39	2
Q8K2W0	Collagen, type IX, alpha 2	12.38	3
Q9DCU6	39S ribosomal protein L4, mitochondrial	12.28	2
P97457	Myosin regulatory light chain 2, skeletal muscle isoform	12.23	3
Q6PER8	Myosin VB	12.22	2
Q149C8	Hexokinase 3	12.15	2
P60882	Multiple epidermal growth factor-like domains protein 8	12.09	3
Q45VK7	Dynein cytoplasmic 2 heavy chain 1	11.87	2
Q8R2X0	EH-domain containing 2	11.83	3
Q62429	Tap1	11.79	3
B9EHR5	Unconventional myosin-VIIb	11.75	2
Q8CFH0	Prolactin-like protein C 3, isoform CRA_a	11.74	2
B2RWS3	Receptor transporter protein 3	11.71	2
E9Q926	Serine protease inhibitor A3M	11.66	2
Q6P5E8	Diacylglycerol kinase theta	11.63	2
Q3UFC6	Desmoglein 3	11.62	2
B9EKA3	Deleted in liver cancer 1	11.59	2
Q8K3W3	Cancer susceptibility candidate 3	11.58	2
O88829	Lactosylceramide alpha-2,3-sialyltransferase	11.58	2
Q8K0T4	Katanin p60 ATPase-containing subunit A-like 1	11.56	2
E9QN15	DNA-dependent protein kinase catalytic subunit	11.54	2
B1PSD9	cAMP-specific 3',5'-cyclic phosphodiesterase 4D	11.52	2
Q14B51	UDP-N-acetyl-alpha-D-galactosamine:polypeptide N-acetylgalactosaminyltransferase 5	11.50	2
Q99NE9	Pre-B-cell leukemia transcription factor 4	11.48	2
Q8BL66	Early endosome antigen 1	11.47	2
B2RS91	RNA polymerase I-specific transcription initiation factor RRN3	11.39	2
Q2T9H5	Vanin 3	11.39	3
B2RWX0	Myosin, heavy polypeptide 1, skeletal muscle, adult	11.36	2

A2AN08	E3 ubiquitin-protein ligase UBR4	11.29	2
Q920Q2	DNA repair protein REV1	11.28	2
B1AQ77	Keratin 15, isoform CRA_a	11.23	2
Q7TRI0	Olfactory receptor 790	11.23	4
Q8K0C6	Kallikrein 1-related peptidase b8	11.20	2
B7ZP32	Zinc finger protein 408	11.17	2
E9QLV2	Dopey-2	11.17	2
Q99PL6	UBX domain-containing protein 6	11.17	2
B2RUG8	Additional sex combs like 2 (Drosophila)	11.16	2
B7ZW99	Formin 1	11.14	2
Q6P3A4	V-set and immunoglobulin domain-containing protein 8	11.13	5
Q99PT1	Rho GDP-dissociation inhibitor 1	11.11	2
Q6PHC1	Enolase 1	11.05	2
B2RT41	Zinc finger, C3H1-type containing	11.04	2
A5X3G4	Kinase suppressor of ras 2	11.03	2
E9QMG5	Sorting nexin-25	11.02	2
P97298	Pigment epithelium-derived factor	11.00	6
Q3TLN1	Peroxisomal biogenesis factor 12, isoform CRA_a	10.95	2
Q2TBA4	Basonuclin 2	10.91	2
A2ADZ8	IQ domain-containing protein C	10.90	2
Q68FM6	Leucine rich repeat and fibronectin type III, extracellular 2	10.89	2
Q3TFK5	G-patch domain-containing protein 4	10.87	2
Q5RKV3	Phosphoglycerate kinase 2	10.82	2
Q05DV1	NADPH--cytochrome P450 reductase	10.78	2
Q155P7	Leucine, glutamic acid, lysine family 1 protein	10.75	2
Q8C1E7	Transmembrane protein 120A	10.71	3
B7ZN53	Armadillo repeat containing 3	10.68	2
B7NZ86	Beta-1,4-galactosyltransferase	10.65	2
B9EIZ9	NLR family, pyrin domain containing 9B	10.62	2
Q9JL95	Proteoglycan 3	10.60	2
P48036	Annexin A5	10.57	2
Q8CD92	Tetratricopeptide repeat protein 27	10.54	2
Q9CWY3	N-lysine methyltransferase SETD6	10.54	2
Q9ES82	Popeye domain-containing protein 2	10.54	2
A2ALD8	LIM homeobox protein 3	10.52	2
Q8BH59	Calcium-binding mitochondrial carrier protein Aralar1	10.52	4
Q3UKC1	Tax1-binding protein 1 homolog	10.51	2
Q8K2Q9	Shootin-1	10.50	3
Q3V036	Coiled-coil domain-containing protein 27	10.49	3

Q7TML3	Solute carrier family 35 member F2	10.47	2
Q91YX0	Thymocyte selection associated family member 2	10.43	3
Q3THK7	GMP synthase [glutamine-hydrolyzing]	10.41	2
Q6P9J5	KN motif and ankyrin repeat domain-containing protein 4	10.39	3
B2RXR2	Pik3r4	10.36	2
B2RXT8	AT rich interactive domain 4A (RBP1-like)	10.35	2
Q8R420	ATP-binding cassette sub-family A member 3	10.27	3
A9C437	Chloride channel protein 2	10.24	2
A6PWV7	Lysosomal amino acid transporter 1 homolog	10.22	2
E9QLS8	ATR-interacting protein	10.20	2
B2RY59	Neuralized homolog 4 (Drosophila)	10.19	2
Q91VJ2	Protein kinase C delta-binding protein	10.19	3
Q05D44	Eukaryotic translation initiation factor 5B	10.18	2
Q0P520	NLR family, pyrin domain containing 4C	10.14	2
Q8BFX3	BTB/POZ domain-containing protein KCTD3	10.12	2
Q01237	3-hydroxy-3-methylglutaryl-coenzyme A reductase	10.11	2
Q3UQU0	Bromodomain-containing protein 9	10.10	2
Q6PGC1	ATP-dependent RNA helicase Dhx29	10.09	4
A2AL17	Rho GTPase-activating protein 11A	10.07	2
Q14DK8	Phospholipase A2, group IVD	10.06	3
Q7TS23	Olfactory receptor 251	10.06	3
Q3UPP8	Centrosomal protein of 63 kDa	10.02	2
Q5SV85	Synergin gamma	10.01	5
Q8R3C6	RNA binding motif protein 19	10.00	2
Q8K3V4	Protein-arginine deiminase type-6	9.94	2
Q61982	Neurogenic locus notch homolog protein 3	9.93	4
Q0P678	Zinc finger CCCH domain-containing protein 18	9.91	3
P68368	Tubulin alpha-4A chain	9.86	2
Q66JW2	Golgi autoantigen, golgin subfamily a, 1	9.86	2
Q8R1T2	Cullin 4A	9.84	2
A9P6P9	Testis-specific serine/threonine protein kinase 5 variant delta	9.78	2
Q9QZA0	Carbonic anhydrase 5B, mitochondrial	9.74	2
O88990	Alpha-actinin-3	9.71	2
D5G1T0	Ankyrin repeat domain 33, isoform CRA_c	9.68	2
Q0P543	Gastric inhibitory polypeptide receptor	9.65	2
A8DUL5	Hemoglobin, beta adult major chain	9.62	2
Q8BW49	Tetratricopeptide repeat protein 12	9.62	3
A8DUL5	Hemoglobin, beta adult major chain	9.62	2
P03995	Glial fibrillary acidic protein	9.62	2
B7ZWK2	Myotubularin-related protein 5	9.61	2

Q67E05	Bactericidal permeability-increasing protein	9.61	6
Q6P5U7	Kiaa1239	9.59	6
A2SW42	Zinc finger protein 462	9.57	2
Q3THE6	Ferritin	9.57	2
B2RT12	Ubiquitin specific peptidase 37	9.52	2
Q9CQT1	Methylthioribose-1-phosphate isomerase	9.52	2
C0LQ88	Syncoilin isoform 3	9.48	2
Q7TS72	Inositol-trisphosphate 3-kinase C	9.47	2
Q920R0	Amyotrophic lateral sclerosis 2 (juvenile)	9.45	3
Q6PIJ4	Nuclear factor related to kappa-B-binding protein	9.40	2
E9QM11	Microtubule-associated protein 1B	9.35	2
Q6PCP7	Probable G-protein coupled receptor 156	9.34	2
Q6PDF3	SV2 related protein homolog (rat)-like	9.31	3
Q8K2I4	Beta-mannosidase	9.31	3
Q9D2L5	Inactive carboxypeptidase-like protein X2	9.31	2
Q8BGV8	Mitochondrial dynamic protein MID51	9.29	2
P59111	Potassium voltage-gated channel subfamily H member 8	9.27	2
Q14DP5	Catenin (Cadherin associated protein), alpha 3	9.27	3
Q5DTI8	Extended synaptotagmin-3	9.27	3
E9QKD7	Dynein heavy chain 5, axonemal	9.25	2
A2AKB9	DDB1- and CUL4-associated factor 10	9.23	2
Q9QZ67	Protein phosphatase 1D	9.23	2
Q62059	Versican core protein	9.20	2
O08850	Regulator of G-protein signaling 5	9.18	2
Q8C3L1	Ssu-2 homolog (C. elegans)	9.16	3
O88783	Coagulation factor V	9.16	2
B7ZNF8	Chromodomain helicase DNA binding protein 9	9.15	2
A6H5W2	Coiled-coil domain-containing protein 87	9.13	2
P11087	Collagen alpha-1(I) chain	9.11	2
Q64092	Transcription factor E3	9.09	3
A2AJG1	Acyl-CoA-binding domain-containing protein 7	9.08	2
D6CHX5	Hepatoma-derived growth factor-related protein 2	9.06	2
E9QL35	Alpha-kinase 2	9.06	2
Q80ZJ6	Zyg-11 related, cell cycle regulator	9.02	2
Q497V3	La ribonucleoprotein domain family, member 2	8.96	3
Q9WVA4	Transgelin-2	8.94	2
Q9WTU0	Lysine-specific demethylase PHF2	8.92	2
P28184	Metallothionein-3	8.90	2
Q5SXY1	Cytospin-B	8.86	2
Q62504	Msx2-interacting protein	8.86	2
B9EHV0	Leucine rich repeat containing 7	8.84	2
O54984	ArsA arsenite transporter, ATP-binding, homolog	8.84	2

	1 (bacterial)		
P62897	Cytochrome c, somatic	8.84	2
E9QM01	E3 SUMO-protein ligase RanBP2	8.82	2
Q8K448	ATP-binding cassette sub-family A member 5	8.81	2
Q9R269	Periplakin	8.81	2
B7ZWG4	Tripartite motif-containing 40	8.77	2
Q8K0Z5	Tropomyosin 3, gamma	8.74	2
B5LBC3	RAD51D transcript variant delta 9,10	8.73	2
Q6P8I3	WD repeat domain 70	8.72	3
Q7TS74	Cytoskeleton-associated protein 2-like	8.72	4
Q8BNJ3	Nicotinamide nucleotide adenylyltransferase 2	8.72	2
Q5SUR0	Phosphoribosylformylglycinamide synthase	8.68	2
Q505K2	Family with sequence similarity 160, member A1	8.67	4
D3Z1J2	Coiled-coil domain-containing protein 112	8.65	3
Q8R4G5	Truncated N-acetylglucosaminyltransferase V	8.64	3
B1ARH0	Hypermethylated in cancer 1 protein	8.59	2
Q059Q1	WD repeat-containing protein 7	8.55	2
C6EQH1	ASL1/Fgf17 fusion protein	8.54	2
Q9JI58	Retinoic acid early-inducible protein 1-delta	8.54	2
P70670	Naca	8.53	2
Q8VC03	Echinoderm microtubule-associated protein-like 3	8.51	2
Q99N99	3-oxo-5-alpha-steroid 4-dehydrogenase 2	8.49	2
E9QPW5	Kinesin-like protein KIF20B	8.48	2
P70351	Histone-lysine N-methyltransferase EZH1	8.47	4
Q8K0M3	Sorbin and SH3 domain containing 3	8.44	3
A2RRJ0	Desmoglein-2	8.42	2
B2RTP7	Keratin 2	8.41	3
Q8CGD2	Cysteine-rich secretory protein LCCL domain-containing 1	8.40	2
Q9WUU9	80 kDa MCM3-associated protein	8.39	2
Q80W71	Pleckstrin homology domain-containing family A member 8	8.39	4
Q149S1	Tektin 4	8.38	2
Q8C3Y4	Kinetochore-associated protein 1	8.38	3
Q8CJF7	AT hook containing transcription factor 1	8.38	3
Q9JHD1	Histone acetyltransferase KAT2B	8.38	2
B7ZWL7	Leucine rich repeat containing 36	8.36	2
P53569	CCAAT/enhancer-binding protein zeta	8.33	3
Q6DIB5	Multiple epidermal growth factor-like domains protein 10	8.30	2
Q08EK4	Keratin 77	8.29	2
Q01853	Transitional endoplasmic reticulum ATPase	8.28	2
Q9Z1W9	STE20/SPS1-related proline-alanine-rich protein	8.27	2

	kinase		
Q9ESC5	GTPase ERA-W	8.24	2
Q62392	Pleckstrin homology-like domain family A member 1	8.19	2
B9EIW5	Nuclear receptor coactivator 7	8.17	2
Q920P3	Deleted in bladder cancer protein 1 homolog	8.17	3
Q8R2C5	Vomeroneasal receptor V1RC29	8.17	2
O88623	Ubiquitin carboxyl-terminal hydrolase 2	8.13	2
Q5SWY7	Family with sequence similarity 83, member G	8.13	3
B7ZP07	Ubiquitin specific peptidase, pseudogene (USP17 homolog)	8.10	2
B9EIV3	Calcium channel, voltage-dependent, alpha 2/delta subunit 4	8.09	2
Q8R4N0	Citrate lyase subunit beta-like protein, mitochondrial	8.08	3
Q8VG71	Olfactory receptor 907	8.08	2
Q8VDE8	Nuclear receptor co-repressor 1	8.07	2
B2RWW0	T-cell activation Rho GTPase-activating protein	8.05	2
Q5SSZ5	Tensin-3	8.03	3
B7ZNF6	Catenin (cadherin associated protein), delta 2	7.96	2
Q80XT6	Lipin 1	7.96	3
Q8K4L2	Supervillin	7.93	3
Q8K4L2	Supervillin	7.93	3
Q61115	Patched homolog 1	7.91	2
C5H7S5	Vascular endothelial growth factor receptor 2	7.90	2
Q8VIN7	Cardiac triadin isoform 3	7.90	3
B1AR51	Dynein, axonemal, heavy chain 9	7.88	2
Q61903	Myeloid secondary granule protein	7.87	3
Q8VDN9	Coiled-coil domain containing 21	7.83	3
Q8BHI4	Kelch repeat and BTB domain-containing protein 3	7.76	2
B2RXW8	Ppfia1 protein	7.74	2
P62192	26S protease regulatory subunit 4	7.73	2
Q3ZAT5	Onecut2 protein	7.73	2
Q3ZAT5	Onecut2 protein	7.73	2
Q8BGU5	Cyclin-Y	7.72	2
B2RXA1	Plcxd2	7.69	2
Q61769	Ki-67 protein	7.69	2
Q09XV5	Chromodomain-helicase-DNA-binding protein 8	7.67	2
Q00941	GM-CSF-R-alpha	7.66	3
Q7M6Z4	Kinesin-like protein KIF27	7.66	3
A0JNY3	Gephyrin	7.65	2
Q8CDC7	Zinc finger and BTB domain-containing protein 9	7.64	2
Q9WV35	Probable C->U-editing enzyme APOBEC-2	7.59	2

P09066	Homeobox protein engrailed-2	7.53	2
Q499F8	Zinc finger protein 445	7.52	3
Q7TMQ7	WD repeat-containing protein 91	7.52	3
Q8VHQ2	Suppressor of cytokine signaling 7	7.52	3
Q8VI46	Canalicular multispecific organic anion transporter 1	7.51	3
B2RY84	Kinesin family member 14	7.47	3
A5J0L5	Interleukin 21	7.47	2
Q2TAW4	Myosin, heavy polypeptide 6, cardiac muscle, alpha	7.42	3
Q8VGG7	Olfactory receptor 1282	7.40	3
Q75WC0	DNA polymerase subunit gamma-1	7.35	3
Q922Y0	Dual specificity tyrosine-phosphorylation-regulated kinase 3	7.34	2
Q8CH25	SAFB-like transcription modulator	7.32	3
Q497I5	Late cornified envelope 3A	7.31	3
Q9D8S3	ADP-ribosylation factor GTPase-activating protein 3	7.31	2
B2RY58	Hyperpolarization-activated, cyclic nucleotide-gated K ⁺ 4	7.30	3
Q9JI44	DNA methyltransferase 1-associated protein 1	7.24	2
Q8K566	Cysteine sulfinic acid decarboxylase	7.23	3
A2AQ50	Solute carrier family 12 member 1	7.22	2
P43142	G-protein coupled receptor 182	7.21	2
B7ZWG5	Coiled-coil domain containing 60	7.20	2
Q6P5H2	Nestin	7.20	3
Q8BWF0	Succinate-semialdehyde dehydrogenase, mitochondrial	7.19	4
B7ZNX6	ErbB2 interacting protein	7.17	2
Q14CH0	Family with sequence similarity 171, member B	7.17	3
Q3U319	E3 ubiquitin-protein ligase BRE1B	7.14	2
Q924W5	Structural maintenance of chromosomes protein 6	7.11	2
Q99JX6	Annexin A6	7.10	2
Q9CRT8	Exportin-T	7.08	2
A2BGH0	BPI fold-containing family B member 4	7.07	2
B2RXZ4	Kcn10a	7.00	2
B2RY11	ATP-binding cassette, sub-family A (ABC1), member 12	7.00	2
E9QPI0	HEAT repeat-containing protein 5A	7.00	2
Q7M6Z8	Kinesin light chain 1F	6.99	3
Q8R1Q3	Angiopoietin-related protein 7	6.96	2
Q8VGD0	Olfactory receptor 25	6.96	2
Q5DTY9	BTB/POZ domain-containing protein KCTD16	6.93	2
Q9WU22	Tyrosine-protein phosphatase non-receptor type 4	6.92	2

P0C5J4	Probable G-protein coupled receptor 52	6.91	2
Q5SSG4	Growth arrest-specific 2 like 1	6.91	2
Q9ER73	Elongator complex protein 4	6.91	2
Q62234	Myomesin-1	6.90	2
Q3MI48	Junctional sarcoplasmic reticulum protein 1	6.88	2
B9EKE4	Periphrin 1	6.87	2
Q6R5P3	Zinc finger protein 677	6.84	4
Q8N7N5	DDB1- and CUL4-associated factor 8	6.84	2
Q91Z67	SLIT-ROBO Rho GTPase-activating protein 2	6.83	2
Q7TNB8	Strawberry notch homolog 2	6.80	2
Q4VAA2	Carnitine deficiency-associated gene expressed in ventricle 3	6.79	3
Q8K087	G-protein coupled receptor 1	6.79	2
Q3URU2	Paternaly-expressed gene 3 protein	6.78	2
Q80YP3	Chromosome-associated kinesin KIF4	6.77	2
Q80U57	Regulating synaptic membrane exocytosis protein 3	6.77	4
Q3UXK8	Biglycan	6.76	2
Q91YD6	Villin-like protein	6.76	3
Q80W93	Hydrocephalus-inducing protein	6.75	2
B9EJA6	Tubulin tyrosine ligase-like family, member 6	6.74	2
Q61193	Ral guanine nucleotide dissociation stimulator-like 2	6.73	3
C3S7Q6	Ojoplano variant B	6.71	2
Q059P4	Filamin A interacting protein 1	6.71	2
Q76HP3	Transmembrane protein 132D	6.70	4
Q62000	Mimecan	6.69	5
Q14C50	Solute carrier family 27 (Fatty acid transporter), member 6	6.66	3
Q52KG5	Kinesin-like protein KIF26A	6.66	3
Q9CX00	Increased sodium tolerance 1 homolog (yeast)	6.65	2
Q3B807	Transcription elongation regulator 1-like protein	6.63	2
B7ZMT5	Multimerin 1	6.60	2
E9QLR6	Serine/threonine-protein kinase SMG1	6.60	2
Q9DBD2	E3 ubiquitin-protein ligase MARCH8	6.60	2
Q0VGI9	Gata5 protein	6.58	2
B7ZNW9	Slit homolog 2 (Drosophila)	6.55	2
A1L343	Transglutininase 3	6.51	2
B2RU69	CUB and zona pellucida-like domain-containing protein 1	6.51	2
Q8BML1	Protein-methionine sulfoxide oxidase MICAL2	6.49	3
B7ZNK9	Spermatogenesis associated 5	6.48	2
B2RWX1	Rho GTPase activating protein 21	6.47	2
Q91W97	Hexokinase domain containing 1	6.47	3

Q9EQW6	Oligodendrocyte transcription factor 2	6.47	2
B9EJ52	ATPase, class V, type 10D	6.46	2
E2IUN6	Shugoshin-like 2B	6.45	2
B2RXY1	Spock1	6.42	2
Q05A56	Hyaluronidase-4	6.40	2
Q8BXV2	Bri3 binding protein	6.40	3
Q8CI43	Myosin light chain 6B	6.39	3
D3Z0W5	Inactive phospholipase C-like protein 1	6.38	2
Q8CGY8	Ogt	6.36	2
Q6PDB6	Prolactin-2C3	6.34	4
Q76LL6	FH1/FH2 domain-containing protein 3	6.33	2
P56384	ATP synthase lipid-binding protein, mitochondrial	6.32	3
Q8C0S1	DIS3 mitotic control homolog (<i>S. cerevisiae</i>)-like	6.31	2
B2RUG6	Dedicator of cytokinesis 4	6.30	2
Q6PFX2	BEN domain-containing protein 6	6.26	2
Q5SX39	Myosin-4	6.26	3
B7ZND5	Purinergic receptor P2X, ligand-gated ion channel, 1	6.23	2
A2AIM4	Tropomyosin beta chain	6.21	2
P47856	Glutamine fructose-6-phosphate amidotransferase 1	6.21	2
A2ALI5	Adherens junction-associated protein 1	6.20	2
Q8QZR5	Alanine aminotransferase 1	6.17	3
Q921I6	SH3 domain-binding protein 4	6.14	2
P47810	Wee1-like protein kinase	6.11	2
Q571C7	Transcription factor TFIIB component B" homolog	6.11	2
Q7TNU9	Regulator of G-protein signaling 16	6.09	5
Q9EST3	Eukaryotic translation initiation factor 4E transporter	6.09	2
Q7TSZ1	Xeroderma pigmentosum, complementation group C	6.09	4
E9QNJ2	Leucine-rich repeat serine/threonine-protein kinase 2	6.06	2
Q7M710	Taste receptor type 2 member 125	6.05	3
Q5ISE2	Zinc finger protein 36, C3H1 type-like 3	6.04	2
Q8R0Z4	Sorting nexin 6	6.04	3
Q5ISE2	Zinc finger protein 36, C3H1 type-like 3	6.04	2
Q8CDK3	IQ and ubiquitin-like domain-containing protein	6.02	3
B1ATT5	Ketosamine-3-kinase	6.01	2
B2KFW1	Zinc finger and SCAN domain-containing protein 20	6.01	2
P60867	40S ribosomal protein S20	6.01	2
Q3U452	ATP synthase subunit alpha	6.01	2

Q3V1I0	Lysozyme g-like protein 2	5.99	3
Q8BI72	CDKN2A-interacting protein	5.95	2
Q8BKY8	mTERF domain-containing protein 3, mitochondrial	5.95	2
E9QKZ9	Proline-rich transmembrane protein 4	5.94	2
D3Z7P3	Glutaminase kidney isoform, mitochondrial	5.94	2
Q8K2G3	DiGeorge syndrome critical region gene 2	5.93	3
Q148W1	Solute carrier organic anion transporter family, member 5A1	5.91	2
Q8K2N9	Annexin A8	5.91	2
A3KGI4	Cancer susceptibility candidate 5	5.89	2
Q61221	Hypoxia-inducible factor 1-alpha	5.77	3
Q80U56	Late secretory pathway protein AVL9 homolog	5.75	3
Q6ZQH8	Nucleoporin NUP188 homolog	5.74	5
Q8R4E6	Purine-rich element-binding protein gamma	5.74	2
Q9QZ83	Gamma actin-like protein	5.72	2
Q8BKT2	Transcription factor HES-7	5.70	4
B2RPV0	Dmrta1	5.69	2
B2RXX1	Centrosomal protein 110	5.69	2
P70277	Alpha-N-acetylgalactosaminide alpha-2,6- sialyltransferase 2	5.68	2
B2RUJ4	ATPase family, AAA domain containing 5	5.67	2
Q8BL06	Inactive ubiquitin carboxyl-terminal hydrolase 54	5.67	3
Q9EPU0	Regulator of nonsense transcripts 1	5.67	2
A7XUZ6	Selection and upkeep of intraepithelial T-cells protein 6	5.67	2
B1AWS8	Angiopoietin-1 receptor	5.65	2
A2AM05	Centlein	5.64	2
Q05D38	RAB27b, member RAS oncogene family	5.63	2
Q9Z247	Peptidyl-prolyl cis-trans isomerase FKBP9	5.63	2
Q7M6Y6	Maestro heat-like repeat-containing protein family member 2B	5.62	4
Q640L5	Coiled-coil domain-containing protein 18	5.60	3
B2RY18	FERM and PDZ domain containing 1	5.58	2
Q0V930	Talin 1	5.58	2
Q80ZQ0	Sperm acrosome membrane-associated protein 4	5.58	4
Q0VGQ5	PI3K-alpha	5.57	3
B2RWS7	Zinc finger protein 609	5.54	2
F1ABR9	Ager	5.54	2
B6ZCE5	Proteinase 3	5.54	2
Q3KPB0	Olfactory receptor 616	5.54	2
Q8JZU4	Forkhead box A3	5.53	2
D3Z6S9	Family with sequence similarity 194, member A	5.52	2
Q148W8	Inactive dual specificity phosphatase 27	5.52	2

B4XVN8	SET domain bifurcated protein 2 variant A.1	5.51	2
P16015	Carbonic anhydrase 3	5.51	2
Q8BIW9	Chromosome transmission fidelity protein 18 homolog	5.49	4
A1L3S7	Gatad2b	5.48	2
Q149F3	Gspt2	5.45	2
Q64163	Transcription factor Dp-2	5.45	2
Q8VED5	Keratin, type II cytoskeletal 79	5.41	2
Q7TPR0	E3 ubiquitin-protein ligase RNF14	5.40	3
Q8CCP0	Nuclear export mediator factor	5.38	2
Q5D0D8	Glucosaminyl (N-acetyl) transferase 1, core 2	5.36	2
Q6PB60	Basic helix-loop-helix domain containing, class B9	5.36	2
Q9CWR8	DNA (cytosine-5)-methyltransferase 3-like	5.35	2
E9Q6U9	Collagen alpha-2(I) chain	5.35	3
Q62381	Toll-like protein 1	5.33	7
Q91Y06	Protocadherin beta 13	5.33	2
Q8CG46	Structural maintenance of chromosomes protein 5	5.33	2
Q52KI9	Zinc finger protein 592	5.32	2
Q5DTM8	E3 ubiquitin-protein ligase BRE1A	5.31	2
Q6NS59	Family with sequence similarity 135, member A	5.30	2
Q99LG0	Ubiquitin carboxyl-terminal hydrolase 16	5.30	2
A2AQ19	RNA polymerase-associated protein RTF1 homolog	5.27	2
B2RWU4	Cordon-bleu	5.27	2
B2RWU4	Zinc finger protein 609	5.27	2
B7ZMU4	Rho-related BTB domain containing 1	5.23	2
Q3LRV6	Voltage-gated chloride channel CIC-4A	5.22	2
A2AA59	PHD Finger protein 15	5.21	2
D3YYK0	Abhydrolase domain containing 11, isoform CRA_b	5.21	3
P50396	Rab GDP dissociation inhibitor alpha	5.21	2
Q6IRU2	Tropomyosin alpha-4 chain	5.20	2
Q8CHE4	Phlpp1	5.19	3
Q8JZQ3	ST8 alpha-N-acetyl-neuraminide alpha-2,8-sialyltransferase 5	5.18	2
Q9D2I5	LisH domain-containing protein ARMC9	5.17	2
Q99K58	Fibulin 2	5.14	3
Q4FZC9	Nesprin-3	5.13	2
A2RT18	Testis expressed gene 16	5.12	2
Q14BE5	Forkhead box B2	5.12	2
Q99J95	Cyclin-dependent kinase 9	5.12	2
A2A6H3	F-box only protein 47	5.11	2
Q8BVN3	Cation channel sperm-associated protein 4	5.06	2

Q6DIC7	Phosphatidylinositol 4-kinase, catalytic, alpha polypeptide	5.04	3
P19001	Keratin, type I cytoskeletal 19	5.00	2
Q05AH2	Zinc finger, CW type with PWWP domain 2	4.99	2
Q64433	10 kDa heat shock protein, mitochondrial	4.99	7
Q7TQU4	Olfactory receptor 1361	4.99	3
P09027	Homeobox protein Hox-D3	4.97	2
Q05BG1	CCR4-NOT transcription complex, subunit 4	4.96	2
E9QKT8	Alstrom syndrome protein 1 homolog	4.93	2
P28654	Decorin	4.93	2
B2RWX5	Centrosomal protein 250	4.91	2
Q5F204	Putative malate dehydrogenase 1B	4.91	8
Q8VI16	B3gnt9	4.88	2
Q2KHP0	Kcna1	4.87	3
E9QNC3	Serine/threonine-protein kinase Nek11	4.86	2
Q9D3D0	Alpha-tocopherol transfer protein-like	4.85	2
P08905	Lysozyme C-2	4.85	2
Q0VGB8	Synaptic nuclear envelope 1	4.83	2
Q8VDU9	Tripartite motif containing 41	4.82	3
B2RRD1	Tudor domain containing 6	4.81	2
Q9JK37	Myozenin-1	4.80	2
Q14AP0	Thioredoxin domain containing 8	4.78	2
Q8C120	SH3 domain-containing RING finger protein 3	4.77	2
Q9WVS5	Chaperonin containing TCP-1 theta subunit	4.77	2
Q0VDP6	Hypocretin (orexin) receptor 1	4.76	3
Q78HU3	Multivesicular body subunit 12A	4.74	2
Q9DD20	Methyltransferase-like protein 7B	4.71	2
E9QJZ4	Fibrillin-2	4.69	2
B9EKK3	IQ motif containing GTPase activating protein 2	4.68	2
P00920	Carbonic anhydrase 2	4.67	2
E9QKV8	Nrde-2 necessary for RNA interference, domain containing	4.65	3
Q3V3F1	Nicotinamide mononucleotide adenylyltransferase 3	4.65	2
A2BE28	Ribosomal biogenesis protein LAS1L	4.64	2
B7ZP22	Heterogeneous nuclear ribonucleoprotein A2/B1	4.64	2
B2RWX4	Rint1	4.63	2
Q05BH2	Tetraspanin-5	4.63	3
B1AXY5	Beta-1,4-galactosyltransferase 1	4.62	2
P11679	Keratin, type II cytoskeletal 8	4.62	2
Q75WD0	Protein-arginine deiminase type-2	4.61	3
P28665	Murinoglobulin-1	4.59	2
Q80TA6	Myotubularin-related protein 12	4.58	3

P59530	Taste receptor type 2 member 7	4.58	2
P51150	Ras-related protein Rab-7a	4.57	2
Q68EF9	Signal peptide, CUB domain, EGF-like 1	4.56	2
D5MP63	Kinesin-like protein KIF26B	4.55	2
B7FAU9	Filamin, alpha	4.54	2
A1A557	Cartilage oligomeric matrix protein	4.52	2
E9QMY2	E3 ubiquitin-protein ligase CBL-B	4.50	2
Q7TNT9	Elk3	4.50	3
C4P6S0	Sperm head and tail associated protein	4.49	2
Q9JJJ0	Calcium transporting protein homolog	4.49	2
Q6PBG2	NADH dehydrogenase (ubiquinone) 1 alpha subcomplex 11	4.47	2
E9Q010	Dynein heavy chain 8, axonemal	4.46	4
Q6SLK2	Protein kinase lysine deficient 1	4.42	4
B2RXT5	Glucose-6-phosphate isomerase	4.39	2
O55124	Myomesin 2	4.38	2
Q62261	Spectrin beta chain, non-erythrocytic 1	4.37	4
O88329	Unconventional myosin-Ia	4.36	2
Q3TIU4	2',5'-phosphodiesterase 12	4.35	2
E3VWA1	Slc4a4	4.31	2
Q8R2H9	Phosphatase, orphan 1	4.31	2
Q9CSH3	Exosome complex exonuclease RRP44	4.30	2
Q810R0	Sycp3 like Y-linked	4.28	4
O70251	Elongation factor 1-beta	4.27	2
A2AHK7	Mucin-15	4.26	2
B2RXX7	Nance-Horan syndrome	4.25	2
E9QM71	Cytoplasmic dynein 1 heavy chain 1	4.24	2
Q8BFZ3	Actin, beta-like 2	4.24	3
Q04899	Cyclin-dependent kinase 18	4.22	3
Q0VB79	T-cell ecto-ADP-ribosyltransferase 1	4.21	2
Q9EQD6	Keratin intermediate filament 16a	4.20	2
Q2WF71	Lrfr1	4.20	2
B8XCJ6	Protein unc-80 homolog	4.18	2
Q6P9Q2	Polymerase (RNA) I polypeptide B	4.18	5
Q9CVL5	CutA divalent cation tolerance homolog	4.16	2
O88799	Zonadhesin	4.15	2
Q9EPL8	Importin-7	4.14	2
Q1ZZX0	Toll-like receptor 5	4.13	2
Q8CIP4	MAP/microtubule affinity-regulating kinase 4	4.13	3
Q9EPS7	Pheromone receptor V3R6	4.13	2
Q921T1	Transforming growth factor, beta 2	4.12	2
E9PZZ1	PR domain zinc finger protein 13	4.10	2
Q2XP45	Phosphatidic acid-preferring phospholipase A1	4.10	2

	variant 2		
E9QMR9	Protocadherin Fat 4	4.07	2
Q91ZF5	Calcium-activated chloride channel CLCA4	4.06	2
P27573	Myelin protein P0	4.06	2
Q99P72	Reticulon-4	4.06	2
B7ZMZ7	DIP2 disco-interacting protein 2 homolog C (Drosophila)	4.04	2
Q91WB5	Androgen binding protein alpha	4.04	2
Q8C963	Coiled-coil domain-containing protein 159	4.01	2
Q8K0J2	B3gnt7	4.01	2
Q8VDV3	Guanine nucleotide exchange factor for Rab-3A	4.01	3
Q8K287	Armadillo repeat containing 5	4.00	2
Q05DC5	Mitochondrial ribosomal protein L3	3.99	2
E9PV27	Pheromone receptor V3R1	3.96	2
Q924J9	Six-transmembrane epithelial antigen of the prostate	3.94	2
B7ZWK3	Spectrin alpha, non-erythrocytic 1	3.89	2
C6EQH2	ASL1/Herc2 fusion protein	3.88	2
P04104	Keratin, type II cytoskeletal 1	3.88	2
P62878	E3 ubiquitin-protein ligase RBX1	3.88	2
B7ZNM9	DNA topoisomerase 1, mitochondrial	3.86	2
Q8R429	Sarcoplasmic/endoplasmic reticulum calcium ATPase 1	3.86	2
B2RQL6	Myosin light chain kinase 3	3.85	2
A2ADF7	Solute carrier family 25 member 34	3.82	2
Q9D2X5	MAU2 chromatid cohesion factor homolog	3.80	2
Q99L13	3-hydroxyisobutyrate dehydrogenase, mitochondrial	3.77	3
Q9JI38	tRNA pseudouridine(38/39) synthase	3.77	2
Q4VBF8	Signal-induced proliferation-associated 1 like 1	3.76	3
Q8C0P0	Microtubule associated serine/threonine kinase-like	3.76	4
E9QAC1	Bromodomain and WD repeat-containing protein 1	3.75	3
Q8R1X8	Oxysterol-binding protein 6	3.75	2
A0AUM9	Translation initiation factor eIF-2B subunit gamma	3.75	2
B1ARM7	Aspm1	3.75	2
A6NAW3	Alpha46-takusan	3.73	2
D3YZF7	V-set and immunoglobulin domain-containing protein 10-like	3.72	4
E3VVQ8	Supervillin muscle-specific isoform	3.72	2
Q6NS69	APC membrane recruitment protein 3	3.72	5
B7ZWN0	Sodium channel, voltage-gated, type IX, alpha	3.69	2

Q0VBT4	Tryptophan 5-hydroxylase 2	3.66	2
B2RY47	Rhotekin 2	3.65	2
B2RXR3	CCR4-NOT transcription complex, subunit 1	3.64	2
Q1XGY5	Fras1 related extracellular matrix protein 2	3.62	3
Q8K203	Endonuclease 8-like 3	3.62	3
Q9JK98	Clusterin	3.62	2
Q61282	Aggrecan core protein	3.62	2
Q922R7	Testis expressed gene 10	3.60	3
B2RSV7	FYVE, RhoGEF and PH domain containing 6	3.57	2
Q99MQ4	Asporin	3.57	3
B2RX10	Fanconi anemia, complementation group M	3.56	3
Q80UM4	Tyrosine-protein phosphatase non-receptor type 12	3.54	2
Q0QJG0	Nanog homeobox pseudogene	3.53	3
Q04447	Creatine kinase B-type	3.52	2
Q6NV59	Lysyl oxidase-like 4	3.48	2
Q8K0R1	Zinc finger protein 644	3.47	3
B1AWC9	Phosphodiesterase 4B, cAMP specific	3.45	2
B9UM22	G-protein-coupled receptor 81	3.45	2
Q03172	Zinc finger protein 40	3.45	3
Q8CFE8	F-box and WD-40 domain protein 17	3.45	3
Q148V8	Family with sequence similarity 83, member H	3.43	3
Q8CH77	Neuron navigator 1	3.43	2
C6EQK3	L1 unspliced fusion gene protein	3.42	2
A2AQ14	Protein Mis18-beta	3.41	2
P15533	Tripartite motif-containing protein 30A	3.36	2
B7ZN63	PRELI domain containing 2	3.33	2
P70124	Serpin B5	3.33	2
Q7M753	Pantothenate kinase 2	3.32	3
Q8BHL3	TBC1 domain family member 10B	3.32	3
Q7TQ32	Hemojuvelin	3.32	2
Q9CQ52	Chymotrypsin-like elastase family member 3B	3.31	3
Q9CQ52	Chymotrypsin-like elastase family member 3B	3.31	3
B7ZNT3	Signal-regulatory protein beta 1C	3.30	2
B8JJ87	Apoptotic chromatin condensation inducer in the nucleus	3.30	2
O35452	Tenascin X	3.30	2
B8JJ87	Apoptotic chromatin condensation inducer in the nucleus	3.30	2
B2RY09	Enhancer trap locus 4	3.29	2
Q6GUA3	Periostin, osteoblast specific factor	3.29	2
B2RY09	Enhancer trap locus 4	3.29	2
B9EKA5	Melanophilin	3.28	2

Q7TMG7	Natriuretic peptide receptor 3	3.28	3
E9QLA1	Adamts20	3.26	2
Q9CR78	Myb/SANT-like DNA-binding domain-containing protein 3	3.24	2
Q91X22	Serpina1b	3.20	3
P43274	Histone H1.4	3.19	4
B7SNM9	Transformed mouse 3T3 cell double minute 1	3.15	2
P08399	Putative per-hexamer repeat protein 5	3.15	2
B7SNM9	Transformed mouse 3T3 cell double minute 1	3.15	2
B2RSU6	Cingulin-like 1	3.14	2
B2RXM4	Alpha N-terminal protein methyltransferase 1B	3.12	2
Q5F259	Ankyrin repeat domain-containing protein 13B	3.10	2
Q58IU7	Cathepsin R	3.07	2
Q91ZQ1	cGMP phosphodiesterase 6C	3.07	3
B2RQR2	Multiple PDZ domain protein	3.06	2
D6RGA8	Coenzyme Q2 homolog, prenyltransferase (yeast)	3.06	2
P63058	Thyroid hormone receptor alpha	3.04	2
B2RRJ9	Adenylate cyclase type 10	3.02	2
A2AFK4	GTP binding protein 5, isoform CRA_a	3.01	2
B9EKT6	IQ motif containing GTPase activating protein 3	3.01	2
P07724	Serum albumin	3.01	2
P51612	DNA repair protein complementing XP-C cells homolog	3.00	2
A2ARZ3	Fibrous sheath-interacting protein 2	2.99	2
Q9CWI9	Bifunctional purine biosynthesis protein PURH	2.98	2
Q61584	Fragile X mental retardation syndrome-related protein 1	2.97	2
Q61584	Fragile X mental retardation syndrome-related protein 1	2.97	2
Q3TJG2	Acyl carrier protein	2.95	2
B2RUA0	Vomerolateral 1 receptor, I2	2.95	2
Q80ZS3	28S ribosomal protein S26, mitochondrial	2.93	3
Q8BZ71	SH3 and cysteine-rich domain-containing protein 3	2.93	2
P97401	Secreted frizzled-related protein 3	2.90	3
Q2NKY1	Thyroglobulin	2.90	3
P70196	TNF receptor-associated factor 6	2.88	4
Q8K4C5	Interleukin-17C	2.87	2
B7ZNH7	Collagen alpha-1(XIV) chain	2.86	2
Q8CFJ9	WD repeat-containing protein 24	2.86	3
P13542	Myosin-8	2.86	2
B1ATA2	CASK-interacting protein 2	2.84	2
Q0P5X1	Leucine-rich repeat and IQ domain-containing protein 1	2.83	2

Q0VIFY6	Zinc finger, DHHC domain containing 17	2.82	3
Q80TR8	Vpr (HIV-1) binding protein	2.81	2
P51885	Lumican	2.80	2
Q9CXZ1	Ndufs4	2.80	2
Q6PG97	CD1d2	2.80	4
P08228	Superoxide dismutase [Cu-Zn]	2.78	2
A9Q751	Primary ciliary dyskinesia protein 1	2.76	2
B8QI35	Liprin-alpha 3	2.76	2
P09542	Myosin light chain 3	2.76	2
Q8C7H1	Methylmalonic aciduria type A homolog, mitochondrial	2.74	2
D3YXT2	ribosomal protein L10A, pseudogene 2	2.72	2
Q6PGN3	Serine/threonine-protein kinase DCLK2	2.72	4
Q6NXJ0	WW, C2 and coiled-coil domain containing 2	2.71	5
Q8R3C0	Mini-chromosome maintenance complex-binding protein	2.71	3
Q05BZ2	Poly (ADP-ribose) polymerase family, member 6	2.71	2
Q543V3	Insulin receptor substrate 1	2.71	4
Q8K1X1	WD repeat-containing protein 11	2.70	2
D3Z6F5	ATP synthase subunit alpha	2.68	2
D3Z6J1	DEP domain containing 1a, isoform CRA c	2.68	3
E9QNM2	Histone-lysine N-methyltransferase ASH1L	2.68	2
P68254	14-3-3 protein theta	2.68	2
Q5M956	BTB/POZ domain-containing protein KCTD1	2.68	2
B6VJS3	5-hydroxytryptamine receptor 7	2.67	2
C9K0Y7	AMPA-selective glutamate receptor 4 flop type	2.61	2
O35409	Glutamate carboxypeptidase 2	2.60	2
B7ZNV8	Ankyrin repeat domain 42	2.54	2
Q5SW50	Olfactory receptor 462	2.51	3
Q6PFZ4	Structural maintenance of chromosomes 3	2.50	3
Q8VCK3	Tubulin gamma-2 chain	2.49	3
Q9CR68	Cytochrome b-c1 complex subunit Rieske, mitochondrial	2.45	2
P97952	Sodium channel subunit beta-1	2.41	2
Q3TDU5	Milk fat globule-EGF factor 8 protein, isoform CRA_a	2.41	2
Q497I4	Keratin, type I cuticular Ha5	2.41	2
A2AEP2	Cyclin B3	2.40	2
P97321	Seprase	2.40	2
P97321	Seprase	2.40	2
B9EKJ4	YEATS domain containing 2	2.39	2
P61982	14-3-3 protein gamma	2.38	2
Q14B48	Coiled-coil domain-containing protein 129	2.37	2

Q14BM5	Nephrocystin-3	2.37	2
Q8R3R8	Gamma-aminobutyric acid receptor-associated protein-like 1	2.37	2
Q8VE11	Myotubularin-related protein 6	2.37	3
Q61166	Microtubule-associated protein RP/EB family member 1	2.36	5
E9QPG9	Extracellular matrix protein FRAS1	2.35	2
Q8CFE4	SCY1-like protein 2	2.35	2
O70577	Solute carrier family 22 member 2	2.30	2
B7ZNI2	Ankyrin and armadillo repeat containing	2.28	2
E9PUH2	Fam208A	2.26	2
D3Z4L1	Mthfsd	2.24	3
B7ZNX0	AF4/FMR2 family, member 4	2.23	2
Q14BE7	Family with sequence similarity 47, member A	2.23	3
Q3UW98	Chloride channel calcium activated 7	2.23	2
B6ZHD0	Erythrocyte protein band 4.1-like 2	2.23	2
E9Q8I9	Furry homolog	2.22	2
Q0V8T7	Contactin-associated protein like 5-3	2.22	2
Q9CQU1	Microfibrillar-associated protein 1	2.21	3
Q61176	Arginase-1	2.19	3
B2RQL2	Storkhead box 1	2.18	2
P27773	Protein disulfide-isomerase A3	2.18	2
E9PYY5	WD repeat-containing protein 78	2.16	2
P20065	Thymosin beta-4	2.16	2
E9QPH5	Sterile alpha motif domain-containing protein 3	2.15	2
Q9R0L7	A-kinase anchor protein 8-like	2.12	2
Q0VBL1	Tigger transposable element-derived protein 2	2.11	2
Q8VIE5	BetaIV-spectrin sigma1	2.10	2
Q08EI4	Matrix metalloproteinase 21	2.07	4
P52480	Pyruvate kinase PKM	2.04	9
Q14BE0	Molybdenum cofactor synthesis 3	2.04	3
Q61884	Meiosis-specific nuclear structural protein 1	2.04	2
Q8QZX2	HAUS augmin-like complex subunit 3	2.04	3
B9EHI6	Oviductal glycoprotein 1, 120kDa	2.03	2
Q8VDU0	G-protein signalling modulator 2	2.03	2
P30933	Seminal vesicle secretory protein 5	2.03	4
Q402U7	Serine protease 44	2.02	3
Q32NZ7	Cingulin	2.00	2
Q8C4X2	Casein kinase 1, gamma 3	2.00	3
Q9D2D7	Zinc finger protein 687	2.00	2
Q9CZP7	Hsp90 co-chaperone Cdc37-like 1	1.99	2
Q059Q0	Coiled-coil domain containing 11	1.97	3
Q8BYK4	Retinol dehydrogenase 12	1.94	3

Q91VK0	Proprotein convertase subtilisin/kexin type 5	1.93	3
B7ZMW6	CD163	1.91	2
Q3TLH4	Proline-rich coiled-coil 2C	1.91	2
Q0KIX1	KIBRA	1.91	4
Q148A4	Protein phosphatase 1 regulatory subunit 32	1.90	3
P13541	Myosin-3	1.90	2
Q9R1A8	E3 ubiquitin-protein ligase RFWD2	1.89	2
A2A9C3	Protein SZT2	1.89	2
Q5XKN4	Jagunal homolog 1	1.88	2
B7ZN50	Syntaxin binding protein 5-like	1.87	2
A0JNY7	Eukaryotic translation initiation factor 4 gamma 2	1.86	2
Q61852	Smooth muscle gamma-actin	1.86	2
D0VLQ5	Tet methylcytosine dioxygenase 2	1.85	2
P29754	Type-1A angiotensin II receptor	1.85	2
Q03142	Fibroblast growth factor receptor 4	1.85	3
Q8BFW9	Slc2a12	1.85	2
Q3UHZ5	Leiomodin-2	1.85	2
C7TQ59	Calcium channel voltage-dependent alpha1c subunit	1.83	2
Q6DFW4	Nucleolar protein 58	1.82	5
B1AR69	Myosin, heavy chain 13, skeletal muscle	1.82	2
Q01097	Glutamate receptor ionotropic, NMDA 2B	1.76	2
Q6PCN6	Microrachidia 2A	1.75	3
Q99JF5	Diphosphomevalonate decarboxylase	1.75	2
Q9DBS8	Centrosomal protein POC5	1.75	2
B2RQS6	DEAH (Asp-Glu-Ala-His) box polypeptide 36	1.74	2
Q8CJ70	Interleukin-19	1.74	2
P51881	ADP/ATP translocase 2	1.72	4
B1B1A8	Myosin light chain kinase, smooth muscle	1.72	2
Q99ML9	E3 ubiquitin-protein ligase Arkadia	1.71	3
C3S7Q5	Ojoplano variant A	1.70	2
P63028	Translationally-controlled tumor protein	1.68	2
Q8C0F9	Inactive serine protease 35	1.68	4
Q5H8C4	Vacuolar protein sorting-associated protein 13A	1.67	4
Q501L5	Osteomodulin	1.64	3
P07744	Keratin, type II cytoskeletal 4	1.63	2
Q8VII7	Receptor activity modifying protein 1	1.62	2
B9EHJ7	Tcf20 protein	1.60	2
E9QMH9	Nuclear receptor coactivator 2	1.60	2
Q8CCX5	Keratin 222	1.59	2
B7ZNV2	GLI-Kruppel family member GLI3	1.58	2
Q8C761	WD repeat-containing protein 60	1.57	3
P62082	40S ribosomal protein S7	1.56	2

B9EKS2	Jumonji domain containing 1B	1.55	2
B9EKC6	Aldehyde oxidase 3-like 1	1.54	2
Q7M759	Alpha/beta hydrolase domain-containing protein 17B	1.47	2
E9QNG9	Serine/threonine-protein kinase B-raf	1.44	2
P08730	Keratin, type I cytoskeletal 13	1.39	2
B7ZND9	Testis expressed gene 9	1.38	2
Q8K224	N-acetyltransferase 10	1.37	2
P17751	Triosephosphate isomerase	1.36	2
E9Q401	Ryanodine receptor 2	1.35	5
Q05D94	Copine VIII	1.35	2
Q0KK56	Family with sequence similarity 184, member B	1.33	4
Q3TRR0	Microtubule-associated protein 9	1.33	2
P53349	Mitogen-activated protein kinase kinase kinase 1	1.29	9
P70452	Syntaxin-4	1.28	2
P61082	NEDD8-conjugating enzyme Ubc12	1.27	2
Q7TQG5	Neogenin	1.27	2
Q3UEH4	Pyruvate kinase liver and red blood cell	1.26	2
E9Q555	E3 ubiquitin-protein ligase RNF213	1.17	5
Q8VG97	Olfactory receptor 1132	1.16	3
Q8VG50	Olfactory receptor 922	1.15	2
Q62018	RNA polymerase-associated protein CTR9 homolog	1.14	2
Q8CHW3	Mitochondrial ribosomal protein L23	1.11	3
Q9JKE5	ELKL motif kinase 2 long form	1.05	2
Q99JY8	Lipid phosphate phosphohydrolase 3	1.04	2
Q9D168	Integrator complex subunit 12	0.96	2
Q61784	ORF1	0.91	2
C9K0Z6	CNTF receptor alpha subunit	0.89	2
Q80UH6	Nucleotide-binding oligomerization domain containing 2	0.89	2
Q0VG46	Calcyphosphine 2	0.85	2
Q7TSF0	Desmoglein-1-gamma	0.84	2
B7ZWF1	DEAD (Asp-Glu-Ala-Asp) box helicase 3, X-linked	0.71	2
Q2YFS4	Zinc finger CW-type PWWP domain protein 1	0.34	2

APPENDIX C

Permission for Reproduction from Springer

SPRINGER LICENSE TERMS AND CONDITIONS

Nov 05, 2014

This is a License Agreement between Matthew R McCann ("You") and Springer ("Springer") provided by Copyright Clearance Center ("CCC"). The license consists of your order details, the terms and conditions provided by Springer, and the payment terms and conditions.

All payments must be made in full to CCC. For payment instructions, please see information listed at the bottom of this form.

License Number	3502441422641
License date	Nov 05, 2014
Licensed content publisher	Springer
Licensed content publication	Journal of Cell Communication and Signaling
Licensed content title	Exploiting notochord cells for stem cell-based regeneration of the intervertebral disc
Licensed content author	Matthew R. McCann
Licensed content date	Jan 1, 2011
Volume number	5
Issue number	1
Type of Use	Thesis/Dissertation
Portion	Excerpts
Author of this Springer article	Yes and you are a contributor of the new work
Order reference number	None
Title of your thesis / dissertation	Mouse models for intervertebral disc development, degeneration and whole-body vibration.
Expected completion date	Dec 2014
Estimated size(pages)	325
Total	0.00 USD
Terms and Conditions	

Introduction

The publisher for this copyrighted material is Springer Science + Business Media. By clicking "accept" in connection with completing this licensing transaction, you agree that the following terms and conditions apply to this transaction (along with the Billing and Payment terms and conditions established by Copyright Clearance Center, Inc. ("CCC"), at the time that you opened your Rightslink account and that are available at any time at <http://myaccount.copyright.com>).

Limited License

With reference to your request to reprint in your thesis material on which Springer Science and Business Media control the copyright, permission is granted, free of charge, for the use indicated in your enquiry.

Licenses are for one-time use only with a maximum distribution equal to the number that you identified in the licensing process.

This License includes use in an electronic form, provided its password protected or on the university's intranet or repository, including UMI (according to the definition at the Sherpa website: <http://www.sherpa.ac.uk/romeo/>). For any other electronic use, please contact Springer at (permissions.dordrecht@springer.com or permissions.heidelberg@springer.com).

The material can only be used for the purpose of defending your thesis limited to university-use only. If the thesis is going to be published, permission needs to be re-obtained (selecting "book/textbook" as the type of use).

Although Springer holds copyright to the material and is entitled to negotiate on rights, this license is only valid, subject to a courtesy information to the author (address is given with the article/chapter) and provided it concerns original material which does not carry references to other sources (if material in question appears with credit to another source, authorization from that source is required as well).

Permission free of charge on this occasion does not prejudice any rights we might have to charge for reproduction of our copyrighted material in the future.

Altering/Modifying Material: Not Permitted

You may not alter or modify the material in any manner. Abbreviations, additions, deletions and/or any other alterations shall be made only with prior written authorization of the author(s) and/or Springer Science + Business Media. (Please contact Springer at (permissions.dordrecht@springer.com or permissions.heidelberg@springer.com))

Reservation of Rights

Springer Science + Business Media reserves all rights not specifically granted in the combination of (i) the license details provided by you and accepted in the course of this licensing transaction, (ii) these terms and conditions and (iii) CCC's Billing and Payment terms and conditions.

Copyright Notice:Disclaimer

You must include the following copyright and permission notice in connection with any reproduction of the licensed material: "Springer and the original publisher /journal title, volume, year of publication, page, chapter/article title, name(s) of author(s), figure number(s), original copyright notice) is given to the publication in which the material was originally published, by adding; with kind permission from Springer Science and Business Media"

Warranties: None

Example 1: Springer Science + Business Media makes no representations or warranties with respect to the licensed material.

Example 2: Springer Science + Business Media makes no representations or warranties with

respect to the licensed material and adopts on its own behalf the limitations and disclaimers established by CCC on its behalf in its Billing and Payment terms and conditions for this licensing transaction.

Indemnity

You hereby indemnify and agree to hold harmless Springer Science + Business Media and CCC, and their respective officers, directors, employees and agents, from and against any and all claims arising out of your use of the licensed material other than as specifically authorized pursuant to this license.

No Transfer of License

This license is personal to you and may not be sublicensed, assigned, or transferred by you to any other person without Springer Science + Business Media's written permission.

No Amendment Except in Writing

This license may not be amended except in a writing signed by both parties (or, in the case of Springer Science + Business Media, by CCC on Springer Science + Business Media's behalf).

Objection to Contrary Terms

Springer Science + Business Media hereby objects to any terms contained in any purchase order, acknowledgment, check endorsement or other writing prepared by you, which terms are inconsistent with these terms and conditions or CCC's Billing and Payment terms and conditions. These terms and conditions, together with CCC's Billing and Payment terms and conditions (which are incorporated herein), comprise the entire agreement between you and Springer Science + Business Media (and CCC) concerning this licensing transaction. In the event of any conflict between your obligations established by these terms and conditions and those established by CCC's Billing and Payment terms and conditions, these terms and conditions shall control.

Jurisdiction

All disputes that may arise in connection with this present License, or the breach thereof, shall be settled exclusively by arbitration, to be held in The Netherlands, in accordance with Dutch law, and to be conducted under the Rules of the 'Netherlands Arbitrage Instituut' (Netherlands Institute of Arbitration). **OR:**

All disputes that may arise in connection with this present License, or the breach thereof, shall be settled exclusively by arbitration, to be held in the Federal Republic of Germany, in accordance with German law.

Other terms and conditions:

v1.3

Questions? customercare@copyright.com or +1-855-239-3415 (toll free in the US) or +1-978-646-2777.

Gratis licenses (referencing \$0 in the Total field) are free. Please retain this printable license for your reference. No payment is required.

APPENDIX D

Permission for Reproduction from The Company of Biologists

THE COMPANY OF BIOLOGISTS LIMITED

Bidder Building, 140 Cowley Road, Cambridge CB4 0DL, UK
Telephone: 44 (0)1223 433319 Fax: 44 (0)1223 423353 E-mail: dmm@biologists.com

LICENCE AGREEMENT: Creative Commons

6 September 2011

Author(s): Matthew R McCann, Owen J Tamplin, Janet Rossant, Cheryle A Seguin (the "Authors")

Title: Tracing notochord-derived cells using a novel Noto-cre mouse: implications for intervertebral disc development. (the "Article")

Journal: Disease Models & Mechanisms

We refer to the above and to your submission of the Article for publication in the Journal. By signing the acknowledgement at the end of this letter you agree to the following terms:

1. In consideration of the publication of your Article in the Journal, you hereby grant to the Company an exclusive (subject to paragraph 4), irrevocable, world wide, non-royalty bearing licence to exercise all rights prohibited by intellectual property protecting the Article including (without limitation) the rights to publish, reproduce, distribute, display and store the Article in both paper, electronic and other formats/ media, whether now known or hereafter developed for the duration of all rights therein (or, where you are a contributor, your contribution to the Article) for exploitation in all forms and media including on an open access basis as set out in paragraph 2. To avoid any doubt the foregoing shall include (without limitation) the rights to translate the Article and create adaptations, summaries, extracts and other derivative works based on the Article. You further grant to the Company the right to license third parties to do any or all of the foregoing. Paragraph 1 shall collectively be known as "Licensed Rights".
2. If the Article is published on an open access basis, it will be made freely available online for non-commercial use immediately following publication and shall be distributed under the terms of the Creative Commons Attribution Non Commercial Share Alike Licence (the terms of which are set out at <http://creativecommons.org/licenses/by-nc-sa/3.0/legalcode>). These terms permit the copying and/or adaptation of the Article and the distribution of the Article or any such adaptation by any means and in any medium or format to any other person, provided that (a) you are credited as the original author, (b) the Article or adaptation is only distributed on a non-commercial free-of-charge basis, and (c) all further distributions of the Article or adaptation (as applicable) must be subject to the same Creative Commons Licence terms. The Company intends to make the Article available on an open access basis via the Company's website.
3. You confirm that:
 - (i) you are the sole author and legal and beneficial owner of all copyright subsisting in the Article (or, where you are a contributor, your contribution to the Article) with full title guarantee;
 - (ii) you have full power to enter into this letter agreement;
 - (iii) the Article (or, where you are a contributor, your contribution to the Article) is an original Article;

<http://submit-dmm.biologists.org/submission/checklist?roleName=author&msedit=checklist...> 9/6/2011

- (iv) the Article (or, where you are a contributor, your contribution to the Article) does not contain anything which is libellous, defamatory, obscene, blasphemous or illegal and all statements in the Article purporting to be facts are true;
 - (v) the Article (or, where you are a contributor, your contribution to the Article) has not previously been published in whole or in part and is not currently under consideration for publication elsewhere;
 - (vi) any excerpt(s) from other Works which are contained in the Article (or, where you are a contributor, your contribution to the Article) have been used with the unrestricted written permission of the copyright owner (evidence of which has been provided to us) and any such excerpt(s) are clearly identified and acknowledged within the Article;
 - (vii) the Article is published with the knowledge and consent of all the authors and owners of any copyright relating to the Article;
 - (viii) nothing in the Article infringes any duty of confidentiality which you owe to any third party and that in providing the Company with the exclusive licence in this letter you are not in breach of any contract, express or implied, which you have with a third party (including without limitation an academic institution where you are employed); and
 - (ix) the exercise of the Licensed Rights will not infringe any rights belonging to any third party.
4. The Company acknowledges that ownership of copyright remains with you. For the avoidance of doubt and provided that you acknowledge reference to the publication of the Article in the Journal, the Company allows you to retain the following non-exclusive rights:
- (i) the right to reproduce the Article in whole or in part in any printed book (including thesis) of which you are the author;
 - (ii) the right for you and any academic institution where you are employed to reproduce in whole or in part the Article for the purpose of teaching students of the academic institution;
 - (iii) the right to post a copy of the Article on your own website provided (a) that the Article has already been published in the Journal; and (b) you provide a link between the web page containing the Article and the Journal's website currently at <http://dmm.biologists.org>; and
 - (iv) to use data and other information created by you and contained in the Article in other Articles created by you.
5. For the avoidance of doubt, if the research was funded in whole or in part by a grant from any organisation or entity that requires that any publication of the results of the research are placed in a publicly available repository (the "Repository") then the Company agrees that the Article may be placed in the relevant Repository provided that (a) that the Article has already been published in the Journal; and (b) you provide a link between the web page containing the Article and the Journal's website currently at <http://dmm.biologists.org>.
6. You hereby agree that responsibility for:
- (i) the accuracy of statements of fact;
 - (ii) the authenticity of scientific findings or observations;
 - (iii) expressions of scientific or other opinions; and

(iv) any other material published in this Article

rests solely with you and any other author(s) of the Article and that no responsibility for such matters is assumed by the Company or the Journal, its owners, publishers or staff (including referees).

7. Without limitation to paragraph 3(vii) if the Article includes illustrations, graphics, designs or any other material ("Material") for which you are not the copyright and related rights owner, you hereby declare that you have obtained full permission from the owners of that copyright and any other relevant rights and any other relevant publisher or licensee to allow the Company to reproduce the Material in paper, electronic and/or other formats for use alongside or incorporated in our Article in the Journal and for any other purpose reasonably ancillary to the Article, including abridgements, spin-off articles, any data compilation required for electronic or other searching/ cross-referencing or compilations etc.
8. You acknowledge that in accordance with UK law, and in particular Data Protection Legislation, authors must explicitly provide consent for their names and addresses to appear alongside the published article. You therefore authorise the Journal to include your name and e-mail address as part of or in relation to any publication containing the article, which may be distributed worldwide.
9. You assert your moral right to be identified as the author of the Work, and we agree to ensure that your name is clearly associated with the Work. Subject to the foregoing, you irrevocably and unconditionally waive all moral rights in respect of the Work to which you may now or at any time in the future be entitled whether arising under Part IV of the Copyright, Designs and Patents Act 1988 or under the law of any other jurisdiction
10. You agree, if so requested by the Company and at the Company's expense, to sign such further documents and do such things as may be necessary or desirable to perfect or confirm the licence of the Licensed Rights and, in territories where the Licensed Rights are registrable, to register the Licensed Rights in such territories as may be specified by the Company and in the Company's name.
11. You authorise the Company to take all steps as the Company considers, in its sole discretion, necessary, in your name and on your behalf, to protect and defend the Company's rights in the Article.

You agree that the terms of this exclusive licence shall be construed in accordance with English law and you agree to submit to the exclusive jurisdiction of the English courts.

.....
For and on behalf of The Company of Biologists Limited

APPENDIX E

Permission for Reproduction from John Wiley and Sons

JOHN WILEY AND SONS LICENSE TERMS AND CONDITIONS

Nov 05, 2014



This is a License Agreement between Matthew R McCann ("You") and John Wiley and Sons ("John Wiley and Sons") provided by Copyright Clearance Center ("CCC"). The license consists of your order details, the terms and conditions provided by John Wiley and Sons, and the payment terms and conditions.

All payments must be made in full to CCC. For payment instructions, please see information listed at the bottom of this form.

License Number	3502450308613
License date	Nov 05, 2014
Licensed content publisher	John Wiley and Sons
Licensed content publication	Arthritis & Rheumatism
Licensed content title	Acute Vibration Induces Transient Expression of Anabolic Genes in the Murine Intervertebral Disc
Licensed copyright line	Copyright © 2013 by the American College of Rheumatology
Licensed content author	Matthew R. McCann, Priya Patel, Kim L. Beaucage, Yizhi Xiao, Corey Bacher, Walter L. Siqueira, David W. Holdsworth, S. Jeffrey Dixon, Cheryle A. Séguin
Licensed content date	Jul 2, 2013
Start page	1853
End page	1864
Type of use	Dissertation/Thesis
Requestor type	Author of this Wiley article
Format	Electronic
Portion	Full article
Will you be translating?	No
Title of your thesis / dissertation	Mouse models for intervertebral disc development, degeneration and whole-body vibration.
Expected completion date	Dec 2014
Expected size (number of pages)	325
Total	0.00 USD
Terms and Conditions	

TERMS AND CONDITIONS

This copyrighted material is owned by or exclusively licensed to John Wiley & Sons, Inc. or one of its group companies (each a "Wiley Company") or handled on behalf of a society with which a Wiley Company has exclusive publishing rights in relation to a particular work

(collectively "WILEY"). By clicking accept in connection with completing this licensing transaction, you agree that the following terms and conditions apply to this transaction (along with the billing and payment terms and conditions established by the Copyright Clearance Center Inc., ("CCC's Billing and Payment terms and conditions"), at the time that you opened your Rightslink account (these are available at any time at <http://myaccount.copyright.com>).

Terms and Conditions

- The materials you have requested permission to reproduce or reuse (the "Wiley Materials") are protected by copyright.
- You are hereby granted a personal, non-exclusive, non-sub licensable (on a stand-alone basis), non-transferable, worldwide, limited license to reproduce the Wiley Materials for the purpose specified in the licensing process. This license is for a one-time use only and limited to any maximum distribution number specified in the license. The first instance of republication or reuse granted by this licence must be completed within two years of the date of the grant of this licence (although copies prepared before the end date may be distributed thereafter). The Wiley Materials shall not be used in any other manner or for any other purpose, beyond what is granted in the license. Permission is granted subject to an appropriate acknowledgement given to the author, title of the material/book/journal and the publisher. You shall also duplicate the copyright notice that appears in the Wiley publication in your use of the Wiley Material. Permission is also granted on the understanding that nowhere in the text is a previously published source acknowledged for all or part of this Wiley Material. Any third party content is expressly excluded from this permission.
- With respect to the Wiley Materials, all rights are reserved. Except as expressly granted by the terms of the license, no part of the Wiley Materials may be copied, modified, adapted (except for minor reformatting required by the new Publication), translated, reproduced, transferred or distributed, in any form or by any means, and no derivative works may be made based on the Wiley Materials without the prior permission of the respective copyright owner. You may not alter, remove or suppress in any manner any copyright, trademark or other notices displayed by the Wiley Materials. You may not license, rent, sell, loan, lease, pledge, offer as security, transfer or assign the Wiley Materials on a stand-alone basis, or any of the rights granted to you hereunder to any other person.
- The Wiley Materials and all of the intellectual property rights therein shall at all times remain the exclusive property of John Wiley & Sons Inc, the Wiley Companies, or their respective licensors, and your interest therein is only that of having possession of and the right to reproduce the Wiley Materials pursuant to Section 2 herein during the continuance of this Agreement. You agree that you own no right, title or interest in or to the Wiley Materials or any of the intellectual property rights therein. You shall have no rights hereunder other than the license as provided for above in Section 2. No right, license or interest to any trademark, trade name, service mark or other branding ("Marks") of WILEY or its licensors is granted hereunder, and you agree that you shall not assert any such right, license or interest with respect thereto.
- NEITHER WILEY NOR ITS LICENSORS MAKES ANY WARRANTY OR

REPRESENTATION OF ANY KIND TO YOU OR ANY THIRD PARTY, EXPRESS, IMPLIED OR STATUTORY, WITH RESPECT TO THE MATERIALS OR THE ACCURACY OF ANY INFORMATION CONTAINED IN THE MATERIALS, INCLUDING, WITHOUT LIMITATION, ANY IMPLIED WARRANTY OF MERCHANTABILITY, ACCURACY, SATISFACTORY QUALITY, FITNESS FOR A PARTICULAR PURPOSE, USABILITY, INTEGRATION OR NON-INFRINGEMENT AND ALL SUCH WARRANTIES ARE HEREBY EXCLUDED BY WILEY AND ITS LICENSORS AND WAIVED BY YOU

- WILEY shall have the right to terminate this Agreement immediately upon breach of this Agreement by you.
- You shall indemnify, defend and hold harmless WILEY, its Licensors and their respective directors, officers, agents and employees, from and against any actual or threatened claims, demands, causes of action or proceedings arising from any breach of this Agreement by you.
- IN NO EVENT SHALL WILEY OR ITS LICENSORS BE LIABLE TO YOU OR ANY OTHER PARTY OR ANY OTHER PERSON OR ENTITY FOR ANY SPECIAL, CONSEQUENTIAL, INCIDENTAL, INDIRECT, EXEMPLARY OR PUNITIVE DAMAGES, HOWEVER CAUSED, ARISING OUT OF OR IN CONNECTION WITH THE DOWNLOADING, PROVISIONING, VIEWING OR USE OF THE MATERIALS REGARDLESS OF THE FORM OF ACTION, WHETHER FOR BREACH OF CONTRACT, BREACH OF WARRANTY, TORT, NEGLIGENCE, INFRINGEMENT OR OTHERWISE (INCLUDING, WITHOUT LIMITATION, DAMAGES BASED ON LOSS OF PROFITS, DATA, FILES, USE, BUSINESS OPPORTUNITY OR CLAIMS OF THIRD PARTIES), AND WHETHER OR NOT THE PARTY HAS BEEN ADVISED OF THE POSSIBILITY OF SUCH DAMAGES. THIS LIMITATION SHALL APPLY NOTWITHSTANDING ANY FAILURE OF ESSENTIAL PURPOSE OF ANY LIMITED REMEDY PROVIDED HEREIN.
- Should any provision of this Agreement be held by a court of competent jurisdiction to be illegal, invalid, or unenforceable, that provision shall be deemed amended to achieve as nearly as possible the same economic effect as the original provision, and the legality, validity and enforceability of the remaining provisions of this Agreement shall not be affected or impaired thereby.
- The failure of either party to enforce any term or condition of this Agreement shall not constitute a waiver of either party's right to enforce each and every term and condition of this Agreement. No breach under this agreement shall be deemed waived or excused by either party unless such waiver or consent is in writing signed by the party granting such waiver or consent. The waiver by or consent of a party to a breach of any provision of this Agreement shall not operate or be construed as a waiver of or consent to any other or subsequent breach by such other party.
- This Agreement may not be assigned (including by operation of law or otherwise) by you without WILEY's prior written consent.
- Any fee required for this permission shall be non-refundable after thirty (30) days

from receipt by the CCC.

- These terms and conditions together with CCC's Billing and Payment terms and conditions (which are incorporated herein) form the entire agreement between you and WILEY concerning this licensing transaction and (in the absence of fraud) supersedes all prior agreements and representations of the parties, oral or written. This Agreement may not be amended except in writing signed by both parties. This Agreement shall be binding upon and inure to the benefit of the parties' successors, legal representatives, and authorized assigns.
- In the event of any conflict between your obligations established by these terms and conditions and those established by CCC's Billing and Payment terms and conditions, these terms and conditions shall prevail.
- WILEY expressly reserves all rights not specifically granted in the combination of (i) the license details provided by you and accepted in the course of this licensing transaction, (ii) these terms and conditions and (iii) CCC's Billing and Payment terms and conditions.
- This Agreement will be void if the Type of Use, Format, Circulation, or Requestor Type was misrepresented during the licensing process.
- This Agreement shall be governed by and construed in accordance with the laws of the State of New York, USA, without regards to such state's conflict of law rules. Any legal action, suit or proceeding arising out of or relating to these Terms and Conditions or the breach thereof shall be instituted in a court of competent jurisdiction in New York County in the State of New York in the United States of America and each party hereby consents and submits to the personal jurisdiction of such court, waives any objection to venue in such court and consents to service of process by registered or certified mail, return receipt requested, at the last known address of such party.

WILEY OPEN ACCESS TERMS AND CONDITIONS

Wiley Publishes Open Access Articles in fully Open Access Journals and in Subscription journals offering Online Open. Although most of the fully Open Access journals publish open access articles under the terms of the Creative Commons Attribution (CC BY) License only, the subscription journals and a few of the Open Access Journals offer a choice of Creative Commons Licenses: Creative Commons Attribution (CC-BY) license [Creative Commons Attribution Non-Commercial \(CC-BY-NC\) license](#) and [Creative Commons Attribution Non-Commercial-NoDerivs \(CC-BY-NC-ND\) License](#). The license type is clearly identified on the article.

Copyright in any research article in a journal published as Open Access under a Creative Commons License is retained by the author(s). Authors grant Wiley a license to publish the article and identify itself as the original publisher. Authors also grant any third party the right to use the article freely as long as its integrity is maintained and its original authors, citation details and publisher are identified as follows: [Title of Article/Author/Journal Title and Volume/Issue. Copyright (c) [year] [copyright owner as specified in the Journal]]. Links to the final article on Wiley's website are encouraged where applicable.

The Creative Commons Attribution License

The [Creative Commons Attribution License \(CC-BY\)](#) allows users to copy, distribute and transmit an article, adapt the article and make commercial use of the article. The CC-BY license permits commercial and non-commercial re-use of an open access article, as long as the author is properly attributed.

The Creative Commons Attribution License does not affect the moral rights of authors, including without limitation the right not to have their work subjected to derogatory treatment. It also does not affect any other rights held by authors or third parties in the article, including without limitation the rights of privacy and publicity. Use of the article must not assert or imply, whether implicitly or explicitly, any connection with, endorsement or sponsorship of such use by the author, publisher or any other party associated with the article.

For any reuse or distribution, users must include the copyright notice and make clear to others that the article is made available under a Creative Commons Attribution license, linking to the relevant Creative Commons web page.

To the fullest extent permitted by applicable law, the article is made available as is and without representation or warranties of any kind whether express, implied, statutory or otherwise and including, without limitation, warranties of title, merchantability, fitness for a particular purpose, non-infringement, absence of defects, accuracy, or the presence or absence of errors.

Creative Commons Attribution Non-Commercial License

The [Creative Commons Attribution Non-Commercial \(CC-BY-NC\) License](#) permits use, distribution and reproduction in any medium, provided the original work is properly cited and is not used for commercial purposes.(see below)

Creative Commons Attribution-Non-Commercial-NoDerivs License

The [Creative Commons Attribution Non-Commercial-NoDerivs License](#) (CC-BY-NC-ND) permits use, distribution and reproduction in any medium, provided the original work is properly cited, is not used for commercial purposes and no modifications or adaptations are made. (see below)

Use by non-commercial users

For non-commercial and non-promotional purposes, individual users may access, download, copy, display and redistribute to colleagues Wiley Open Access articles, as well as adapt, translate, text- and data-mine the content subject to the following conditions:

- The authors' moral rights are not compromised. These rights include the right of "paternity" (also known as "attribution" - the right for the author to be identified as such) and "integrity" (the right for the author not to have the work altered in such a way that the author's reputation or integrity may be impugned).
- Where content in the article is identified as belonging to a third party, it is the obligation of the user to ensure that any reuse complies with the copyright policies of the owner of that content.

- If article content is copied, downloaded or otherwise reused for non-commercial research and education purposes, a link to the appropriate bibliographic citation (authors, journal, article title, volume, issue, page numbers, DOI and the link to the definitive published version on **Wiley Online Library**) should be maintained. Copyright notices and disclaimers must not be deleted.
- Any translations, for which a prior translation agreement with Wiley has not been agreed, must prominently display the statement: "This is an unofficial translation of an article that appeared in a Wiley publication. The publisher has not endorsed this translation."

Use by commercial "for-profit" organisations

Use of Wiley Open Access articles for commercial, promotional, or marketing purposes requires further explicit permission from Wiley and will be subject to a fee. Commercial purposes include:

- Copying or downloading of articles, or linking to such articles for further redistribution, sale or licensing;
- Copying, downloading or posting by a site or service that incorporates advertising with such content;
- The inclusion or incorporation of article content in other works or services (other than normal quotations with an appropriate citation) that is then available for sale or licensing, for a fee (for example, a compilation produced for marketing purposes, inclusion in a sales pack)
- Use of article content (other than normal quotations with appropriate citation) by for-profit organisations for promotional purposes
- Linking to article content in e-mails redistributed for promotional, marketing or educational purposes;
- Use for the purposes of monetary reward by means of sale, resale, licence, loan, transfer or other form of commercial exploitation such as marketing products
- Print reprints of Wiley Open Access articles can be purchased from:
corporatesales@wiley.com

Further details can be found on Wiley Online Library
<http://olabout.wiley.com/WileyCDA/Section/id-410895.html>

Other Terms and Conditions:

v1.9

Questions? customercare@copyright.com or +1-855-239-3415 (toll free in the US) or +1-978-646-2777.

Gratis licenses (referencing \$0 in the Total field) are free. Please retain this printable license for your reference. No payment is required.

APPENDIX F

Ethics Approval of Animal Use



AUP Number: 2009-050

PI Name: Seguin, Cheryle

AUP Title: Mouse Models To Characterize Intervertebral Disc Development And Disc Disease

Approval Date: 07/25/2013

Official Notice of Animal Use Subcommittee (AUS) Approval: Your new Animal Use Protocol (AUP) entitled "Mouse Models To Characterize Intervertebral Disc Development And Disc Disease

" has been APPROVED by the Animal Use Subcommittee of the University Council on Animal Care. This approval, although valid for four years, and is subject to annual Protocol Renewal.2009-050::5

1. This AUP number must be indicated when ordering animals for this project.
2. Animals for other projects may not be ordered under this AUP number.
3. Purchases of animals other than through this system must be cleared through the ACVS office. Health certificates will be required.

The holder of this Animal Use Protocol is responsible to ensure that all associated safety components (biosafety, radiation safety, general laboratory safety) comply with institutional safety standards and have received all necessary approvals. Please consult directly with your institutional safety officers.

Submitted by: Copeman, Laura
on behalf of the Animal Use Subcommittee
University Council on Animal Care

The University of Western Ontario
Animal Use Subcommittee / University Council on Animal Care
Health Sciences Centre, • London, Ontario • CANADA – N6A 5C1
PH: 519-661-2111 ext. 86768 • FL 519-661-2028
Email: auspc@uwo.ca • <http://www.uwo.ca/animal/website/>

CURRICULUM VITAE

Matthew Robert McCann

PERSONAL DATA

Date of Birth: April 6th, 1986

Citizenship: Canadian

EDUCATION

Sept 2009 -
Dec 2014 **Doctor of Philosophy in Physiology,
Specialization in Musculoskeletal Health Research &
Developmental Biology**
Schulich School of Medicine and Dentistry
University of Western Ontario, London, Ontario, Canada.
Supervisor: Dr. Cheryle Séguin Co-Supervisor: Dr. Frank Beier
Thesis Topic: Mouse Models of Intervertebral Disc Development,
Degeneration and Mechanical Loading

Sept 2005 -
June 2009 **Honors B.Sc. Specialization in Biology & Minor in Anatomy
and Cell Biology**
University of Western Ontario, London, Ontario, Canada.
Supervisor: Dr. Andrew Leask
Thesis Topic: Role of microsomal Prostaglandin E₂ Synthases-1
(mPGES-1) in bleomycin induced fibrosis
(Conferred in June 2009)

TEACHING EXPERIENCE

Sept 2012 -
Dec 2013 **Teaching Assistant: Physiology 3140a “Cellular Physiology”**
Department of Physiology and Pharmacology
The University of Western Ontario, London, Ontario, Canada

Sept 2012 -
Dec 2013 **Teaching Assistant: Biology 2244a “Analysis and
Interpretation of Biological Data”**
Department of Biology and Mathematics
(Consent from Dept. of Physiology and Pharmacology),
The University of Western Ontario, London, Ontario, Canada

SUPERVISORY EXPERIENCE

Sept 2014 - Present	Thesis Advisor Khander Zimmo - Hon. Physiology Student <i>"Transcriptional profiling the nucleus pulposus during aged induced degeneration"</i>
June 2014 - Present	Mentor Cynthia Yeung - Scholar's Elective Student <i>"The role of notochord cells in aging and injury induced degeneration of the intervertebral disc"</i>
Sept 2012 - Apr 2013	Thesis Advisor Jimin Lee - Scholar's Elective Student <i>"Parameters for isolation and growth of notochordal cells in vitro"</i>
Sept 2012 - Sept 2013	Mentor Megan Kamphuis - High School Co-op Student <i>"Developing novel assessment parameters to determine quality of collagen structure within the intervertebral disc – implications in whole body vibration induced degeneration"</i>
Sept 2011 - Aug 2013	Thesis Advisor Matthew Ernst - Hon. Physiology Student <i>"Cell type-specific purinergic signaling in the intervertebral disc."</i>
June 2011 - Aug 2011	Thesis Advisor Priya Patel - Hon. Medical Sciences Student <i>"Effects of whole-body vibration on the musculoskeletal system"</i>
June 2011 - Apr 2013	Thesis Advisor Salma Shiak - Hon. Medical Sciences Student <i>"Isolation of nucleus pulposus-derived cells from the intervertebral disc of Noto^{Cre/+};ROSA26^{mT/mG} Mus Musculus"</i>
Sept 2010 - Apr 2011	Thesis Advisor Corey Bacher - Hon. Medical Sciences Student <i>"Effect of acute vibration on intervertebral disc homeostasis in a mouse model"</i>

AWARDS AND SCHOLARSHIPS

(Selected)

Date	Award
Jun. 2014	20 th Canadian Connective Tissue Conference Best Presentation London, Ontario, Canada <i>Value \$150</i>
Mar. 2014 - Jun. 2014	Canadian Institutes for Health Research Michael Smith Foreign Study Supplement , Icahn School of Medicine at Mount Sinai, New York City <i>Value: \$5,478</i>
Jan. 2014	Bone and Joint Injury and Repair Conference Poster Award: Novel Therapies London, Ontario, Canada <i>Value: \$100</i>
Nov. 2013	Physiology and Pharmacology Research Day Poster Award in Cell & Developmental Biology University of Western University, London, Ont. <i>Value: \$100</i>
Oct. 2013	Chordoma Foundation Travel Award Boston, Massachusetts <i>Value: \$500</i>
Mar. 2012	The Dr. Suzanne Bernier Memorial Award in Skeletal Biology University of Western University, London, Ont. <i>Value: \$5000</i>
Mar. 2012	London Health Research Day Podium Presentation Award London, Ontario, Canada <i>Value: \$600</i>
May 2011 - May 2014	CIHR Frederick Banting & Charles Best Canada Scholarship Doctoral Scholarship University of Western University, London, Ont. <i>Value: \$105,00 (35,000 per annum)</i>
May 2011	17 th Canadian Connective Tissue Conference Best Presentation Montreal, Quebec, Canada <i>Value: \$200</i>

Mar. 2011	Gordon Research Conference: Cartilage Biology & Pathology Poster Award Ventura, California, United States <i>Value: \$500</i>
Mar. 2011	CIHR: Institute for Musculoskeletal Health and Arthritis Travel Award University of Western University, London, Ont. <i>Value: \$900</i>
Feb. 2011	Schulich School of Medicine Graduate Research Bursary University of Western University, London, Ont. <i>Value: \$300</i>
Oct. 2011	Canadian Arthritis Network's Conference Travel Award Gatineau, Quebec <i>Value: \$1,500</i>
Aug. 2010 - June 2011	Collaborative Developmental Biology Program Scholarship University of Western University, London, Ont. <i>Value: \$1,250</i>
Jan. 2010 - Aug. 2011	CIHR Joint Motion Program Scholarship University of Western University, London, Ont. <i>Value: \$10,500</i>
Nov. 2010	Canadian Arthritis Network's Conference Travel Award Vancouver, British Columbia. <i>Value: \$2,000</i>
Sept. 2009 - Aug. 2011	Schulich School of Medicine and Dentistry Entrance Scholarship University of Western University, London, Ont. <i>Value: \$44,500 (8,990 per annum)</i>
Apr. 2009	Honours Biology Thesis Day Best Presentation University of Western University, London, Ont. <i>Distinction</i>
Mar. 2009	Ontario Biology Day Best Poster Presentation University of Windsor, Windsor, Ont. <i>Distinction</i>

ACADEMIC SERVICE

(Selected)

Dec 2014 - Present	Journal Reviewer - PLOS ONE
Nov. 2010 - Present	Student Rep to the Program Operations Committee Joint Motion Program University of Western University, London, Ont.
Sep. 2010 - Apr 2014	Vice Chair Physiology and Pharmacology Grad Council University of Western University, London, Ont.
Nov. 2010 - Apr. 2014	Physiology Graduate Student Webmaster Department of Physiology and Pharmacology University of Western University, London, Ont.
Mar. 2010 - Sep. 2012	Graduate Rep to Schulich Educational Award Committee Schulich School of Medicine and Dentistry University of Western University, London, Ont.
Mar. 2010 - Sep. 2012	Physiology Grad Rep to Schulich Council Schulich School of Medicine and Dentistry University of Western University, London, Ont.
Sept 2010 - Sept 2011	Developmental Biology Grad Rep; Course Rep. Collaborative Program in Developmental Biology University of Western University, London, Ont.

PUBLICATIONS:

(Sorted by Date Submitted)

1. **McCann M.R.**, Patel P., Pest M.A., Ratneswaran A., Kamphuis M.P., Esmail Z., Lee J., Barbalinardo M., Beaucage K.L, Holdsworth D.W., Beier F., Dixon S.J, Séguin C.A. Repeated exposure to high-frequency low-amplitude vibration induce degeneration of intervertebral disc and knee joint in a murine model. (In revision at *Arthritis & Rheumatology* - Dec 2, 2014)
2. **McCann M.R.**, Patel P., Frimpong A., Xiao Y., Siqueira W.L., Séguin C.A. Proteome signature of the murine intervertebral disc. (In revision at *PLOS One*; Oct 3, 2014)
3. Bedore J., Sha W., **McCann M.R.**, Leask A., Séguin C.A. Loss of notochord-derived CCN2 results in impaired intervertebral disc development and premature disc degeneration. *Arthritis & Rheumatism*. 2013 Oct;65(10):2634-44. *Selected for cover art

4. **McCann M.R.***, Patel P.*, Beaucage K.L, Xiao Y., Bacher C.A., Siqueira W.L., Holdsworth D.W., Dixon S.J, Séguin C.A. Acute vibration induces transient expression of anabolic genes in the intervertebral disc in a frequency dependent manner. *Arthritis and Rheumatism*. 2013 Jul;65(7):1853-64. R6 *Equal first author contribution
5. **McCann M.R.** Tamplin O.J., Rossat J., Séguin C.A. Tracing notochord-derived cells using a novel Noto-cre mouse: implications for intervertebral disc development. *Disease Models and Mechanisms*, 2012 Jan;5(1):73-82. *Selected for cover artwork
6. **McCann M.R.***, Monemdjou R.*, Ghassemi-Kakroodi P., Fahmi H., Perez G., Liu S., Shi-wen X., Parapuram S.K., Kojima F., Denton C.P., Abraham D.J., Martel-Pelletier J., Crofford L.J., Leask A., Kapoor M. mPGES-1 null mice are resistant to bleomycin-induced skin fibrosis. *Arthritis Research & Therapy*, 2011, 13:R6 *Equal first author contribution
7. **McCann M.R.**, Bacher C.A., and Séguin C.A. Exploiting notochord cells for stem cell-based regeneration of the intervertebral disc. *Journal of Cell Communication and Signaling*. 2011, 5 (1):39-43
8. Kapoor M, **McCann M.R.**, Liu S, Huh K, Denton CP, Abraham DJ, Leask A. Loss of PPAR γ in mouse fibroblasts results in enhanced responsiveness to the bleomycin-induced model of skin scleroderma. *Arthritis and Rheumatism*. 2009 Sep;60(9):2822-9.

IN PREPERATION

9. **McCann M.R.**, Carter D.E., Séguin C.A. Elucidating the specific phenotype of notochord cells and how these cellular properties change with age. (To be submitted to *Osteoarthritis and Cartilage*; Dec 2014)
10. **McCann M.R.**, Patel P., Xiao Y., Siqueira W.L., Séguin C.A. Acute vibrational effects on the proteome of the murine intervertebral disc. (To be submitted to *Proteomics*; Dec 2014)

SELECT CONFERENCES

1. **McCann M.R.**, Patel P., Barbalinardo M., Pest M.A., Beaucage K.L., Kamphuis M.K., Beier F., Holdsworth D.W., Dixon S.J., Séguin C.A. (June 2014) Whole body vibration results in degeneration of the intervertebral disc and knee joint in a mouse model: is fibrocartilage the culprit? 20th Annual Canadian Connective Tissue Conference. London, Ontario, Canada. Podium Presentation.
2. **McCann M.R.**, Patel P., Frimpong A., Xiao Y., Siqueira W.L., Séguin C.A. (June 2014) Proteome signature of the murine intervertebral disc. 20th Annual Canadian Connective Tissue Conference. London, Ontario, Canada. Poster Presentation.
3. **McCann M.R.**, Patel P., Barbalinardo M., Pest M.A., Beaucage K.L., Kamphuis M.K., Beier F., Holdsworth D.W., Dixon S.J., Séguin C.A. (January 2014) Repeated daily exposure to high-frequency low-amplitude vibration negatively affects cartilaginous joints. Bone and Joint Injury and Repair Conference. London, Ontario, Canada. Podium Presentation.
4. **McCann M.R.**, Patel P., Barbalinardo M., Pest M.A., Beaucage K.L., Kamphuis M.K., Beier F., Holdsworth D.W., Dixon S.J., Séguin C.A. (April 2013) Repeated daily exposure to high-frequency low-amplitude vibration negatively affects cartilaginous joints. 2013 Gordon Research Conference: Cartilage Biology and Pathology. Les Diablerets, Switzerland Poster Presentation.
5. **McCann M.R.**, Patel P., Barbalinardo M., Pest M.A., Beaucage K.L., Kamphuis M.K., Beier F., Holdsworth D.W., Dixon S.J., Séguin C.A. (March 2013) Repeated daily exposure to high-frequency low-amplitude vibration negatively affects cartilaginous joints. 2012 London Health Research Day. London, Ontario, Canada. Podium Presentation.
6. Patel P.*, **McCann M.R.***, Beaucage K.L., Bacher C.A., Holdsworth D.W., Dixon S.J., Séguin C.A. (June 2012). Acute vibration induces transient expression of anabolic genes in the intervertebral disc in a frequency dependent manner. 18th Annual Canadian Connective Tissue Conference. Toronto, Ontario, Canada. *Equal first author contribution. Poster Presentation.
7. **McCann M.R.***, Patel P.*, Beaucage K.L., Bacher C.A., Holdsworth D.W., Dixon S.J., Séguin C.A. (April 2012). Acute vibration induces transient expression of anabolic genes in the intervertebral disc in a frequency dependent manner. 2012 London Health Research Day. London, Ontario, Canada. *Equal first author contribution. Podium Presentation.

8. **McCann M.R.***, Patel P.*, Beaucage K.L, Bacher C.A., Holdsworth D.W., Dixon S.J, Séguin C.A. (November 2011) Acute vibration induces transient expression of anabolic genes in the intervertebral disc in a frequency dependent manner. Philadelphia Spine Symposium, Philadelphia, U.S.A. *Equal first author contribution. Poster Presentation.

9. **McCann M.R**, Tamplin O.J., Rossant J., Séguin C.A. (June 2011) Origins of the nucleus pulposus: implications for notochord cell based therapy. 17th Annual Canadian Connective Tissue Conference. Montreal, Quebec, Canada. Podium Presentation.

10. **McCann M.R**, Tamplin O.J., Rossant J., Séguin C.A. (June 2011) Origins of the Nucleus Pulposus; Implications for stem cell therapy of the Developmental Disc Disease. 9th International Society for Stem Cell Research Conference, Toronto, Ontario, Canada. Poster Presentation.

11. **McCann M.R**, Tamplin O.J., Rossant J., Séguin C.A. (March 2011) The embryonic notochord forms the nucleus pulposus during intervertebral disc development. Gordon Research Conferences: Cartilage Biology and Pathology. Ventura, California, U.S.A. Poster Presentation.

12. **McCann M.R**, Tamplin O.J., Rossant J., Séguin C.A. (March 2011) Origins of the nucleus pulposus: implications for notochord cell based therapy. Great Lakes Mammalian Development Meeting. Toronto, Ontario, Canada. Podium Presentation.

13. **McCann M.R**, Tamplin O.J., Rossant J., Séguin C.A. (October 2010) Determining the Developmental Origins of the Nuclues Pulposus; Implications in Intervertebral Disc Degeneration. Canadian Arthritis Network's Annual Scientific Conference, Gatineau, Quebec, Canada. Poster Presentation.

14. **McCann M.R**, Tamplin O.J., Rossant J., Séguin C.A. (November 2010) Role of the Notochord during Disc Development; A Cross Discipline Approach. CIHR Joint Motion Program in Musculoskeletal Health Workshop. University of Western Ontario. London, Ontario, Canada. Podium Presentation.